NEURO-OTOLOGY EDITOR'S PICK 2021

EDITED BY: Michael Strupp
PUBLISHED IN: Frontiers in Neurology

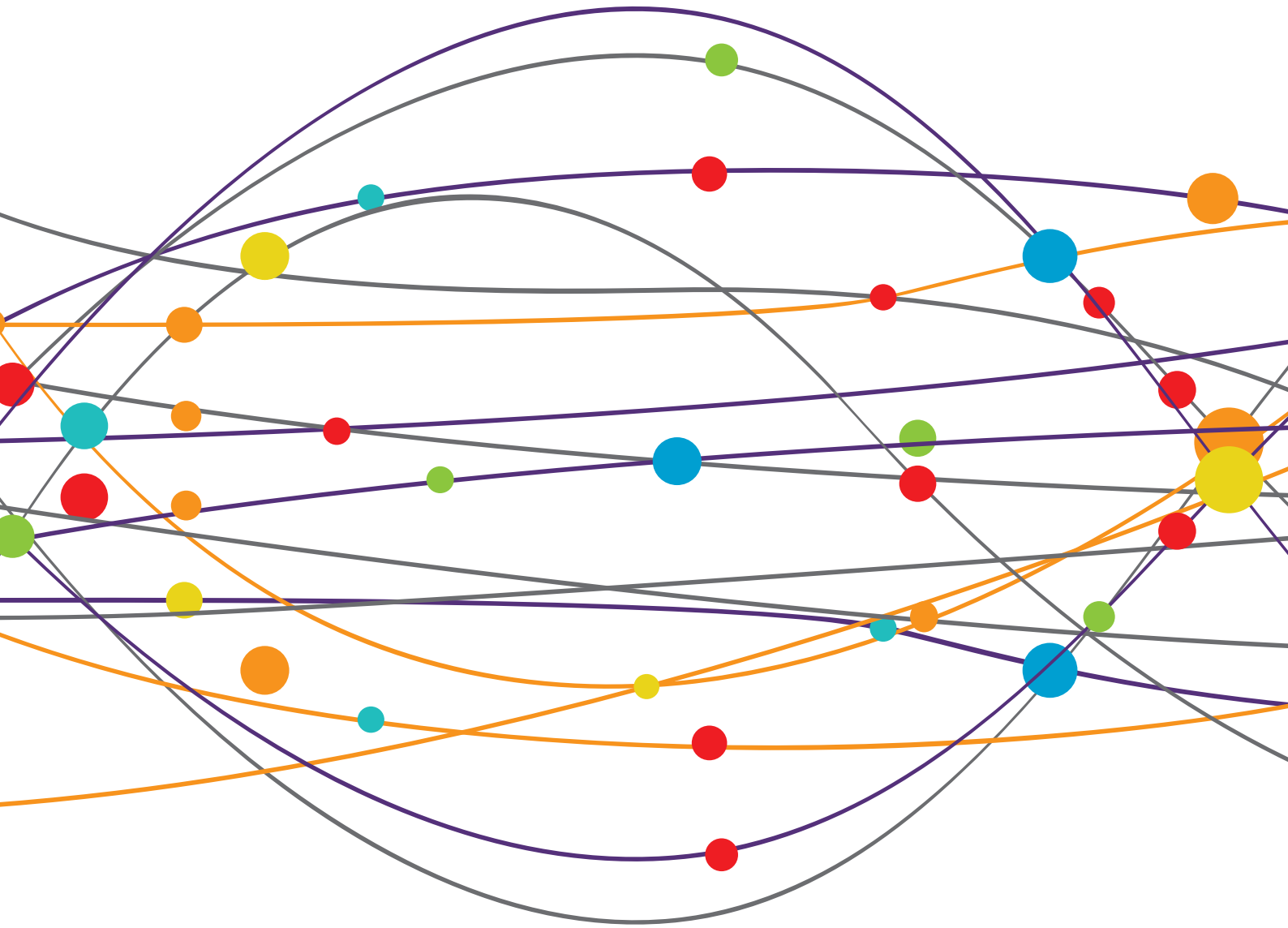

frontiers Research Topics

frontiers

ISSN 1664-8714
ISBN 978-2-88971-176-5
DOI 10.3389/978-2-88971-176-5

About Frontiers

Frontiers is more than just an open-access publisher of scholarly articles: it is a pioneering approach to the world of academia, radically improving the way scholarly research is managed. The grand vision of Frontiers is a world where all people have an equal opportunity to seek, share and generate knowledge. Frontiers provides immediate and permanent online open access to all its publications, but this alone is not enough to realize our grand goals.

Frontiers Journal Series

The Frontiers Journal Series is a multi-tier and interdisciplinary set of open-access, online journals, promising a paradigm shift from the current review, selection and dissemination processes in academic publishing. All Frontiers journals are driven by researchers for researchers; therefore, they constitute a service to the scholarly community. At the same time, the Frontiers Journal Series operates on a revolutionary invention, the tiered publishing system, initially addressing specific communities of scholars, and gradually climbing up to broader public understanding, thus serving the interests of the lay society, too.

Dedication to Quality

Each Frontiers article is a landmark of the highest quality, thanks to genuinely collaborative interactions between authors and review editors, who include some of the world's best academicians. Research must be certified by peers before entering a stream of knowledge that may eventually reach the public - and shape society; therefore, Frontiers only applies the most rigorous and unbiased reviews.
Frontiers revolutionizes research publishing by freely delivering the most outstanding research, evaluated with no bias from both the academic and social point of view. By applying the most advanced information technologies, Frontiers is catapulting scholarly publishing into a new generation.

What are Frontiers Research Topics?

Frontiers Research Topics are very popular trademarks of the Frontiers Journals Series: they are collections of at least ten articles, all centered on a particular subject. With their unique mix of varied contributions from Original Research to Review Articles, Frontiers Research Topics unify the most influential researchers, the latest key findings and historical advances in a hot research area! Find out more on how to host your own Frontiers Research Topic or contribute to one as an author by contacting the Frontiers Editorial Office: frontiersin.org/about/contact

NEURO-OTOLOGY EDITOR'S PICK 2021

Topic Editor:
Michael Strupp, Ludwig Maximilian University of Munich, Germany

Citation: Strupp, M., ed. (2021). Neuro-Otology Editor's Pick 2021. Lausanne: Frontiers Media SA. doi: 10.3389/978-2-88971-176-5

Table of Contents

frontiers in Neurology

ORIGINAL RESEARCH
published: 25 February 2019
doi: 10.3389/fneur.2019.00147

Ginkgo biloba Extract EGb 761 Improves Vestibular Compensation and Modulates Cerebral Vestibular Networks in the Rat

*Magdalena Lindner[1], Astrid Gosewisch[1], Eva Eilles[1], Christina Branner[1], Anja Krämer[1], Rosel Oos[2], Eckhard Wolf[3], Sibylle Ziegler[1,2], Peter Bartenstein[1,2,4], Thomas Brandt[1,5], Marianne Dieterich[1,4,6] and Andreas Zwergal[1,6]**

[1] German Center for Vertigo and Balance Disorders, DSGZ, Ludwig-Maximilians-University of Munich, Munich, Germany, [2] Department of Nuclear Medicine, Ludwig-Maximilians-University of Munich, Munich, Germany, [3] Department of Veterinarian Medicine, Ludwig-Maximilians-University of Munich, Munich, Germany, [4] Munich Cluster of Systems Neurology, SyNergy, Munich, Germany, [5] Clinical Neuroscience, Ludwig-Maximilians-University of Munich, Munich, Germany, [6] Department of Neurology, Ludwig-Maximilians-University of Munich, Munich, Germany

OPEN ACCESS

Edited by:
Paul Smith,
University of Otago, New Zealand

Reviewed by:
Lacour Michel,
Aix-Marseille Université, France
Sung-Hee Kim,
Kyungpook National University, South Korea
Rachael L. Taylor,
The University of Auckland, New Zealand

***Correspondence:**
Andreas Zwergal
andreas.zwergal@med.uni-muenchen.de

Specialty section:
This article was submitted to Neuro-Otology, a section of the journal Frontiers in Neurology

Received: 01 October 2018
Accepted: 05 February 2019
Published: 25 February 2019

Citation:
Lindner M, Gosewisch A, Eilles E, Branner C, Krämer A, Oos R, Wolf E, Ziegler S, Bartenstein P, Brandt T, Dieterich M and Zwergal A (2019) Ginkgo biloba Extract EGb 761 Improves Vestibular Compensation and Modulates Cerebral Vestibular Networks in the Rat. Front. Neurol. 10:147. doi: 10.3389/fneur.2019.00147

Unilateral inner ear damage is followed by behavioral recovery due to central vestibular compensation. The dose-dependent therapeutic effect of *Ginkgo biloba* extract EGb 761 on vestibular compensation was investigated by behavioral testing and serial cerebral [^{18}F]-Fluoro-desoxyglucose ([^{18}F]-FDG)-μPET in a rat model of unilateral labyrinthectomy (UL). Five groups of 8 animals each were treated with EGb 761-supplemented food at doses of 75, 37.5 or 18.75 mg/kg body weight 6 weeks prior and 15 days post UL (groups A,B,C), control food prior and EGb 761-supplemented food (75 mg/kg) for 15 days post UL (group D), or control food throughout (group E). Plasma levels of EGb 761 components bilobalide, ginkgolide A and B were analyzed prior and 15 days post UL. Behavioral testing included clinical scoring of nystagmus, postural asymmetry, head roll tilt, body rotation during sensory perturbation and instrumental registration of mobility in an open field before and 1, 2, 3, 5, 7, 15 days after UL. Whole-brain [^{18}F]-FDG-μPET was recorded before and 1, 3, 7, 15 days after UL. The EGb 761 group A (75 mg/kg prior/post UL) showed a significant reduction of nystagmus scores (day 3 post UL), of postural asymmetry (1, 3, 7 days post UL), and an increased mobility in the open field (day 7 post UL) as compared to controls (group E). Application of EGb 761 at doses of 37.5 and 18.75 mg/kg prior/post UL (groups B,C) resulted in faster recovery of postural asymmetry, but did not influence mobility relative to controls. Locomotor velocity increased with higher plasma levels of ginkgolide A and B. [^{18}F]-FDG-μPET revealed a significant decrease of the regional cerebral glucose metabolism (rCGM) in the vestibular nuclei and cerebellum and an increase in the hippocampal formation with higher plasma levels of ginkgolides and bilobalide 1 and 3 days post UL. Decrease of rCGM in the vestibular nucleus area and increase in the hippocampal formation with higher plasma levels persisted until day 15 post UL. In conclusion, *Ginkgo biloba* extract EGb 761 improves vestibulo-ocular motor, vestibulo-spinal compensation, and mobility after UL. This rat study supports the translational approach to investigate EGb 761 at higher dosages for acceleration of vestibular compensation in acute vestibular loss.

Keywords: unilateral vestibulopathy, vestibular compensation, *Ginkgo biloba* extract EGb 761, small animal PET, vertigo, pharmacotherapy, *in vivo* cerebral imaging

INTRODUCTION

Unilateral damage to the peripheral vestibular organ induces characteristic signs of vestibular imbalance, including spontaneous nystagmus, head tilt, and falling to the lesion side. Even if the damage to the labyrinth persists, initial symptoms recover over days to weeks due to central vestibular compensation (VC). VC is not a unique global process but comprises various structural and functional processes with separate and distinct time courses. It implicates neuronal plasticity in various hubs of cerebral and spinal vestibular networks (1–4). Most important regions for reorganization are the vestibular nuclei, the vestibulocerebellum, the thalamus and hippocampus (3–7). Mechanisms of VC can be examined on a cellular and neuronal level by various histological and electrophysiological techniques or on a whole brain network level using *in vivo* methods like serial positron emission tomography (PET) (8–10). Characteristic changes of regional cerebral glucose metabolism (rCGM) have been depicted recently after unilateral labyrintectomy (UL) in the rat using [^{18}F]-Fluoro-desoxyglucose ([^{18}F]-FDG)-μPET (9). The asymmetry of rCGM in the vestibular nuclei, vestibulocerebellum, thalamus and temporoparietal cortex directly after UL was followed by an adjustment of rCGM in the vestibular nuclei, rCGM increase in the ipsilesional spinal trigeminal nucleus, and increased vestibulocerebellar rCGM over time (9). [^{18}F]-FDG-μPET imaging was also feasible to quantify rCGM changes in cerebral vestibular networks by pharmacological interventions with 4-aminopyridine and N-acetyl-DL-leucine following inner ear damage (11, 12).

A possible therapeutic strategy for acute unilateral vestibular disorders is to improve and accelerate VC by medication such as betahistine, N-acetyl-DL-leucine or *Ginkgo biloba* extract EGb 761 [for review see (13)]. The pharmacon EGb 761 is a standardized extract of *Ginkgo biloba*, which contains flavonoids and terpene lactones at defined doses (14, 15). Previous studies have shown improvement of vestibular symptoms by EGb 761 after unilateral vestibular damage in rats, cats, and guinea pigs (16–18). Placebo-controlled trials in patients with unilateral peripheral and central vestibular lesions gave first evidence for an augmentation of exercise-induced effects on VC by EGb 761 (19). However, the mode of action and the pharmacological substrate by which the polyvalent EGb 761 extract improves VC are still not clear. Experimental data from neurodegenerative animal models suggest multiple effects of EGb 761 on neural plasticity, including modulation of long-term potentiation, neuronal spine morphology and density, neurito- and neurogenesis mostly by terpene lactones (20). The aim of this study was to determine systematically dose-, substrate-, and time-dependent effects of EGb 761 on vestibulo-ocular motor, vestibular-spinal, locomotor, and orientational symptoms after UL in the rat by behavioral testing. To further elucidate the EGb 761 mode of action during VC, serial [^{18}F]-FDG-μPET was performed at various stages in the course of compensation. We hypothesized that EGb 761 accelerates compensation of spontaneous nystagmus and postural asymmetry and improves mobility after UL. We expected EGb 761-induced rCGM changes to appear at various central vestibular network levels during VC.

METHODS

Animals

All animal experiments were approved by the government of Upper Bavaria and performed in accordance with the guidelines for the use of living animals in scientific studies and the German Law for the Protection of Animals. Male Sprague-Dawley rats (mean 400 ± 20 g, age 3 months at time of UL, Charles River Ltd, UK) were housed two animals per cage in a temperature- and humidity-controlled room with a 12 h light/dark cycle, with free access to food and water. In total 46 animals were included in the study.

EGb 761 Food

Phytoestrogen-free food with and without *Ginkgo biloba* extract EGb 761 supplement was provided by Altromin Spezialfutter GmbH & Co. KG, Germany. EGb 761® was provided by Dr. Willmar Schwabe Pharmaceuticals, Karlsruhe, Germany. It is a dry extract from *Ginkgo biloba* leaves (35–67:1) with extraction solvent: acetone 60% (w). The extract is adjusted to 22–27% Ginkgo flavonoids calculated as Ginkgo flavone glycosides, 5–7% terpene lactones consisting of 2.8–3.4% ginkgolides A, B, C, and 2.6–3.2% bilobalide and contains <5 ppm ginkgolic acids[1]. Food contained either EGb 761 in a dose of 735 or 367.5 mg or 184 mg per kg food or no supplement (control food). Food was prepared in 10 mm palletization and color-coded to avoid carry-over or mix-up (EGb 761 food: yellow, control food: green). Animals were allowed to consume the food *ad libitum*. Food was exchanged weekly and the extent of food consumption documented. Based on mean food uptake per body weight, 735, 367.5, and 184 mg EGb 761 per kg food equated to 75, 37.5, and 18.75 mg per kg body weight and day.

Experimental Design

Different food application protocols were tested to investigate effects of dose and treatment duration: (1) Eight animals received EGb 761 at a dose of either 75 mg/kg (group A), 37.5 mg/kg (group B), or 18.75 mg/kg body weight (group C) per day 6 weeks prior to and 15 days post UL. (2) Eight animals were treated with EGb 761-free control food 6 weeks prior to and EGb 761 food (75 mg/kg body weight per day) 15 days post UL (group D). (3) Eight animals received control food 6 weeks prior to and 15 days post UL (group E). All animals underwent behavioral testing by clinical scoring of vestibular imbalance and instrumental analysis of locomotion before and on days 1, 2, 3, 5, 7, and 15 after UL. Sequential whole-brain [^{18}F]-FDG-μPET was recorded prior to and 1, 3, 7, and 15 days post UL. Blood samples were drawn before and 15 days after UL in all animals and analyzed for the EGb 761 components bilobalide, ginkgolide A and B (**Figure 1**).

[1]EGb 761® is the active ingredient of Tebonin® intens, Dr. Willmar Schwabe Pharmaceuticals, Karlsruhe, Germany.

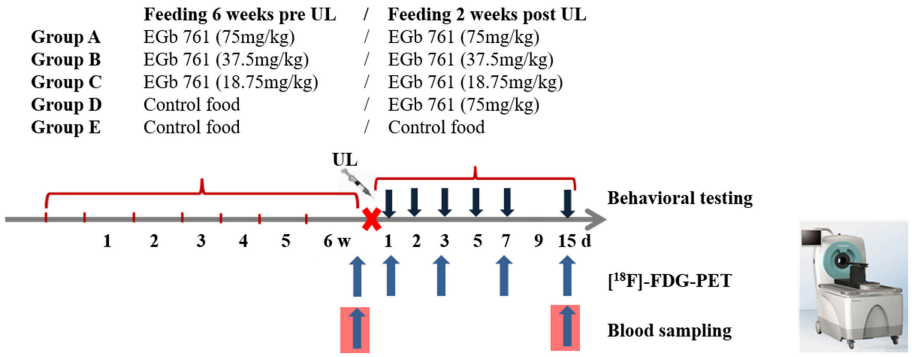

FIGURE 1 | Study design and time course of treatment, behavioral testing, and [^{18}F]-FDG-μPET-scanning. Groups of 8 rats were treated with EGb 761 food at a dose of 75 mg/kg (group A), 37.5 mg/kg (group B), or 18.75 mg/kg body weight (group C) 6 weeks prior and 15 days post UL. Another group of 8 rats was treated with control food prior and EGb 761 food (75 mg/kg body weight) for 15 days post UL (group D). Finally, a group received control food throughout (group E). Clinical scoring for vestibular imbalance and automated analysis of locomotor and spatial exploration behavior was performed on days 1, 2, 3, 5, 7, and 15 post UL. Cerebral glucose metabolism was depicted by serial [^{18}F]-FDG-μPET at baseline and days 1, 3, 7, and 15 post UL. Blood samples were drawn before UL and 15 days post UL. UL, unilateral labyrinthectomy; [^{18}F]-FDG-PET, [^{18}F]-Fluorodeoxyglucose-positron-emission tomography; w, weeks; d, days.

Chemical Unilateral Labyrinthectomy

Chemical unilateral labyrinthectomy was performed as described earlier (9, 21–23). Animals were anesthetized with 1.5% isoflurane in O_2 delivered up to 1.2 l/min O_2 via a mask. For surgical analgesia 1.5 mg/kg meloxicam was injected s.c. before and 3 days after surgery. An additional 5 ml saline was injected s.c. as a bolus. After local anesthesia with 1% bupivacaine hydrochloride, a left paramedian incision was made to expose the lamboidal ridge and the external ear canal. The external ear canal was opened just anterior to the exit point of the facial nerve. With a 26-gauge needle the tympanic membrane was perforated caudally to the hammer shaft, and about 0.150 ml of a 20% bupivacaine solution was instilled into the tympanic cavity. After about 2 min the bupivacaine solution was aspirated and instilled slowly again (three repetitions in total). After the local anesthesia was instilled, the same procedure was followed to instill 0.150 ml of a 10% solution of p-arsanilic acid, which irreversibly desensitized the primary sensory cells of the inner ear (23). After the last thorough aspiration, the wound was closed by skin suture and for preventive antibiosis 2 mg/kg marbofloxacin was injected s.c. for 3 days.

Criteria for Exclusion

Animals were excluded from the study if the following symptoms were observed:

- loss of body weight equal to more than 20% of the pre-treatment value
- ulcer of the cornea, which could occur due to an inadvertent lesion of the facial nerve during UL
- bleeding from the tympanic cavity, which could prevent the diffusion of bupivacaine or p-arsanilic acid into the inner ear
- abnormalities in behavioral scoring, i.e., convulsions, paresis, hemiataxia, etc.

Based on these criteria, four animals had to be excluded.

Clinical Scoring of Vestibular Asymmetry After UL

Behavioral symptoms of vestibular imbalance were scored by two experienced veterinarians blinded for the treatment condition for four components after unilateral vestibular ablation [based on (24)]: nystagmus, postural asymmetry, head roll tilt, and elevation tail test. Scores were depicted as mean values of two raters. Each component was given a score of up to 10:

- *Nystagmus* was observed visually. Intensity of spontaneous nystagmus was scored with 6–10 points, with 1 point for every 60 beats per minute (bpm). In the absence of spontaneous nystagmus at rest, the animal was touched slightly. If nystagmus was evoked, it was scored 1–5 points, with 1 point for every 60 bpm.
- *Postural deficits* were scored as follows: spontaneous barrel rolling—10 points; barrel rolling evoked by light touch or air-puff—9 points; recumbent position on lesion side without leg support—8 points; some ipsilesional leg support—7 points; moving around on one side or using ipsilesional legs for recumbent support—6 points; moving around with bilateral leg support—5 points; moving around with occasional falls to the ipsilesional side—4 points; moving around leaning toward the ipsilesional side—3 points; hardly noticeable asymmetry—2 points; postural asymmetry only noticeable when picked up—1 point.
- Spontaneous *head roll tilt* was scored by estimating the angle between the jaw plane and the horizontal, with 10 points given either for a 90° angle or if the animal rested recumbent on the lesion side or showed barrel-rolling toward that side. Seven points correlated to a 60° and 5 points to a 45° angle.
- Influence of perceptive somatosensory input to postural control during VC was examined by the *elevation tail test* (ETT). Animals were picked up from the ground at the radix of their tail and body rotation was scored by estimating in degrees, with 10 points given for more than 360°, 8

points for 180–360°, 6 points for <180° and 0 points for no relevant rotation.

Instrumental Locomotor Analysis

Testing of locomotor behavior was performed in the open field using automated video tracking (EthoVision System, Noldus, Netherlands). Animals were allowed to move freely in the rectangular open field (side length 70 cm) over 10 min. Position of nose, body center, and tail were automatically detected by video software. Mean locomotor velocity, cumulative duration of movement, changes in mobility state, frequency of rotation, and cumulative duration of stay in the center or at the edges of the maze were quantified. Locomotor velocity was taken as an overall estimate of mobility, the time in center zone as a measure of mobility and spatial exploration behavior. Heat maps of position at place were generated to indicate overall movement in open space.

Blood Sampling and Substrate Analysis

Blood samples were taken before and 15 days after UL in all animals (500 µl in mean). Blood sampling was restricted to these time points to avoid side effects of a regular haemodilution. The blood was collected in vials that were coated with lithium heparin and centrifuged immediately (10 min/2,000 rotations per min). The plasma was separated and mixed with 1% hydrogen chloride (10% of obtained plasma volume). The samples were stored at −20°C. Analysis for bilobalide and ginkgolide A and B was performed using liquid chromatography-electrospray ionization-tandem mass spectrometry as described earlier (25).

µPET Imaging

Anesthesia was induced with isoflurane (as described above) and a cannula was placed in a tail vein. Before the animals awakened from anesthesia, a [^{18}F]-FDG (50 MBq) bolus was injected (in 0.5 ml saline) and the animals were allowed to move freely until anesthesia was induced again with isoflurane (1.8%) for the µPET-scan. The scan was started 30 min after [^{18}F]-FDG injection. Animals were positioned in the Siemens Inveon PET scanner (Siemens Healthineers, Erlangen, Germany) and were kept warm with a heating pad. In order to avoid head movement, the head position was fixed using a custom-made head-holder. A 30-min-long emission recording was initiated followed by a 7 min transmission scan using a rotating [^{57}Co] point source. Upon recovery from anesthesia the rats were returned to their home cages.

Image Processing and Statistical Analysis

Emission recordings were reconstructed with iterative reconstruction employing the Ordered Subsets Expectation Maximization (OSEM-3D) algorithm which includes scatter and attenuation correction (Siemens Healthineers, Erlangen, Germany) and results in a final 128 × 128 × 159 matrix. For attenuation correction, the corresponding transmission measurements at the end of the emission scan were used. The voxel dimensions of the reconstructed images were 0.59 × 0.59 × 0.79 mm^3. [^{18}F]-FDG distribution in the reconstructed images was used as measure of regional cerebral glucose metabolism (rCGM). Data processing and statistical analysis were performed by means of custom-made protocols implemented in the statistical parametric mapping software SPM8 (Wellcome Department of Cognitive Neurology, Great Britain). Using automated algorithms, all individual [^{18}F]-FDG-µPET images were stereotactically normalized co-registered to a custom-made [^{18}F]-FDG template (average of 20 healthy rats), which was manually co-registered to a digital high-resolution cryosection-based atlas of rat brain. [^{18}F]-FDG data were normalized to the mean activity value in a whole-brain atlas region, in order to remove differences in the individual count levels. Images were compared in a voxel-wise manner between time points and conditions using SPM8. A correlation analysis of rCGM with individual plasma levels of ginkgolide A, ginkgolide B and bilobalide across the EGb 761 groups A, B and C was performed on day 1 and 3 (using plasma levels before UL) and day 15 post UL (with plasma levels from the same day).

Statistics

IBM SPSS Statistics (version 23.0; SPSS, Chicago, IL) was used for all statistical tests. Kolmogorov-Smirnov-Test indicated that none of the parameters (nystagmus, postural asymmetry, head roll tilt, elevated tail test, locomotor velocity, time in center-zone) was normally distributed. Statistical group comparison for behavioral scoring was performed by the non-parametric Kruskal-Wallis H test and *post hoc* testing with Bonferroni correction to analyse significant differences between time points and groups after UL. Blood levels for bilobalide, ginkgolides A and B at baseline and 15 days after UL were compared between time points and groups using the non-parametric Kruskal-Wallis H test and *post hoc* testing with Bonferroni correction. Pearson's coefficient of correlation was calculated between individual values for plasma levels of bilobalide, ginkgolides A and B (mean of baseline and post-UL values) and the slope of locomotor velocity, nystagmus and postural asymmetry over time, respectively. For each rat the average change of locomotor velocity and postural asymmetry per day was computed by the slope of the linear function starting on day 2 and ending at day 15 post UL.

RESULTS

High-Dose EGb 761 Improves Vestibular Imbalance, Locomotor and Exploratory Behavior After UL

After UL, animals showed severe signs of vestibular imbalance including spontaneous nystagmus, postural asymmetry, head roll tilt and body turns on elevated tail rotation test. In all groups, nystagmus peaked at day 1 (Control group: 8.9; Control/EGb 761: 8.5; EGb 761/EGb 761 75 mg/kg: 7.6) and disappeared completely in the first 7 days post UL. However, for group comparison the Kruskal-Wallis H test showed a significant difference of nystagmus scores on day 2 ($\chi^2 = 14.2$, $p = 0.007$) and day 3 ($\chi^2 = 14.2$, $p = 0.007$). *Post hoc* tests indicated a decrease of nystagmus in the Control/EGb 761 group D vs. Control group E on day 2 ($z = 17.1$, $p = 0.023$) and the EGb 761/EGb 761 75

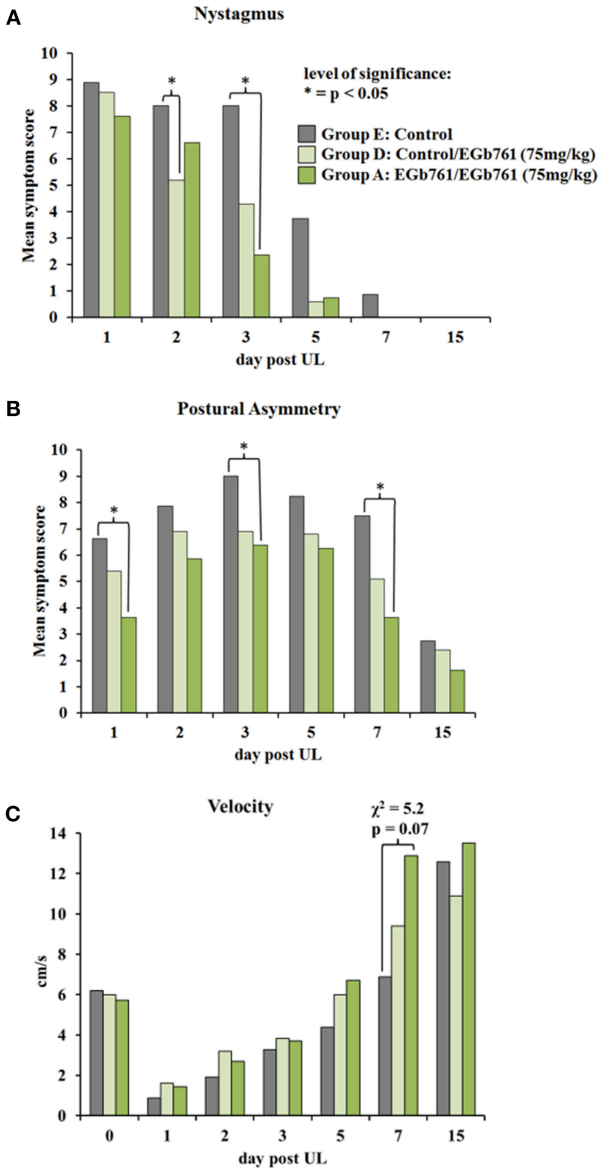

FIGURE 2 | Effects of EGb 761 on clinical scores of vestibular imbalance and locomotor velocity. **(A)** Nystagmus scores were significantly lower in the EGb 761/EGb 761 group (75 mg/kg) (group A) on day 3 and in the Control/EGb 761 group (75 mg/kg) (group D) on day 2 post UL compared to Controls (group E). **(B)** In the EGb 761/EGb 761 75 mg/kg group A postural asymmetry scores were significantly lower on days 1, 3 and 7 post UL relative to the Control group. **(C)** The Kruskal-Wallis H test between groups A, D and E showed only some trend to a different locomotor velocity on day 7 ($\chi^2 = 5.2$, $p = 0.07$). Solid lines and asterisk indicates a level of significance of $p < 0.05$ in Kruskal-Wallis H *post hoc* test.

mg/kg (group A) relative to the Control group E on day 3 ($z = 21.4$, $p = 0.003$). Nystagmus scores in the EGb 761/EGb 761 (group A) and Control/EGb 761 (group D) were not statistically different on all days (**Figure 2A**). Postural asymmetry increased in all groups within the first 3 days due to delayed toxicity effects of p-arsanilic acid. In all groups, the postural asymmetry scores decreased significantly from day 3 until day 15 post UL (Control group E: peak mean score on day 3: 9.0 vs. mean score on day 15: 2.8, $p = 0.003$; EGb 761/EGb 761 75 mg/kg (group A): peak mean score on day 3: 6.3 vs. mean score on day 15: 1.6, $p = 0.002$; Control/EGb 761 (group D): peak mean score on day 3: 7.0 vs. mean score on day 15: 2.4, $p < 0.001$). Intergroup comparison showed a significant difference of postural asymmetry scores between groups on day 1 ($\chi^2 = 16.9$, $p = 0.002$), day 3 ($\chi^2 = 15.4$, $p = 0.004$), and day 7 post UL ($\chi^2 = 12.9$, $p = 0.012$). *Post hoc* tests with Bonferroni correction revealed a significant decrease of postural asymmetry scores in the EGb 761/EGb 761 (group A) relative to the Control group E on day 1 ($z = 19.6$, $p = 0.002$), day 3 ($z = 20.0$, $p = 0.009$) and day 7 ($z = 19.25$, $p = 0.015$) and a significant reduction of scores for the Control/EGb 761 group D vs. the Control group E on day 3 post UL ($z = 15.8$, $p = 0.05$) (**Figure 2B**). The course of postural compensation accelerated by about 7 days in the EGb 761/EGb 761 group A. Head roll tilt persisted until day 15 post UL in all groups. Kruskal-Wallis H test showed no significant difference between groups at any time point, except a tendency on day 3 ($\chi^2 = 9.0$, $p = 0.061$). Head roll tilt scores on day 3 were lower in the EGb 761/EGb 761 group A (9.1 ± 0.7) and in the Control/EGb 761 group D (9.2 ± 0.6) compared to the Control group E (10.0 ± 0.0). The elevated tail rotation test also persisted to be pathological with mean scores above 7 until day 15 post UL in all groups. Scores in the EGb 761/EGb 761 group A and in the Control/EGb 761 group D were not statistically different from the Control group E in the Kruskal-Wallis H test for the different time points (data not shown).

After UL, mean locomotor velocity and cumulative duration of movement decreased in the Control, EGb761/EGb 761 (75 mg/kg), and Control/EGb761 (75 mg/kg) group (groups E, A, D) as compared to baseline. Over time both parameters increased in all groups significantly and were above baseline level after day 7 post UL. The Kruskal-Wallis H test between groups A, D and E showed only some trend to a different locomotor velocity on day 7 ($\chi^2 = 5.2$, $p = 0.07$). Mean locomotor velocity in the EGb 761/EGb 761 group A was more than double as high than the Control group E (13.9 ± 2.8 cm/s vs. 6.8 ± 1.5 cm/s) and higher than the Control/EGb 761 group D (9.4 ± 2.2 cm/s) (**Figure 2C**).

Analysis of spatial exploration patterns in the open field indicated that on days 1, 2, and 3 after UL rats in all groups stayed mostly at the border zone. After day 3 post UL, the EGb 761/EGb 761 75 mg/kg (group A) showed a statistically increased exploration in the central zone of the open field (**Figure 3A**). Cumulative time of stay in the central zone was significantly different between groups A, D and E on day 7 post UL ($\chi^2 = 16.6$, $p = 0.002$). *Post hoc* test revealed a higher duration of in center stay for the EGb 761/EGb 761 75mg/kg (group A) vs. the Control group ($z = 19.62$, $p = 0.014$) (**Figure 3B**).

Dose-Dependency of EGb 761 Effects on Vestibular Imbalance and Locomotor Velocity

Dose-response experiments in groups treated with EGb 761 doses of 75 mg/kg (group A), 37.5 mg/kg (group B), 18.75 mg/kg (group

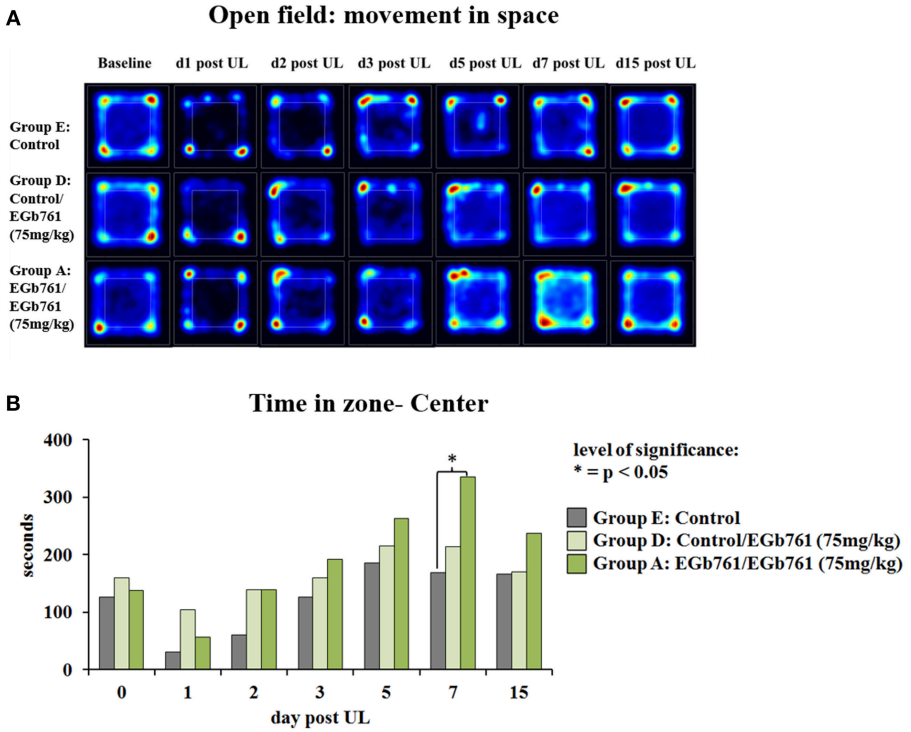

FIGURE 3 | Effects of EGb 761 on spatial exploration behavior in the open field. **(A)** Analysis of spatial exploration patterns in the open field indicated that on days 1, 2, and 3 after UL rats in all groups stayed mostly at the border zone. After day 3 post UL, the EGb 761/EGb 761 75 mg/kg group A showed an increased exploration in the central zone of the open field. Heatmaps indicate the cumulative time at place (blue to red scale increasing duration). **(B)** Cumulative time in the central zone was significantly higher on day 7 post UL in the EGb 761/EGB 761 75 mg/kg group A as compared to Controls group E. Asterisk indicates a level of significance in Kruskal-Wallis *post hoc* test of $p < 0.05$; d, day; UL, unilateral labyrinthectomy.

C), or Control food (group E) 6 weeks prior and 15 days post UL showed the following results: For nystagmus scores Kruskal-Wallis H test indicated significant differences between groups on day 1 ($\chi^2 = 13.3$, $p = 0.01$), day 3 ($\chi^2 = 14.2$, $p = 0.007$), and day 5 ($\chi^2 = 9.8$, $p = 0.043$). Nystagmus scores were significantly lower in the EGb 761/EGb 761 75 mg/kg (group A) vs. 37.5 mg/kg (group B) ($z = 19.4$, $p = 0.01$), as well as 18.75 mg/kg (group C) ($z = 16.6$, $p = 0.047$) on day 1 only, whereas there were no significant differences between the treatment groups A, B and C at later time points (**Figure 4A**). Postural asymmetry scores were significantly different between groups on day 1 ($\chi^2 = 16.9$, $p = 0.002$), day 2 ($\chi^2 = 11.1$, $p = 0.025$), day 3 ($\chi^2 = 15.4$, $p = 0.004$), day 5 ($\chi^2 = 12.2$, $p = 0.016$), and day 7 ($\chi^2 = 12.9$, $p = 0.012$). Postural asymmetry scores were lower in the EGb 761/EGb 761 75 mg/kg (group A) vs. the 18.75 mg/kg (group C) ($z = 19.6$, $p = 0.011$) and the Control group E ($z = 22.5$, $p = 0.002$) on day 1. While the postural asymmetry scores for treatment groups A, B and C vs. Control group E were lower on days 2, 3, 5, and 7, with some comparisons reaching significance (**Figure 4B**), again there were no significant differences between the EGb 761 groups at later time points. There were no significant group differences for head roll tilt or elevated tail rotation scores on any time point. Open field testing indicated a significant difference in velocity ($\chi^2 = 9.9$, $p = 0.042$) and moving duration between group ($\chi^2 = 10.8$, $p = 0.03$) only on day 15 post UL. *Post hoc* testing revealed that the EGb 761/ EGb 761 high dose group A had significantly increased locomotor velocity ($z = 17.6$, $p = 0.04$) and moving duration ($z = 19.1$, $p = 0.018$) compared to the low dose group C (**Figure 4C**). Duration of stay in the open field central zone was significantly different between groups on day 5 ($\chi^2 = 15.1$, $p = 0.005$) and day 7 post UL ($\chi^2 = 16.2$, $p = 0.002$). In *post hoc* analysis on day 5 ($z = 21.2$, $p = 0.005$) and day 7 ($z = 21.1$, $p = 0.002$) the EGb 761/EGb 761 75 mg/kg (group A) stayed longer in the central zone compared to the 18.75 mg/kg (group C) (data not shown).

Blood Levels of Bilobalide, Ginkgolides A and B Correlate With Behavioral Parameters

Plasma levels of the terpene lactones bilobalide and ginkgolides A and B were as follows: prior to UL, Kruskal-Wallis H test revealed a significant difference for bilobalide ($\chi^2 = 38.0$, $p < 0.001$), ginkgolide A ($\chi^2 = 38.7$, $p < 0.001$), and ginkgolide B plasma levels ($\chi^2 = 30.6$, $p < 0.001$). *Post hoc* analysis showed significantly higher plasma levels for bilobalide and ginkgolide A in the EGb 761/EGb 761 75 mg/kg (group A) and 37.5 mg/kg (group B) compared to the Control group E and the Control/ EGb 761 group D, respectively. Ginkgolide B levels additionally were higher in the EGb 761/EGb 761 groups A compared to group C.

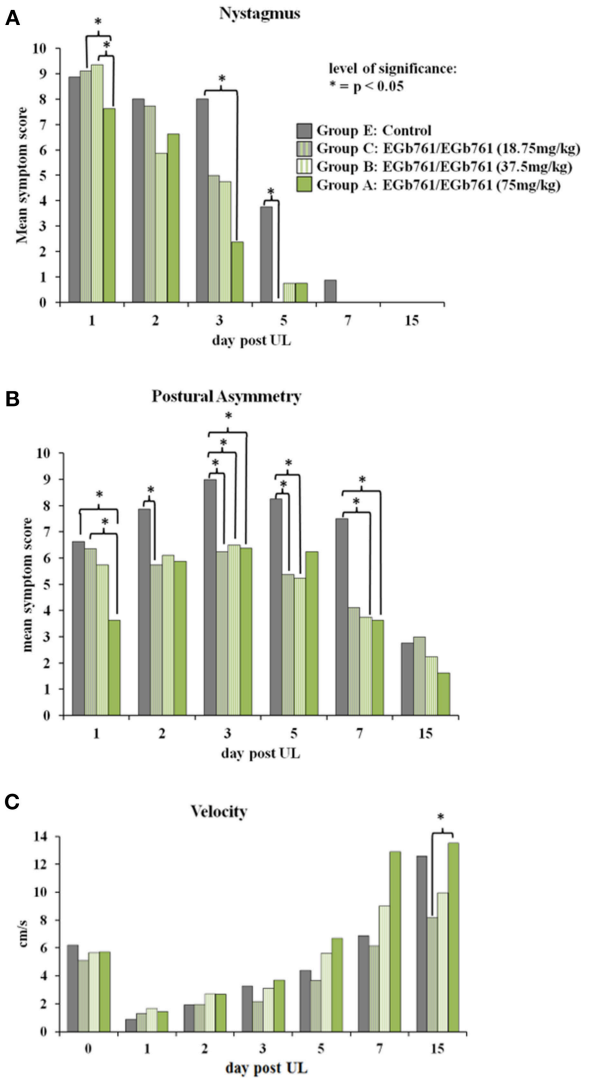

FIGURE 4 | Dose-dependency of EGb 761 on behavioral scores of vestibular imbalance and locomotor velocity. **(A)** Nystagmus scores were significantly lower on day 1 in the EGb 761/EGb 761 75 mg/kg group A compared to groups B and C and on day 3 in the EGb 761 group A compared to Controls. The EGb 761/EGb 761 18.75 mg/kg group C had lower nystagmus scores than Controls on day 5 post UL. **(B)** Postural asymmetry scores were lower in the EGb 761/EGb 761 75 mg/kg group A on days 1, 3, and 7, in the EGb 761/EGb 761 37.5 mg/kg group B on days 3, 5 and 7 and in the EGb 761/EGb 761 18.75 mg/kg group C on days 2, 3, and 5 post UL relative to Controls. Group A had lower nystagmus scores on day 1 post UL compared to group C. **(C)** Open field testing indicated a significant increase in locomotor velocity on day 15 post UL in the EGb 761/EGb 761 75 mg/kg group A compared to the 18.75 mg/kg group C. Asterisk indicates a level of significance in Kruskal-Wallis *post hoc* test of $p < 0.05$.

On day 15 post UL, bilobalide ($\chi^2 = 34.7$, $p < 0.001$), ginkgolide A ($\chi^2 = 35.7$, $p < 0.001$), and ginkgolide B ($\chi^2 = 30.6$, $p < 0.001$) were significantly different between groups. Bilobalide levels were higher for the EGb 761/EGb 761 group A ($z = 31.9$, $p < 0.001$) and B ($z = 17.1$, $p = 0.04$), but not C, and the Control/EGb 761 group D vs. the Control group E ($z = 24.4$, $p < 0.001$). Additionally, higher bilobalide levels were found in EGb 761/EGb 761 group A vs. group C ($z = 22.9$, $p = 0.002$). For ginkgolide A, plasma levels in the EGb 761/EGb 761 group A ($z = 27.1$, $p < 0.001$) and Control/EGb 761 group D ($z = 29.1$, $p < 0.001$) were significantly higher than in Controls and the EGb 761/EGb 761 group C ($z = 18.5$, $p = 0.027$; $z = 20.4$, $p = 0.003$). Finally, ginkgolide B plasma levels were higher in the EGb 761/EGb 761 group A ($z = 27.6$, $p < 0.001$) and Control/EGb 761 group D ($z = 21.2$, $p = 0.001$) vs. the Control group E, as well as relative to EGb 761/EGb 761 group C ($z = 24.5$, $p < 0.001$; $z = 18.1$, $p = 0.009$). Levels in group A were significantly higher than in group B ($z = 20.0$, $p = 0.008$) (**Figure 5A**).

Correlations of plasma levels for bilobalide, ginkgolide A and B with the slope of locomotor velocity, nystagmus, or postural asymmetry over time revealed the following results: Locomotor velocity after UL moderately, but significantly increased over time with higher plasma levels of ginkgolide A ($R = 0.47$, $p = 0.0062$), ginkgolide B ($R = 0.46$, $p = 0.0068$), and bilobalide ($R = 0.35$, $p = 0.047$) (**Figure 5B**). The slope of postural compensation over time showed some mild but not significant correlation with plasma levels of ginkgolide A and B ($R = -0.25$) as well as bilobalide ($R = -0.30$). Nystagmus compensation did not correlate to plasma levels of terpene lactones.

Dose-Dependent Effects of EGb 761 on Regional Cerebral Glucose Metabolism After UL

Correlation analysis of increases and decreases of regional cerebral glucose metabolism (rCGM) to the individual plasma levels of ginkgolide A, B and bilobalide on days 1, 3, and 15 post UL in all animals of the EGb 761 75, 37.5, and 18.75 mg/kg groups A, B, and C revealed the following patterns: On day 1, rCGM decreased with higher ginkgolide A, ginkgolide B, and bilobalide levels, respectively, in the vestibular nuclei, cerebellum and inferior colliculi on both sides and right temporoparietal cortex. An rCGM increase with plasma levels was found in the hippocampus (lateral C2/3 region bilaterally). On day 3, a decrease of rCGM appeared in the vestibular nuclei, the cerebellum and right temporoparietal cortex and an increase in the hippocampus bilaterally with higher plasma levels of ginkgolides and bilobalide. On day 15, rCGM relatively decreased with increasing plasma levels of ginkgolide A, B and bilobalide between the vestibular nuclei (commissural system), in the right inferior colliculus and right amydala. rCGM increased in the lateral hippocampus and thalamus with higher levels of ginkgolide A, ginkgolide B and bilobalide on this day ($p < 0.005$, uncorrected) (**Figure 6**).

Comparison of the EGb 761/EGb 761 75, 37.5, and 18.75 mg/kg groups (groups A, B, and C) to the Control group (group E) revealed the following rCGM decreases and increases ($p < 0.005$, uncorrected): In the EGb 761/EGb 761 75 mg/kg (group A), rCGM was significantly decreased in the cerebellum on day 1 (paraflocculus and lobulus simplex), day 3 (nodulus), and day 15 (right vermis) post UL compared to the Control group E. In the EGb 761/EGb 761 37.5 mg/kg (group B), rCGM was significantly reduced in the vestibular nuclei and cerebellum

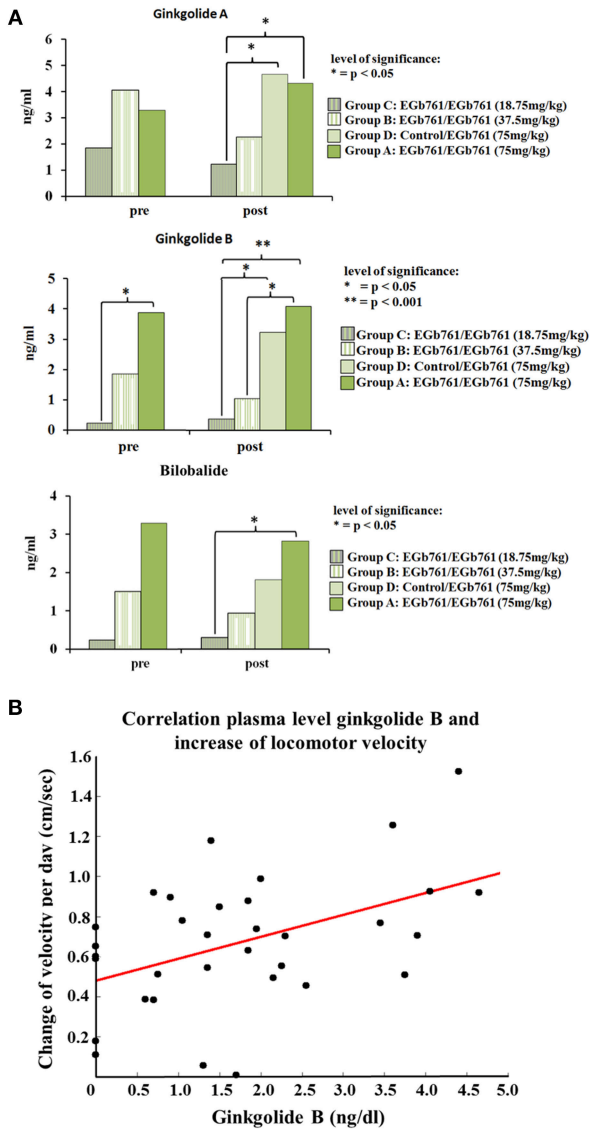

FIGURE 5 | Plasma levels of EGb 761 substrates and correlation to behavioral scores. **(A)** Before UL, plasma levels of ginkgolide A and bilobalide were significantly higher in the EGb 761/EGb 761 group A and B compared to Controls. Ginkgolide B levels were higher in the group A compared to group C. Fifteen days post UL, ginkgolide A and B levels were significantly higher in the EGb 761/EGb 761 75 mg/kg group A and the Control/EGb 761 group D compared to the 18.75 mg/kg group C. Additionally, gingkolide B levels were higher in the EGb 761/EGb 761 75 mg/kg group A compared to the 37.5 mg/kg group B. Levels of bilobalide were significantly higher in the EGb 761/EGb 761 75 mg/kg group A compared to the group C. **(B)** Locomotor velocity after UL moderately but significantly increased over time with higher plasma levels of ginkgolide B ($R = 0.46$, $p = 0.0068$). Asterisk indicates a level of significance in Kruskal-Wallis *post hoc* test of $p < 0.05$.

on day 1 (paraflocculus bilaterally), cerebellum on day 7 (right paraflocculus), and day 15 post UL (right vermis) relative to Controls. In the EGb 761/EGb 761 18.75 mg/kg group C, rCGM was lower in the cerebellum (nodulus) on day 3 post UL compared to the Control group E (**Figure S1**, left side).

In the EGb 761/EGb 761 75 mg/kg (group A) a significant increase of rCGM appeared in the hippocampus (lateral CA2/3 region bilateral and fibria of the hippocampus right) on day 1 post UL, which decreased until day 3 (lateral CA2/3 region and fimbria of the hippocampus right) (compared to the Control group E, respectively). In the EGb 761/EGb 761 37.5 mg/kg (group B) there was no hippocampal activation over time compared to Controls. In the EGb 761/EGb 761 18.75 mg/kg (group C) a significant rCGM increase was only found in the left posterolateral thalamus on day 1 post UL compared to Controls. On days 3 and 7 post UL, there were no significant rCGM increases in this group. On day 15 post UL rCGM was increased in the right amygdaloid nucleus in the low-dose group (group C) compared to Controls (**Figure S1**, right side).

DISCUSSION

The major findings of this study were the following: (1) Oral application of *Ginkgo biloba* extract EGb 761 accelerates compensation of nystagmus and postural asymmetry and improves mobility after unilateral labyrinthectomy in the rat. (2) Plasma levels of ginkgolide A, ginkgolide B, and bilobalide correlate significantly with an increase in spontaneous locomotor velocity over time. (3) EGb 761 improves vestibular compensation also when started after onset of vestibular imbalance. (4) EGb 761 modulates cerebral glucose metabolism in the vestibular nuclei, cerebellar, thalamic, hippocampal, and temporoparietal networks dose-dependently after unilateral labyrinthectomy.

Differential and Dose-Dependent Effects of EGb 761 Extract on Behavioral Vestibular Compensation

The polyvalent *Ginkgo biloba* extract EGb 761 has been in clinical use for the treatment of vestibular disorders for decades (26–28). Previous animal experiments have reported improvement of symptoms after unilateral vestibular damage by EGb 761: In the rat model of chemical UL, EGb 761 application (50 mg/kg i.p. for 10 weeks) improved recovery of nystagmus and static postural symptoms (16). Similarly, Lacour et al. showed an acceleration of postural and locomotor balance recovery as well as earlier restoration of vestibulo-collic reflex after UL in the cat by intraperitoneal injection of 50 mg/kg EGb 761 over 30 days (17). In the guinea pig UL model, the EGb 761 component ginkgolide B improved compensation of spontaneous nystagmus at a dose of 25 mg/kg i.p., but not at higher doses (18). Schlatter et al. criticized these studies for the lack of either a control group with solution vehicle only or dose-response groups (29). In their experiments, i.p. application of EGb 761 at doses of 25, 50, and 100 mg/kg for 3 days after UL in the guinea pig failed to induce significant dose-dependent improvements of static vestibular symptoms as compared to vehicle application (29). The discrepancy of findings was attributed partly to differences in time course of application and effects of the vehicle. Furthermore, it was speculated that EGb 761 may have differential effects on compensation of

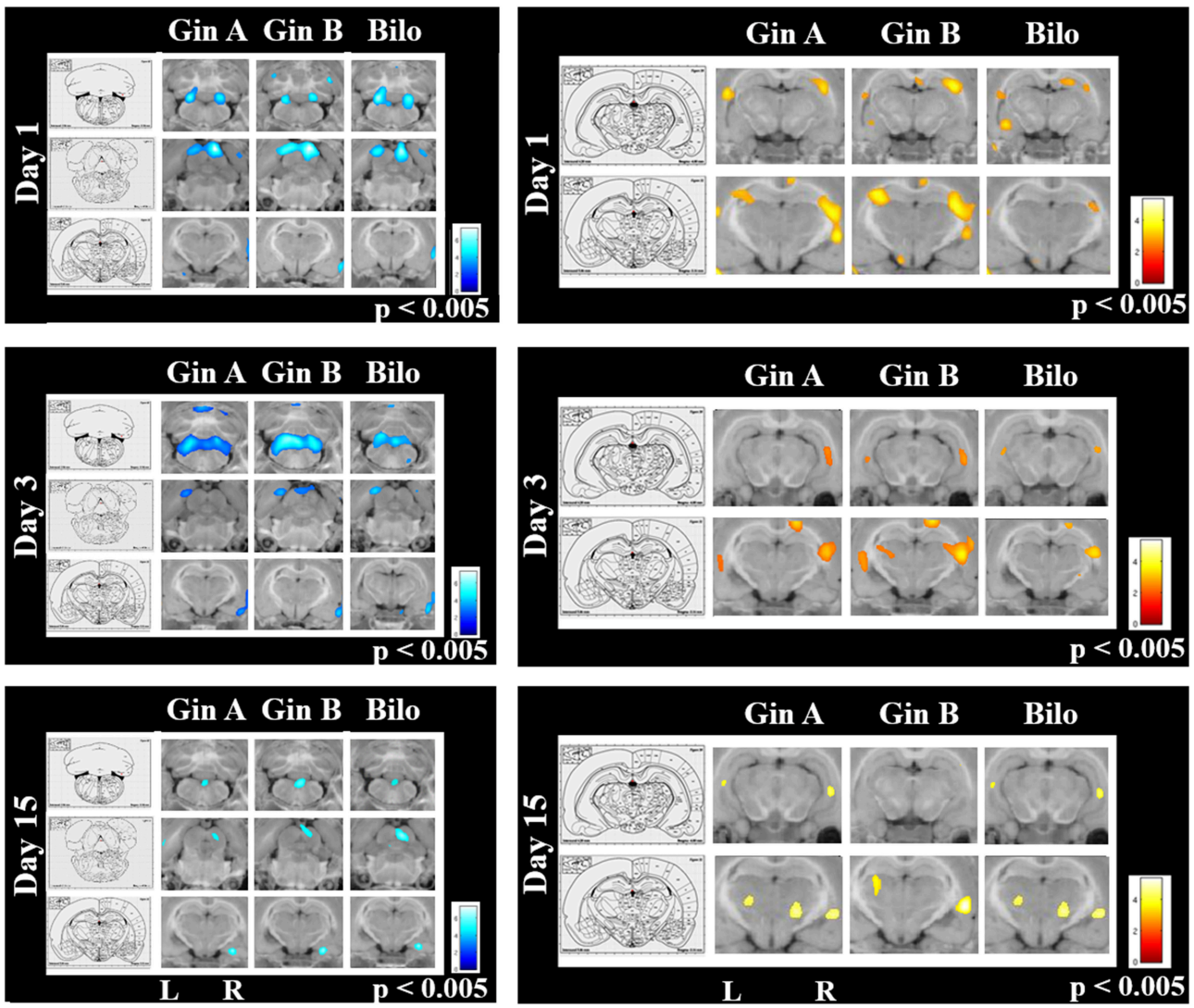

FIGURE 6 | Correlation analysis of regional cerebral glucose metabolism and plasma levels for ginkgolide A, ginkgolide B, and bilobalide on days 1, 3, and 15 post UL. On day 1, rCGM decreased with higher ginkgolide A, ginkgolide B, and bilobalide levels, respectively, in the vestibular nuclei, cerebellum and inferior colliculi on both sides and right temporoparietal cortex (upper row, left). An rCGM increase with plasma levels was found in the hippocampus (lateral C2/3 region bilaterally) (upper row, right). On day 3, a decrease of rCGM appeared in the vestibular nuclei, the cerebellum and right temporoparietal cortex and an increase in the hippocampus bilaterally with higher plasma levels of ginkgolides and bilobalide (middle row). On day 15, rCGM relatively decreased with increasing plasma levels of ginkgolide A, B, and bilobalide between the vestibular nuclei (commissural system), in the right inferior colliculus and right amydala (lower row, left). rCGM increased in the lateral hippocampus and thalamus with higher levels of ginkgolide A, ginkgolide B, and bilobalide on this day (lower row, right). Level of significance: $p < 0.005$. L, left, R, right; Gin A, ginkgolide A; Gin B, ginkgolide B; Bilo, bilobalide.

static and dynamic vestibular imbalance. To address these open questions, we conducted a study in the rat model, which used an alternative mode of application via the oral route, examined compensation of both static and dynamic signs of vestibular asymmetry, compared effects of dose and time course of EGb 761 administration, controlled plasma levels of the most important EGb 761 substrates, and correlated them to behavior and cerebral glucose metabolism. In our study, oral administration of EGb 761 improved compensation of static signs of vestibular asymmetry, such as nystagmus (vestibulo-ocular motor function) and postural imbalance (vestibulo-spinal function), as well as of dynamic function indicated by an increase in spontaneous mobility and locomotor velocity (**Figures 2**, **3**). The effects of EGb 761 on static compensation appeared earlier than the effects on dynamic compensation. The beneficial effects on recovery of nystagmus and postural asymmetry persisted, when EGb 761 administration started at the time of UL, suggesting immediate alongside more delayed effects of the extract on vestibular

compensation (**Figure 2**). Unspecific effects of a solution vehicle (as suggested for DMSO) or byproducts were unlikely, because EGb 761 was applied orally, and treatment and control groups differed in their time course of compensation (18). Effects of EGb 761 on vestibular compensation were partially dose-dependent in our study: decrease of nystagmus and postural asymmetry on day 1 post UL was significantly higher for the 75 mg/kg than the 18.75 mg/kg group. Locomotor velocity and mobility improved more in the high-dose EGb 761 group compared to the low-dose group on day 15 post UL. In contrast, postural asymmetry on day 3 post UL decreased to an equal extent in all EGb 761 groups and on day 7 post UL in the EGb 761 high- and middle-dose group, suggesting some saturation of the dose-response effect for this parameter.

EGb 761 Mechanisms of Action on Vestibular Compensation: Chemical Substrates and Cerebral Networks

The effects of EGb 761 on various mechanisms of neuroplasticity, including changes in cellular excitability, synaptic function, neurito- and neurogenesis, were reported previously (20, 30, 31). The specific mode of action of EGb 761 on central plasticity following vestibular lesions remains to be determined. The most important open questions are: which substrates of the polyvalent EGb 761 extract modulate vestibular compensation at which dose, which cerebral networks are involved, and which mechanisms of central plasticity (early vs. delayed) are affected by EGb 761. The EGb 761 extract contains two well-characterized biochemical components (terpene lactones and flavonoids). Flavonoids are abundantly present in herbs and vegetables, whereas terpene lactones (e.g., bilobalide, ginkgolide A and B) are components specific to *Ginkgo biloba* (30, 32). The special extract of *Ginkgo biloba* leaves–EGb 761–contains standardized amounts of flavonoids (22–27%) and terpene lactones (5–7%). In a previous study, ginkgolide B but not A effectively reduced nystagmus after UL in the guinea pig (18). Compensation of postural asymmetry or head roll tilt was not affected by either substrate. Another study suggested that the non-terpenic fraction of the polyvalent EGb 761 extract was pharmacologically active in compensation of locomotor dysequilibrium after UL in cats (33). However, non-specific effects of the solution vehicle could not be excluded (29). The correlation analysis of terpene lactone plasma levels and behavior in the current study showed differential effects of EGb 761 substrates: higher ginkgolide A and B and, to a lesser extent, bilobalide plasma levels significantly correlated with a faster increase in locomotor velocity over time after UL. Plasma levels of bilobalide more than gingkolide A and B tended to inversely correlate with the slope of postural compensation. In contrast to data reported by Maclennan and colleagues, no significant correlations were found between compensation of nystagmus and terpene lactones plasma levels. Based on our data, one can assume that EGb 761 components have pleiotrophic effects on static and dynamic vestibular compensation.

The questions remain, in which cerebral networks and by which mechanisms EGb 761 improves vestibular compensation after inner ear lesions. Overall, CNS uptake of EGb compounds ginkgolide A, B, and bilobalide is rapid after oral administration in the rat, whereas ginkgolide C does not penetrate the blood-brain barrier (15). About 60% of radiolabeled EGb 761 passes into the brain within 72 h after oral application (34). About 90% of EGb 761 substrates are distributed in the hippocampus, frontal cortex, striatum, and cerebellum (35). Previous experiments on the modes of action of EGb 761 in vestibular animal models mostly have focused on the vestibular nuclei. Yabe et al. showed a suppression of the horizontal vestibulo-ocular reflex gain in normal guinea pigs 2 h after i.p. injection of EGb 761 at a dose of 50 mg/kg (36). Ginkgolide B (25 mg/kg i.p. single dose) accelerated suppression of spontaneous nystagmus in a UL guinea pig model, suggesting action on the level of the vestibular nuclei (37). Functionally, it was hypothesized that EGb 761 may modulate neuronal excitability in the vestibular nuclei (36). Lacour et al. identified structural changes at the level of the vestibular nuclei induced by EGb 761 in UL cats, which consisted of a more rapid synaptic reoccupation in the deafferented medial vestibular nucleus (17). Another study reported an increase of protein synthesis on a brainstem level by EGb 761 (38). The time constant of the latter effects however exceeded the behavioral compensation of vestibular imbalance (17). These data therefore suggest that EGb 761 extract has immediate functional effects on vestibular asymmetry and delayed structural effects on consolidation of vestibular networks. In the current study, regional cerebral glucose metabolism decreased in the vestibular nuclei and cerebellum with higher plasma levels of ginkgolides and bilobalide on days 1 and 3 post UL, following the temporal dynamics of compensation of static vestibular functions. In accordance, a previous autoradiographic study in the rat also revealed a significant decrease of glucose consumption in the cerebellar cortex and pons following application of EGb 761 (50 mg/kg dose p.o. for 15 days) (39). One can only speculate whether the decreased glucose uptake in the vestibular nuclei reflects a regional reduction of neuronal activity or excitability by changes in membrane properties or neurotransmission. From a functional perspective, a reduced excitability in the vestibular nuclei on both sides would help to restore vestibular symmetry and thus would contribute to static vestibular compensation. The second significant effect of EGb 761 on cerebral glucose consumption was an increased uptake in the hippocampus in the high-dose group until day 7 post UL (**Figure 6**). The hippocampus is a well-known target for EGb 761 action and a hub of the cerebral vestibular networks (5, 20, 40). EGb 761-induced changes of hippocampal long-term potentiation, neurito- and neurogenesis are documented (20). The time course of glucose changes in the UL model would point toward a change in hippocampal neuronal activity rather than structural changes on network levels. Accordingly, spatial exploration behavior in the open field significantly differed in the EGb 761 (75 mg/kg) group and controls on days 3, 5, and 7 post UL. A longer duration of in-center stays would indicate reduced spatial anxiety and increased interest in spatial exploration. One cannot exclude the possibility that the altered hippocampal glucose consumption in the high-dose EGb 761 group was rather a consequence of improved overall mobility.

Translational Perspectives for the Use of EGb 761 in Vestibular Disorders

In pharmacologic research the translation of animal data into the clinical context can be limited by differences in the route, time course and dose of application, metabolism and neurobiology between species. In the current study, we chose oral EGb 761 administration and included a starting point for treatment after onset of vestibular imbalance to resemble the clinical situation of a patient with an acute unilateral vestibulopathy. Effective plasma levels for bilobalide, ginkgolide A and B in our high-dose EGb 761 group (75 mg/kg) were similar to previously reported values in healthy humans taking a maximal standard dose of approved *Ginkgo biloba* extract drugs (25). Indeed, controlled clinical studies have also reported benefits of EGb 761 on vestibular compensation: Haguenauer et al. described a significant improvement of subjective vertigo symptoms and quality of life in 70 patients with unilateral vestibulopathies after 3 months of EGb 761 treatment as compared to placebo (28). Other clinical trials showed an augmentation of exercise-induced postural recovery by EGb 761 vs. placebo administration in patients with vestibular disorders (41, 42). It therefore seems likely that the experimental effects of EGb 761 in vestibular animal models can, in principle, be translated to patients with vestibular disorders (19). Further controlled studies will have to be conducted in order to determine the optimal time course and dose of EGb 761 administration in patients with acute and chronic vestibulopathies.

EGb 761 induced changes of regional cerebral glucose metabolism in the vestibular nuclei, vestibulocerebellum, thalamus, hippocampus, and temporoparietal cortex after UL in the rat model. From a translational perspective, EGb 761 seems to target vestibular hubs, which are also found to be modulated in patients with acute unilateral vestibular syndromes: in acute vestibular neuritis, an increase of glucose metabolism was reported in the pontomesencephalic brainstem, posterolateral thalamus, parietoinsular vestibular cortex and hippocampus (43). In patients with Wallenberg syndrome, vestibulocerebellar activations were found during the acute stage (44). These regions show a striking overlap with the networks and hubs modulated by EGb 761 in the rat model of vestibular imbalance.

Limitations of the Study

The relatively short follow-up post UL may not be sufficient to pick up delayed effects of EGb 761 administration on vestibular compensation and plasticity. As the method of serial [^{18}F]-FDG-μPET imaging is concerned, the authors are aware that changes in glucose metabolism do not allow conclusions on molecular mechanisms underlying EGb 761 effects. Correlations of terpene lactone plasma levels with behavioral parameters of vestibular compensation may not be misinterpreted as a proof of causation. Plasma levels of flavonoids were not measured. A strict dose-dependency could not be proven for all read-out parameters tested. It was present for nystagmus and postural asymmetry only on day 1 post UL and for locomotor velocity on day 15 post UL. For the intermediate time points dose-response effects were less clear. Correlation of plasma levels of ginkgolides and bilobalide with cerebral glucose consumption, however, showed a clear dose-dependency for effects in the vestibular nuclei, cerebellum and hippocampus on day 1, 3, and 15 post UL.

Conclusions

The current study shows beneficial effects of the oral *Ginkgo biloba* extract EGb 761 application on compensation of static and dynamic vestibular function following inner ear damage. Improvement of nystagmus, postural asymmetry, and locomotor behavior indicates a modulation of vestibulo-ocular motor, vestibulo-spinal, and cortico-striatal networks. Changes in spatial exploration behavior suggest additional EGb 761 effects on vestibulo-hippocampal circuits. Terpene lactones like ginkgolide A and B as well as bilobalide probably account for some of the effects on mobility, whereas compensation of nystagmus and postural asymmetry may involve other pharmacologically active substrates of the polyvalent extract. This rat study supports the translational approach of using EGb 761 at higher dosages for medical acceleration of vestibular compensation in surgical or disease related acute vestibular loss. Serial imaging of cerebral glucose metabolism indicates a modulation of the vestibular nuclei, cerebellar, thalamic, hippocampal and temporoparietal networks by EGb 761 during vestibular compensation. The observed mechanisms might account for some of the EGb 761 benefits reported in controlled clinical trials in patients with vestibular disorders.

AUTHOR CONTRIBUTIONS

ML: acquisition of data, analysis and interpretation of data, statistical analysis; AG: analysis and interpretation of data, statistical analysis; EE, CB, and AK: acquisition of data, analysis and interpretation of data; RO: acquisition of data; EW, SZ, and PB: study concept and design, revising the manuscript; TB: interpretation of data, revising the manuscript; MD: study concept and design, analysis, and interpretation of data, revising the manuscript; AZ: drafting, revising the manuscript, study concept and design, acquisition of data, analysis and interpretation of data, statistical analysis.

FUNDING

The study was supported by the German Federal Ministry of Education and Research (BMBF) in the context of the foundation of the German Center for Vertigo and Balance Disorders (DSGZ) (grant number 01 EO 0901) and Dr. Willmar Schwabe GmbH.

ACKNOWLEDGMENTS

We thank Katie Göttlinger for copyediting of the manuscript.

SUPPLEMENTARY MATERIAL

The Supplementary Material for this article can be found online at: https://www.frontiersin.org/articles/10.3389/fneur.2019.00147/full#supplementary-material

Figure S1 | Sequential increases and decreases of the cerebral glucose metabolism in the EGb 761 treated groups relative to controls. In the EGb 761/EGb 761 75 mg/kg group rCGM was significantly decreased in the cerebellum on days 1, 3 and day 15 post UL as well as in the ventral intermediate thalamus on day 1 post UL compared to the Control group. In the EGb 761/EGb 761 37.5 mg/kg group B, rCGM was significantly reduced in the vestibular nuclei and cerebellum on day 1, 7, and 15 as well as in the ventrointermediate thalamus on days 1 and 3 post UL as compared to Controls. In the EGb 761/EGb 761 18.75 mg/kg group, rCGM was lower in the cerebellum on day 3 post UL compared to the Control group E. In the EGb 761/EGb 761 75 mg/kg group a significant increase of rCGM appeared in the hippocampus on day 1 post UL, which decreased until day 3 compared to the Control group, respectively. In the EGb 761/EGb 761 37.5 mg/kg group there was no hippocampal activation over time, but instead an rCGM increase in the left striatum on day 1, left thalamus and right striatum on day 3 post UL (compared to Controls). In the EGb 761/EGb 761 18.75 mg/kg group C a significant rCGM increase was only found in the left posterolateral thalamus on day 1 post UL compared to Controls. On day 15 post UL rCGM was increased in the right amygdaloid nucleus in the low-dose group compared to Controls. Level of significance: $p < 0.005$. L, left; R, right.

REFERENCES

1. Brandt T, Strupp M, Arbusow V, Dieringer N. Plasticity of the vestibular system: central compensation and sensory substitution for vestibular deficits. *Adv Neurol.* (1997) 73:297–309.
2. Cullen KE, Minor LB, Beraneck M, Sadeghi SG. Neural substrates underlying vestibular compensation: contribution of peripheral vs. central processing. *J Vestib Res.* (2009) 19:171–82. doi: 10.3233/VES-2009-0357
3. Dutia MB. Mechanisms of vestibular compensation: recent advances. *Curr Opin Otolaryngol Head Neck Surg.* (2010) 18:420–4. doi: 10.1097/MOO.0b013e32833de71f
4. Lacour M, Helmchen C, Vidal PP. Vestibular compensation: the neuro-otologist's best friend. *J Neurol.* (2016) 263(Suppl. 1):S54–64. doi: 10.1007/s00415-015-7903-4
5. Smith PF, Horii A, Russell N, Bilkey DK, Zheng Y, Liu P, et al. The effects of vestibular lesions on hippocampal function in rats. *Prog Neurobiol.* (2005) 75:391–405. doi: 10.1016/j.pneurobio.2005.04.004
6. Straka H, Vibert N, Vidal PP, Moore LE, Dutia MB. Intrinsic membrane properties of vertebrate vestibular neurons: function, development and plasticity. *Prog Neurobiol.* (2005) 76:349–92. doi: 10.1016/j.pneurobio.2005.10.002
7. Beraneck M, McKee JL, Aleisa M, Cullen KE. Asymmetric recovery in cerebellar-deficient mice following unilateral labyrinthectomy. *J Neurophysiol.* (2008) 100:945–58. doi: 10.1152/jn.90319.2008
8. Straka H, Zwergal A, Cullen KE. Vestibular animal models: contributions to understanding physiology and disease. *J Neurol.* (2016) (Suppl. 1):S10–23. doi: 10.1007/s00415-015-7909-y
9. Zwergal A, Schlichtiger J, Xiong G, Beck R, Günther L, Schniepp R, et al. Sequential [(18)F]FDG μPET whole-brain imaging of central vestibular compensation: a model of deafferentation-induced brain plasticity. *Brain Struct Funct.* (2016) 221:159–70. doi: 10.1007/s00429-014-0899-1
10. Zwergal A, Günther L, Brendel M, Beck R, Lindner S, Xiong G, et al. *In vivo* imaging of glial activation after unilateral labyrinthectomy in the rat: a [18F] GE180-PET study. *Front Neurol.* (2017) 8:665. doi: 10.3389/fneur.2017.00665
11. Beck R, Günther L, Xiong G, Potschka H, Böning G, Bartenstein P. et al. The mixed blessing of treating symptoms in acute vestibular failure–evidence from a 4-aminopyridine experiment. *Exp Neurol.* (2014) 261:638–45. doi: 10.1016/j.expneurol.2014.08.013
12. Günther L, Beck R, Xiong G, Potschka H, Jahn K, Bartenstein P. et al. N-acetyl-L-leucine accelerates vestibular compensation after unilateral labyrinthectomy by action in the cerebellum and thalamus. *PLoS ONE* (2015) 10:e0120891. doi: 10.1371/journal.pone.0120891
13. Chabbert C. Principles of vestibular pharmacotherapy. *Handb Clin Neurol.* (2016) 137:207–18. doi: 10.1016/B978-0-444-63437-5.00014-5
14. Strømgaard K, Nakanishi K. Chemistry and biology of terpene trilactones from *Ginkgo biloba*. *Angew Chem Int Ed Engl.* (2004) 43:1640–58. doi: 10.1002/anie.200300601
15. Ude C, Schubert-Zsilavecz M, Wurglics M. *Ginkgo biloba* extracts: a review of the pharmacokinetics of the active ingredients. *Clin Pharmacokinet.* (2013) 52:727–49. doi: 10.1007/s40262-013-0074-5
16. Denise P, Bustany A. The effect of extract of Gingko biloba (EGb 761) on central compensation of a total unilateral peripheral vestibular deficit in the rat. In: Lacour M, Toupet M, Denise P, Christen Y, editors. *Vestibular Compensation: Facts, Theories, and Clinical Perspectives.* Paris: Elsevier (1989). p. 201–8.
17. Lacour M, Ez-Zaher L, Raymond J. Plasticity mechanisms in vestibular compensation in the cat are improved by an extract of *Ginkgo biloba* (EGb 761). *Pharmacol Biochem Behav.* (1991) 40:367–79. doi: 10.1016/0091-3057(91)90568-M
18. Maclennan KM, Smith PF, Darlington CL. The effects of ginkgolide B (BN52021) on guinea pig vestibular nucleus neurons *in vitro*: importance of controlling for effects of dimethylsulphoxide (DMSO) vehicles. *Neurosci Res.* (1996) 26:395–9. doi: 10.1016/S0168-0102(96)01118-2
19. Hamann KF. Special ginkgo extract in cases of vertigo: a systematic review of randomised, double-blind, placebo controlled clinical examinations. *HNO* (2007) 55:258–63. doi: 10.1007/s00106-006-1440-5
20. Müller WE, Heiser J, Leuner K. Effects of the standardized *Ginkgo biloba* extract EGb 761® on neuroplasticity. *Int Psychogeriatr.* (2012) (Suppl. 1):S21–4. doi: 10.1017/S1041610212000592
21. Anniko M, Wersäll J. Experimentally (atoxyl) induced ampullar degeneration and damage to the maculae utriculi. *Acta Otolaryngol.* (1977) 83:429–40. doi: 10.3109/00016487709128868
22. Magnusson AK, Ulfendahl M, Tham R. Early compensation of vestibulo-oculomotor symptoms after unilateral vestibular loss in rats is related to GABA(B) receptor function. *Neuroscience* (2002) 111:625–34. doi: 10.1016/S0306-4522(01)00618-2
23. Vignaux G, Chabbert C, Gaboyard-Niay S, Travo C, Machado ML, Denise P, et al. Evaluation of the chemical model of vestibular lesions induced by arsanilate in rats. *Toxicol Appl Pharmacol.* (2012) 258:61–71. doi: 10.1016/j.taap.2011.10.008
24. Bergquist F, Ludwig M, Dutia MB. Role of the commissural inhibitory system in vestibular compensation in the rat. *J Physiol.* (2008) 586:4441–52. doi: 10.1113/jphysiol.2008.155291
25. Woelkart K, Feizlmayr E, Dittrich P, Beubler E, Pinl F, Suter A, et al. Pharmacokinetics of bilobalide, ginkgolide A and B after administration of three different *Ginkgo biloba* L,. preparations in humans. *Phytother Res.* (2010) 24:445–50. doi: 10.1002/ptr.3074
26. Guerrier Y, Basseres F, Artieres J. Le Tanakan® dans le traitement des vertiges. A propos de 26 observations. *Les Cahiers d'O.R.L.* (1978) 13:421–8.
27. Schwerdtfeger F. Elektronystagmographisch und klinisch dokumentierte Therapieerfahrungen mit rökan® bei Schwindelsymptomatik. *Therapiewoche* (1981) 31:8658–67.
28. Haguenauer JP, Cantenot F, Koskas H, Pierart H. Traitement des troubles de l'équlibre par l'extrait de *Ginkgo biloba*. *Presse Med.* (1986) 15:1569–72.
29. Schlatter M, Kerr DR, Smith PF, Darlington CL. Evidence that the ginkgo biloba extract, EGb 761, neither accelerates nor enhances the rapid compensation of the static symptoms of unilateral vestibular deafferentation in guinea pig. *J Vestib Res.* (1999) 9:111–8.
30. Maclennan KM, Darlington CL, Smith PF. The CNS effects of *Ginkgo biloba* extracts and ginkgolide B. *Prog Neurobiol.* (2002) 67:235–57. doi: 10.1016/S0301-0082(02)00015-1
31. Kiewert C, Kumar V, Hildmann O, Rueda M, Hartmann J, Naik RS, et al. Role of GABAergic antagonism in the neuroprotective effects of bilobalide. *Brain Res.* (2007) 1128:70–8. doi: 10.1016/j.brainres.2006.10.042

32. Islam MT, da Silva CB, de Alencar MV, Paz MF, Almeida FR, de Carvalho Melo-Cavalcante AA. Diterpenes: advances in neurobiological drug research. *Phytother Res.* (2016) 30:915–28. doi: 10.1002/ptr.5609
33. Tighilet B, Lacour M. Pharmacological activity of the *Ginkgo biloba* extract (EGb 761) on equilibrium function recovery in the unilateral vestibular neurectomized cat. *J Vestib Res.* (1995) 5:187–200. doi: 10.1016/0957-4271(94)00030-6
34. Moreau JP, Eck CR, McCabe J, Skinner S. Absorption, distribution, and excretion of tagged *Ginkgo biloba* leaf extract in the rat. In: Fünfgeld EW, editor. *Rökan*. Berlin; Heidelberg: Springer (1998). p. 37–45.
35. Rangel-Ordóñez L, Nöldner M, Schubert-Zsilavecz M, Wurglics M. Plasma levels and distribution of flavonoids in rat brain after single and repeated doses of standardized *Ginkgo biloba* extract EGb 761®. *Planta Med.* (2010) 76:1683–90. doi: 10.1055/s-0030-1249962
36. Yabe T, Chat M, Malherbe E, Vidal PP. Effects of *Ginkgo biloba* extract (EGb 761) on the guinea pig vestibular system. *Pharmacol Biochem Beh.* (1992) 42:595–604. doi: 10.1016/0091-3057(92)90004-Y
37. Maclennan K, Smith PF, Darlington CL. Ginkgolide B accelerates vestibular compensation of spontaneous ocular nystagmus in guinea pig following unilateral labyrinthectomy. *Exp Neurol.* (1995) 131:273–8.
38. Bustany P, Denise P, Pottier M, Moulin M. Brain protein synthesis after unilateral labyrinthectomy: natural one month and EGb 761® treatment effect. In: Christen Y, Costentin J, Lacour M, editors. *Effects of Ginkgo biloba Extract on the Central Nervous System*. Paris: Elsevier (1992). p 57–74.
39. Duverger D, DeFeudis FV, Drieu K. Effects of repeated treatments with an extract of *Ginkgo biloba* (EGb 761) on cerebral glucose utilization in the rat: an autoradiographic study. *Gen Pharmacol.* (1995) 26:1375–83. doi: 10.1016/0306-3623(94)00309-B
40. Brandt T, Schautzer F, Hamilton DA, Brüning R, Markowitsch HJ, Kalla R. et al. Vestibular loss causes hippocampal atrophy and impaired spatial memory in humans. *Brain* (2005) 128:2732–41. doi: 10.1093/brain/awh617
41. Hamann KF. Physikalische therapie des vestibulären schwindels in verbindung mit ginkgo-biloba-extrakt. *Therapiewoche* (1985) 35:4586–90.
42. Orendorz-Fraczkowska K, Pospiech L, Gawron W. Results of combined treatment of vestibular receptor impairment with physical therapy and *Ginkgo biloba* extract (EGb 761®). *Otolaryngol Pol.* (2002) 65:83–8.
43. Bense S, Bartenstein P, Lochmann M, Schlindwein P, Brandt T, Dieterich M. Metabolic changes in vestibular and visual cortices in acute vestibular neuritis. *Ann Neurol.* (2004) 56:624–30. doi: 10.1002/ana.20244
44. Becker-Bense S, Buchholz HG, Best C, Schreckenberger M, Bartenstein P, Dieterich M. Vestibular compensation in acute unilateral medullary infarction: FDG-PET study. *Neurology* (2013) 80:1103–9. doi: 10.1212/WNL.0b013e31828868a6

Conflict of Interest Statement: AZ received speaker's honoria from Dr. Willmar Schwabe GmbH.

The remaining authors declare that the research was conducted in the absence of any commercial or financial relationships that could be construed as a potential conflict of interest.

frontiers in Neurology

ORIGINAL RESEARCH
published: 05 April 2019
doi: 10.3389/fneur.2019.00303

Endotype-Phenotype Patterns in Meniere's Disease Based on Gadolinium-Enhanced MRI of the Vestibular Aqueduct

*David Bächinger[1,2], Catrin Brühlmann[2], Tim Honegger[2], Eleftheria Michalopoulou[3], Arianne Monge Naldi[4], Vincent G. Wettstein[1,2], Stefanie Muff[3], Bernhard Schuknecht[5] and Andreas H. Eckhard[1,2]**

[1] Department of Otorhinolaryngology, Head and Neck Surgery, University Hospital Zurich, Zurich, Switzerland, [2] University of Zurich, Zurich, Switzerland, [3] Department of Biostatistics, Institute for Epidemiology, Biostatistics, and Prevention, University of Zurich, Zurich, Switzerland, [4] Department of Otorhinolaryngology, University Children's Hospital Zurich, Zurich, Switzerland, [5] Medical Radiological Institute (MRI), Zurich, Switzerland

OPEN ACCESS

Edited by:
Jose Antonio Lopez-Escamez, Junta de Andalucía de Genómica e Investigación Oncológica (GENYO), Spain

Reviewed by:
Eduardo Martin-Sanz, Hospital de Getafe, Spain
Sung Huhn Kim, Yonsei University, South Korea

***Correspondence:**
Andreas H. Eckhard
andreasheinrich.eckhard@usz.ch

Specialty section:
This article was submitted to Neuro-Otology, a section of the journal Frontiers in Neurology

Received: *22 January 2019*
Accepted: *11 March 2019*
Published: *05 April 2019*

Citation:
Bächinger D, Brühlmann C, Honegger T, Michalopoulou E, Monge Naldi A, Wettstein VG, Muff S, Schuknecht B and Eckhard AH (2019) Endotype-Phenotype Patterns in Meniere's Disease Based on Gadolinium-Enhanced MRI of the Vestibular Aqueduct. Front. Neurol. 10:303. doi: 10.3389/fneur.2019.00303

Two histopathological subtypes of Meniere's disease (MD) were recently described in a human post-mortem pathology study. The first subtype demonstrated a degenerating distal endolymphatic sac (ES) in the affected inner ear (subtype MD-dg); the second subtype (MD-hp) demonstrated an ES that was developmentally hypoplastic. The two subtypes were associated with different clinical disease features (phenotypes), suggesting that distinct endotype-phenotype patterns exist among MD patients. Therefore, clinical endotyping based on ES pathology may reveal clinically meaningful MD patient subgroups. Here, we retrospectively determined the ES pathologies of clinical MD patients ($n = 72$) who underwent intravenous delayed gadolinium-enhanced inner ear magnetic resonance imaging using previously established indirect radiographic markers for both ES pathologies. Phenotypic subgroup differences were evidenced; for example, the MD-dg group presented a higher average of vertigo attacks (ratio of vertigo patterns daily/weekly/other vs. monthly, MD-dg: 6.87: 1; MD-hp: 1.43: 1; $p = 0.048$) and more severely reduced vestibular function upon caloric testing (average caloric asymmetry ratio, MD-dg: 30.2% ± 30.4%; MD-hp: 13.5% ± 15.2%; $p = 0.009$), while the MD-hp group presented a predominantly male sex ratio (MD-hp: 0.06:1 [f/m]; MD-dg: 1.2:1 [f/m]; $p = 0.0004$), higher frequencies of bilateral clinical affection (MD-hp: 29.4%; MD-dg: 5.5%; $p = 0.015$), a positive family history for hearing loss/vertigo/MD (MD-hp: 41.2%; MD-dg: 15.7%; $p = 0.028$), and radiographic signs of concomitant temporal bone abnormalities, i.e., semicircular canal dehiscence (MD-hp: 29.4%; MD-dg: 3.6%; $p = 0.007$). In conclusion, this new endotyping approach may potentially improve the diagnosis, prognosis and clinical decision-making for individual MD patients.

Keywords: endolymphatic sac, patient subgroups, phenotype, degeneration, hypoplasia

INTRODUCTION

A major challenge in diagnosing and managing patients with Meniere's disease (MD) is its heterogeneous clinical presentation (i.e., phenotypic differences among patients) (1). For example, vestibular and auditory symptoms may occur together or in a temporally independent manner, in varying frequency patterns (e.g., daily, monthly, episodically), and with some symptoms predominating over others (e.g., more pronounced vestibular than auditory symptoms) (2, 3). Symptom attacks may occur in response to identifiable triggers [e.g., high sodium intake, caffeine, stress, reviewed in (1, 4)] or in random patterns. In many cases, the disease remains unilateral (one inner ear clinically affected), whereas progression to bilateral disease is observed in ∼40% of cases (2, 5). In the long-term, the degree of permanent hearing loss and vestibular hypofunction can remain mild to moderate or progress to severe levels (2). Identifying distinct phenotypic patterns among MD patients would potentially enable clinicians to predict clinical features or the disease course in individual MD patients.

In a recent post-mortem histopathology study on inner ear tissues from MD patients (6), we identified two histopathological subtypes of the disease: (i) epithelial degeneration of the endolymphatic sac (ES) and (ii) organ hypoplasia of the ES. Both ES pathologies result in loss of the normal ES epithelium and its ion transport functions. Loss of ES function presumably underlies the endolymphatic hydrops generation in MD and is believed to be a necessary precondition for MD's clinical symptomatology. We therefore consider the two ES pathologies to be etiopathologically distinct MD "endotypes" that may be associated with different phenotypical features. To investigate endotype-phenotype patterns in clinical patients, we previously developed a high-resolution computed tomography (HRCT)-based imaging method to distinguish the two ES pathologies (7).

The present study aimed to (i) adapt the method to distinguish ES pathologies based on gadolinium-enhanced magnetic resonance imaging (Gd-MRI); (ii) retrospectively subgroup a series of MD patients based on their ES pathology; and (iii) investigate, based on clinical data, whether these endotypes separate into clinically meaningful patient subgroups.

METHODS

Study Design and Approval

This retrospective explorative study was approved by the local Ethics Committee (application KEK-ZH-Nr. 2016-01619, Kantonale Ethikkommission, Zurich, Switzerland) in accordance with the Helsinki declaration and its amendments. Written informed general consent was obtained from all participants.

Study Population

We retrospectively assessed consecutive patients who attended our interdisciplinary center for vertigo and balance disorders at the University Hospital Zurich (tertiary referral center) from January 2010 to December 2015 for eligibility to be included in the study. The inclusion criteria were available data from Gd-MRI of the inner ears [(8); $n = 187$] and a final diagnosis of uni or bilateral definite MD [(9); $n = 92$]. We excluded patients with a Meniere's-like symptom complex due to a secondary pathology [e.g., otosclerosis, vestibular schwannoma, history of temporal bone fracture, and Cogan's syndrome, reviewed in (10)], patients who fulfilled the diagnostic criteria for possible or probable MD (9), and patients who were ultimately assigned another vertigo-associated diagnosis (e.g., vestibular migraine). Of the 92 primarily included MD patients, 20 were excluded after Gd-MRI data analysis (see "Vestibular aqueducts (VA) measurements and patient endotyping"). Finally, 72 patients' data were statistically analyzed (**Figure 1**).

Temporal Bone Imaging

During the routine clinical work-up, patients underwent 3-T MR imaging of the temporal bones 4 h after intravenous contrast (Gd) was administered to detect endolymphatic hydrops based on previously established protocols (8, 11). The endolymphatic hydrops grade (8) and signs of semicircular canal (SCC)

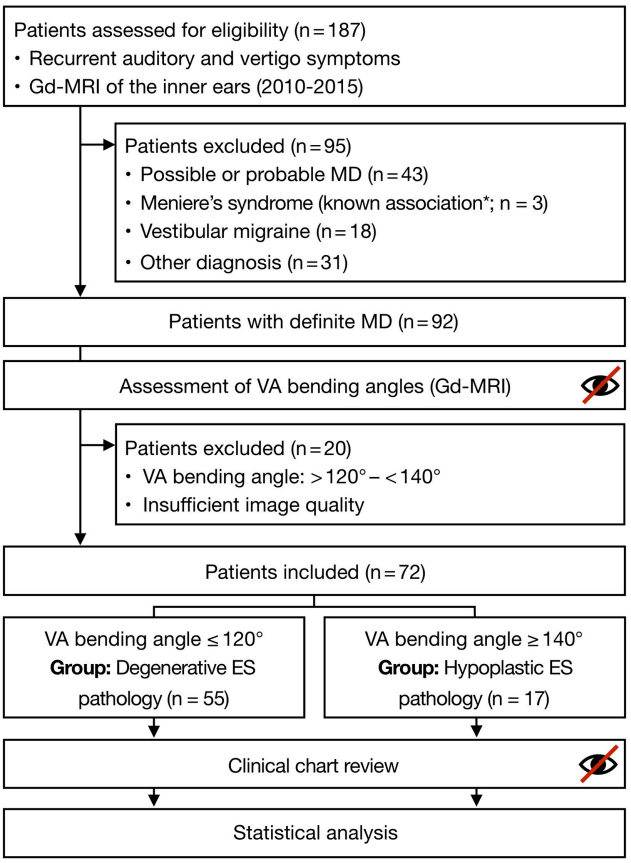

FIGURE 1 | Study flowchart. MD was definitively diagnosed per the guidelines from the Committee on Hearing and Equilibrium of the American Academy of Otolaryngology-Head and Neck Surgery for the Definition of Meniere's Disease from 1995 (9). VA bending angles and clinical chart reviews were assessed in a blinded manner (see text for details). *according to Merchant and Nadol (10). (Gd-MRI, gadolinium-enhanced magnetic resonance imaging; ES, endolymphatic sac; MD, Meniere's disease; VA, vestibular aqueduct).

dehiscence (i.e., absence of low-signal bone margins around the SCCs) were evaluated by experienced neuroradiologists at the time the images were taken. Additional dedicated temporal bone HRCT imaging was available for a subset of patients ($n = 16$). HRCT data were reconstructed separately for each temporal bone in the axial plane using a standard bone algorithm.

Vestibular Aqueduct (VA) Measurements and Patient Endotyping

We recently established a method to clinically distinguish the two histopathological subtypes (ES degeneration vs. ES hypoplasia) using the vestibular aqueduct angular trajectory (ATVA) as a radiographic surrogate marker (7). We demonstrated that the two ES pathologies are associated with significantly different VA bending angles (α_{exit}), which can be reliably determined using temporal bone HRCT imaging data and custom-developed software (12). Here, we validated the method for use with the Gd-MRI data by performing α_{exit} measurements based on HRCT and Gd-MRI (T2 space or 3D inversion recovery sequence) data from the same MD patients ($n = 16$). The imaging datasets were presented to an investigator (DB) who performed all measurements in a randomized order. The measured angles revealed a strong intermodal correlation between the HRCT and Gd-MRI (Spearman correlation coefficient $r = 0.95$, $p < 0.0001$; **Figure 2**).

Previously determined reference values for α_{exit} were used to endotype the MD patients (7). In clinically affected inner ears, angles $\leq 120°$ indicated a degenerative ES pathology. This subgroup is hereafter referred to as "MD-dg" patients. Angles $\geq 140°$ indicated a hypoplastic ES pathology, hereafter referred to as "MD-hp" patients. Of the 92 patients whose Gd-MRI-based ATVA was measured, 20 were excluded from the final analysis because of inconclusive α_{exit} values ($>120°$ and $<140°$) likely due to insufficient image quality from the Gd-MRI data.

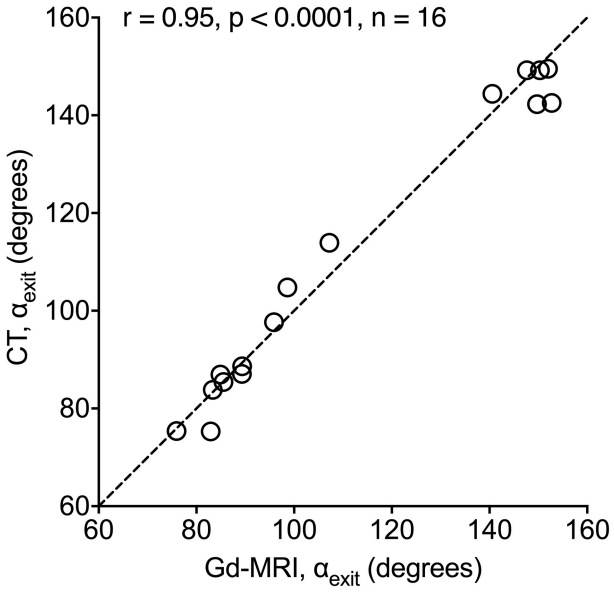

FIGURE 2 | CT vs. Gd-MRI correlation for α_{exit}. Angles were measured from HRCT and Gd-MRI data from the same 16 MD patients.

Reproducibility of the ATVA Measurements

Internal consistency of the Gd-MRI-based angle measurements and patient endotyping was tested by two independent investigators (AE and DB) who reassessed the Gd-MRI data from a randomly selected 14% of the cases. The investigators were blinded to the previous measurements when remeasuring α_{exit} and assigning cases to the endotype subgroups per the procedures described above. The interobserver test-retest reliability of the endotype assignments (MD-dg vs. MD-hp) was determined using Cohen's kappa coefficient (x). A x-value of 0.78 was determined, indicating excellent test-retest agreement per (13).

Clinical Data Collection and Processing

Clinical records, audiometric and vestibular test data, and radiology reports were reviewed by two investigators (CB and TH), who were blinded to the original imaging data and endotyping results. All data were collected in a structured digital database with predefined variables and categories. After collecting the data, all variables in the database were checked for categories with excessively low cell frequencies (<4). Those categories were merged with others from the same variable based on clinical meaningfulness to retain sufficient statistical power.

Statistical Analysis

Null hypotheses were formulated and statistical tests were selected before collecting the data. Second-step statistical analysis (*post hoc* testing) was clearly indicated (see respective paragraph). For binary variables, a chi-square test was performed if all category frequencies were greater than five; otherwise, Fisher's exact test was performed. Continuous variables were analyzed using a two-tailed Student's *t*-test for independent samples if the data were normally distributed; otherwise, a two-tailed Mann-Whitney U-test was performed. If not otherwise specified, statistical analyses were performed using IBM SPSS Statistics, version 24 (IBM Corp., Armonk, NY, USA). *P*-values were categorized into levels of evidence against H_0 (very strong evidence, $p < 0.001$; strong evidence, $p = 0.001$–0.01; evidence, $p = 0.01$–0.05; weak evidence, $p = 0.05$–0.1; and little or no evidence, $p > 0.1$) per (14).

Multiple Testing Correction

Twenty-eight independent null hypotheses were tested on the sample data. (A Benjamini–Hochberg procedure for multiple comparisons was used to control the false discovery rate (FDR) (15) see also the following paragraph). Subsequent *p*-values are followed by a statement regarding their significance per the Benjamini-Hochberg procedure (significant [sig.] or not significant [n. s.]) (16).

Rationale for Choosing the FDR's Critical Value

This study's purpose was to exploratively and exhaustively screen for clinical variables that differed between the two predefined patient subgroups and that would potentially contribute to the

variable's clinical meaningfulness. Therefore, in our statistical analysis, we intended to minimize the risk of false negatives (type II error) while retaining an appropriate risk of false positives (type I error), which was controlled by the FDR (15). In contrast to large-scale multiple-testing studies (e.g., genomics studies with $>10^3$ null hypotheses) that typically apply an FDR of 0.05 to minimize the type I error probability, we chose an FDR of 0.15. This value is associated with a reduced type II error rate and is commonly used in explorative and proof-of-concept studies (17, 18) in which not overlooking any true-positive results is prioritized.

Post hoc Analysis

In all contingency tables where significant differences were detected (based on an FDR of 0.15) between the groups, we performed *post hoc* testing per (19), enabling rigorous control of type I error rates: all three possible pairwise comparisons were performed between one variable and the other two, followed by a Bonferroni correction (in which the *p*-value is divided by the number of tests).

Longitudinal Analysis

To investigate whether the two MD endotypes differed in hearing loss progression over time (i.e., the slope of pure-tone averages [PTAs] respective of time), we performed a longitudinal analysis on data from each patient's repeated audiometric measurements. In bilateral cases, each ear was considered a separate case. A linear mixed-effects model was used with a subject-specific random intercept and a random slope for time. This model enabled varying baseline measurements and time-varying trends among subjects, considering data imbalance and unequal time-spacing. PTA measurements constituted the response, while time and endotype were the explanatory variables. Moreover, an interaction term between pathology type and time was included in the model to allow a pathology-specific time trend. The longitudinal analysis was performed in the R programming language using the function, *lmer()*, from the analysis-specific package, *lme4* (20, 21).

Volume Reconstructions

Inner ear volumes (**Figure 3**) were reconstructed from Gd-MRI data using 3D Slicer software [version 4.8.1 for Mac OS X (22)].

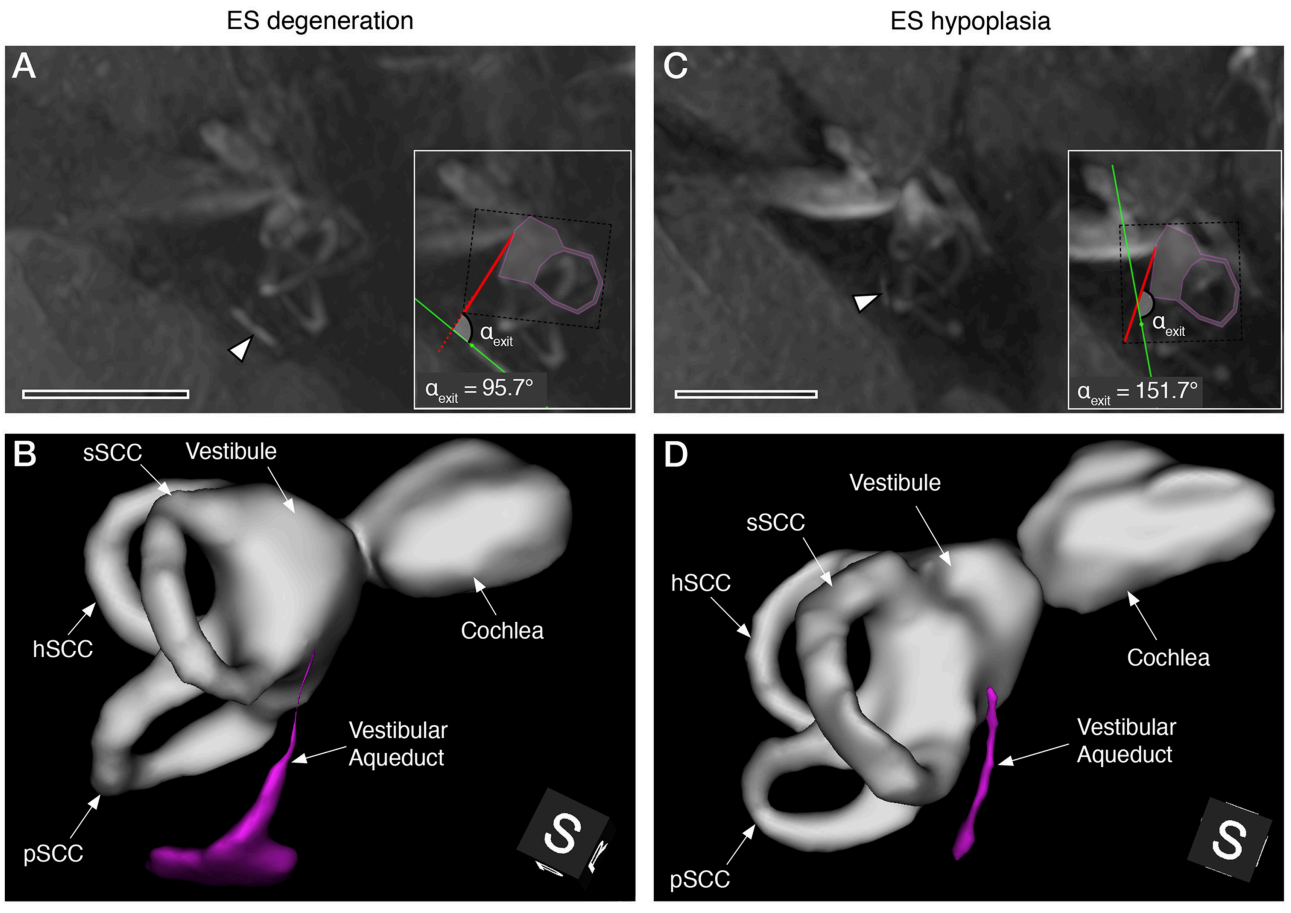

FIGURE 3 | Gd-MRI VA morphology in representative MD cases with degenerative **(A,B)** and hypoplastic **(C,D)** ES pathology. Maximum intensity projections of axial plane images **(A,C)**, and 3D reconstructions (postero-superior view) of the labyrinthine fluid spaces with the VA shown in magenta **(B,D)**. Arrowheads in **(A,C)** indicate the VA in the opercular region. Insets in **(A,C)** show angle measurements of the VA's angular trajectory as described previously (7) (sSCC, superior semicircular canal; hSCC, lateral semicircular canal; pSCC, posterior semicircular canal). Scale bars, 10 mm.

TABLE 1 | Key baseline characteristics of the study sample.

	Total MD patients included ($n = 72$)
Female:male ratio	41 (56.9%): 31 (43.1%)
Unilateral:bilateral ratio	64 (88.9%): 8 (11.1%)
Disease duration (*)	10.1 (6.1) years
Age at first MD symptoms	46.8 (12.0) years
Age at inclusion	56.8 (12.7) years

*Mean (SD) or absolute numbers (percentage). *Mean disease durations at inclusion were similar in both subgroups (MD-dg: 9.8 ± 6.4 years MD-hp: 10.6 ± 5.1 years; p = 0.685).*

RESULTS

Patient Endotyping and Baseline Characteristics

Of the 72 patients who were ultimately included, 55 (76.4%) demonstrated angles (α_{exit}) $\leq 120^{\circ}$ in the clinically affected inner ear(s). This subgroup was histopathologically diagnosed with ES degeneration (6) and is hereafter referred to as the MD-dg subgroup (**Figures 3A,B**). In 17 patients (23.6%), angles (α_{exit}) $\geq 140^{\circ}$ were observed, corresponding to a histopathological diagnosis of ES hypoplasia [(7); MD-hp subgroup; **Figures 3C,D**]. **Table 1** shows the 72 endotyped patients' baseline characteristics.

Between-Endotype Clinical Differences

From 28 clinical variables (**Table 2**), seven variables showed evidence to very strong evidence (14) for group differences (MD-dg vs. MD-hp endotypes), which are highlighted together with other potentially clinically meaningful variables (**Figure 4**).

Very strong evidence was found for a different sex distribution ($p = 0.0004$, sig.; **Figure 4A**), with a strong preponderance of male patients in the MD-hp group (male-to-female ratio = 1:0.06) and a nearly balanced male-to-female ratio in the MD-dg group (1:1.2). The Gd-MRI data strongly evidenced radiological signs of SCC dehiscence (**Figure 4B**; i.e., no clear spatial separation of signals from the superior, posterior or both SCCs and the cerebrospinal fluid space) more often in the MD-hp group (5/17 [29.4%]) than in the MD-dg group [2/55 [3.6%]; $p = 0.007$, sig.]. The objective vestibular test data strongly evidenced, on average, greater reductions of bithermal caloric responses (**Figure 4C**) on the clinically affected side in the MD-dg group (30.2 ± 30.4% asymmetry, $n = 48$) than in the MD-hp group (13.5 ± 15.2% asymmetry, $n = 12$; $p = 0.009$, sig.). Notably, there was no evidence that the mean age at caloric testing differed between groups (MD-dg group: 54.9 ± 13.5 years; MD-hp group 52.4 ± 8.7 years, $p = 0.38$). We found further evidence for a higher frequency of bilateral clinical manifestations (**Figure 4D**) in the MD-hp group (5/17 [29.4%]) than in the MD-dg group (3/55 [5.5%]; $p = 0.015$, sig.), as well as for different frequency patterns of vertigo symptoms (**Figure 4E**) between groups ($p = 0.023$, sig.). *Post hoc* comparisons (**Table 3**) evidenced a group difference when testing the frequency pattern "monthly" (MD-dg: 12.7%, MD-hp: 41.2% of patients) vs. the other two frequency patterns ("daily/weekly" and "less than once per month"; $p = 0.048$, Bonferroni corrected). Although the initial analysis revealed no evidence of group differences regarding a positive family history for MD, non-age-related hearing loss or vertigo and migraine (**Figure 4F**), *post hoc* analysis for MD and hearing loss/vertigo symptoms only (**Table 3**) was more prevalent in relatives of MD-hp patients (41.2%; MD-dg group: 15.7%, data available from $n = 51$; $p = 0.028$, Bonferroni corrected).

For the remaining variables, no evidence of group differences was found, or no statistical analysis was performed. Those variables nonetheless represent clinically meaningful and potentially endotype-segregating features (see Discussion section). Although strong evidence suggested that headache symptom frequencies differed between the two groups in the primary statistical analysis ($p = 0.004$, sig., **Table 2**), *post hoc* analysis (**Table 3**) revealed no evidence of a group difference when only male patients in both groups were compared to eliminate sex as a confounding factor [higher prevalence of migraine headaches in women than in men in the general population (23)]. In the MD-hp group, unilateral hypoplastic ES pathology was invariably associated with ipsilateral endolymphatic hydrops and ipsilateral MD. However, among the eight patients with bilateral ES hypoplasia, five demonstrated endolymphatic hydrops and MD symptoms in both inner ears, while three had only one ear affected (**Figure 4G**). The mean age when MD symptoms first manifested was slightly earlier in the MD-hp group (43.1 ± 8.9 years) than in the MD-dg group (47.9 ± 12.6 years; $p = 0.152$, n. s.; **Figure 4H**). Endolymphatic hydrops without evidence of clinical affection [i.e., "clinically silent" endolymphatic hydrops (8, 24)] was exclusively observed in the contralateral inner ears from unilaterally affected MD-dg patients (19.2% of patients; $p = 0.186$, n. s.; **Figure 4I**).

DISCUSSION

The following sections discuss the endotype-specific clinical characteristics and their potential implications for clinically managing MD patients (synopsis in **Table 4**).

Endotype "ES Hypoplasia" (MD-hp Subgroup)

ES hypoplasia was present in 23.6% of our cohort. Unilateral ES hypoplasia was invariably associated with ipsilateral endolymphatic hydrops and MD but not with any radiological/clinical signs for contralateral affection. In those cases, the risk of developing MD in the contralateral inner ear (normal VA angle) is probably low, most likely comparable to the risk of MD with an ES degenerative endotype in the general population [i.e., ∼0.15% per a calculation based on data from this study and (26)], and they may be suitable candidates for ablative therapies [e.g., gentamicin injections) in the affected ear if clinically indicated. MD-hp patients should be considered with caution for ES surgical procedures [decompression, shunting, or endolymphatic duct blockage; reviewed in (28, 29)] since the hypoplastic operculum of the VA is considerably smaller than normal, and the extraosseous

TABLE 2 | Demographic and clinical characteristics tested for between-group differences.

Variable	Degeneration ($n = 55$)	Hypoplasia ($n = 17$)	Difference (95% CI)	*p*-value	Benjamini-Hochberg significance
Female:male ratio	30 (54.5%): 25 (45.5%)	1 (5.9%): 16 (94.1%)	n. a.	0.0004	sig.
Headache type					
- Migraineous	20 (36.4%)	4 (23.5%)			
- Non-migraineous	5 (9.1%)	8 (47.1%)	n. a.	0.004	sig.
- None	30 (54.5%)	5 (29.4%)			
SCC dehiscence on affected side	2 (3.6%)	5 (29.4%)	n. a.	0.007	sig.
Caloric response asymmetry (unilateral cases)—% asymmetry	30.2 ± 30.4 ($n = 48$)	13.5 ± 15.2 ($n = 12$)	16.7 (4.4 to 29.1)	0.009	sig.
Laterality					
- Unilateral	52 (94.5%)	12 (70.6%)	n. a.	0.015	sig.
- Bilateral	3 (5.5%)	5 (29.4%)			
Vertigo frequency					
- Daily/weekly	36 (65.5%)	9 (52.9%)			
- Monthly	7 (12.7%)	7 (41.2%)	n. a.	0.023	sig.
- Other	12 (21.8%)	1 (5.9%)			
Family history					
- MD	2 (3.6%)	2 (11.8%)			
- Hearing loss/vertigo	6 (10.9%)	5 (29.4%)			
- Migraine	6 (10.9%)	0 (0.0%)	n. a.	0.141	n. s.
- None	37 (67.3%)	10 (58.8%)			
- No data	4 (7.3%)	0 (0.0%)			
Age at first symptoms	47.9 ± 12.6	43.1 ± 8.9	4.8 (−0.8 to 10.3)	0.152	n. s.
Cardiovascular comorbidities	20 (36.4%)	3 (17.6%)	n. a.	0.234	n. s.
Hearing aid(s)	20 (36.4%)	9 (52.9%)	n. a.	0.265	n. s.
Vegetative symptoms	47 (85.5%)	12 (70.6%)	n. a.	0.277	n. s.
Hydrops grade—median (25th−75th percentiles)	1.3 (1.0 to 2.0)	1.0 (0.9 to 1.5)	n. a.	0.289	n. s.
oVEMP asymmetry ratio	6.5 ± 24.3 ($n = 41$)	13.0 ± 19.4 ($n = 13$)	6.5 (−7.1 to 20.0)	0.324	n. s.
cVEMP asymmetry ratio	6.9 ± 22.4 ($n = 38$)	15.8 ± 22.8 ($n = 13$)	8.9 (−0.5 to 14.2)	0.333	n. s.
Dynamic visual acuity loss (logMAR)—median (25th−75th percentiles)	0.4 (0.5 to 0.6) ($n = 40$)	0.3 (0.4 to 0.6) ($n = 7$)	n. a.	0.349	n. s.
Hearing loss (last PTA)—median (25th−75th percentiles)	40.0 (19.9 to 54.6)	42.1 (26.8 to 42.1)	n. a.	0.403	n. s.
Head impulse test gain ratios—median (25th−75th percentiles)	1.1 (0.9 to 1.3) ($n = 49$)	1.0 (0.8 to 1.3) ($n = 9$)	n. a.	0.410	n. s.
Neck or spine problems	9 (16.4%)	1 (5.9%)	n. a.	0.434	n. s.
Hearing loss (first PTA)—median (25th−75th percentiles)	28.3 (10.8 to 45.5)	28.25 (19.3 to 44.4)	n. a.	0.443	n. s.
Maximal MD therapy					
- Betahistine/cinnarizine	17 (30.9%)	6 (35.3%)			
- Intratympanic dexamethasone/lidocaine	34 (61.8%)	11 (64.7%)	n. a.	0.665	n. s.
- Intratympanic gentamicin	4 (7.3%)	0 (0.0%)			
Photo-/phono-phobia	17 (30.9%)	6 (35.3%)	n. a.	0.735	n. s.
Hearing loss pattern (first PTA)					
- Low	6 (10.9%)	0 (0.0%)			
- High and low (peak)	25 (45.5%)	9 (52.9%)			
- High/other	9 (16.4%)	3 (17.6%)	n. a.	0.737	n. s.
- All frequencies	13 (23.6%)	5 (29.4%)			
- No hearing loss	2 (3.6%)	0 (0.0%)			
Migraineous aura	11 (20.0%)	3 (17.6%)	n. a.	0.830	n. s.

(Continued)

TABLE 2 | Continued

Variable	Degeneration ($n = 55$)	Hypoplasia ($n = 17$)	Difference (95% CI)	p-value	Benjamini-Hochberg significance
Maximal migraine therapy					
- Magnesium, vitamin B2, flunarizine	13 (23.7%)	4 (23.5%)			
- Valproate, triptans	10 (18.1%)	4 (23.5%)	n. a.	0.928	n. s.
- None	32 (58.2%)	9 (52.9%)			
Hearing loss pattern (last PTA)					
- Low	1 (1.8%)	0 (0.0%)			
- High and low	17 (30.9%)	6 (35.3%)			
- High/other	10 (18.2%)	2 (11.8%)	n. a.	0.929	n. s.
- All frequencies	23 (41.8%)	8 (47.1%)			
- No hearing loss	3 (5.5%)	0 (0.0%)			
- No data	1 (1.8%)	1 (5.9%)			
First MD symptom					
- Hearing loss	13 (23.6%)	4 (23.5%)			
- Vertigo	11 (20.0%)	5 (29.4%)			
- Tinnitus/aural fullness	5 (9.1%)	1 (5.9%)	n. a.	0.929	n. s.
- Multiple	21 (38.2%)	7 (41.2%)			
- No data	5 (9.1%)	0 (0.0%)			
Allergies	6 (10.9%)	2 (11.8%)	n. a.	0.992	n. s.
Vertigo quality					
- Rocking	12 (21.8%)	4 (23.5%)			
- Spinning	41 (74.6%)	13 (76.5%)	n. a.	1.000	n. s.
- Other	2 (3.6%)	0 (0.0%)			

Values are reported as absolute numbers (percentage), mean ± SD or median with 25th and 75th percentiles. The number in brackets indicates the number of patients included in the analysis if some patients in the group were excluded. 95% CI, 95% confidence interval; cVEMP/oVEMP, cervical/ocular vestibular-evoked myogenic potentials; logMAR, logarithm of minimum angle of resolution; MD, Meniere's disease; n. a., not applicable; n. s., not significant; PTA1, first available pure-tone audiometry; PTA4, last available pure-tone audiometry; SCC, semicircular canal; sig., significant.

ES portion is mostly absent (6). A recent retrospective study showed that during ES surgery in MD patients, intraoperatively visualizing the operculum was impossible in 28% of the cases (25). This number very closely matches the hypoplastic ES-endotype prevalence found in the present study (23.6%). In almost all MD-hp patients, bilateral ES hypoplasia was associated with bilateral endolymphatic hydrops and MD; however, three of those patients showed only unilateral hydrops and clinical symptoms at the time of data collection (**Figure 4G**). These three patients are expected to develop bilateral MD later in life based on the consistent association between ES hypoplasia and clinical symptoms that we found previously in post-mortem cases (6, 7). Thus, in all MD-hp patients with bilateral ES hypoplasia, a bilaterally impaired audiovestibular function (bilateral MD) with a significantly impacted quality of life should be expected, and those patients should be considered with caution for ablative therapies. Furthermore, MD-hp patients may have an increased risk of concomitant audiovestibular symptoms caused by SCC dehiscence syndrome, as suggested by the higher prevalence (29.4%) of suspected (posterior) SCC dehiscence on the MRI data. In contrast, SCC dehiscence was suspected radiologically in only 3.6% of MD-dg patients, mostly of the superior SCC, which is comparable to the reported overall prevalence of superior SCC dehiscence in the general population [3–10% (30–32)]. The epidemiological features associated with this endotype (predominantly men, familial clustering of MD, and tendency toward earlier disease onset) support the hypothesis of a genetic/developmental cause. Therefore, the endotype's specific radiological feature (VA bending angle $\geq 140°$) may be useful for predictive clinical screenings (e.g., in family members of MD-hp patients) for this potentially inheritable inner ear pathology and to prognosticate the risk of developing MD.

Endotype "ES Degeneration" (MD-dg Subgroup)

ES degeneration was observed in 76.4% ($n = 55$; MD-dg group) of patients. This endotype (VA angle $\leq 120°$) is radiologically diagnosed by excluding the hypoplastic endotype (VA angle $\geq 140°$), but it cannot be distinguished from a normal ES (VA angle $\leq 120°$) using the Gd-MRI-based criteria described herein. Thus, in contrast to the hypoplastic endotype, no potential prognostic marker for future bilateral manifestation is available to date. This endotype was exclusively associated with contralateral "clinically silent" endolymphatic hydrops (i.e., hydrops without clinical signs of inner ear dysfunction, particularly without MD). Clinically silent hydrops was observed

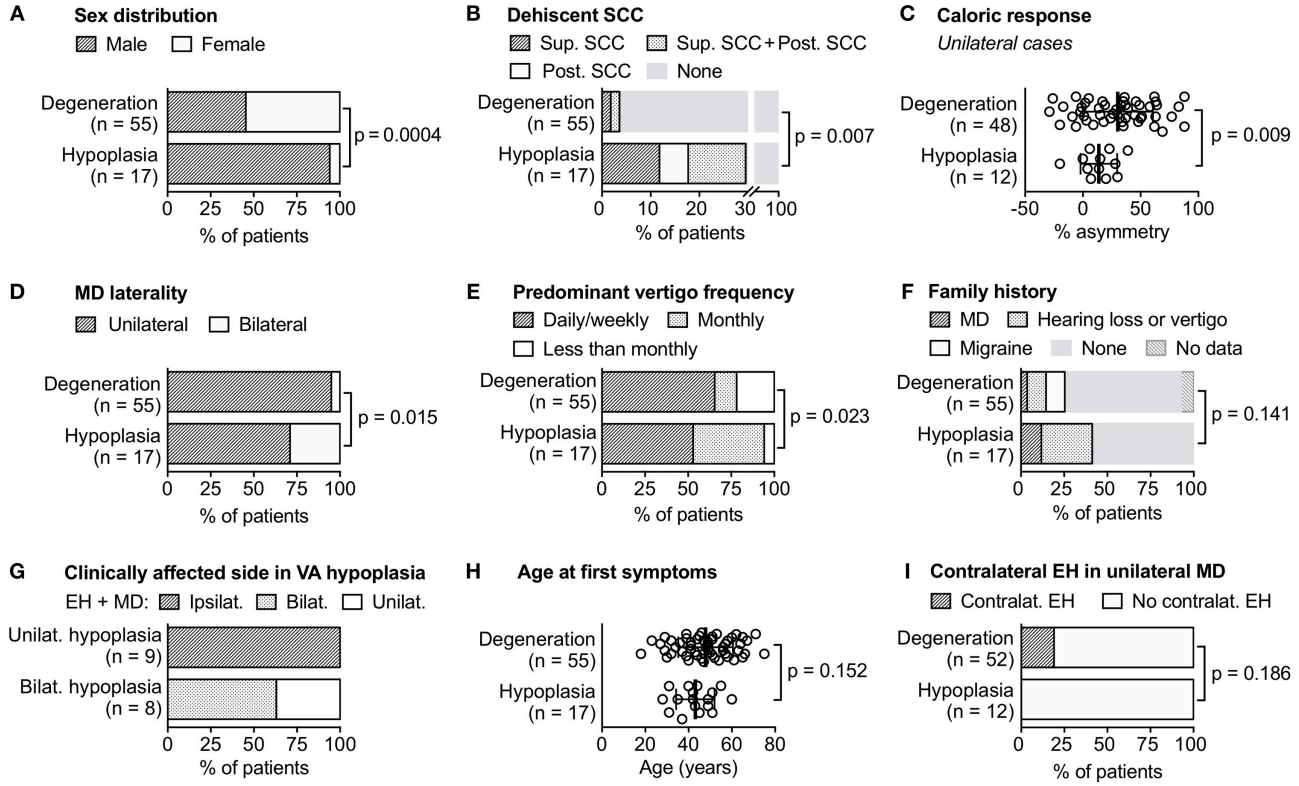

FIGURE 4 | Clinical differences between and within the two MD endotypes. Data from **(A–F,H)** are also shown in **Table 2**, data from **(G)** and **(I)** were not part of the initial null hypotheses. Bilat, bilateral; contralat, contralateral; EH, endolymphatic hydrops; ipsilat, ipsilateral; MD, Meniere's disease; post, posterior; SCC, semicircular canal; sup, superior; unilat, unilateral; VA, vestibular aqueduct.

in 19.2% of all unilateral MD-dg patients, which is consistent with previously reported numbers from MRI studies investigating unilaterally affected MD patients [16.0–23.3% (8, 33)]. Since clinically silent hydrops reportedly progresses to MD in 33% of cases (34), MD-dg patients with contralateral hydrops may have an elevated risk of developing bilateral MD and should be considered for ablative therapy with caution. However, MD-dg patients may be generally considered suitable candidates for ES surgery (decompression or shunting) since the operculum, which exhibits normal anatomy in these cases, allows its reliable intraoperative visualization. However, per our previous human pathology study (6), the extraosseous ES portion is degenerating in these cases, which calls into question the proposed mode of function of these treatments. On average, a higher frequency of vertigo attacks and a more severely impaired vestibular (caloric) function was associated with this endotype. These findings may be explained by a supposedly more sudden manifestation of ES degeneration in the matured inner ear, as opposed to the developmentally inherent ES hypoplasia. ES degeneration therefore probably has a more disruptive effect on vestibular function due to the adult inner ear's limited capability to develop compensating homeostatic mechanisms. In contrast in the developing inner ear, in the presence of ES hypoplasia, such compensatory function may be established more efficiently.

Between-Endotype Comparisons With Little or No Evidence for Group Differences

Of the 28 tested clinical variables, we found weak to no evidence for endotype differences for 21 variables (**Table 2**) and for a longitudinal analysis of hearing loss progression (**Supplementary Figure 1**; Benjamini-Hochberg significance: n. s.). However, our retrospective explorative approach does not categorically rule out those 21 variables as clinically meaningful, endotype-segregating features. Specifically, variables such as migraine headache prevalence, age at first MD symptom onset, and prevalence of "clinically silent" contralateral endolymphatic hydrops should, in our view, remain of interest in future endotyping studies.

Although the migraine headache prevalence did not differ between endotypes, the overall prevalence of migraine symptoms in our cohort (59.9%) was similar to that of a previous study [56% (35)] and considerably higher than the prevalence in the general population [11–18% (36–38)]. Future studies should more specifically address questions such as whether migraines are associated—or even share a common etiopathology—with a distinct MD endotype.

An earlier age of onset of the first MD symptoms in MD-hp patients was evident in our previous temporal bone study (6) (MD-hp: 37.7 ± 19.0 years; MD-dg: 58.1 ± 20.5 years; $p = 0.038$) but not in the present study (MD-hp: 43.1 ± 8.9 years;

TABLE 3 | *Post-hoc* tests.

Clinical feature	Category	ES pathology		*p*-value (Bonferroni corrected)
		Degeneration	Hypoplasia	
Vertigo	Monthly	7 (12.7%)	7 (41.2%)	$p = 0.048$
	Daily/weekly or less than once per month	48 (87.3%)	10 (58.8%)	
Headache type (males)	Migraineous	6	4	$p = 0.211$
	Non-migraineous	5	7	
	Other	14	5	
Family history	MD, hearing loss and/or vertigo	8 (15.7%)	7 (41.2%)	$p = 0.028$
	No family history	43 (84.3%)	10 (58.8%)	

TABLE 4 | Endotype-specific clinical considerations.

Endotype (patient subgroup)	Laterality	Endotype frequency	Characteristics/considerations
ES hypoplasia (MD-hp patients)	Overall	23.6%	• Specific radiological feature (VA bending angle ≥140°) • Prognostic radiological screening possible • Possible concomitant SSC dehiscence syndrome • ES not visualizable for surgical ES enhancement/shunting (*)
	Unilateral	16.7%	• Very low risk of developing bilateral MD (†) • Most suitable for vestibular ablative therapy
	Bilateral	6.9%	• Very high risk of developing bilateral MD • Avoid performing vestibular ablative therapy (‡) • Significant impact on auditory/vestibular function and quality of life must be expected
ES degeneration (MD-dg patients)	Overall	76.4%	• Suitable for ES surgery if considered (§) • Consider average higher frequency of vertigo symptoms, more severe vestibular hypofunction when establishing treatment • Consider sequential imaging to rule out ES tumors if symptomatology increases over baseline fluctuations (‖)
	Unilateral	72.2%	• "Clinically silent" contralateral EH (19.2%) • Unknown risk for progression to bilateral disease • Increased risk to perform vestibular ablative treatment
	Bilateral	4.2%	• Least frequent endotype, 4.2% of patients

**Considering the anticipated low chance of intraoperatively identifying the operculum (25). (†) equal to the overall risk of developing MD with degenerative ES pathology in the general population [i.e., 0.15% based on the MD prevalence of 0.2% (26) and a prevalence of degenerative ES pathology of 76.4% among MD patients in the present study]. (‡) upon initial presentation with clinically unilateral symptoms. (§) due to degenerative changes of extraosseous ES in these patients (6), we consider the rationale for ES surgery questionable. (‖) according to Kirsh et al. (27). In MD-hp patients, ES hypoplasia sufficiently explains the etiology.*

MD-dg: 47.9 ± 12.6; $p = 0.152$, n. s.). An earlier symptom onset in the MD-hp group (although not evident in the present study) could be explained by the likely prenatally determined hypoplastic ES pathology (7), which presumably renders the inner ear susceptible to precipitating factors that ultimately cause MD. In contrast, ES degeneration in MD-dg patients is thought to be an acquired pathology, possibly associated with age-related factors, and therefore may explain MD's tendency to manifest later in life.

A "clinically silent" (no MD symptoms) endolymphatic hydrops is a frequent [5–26%, (8, 24, 39)] histological and radiological entity in the contralateral ears from unilaterally affected Meniere's patients, and was in the present study found exclusively in the MD-dg endotype (19.2%; $p = 0.186$, n. s.). The frequent association of this endotype with bilateral hydrops may suggest limited or still progressing ES degeneration as the cause for contralateral, clinically silent hydrops, and further suggests a systemic (e.g. immune-mediated or vascular) etiology of degenerative ES pathology. Although progression to bilateral MD was rarely observed in the MD-dg group (4.2%); longer prospective observations are required to determine whether clinically silent hydrops represents a precursor lesion of MD.

Patient Subgrouping Approaches in MD

Patient stratification algorithms in MD can be divided into phenomenology (clinical features)-based "top-down" algorithms, and etiology (endotype)-based "bottom-up" algorithms. Frejo et al. used disease laterality (uni vs. bilateral) as a principal group classifier, and, in a second step, applied data mining procedures (cluster analysis) to identify clinical features (autoimmune disorders, migraine, MD family history, synchronic vs. metachronic onset of hearing loss) that segregated five discrete subgroups of uni and bilateral MD patients, respectively (40, 41). In a follow-up study, Frejo et al. then used an etiology-based approach and distinguished two subgroups with different cytokine profiles

among uni and bilateral MD patients (42). They suggested an immune-mediated etiology in the subgroup that exhibited elevated interleucin-1β plasma levels as well as mold-induced TNF-α secretion. Notably, some subgroups defined by Frejo et al. share certain group-defining features with the MD-dg and MD-hp endotypes. Further studies that combine the described subgrouping/endotyping algorithms will determine whether the subgroups defined by the different approaches truly overlap.

Limitations of the Study

The overall study design was retrospective and exploratory. Thus, for statistical between-group comparisons, an FDR was chosen that allowed us to identify many endotype-specific clinical features. Moreover, few patients ($n = 72$) were available for this study. Consequently, the statistical power for some group comparisons was low, and the results from this investigation should be verified in a larger prospective cohort study.

For the 20 excluded patients, α_{exit} angles between 120 and 140° were measured, or the VA could not be visualized (**Figure 1**). Since such α_{exit} values or non-visualization of the VA were lacking in a previous retrospective MD case series ($n = 64$) in which HRCT temporal bone data were measured (7), we consider this a problem of insufficient Gd-MRI resolution, likely due to movement artifacts in individual datasets.

For most included patients, the initial diagnostic test data (PTA, vestibular diagnostics) were acquired at the time of diagnosis, whereas for a minority of patients, these initial tests were performed several months or years after being diagnosed. This inhomogeneity of the available data is a confounding factor, particularly in the longitudinal analysis of hearing thresholds (**Supplementary Figure 1**).

CONCLUSION

This novel endotype-driven diagnostic approach allowed distinguishing clinically meaningful MD patient subgroups with different etiologies and phenotypes. This approach may (i) help select more homogeneous patient cohorts for future clinical studies, (ii) refine clinical diagnoses, (iii) improve clinical decision-making, and (iv) help prognosticate the disease course in individual patients. The results from this retrospective study require validation in prospective cohort studies.

AUTHOR CONTRIBUTIONS

AE: study conception and design; DB, CB, TH, and AE: data acquisition; DB, CB, TH, EM, SM, and AE: data analysis and interpretation; DB and AE: drafted the manuscript; AM, VW, SM, and BS: critically reviewed and revised the manuscript.

FUNDING

This work was supported by a principal grant from the British Ménière's Society. DB was supported by a national M.D.-Ph.D. scholarship of the Swiss National Science Foundation. AE was supported by a career development grant from the University of Zurich.

ACKNOWLEDGMENTS

The authors thank Dr. Niels Hagenbuch for biostatistical support.

SUPPLEMENTARY MATERIAL

The Supplementary Material for this article can be found online at: https://www.frontiersin.org/articles/10.3389/fneur.2019.00303/full#supplementary-material

REFERENCES

1. Rauch S. Clinical hints and precipitating factors in patients suffering from Meniere's disease. *Otolaryngol Clin North Am.* (2010) 43:1011–17. doi: 10.1016/j.otc.2010.05.003
2. Friberg U, Stahle J, Svedberg A. The natural course of Meniere's disease. *Acta Otolaryngol Suppl.* (1984) 406:72–7.
3. Gürkov R, Jerin C, Flatz W, Maxwell R. Clinical manifestations of hydropic ear disease (Menière's). *Eur Arch Otorhinolaryngol.* (2018) 276:27–40. doi: 10.1007/s00405-018-5157-3
4. Merchant SN, Rauch SD, Nadol JBJ, Nadol JB Jr. Meniere's disease. *Eur Arch Otorhinolaryngol.* (1995) 252:63–75.
5. Kitahara M. Bilateral aspects of meniere's disease: Meniere's disease with bilateral fluctuant hearing loss. *Acta Otolaryngol.* (1991) 485:74–7.
6. Eckhard AH, Zhu M, O'Malley JT, Williams GH, Loffing J, Rauch SD, et al. Inner ear pathologies impair sodium-regulated ion transport in Meniere's disease. *Acta Neuropathol.* (2019) 137:343–57. doi: 10.1007/s00401-018-1927-7
7. Bächinger D, Luu N-N, Kempfle JS, Barber S, Zürrer D, Lee DJ, et al. Vestibular aqueduct morphology correlates with endolymphatic sac pathologies in Meniere's disease – a correlative histology and computed tomography study. *Otol Neurotol.* (in press). doi: 10.1097/MAO.0000000000002198
8. Baráth K, Schuknecht B, Monge Naldi A, Schrepfer T, Bockisch CJ, Hegemann SCA. Detection and grading of endolymphatic hydrops in meniere disease using MR imaging. *Am J Neuroradiol.* (2014) 35:1387–92. doi: 10.3174/ajnr.A3856
9. Monsell M, Balkany TA, Gates GA, Goldenberg RA, William L, House JW. Committee on hearing and equilibrium guidelines for the diagnosis and evaluation of therapy in Menière's disease. American Academy of Otolaryngology-Head and Neck Foundation, Inc. *Otolaryngol Head Neck Surg.* (1995) 113:181–5.
10. Merchant SN, Nadol JB. *Schuknecht's Pathology of the Ear*. 3rd ed. Shelton, CT: People's Medical Publishing House-USA (2010).
11. Naganawa S, Ishihara S, Iwano S, Sone M, Nakashima T. Three-dimensional (3D) visualization of endolymphatic hydrops after intratympanic injection of Gd-DTPA: optimization of a 3D-real inversion-recovery turbo spin-echo (TSE) sequence and application of a 32-channel head coil at 3T. *J Magn Reson Imaging.* (2010) 31:210–14. doi: 10.1002/jmri.22012
12. Zürrer D. *CoolAngleCalc*. Available online at: https://danielzuerrer.github.io/CoolAngleCalcJS/ (accessed January 20, 2019).
13. Landis JR, Koch GG. Agreement measures for categorical data. *Biometrics.* (1977) 33:159–74. doi: 10.2307/2529310
14. Bland JM. *An Introduction to Medical Statistics*. 4th ed. Oxford, UK: Oxford University Press (2015).

15. Benjamini Y, Hochberg Y. Controlling the false discovery rate: a practical and powerful approach to multiple testing. *J R Stat Soc.* (1995) 57:289–300. doi: 10.1111/j.2517-6161.1995.tb02031.x
16. McDonald JH. *Handbook of Biological Statistics*. 3rd ed. Baltimore, MA: Sparky House Publishing (2014).
17. Linnstaedt SD, Walker MG, Parker JS, Yeh E, Sons RL, Zimny E, et al. MicroRNA circulating in the early aftermath of motor vehicle collision predict persistent pain development and suggest a role for microRNA in sex-specific pain differences. *Mol Pain.* (2015) 11:66. doi: 10.1186/s12990-015-0069-3
18. Ferrario M, Cambiaghi A, Brunelli L, Giordano S, Caironi P, Guatteri L, et al. Mortality prediction in patients with severe septic shock: a pilot study using a target metabolomics approach. *Sci Rep.* (2016) 6:20391. doi: 10.1038/srep20391
19. MacDonald PL, Gardner RC. Type I error rate comparisons of *post hoc* procedures for I × J chi-square tables. *Educ Psychol Meas.* (2000) 60:735–54. doi: 10.1177/00131640021970871
20. R Foundation for Statistical Computing. *R: A Language and Environment for Statistical Computing* (2011).
21. Bates D, Maechler M. *Package "Lme4"* (2010).
22. Fedorov A, Beichel R, Kalpathy-Cramer J, Finet J, Fillion-Robin JC, Pujol S, et al. 3D Slicer as an image computing platform for the Quantitative Imaging Network. *Magn Reson Imaging.* (2012) 30:1323–41. doi: 10.1016/j.mri.2012.05.001
23. Smitherman TA, Burch R, Sheikh H, Loder E. The prevalence, impact, and treatment of migraine and severe headaches in the United States: a review of statistics from national surveillance studies. *Headache.* (2013) 53:427–36. doi: 10.1111/head.12074
24. Rauch SD, Merchant SN, Thedinger BA. Meniere's syndrome and endolymphatic hydrops. Double-blind temporal bone study. *Ann Otol Rhinol Laryngol.* (1989) 98:873–83.
25. Kitahara T, Yamanaka T. Identification of operculum and surgical results in endolymphatic sac drainage surgery. *Auris Nasus Larynx.* (2017) 44:116–18. doi: 10.1016/j.anl.2016.02.017
26. Alexander TH, Harris JP. Current epidemiology of Meniere's syndrome. *Otolaryngol Clin North Am.* (2010) 43:965–70. doi: 10.1016/j.otc.2010.05.001
27. Kirsh ER, Kozin ED, Knoll RM, Wong K, Faquin W, Reinshagen KL, et al. Sequential imaging in patient with suspected Menière's disease identifies endolymphatic sac tumor. *Otol Neurotol.* (2018) 39:e856–9. doi: 10.1097/MAO.0000000000001952
28. Pullens B, Verschuur HP, van Benthem PP. Surgery for Ménière's disease. *Cochrane Database Syst Rev.* (2013) 2:CD005395. doi: 10.1002/14651858.CD005395.pub2
29. Sood AJ, Lambert PR, Nguyen SA, Meyer TA. Endolymphatic sac surgery for Ménière's disease: a systematic review and meta-analysis. *Otol Neurotol.* (2014) 35:1033–45. doi: 10.1097/MAO.0000000000000324
30. Crovetto M, Whyte J, Rodriguez OMM, Lecumberri I, Martinez C, Eléxpuru J. Anatomo-radiological study of the Superior Semicircular Canal Dehiscence. *Eur J Radiol.* (2010) 76:167–72. doi: 10.1016/j.ejrad.2009.05.038
31. Stimmer H, Hamann KF, Zeiter S, Naumann A, Rummeny EJ. Semicircular canal dehiscence in HR multislice computed tomography: distribution, frequency, and clinical relevance. *Eur Arch Otorhinolaryngol.* (2012) 269:475–80. doi: 10.1007/s00405-011-1688-6
32. Bi WL, Brewster R, Poe D, Vernick D, Lee DJ, Eduardo Corrales C, et al. Superior semicircular canal dehiscence syndrome. *J Neurosurg.* (2017) 72:1–9. doi: 10.3171/2016.9.JNS16503
33. Wu H. Endolymphatic hydrops detected by 3-dimensional fluid-attenuated inversion recovery MRI following intratympanic injection of gadolinium in the asymptomatic contralateral ears of patients with unilateral Ménière's disease. *Med Sci Monit.* (2015) 21:701–7. doi: 10.12659/MSM.892383
34. House JW, Doherty JK, Fisher LM, Derebery MJ, Berliner KI. Meniere's disease: prevalence of contralateral ear involvement. *Otol Neurotol.* (2006) 27:355–61. doi: 10.1097/00129492-200604000-00011
35. Radtke A, Lempert T, Gresty MA, Brookes GB, Bronstein AM, Neuhauser H. Migraine and Ménière's disease: is there a link? *Neurology.* (2002) 59:1700–4. doi: 10.1212/01.WNL.0000036903.22461.39
36. Rasmussen BK, Jensen R, Schroll M, Olesen J. Epidemiology of headache in a general population-a prevalence study. *J Clin Epidemiol.* (1991) 44:1147–57. doi: 10.1016/0895-4356(91)90147-2
37. Goebel H, Petersen-Braun M, Soyka D. The epidemiology of headache in Germany: a nationwide survey of a representative sample on the basis of the headache classification of the International Headache Society. *Cephalalgia.* (1994) 14:97–106. doi: 10.1046/j.1468-2982.1994.1402097.x
38. Launer LJ, Terwindt GM, Ferrari MD. The prevalence and characteristics of migraine in a population-based cohort: the GEM Study. *Neurology.* (1999) 53:537–42. doi: 10.1212/WNL.53.3.537
39. Merchant SN, Adams JC, Nadol JB. Pathophysiology of Meniere's syndrome: are symptoms caused by endolymphatic hydrops? *Otol Neurotol.* (2005) 26:74–81. doi: 10.1097/00129492-200501000-00013
40. Frejo L, Soto-Varela A, Santos-Perez SS, Aran I, Batuecas-Caletrio A, Perez-Guillen V, et al. Clinical subgroups in bilateral meniere disease. *Front Neurol.* (2016) 7:182. doi: 10.3389/fneur.2016.00182
41. Frejo L, Martin-Sanz E, Teggi R, Trinidad G, Soto-Varela A, Santos-Perez S, et al. Extended phenotype and clinical subgroups in unilateral Meniere disease: a cross-sectional study with cluster analysis. *Clin Otolaryngol.* (2017) 42:1172–80. doi: 10.1111/coa.12844
42. Frejo L, Gallego-Martinez A, Requena T, Martin-Sanz E, Amor-Dorado JC, Soto-Varela A, et al. Proinflammatory cytokines and response to molds in mononuclear cells of patients with Meniere disease. *Sci Rep.* (2018) 8:5974. doi: 10.1038/s41598-018-23911-4

Conflict of Interest Statement: The authors declare that the research was conducted in the absence of any commercial or financial relationships that could be construed as a potential conflict of interest.

frontiers in Neurology

METHODS
published: 09 April 2019
doi: 10.3389/fneur.2019.00326

Clinical Findings in Patients With Persistent Positional Nystagmus: The Designation of "Heavy and Light Cupula"

Xiaowu Tang[1,2,3†], *Qiuhong Huang*[1,2,3†], *Ling Chen*[1,2,3], *Peng Liu*[1,2,3], *Tianci Feng*[1,2,3], *Yongkang Ou*[1,2,3*] *and Yiqing Zheng*[1,2,3*]

[1] *Department of Otolaryngology-Head and Neck Surgery, Sun Yat-sen Memorial Hospital, Sun Yat-sen University, Guangzhou, China,* [2] *Institute of Hearing and Speech-language Science, Sun Yat-Sen University, Guangzhou, China,* [3] *Xinhua College Sun Yat-Sen University, Guangzhou, China*

OPEN ACCESS

Edited by:
Louis Murray Hofmeyr, Stellenbosch University, South Africa

Reviewed by:
Jose Antonio Lopez-Escamez, Junta de Andalucía de Genómica e Investigación Oncológica (GENYO), Spain
Abhineet Lall, Holy Spirit Hospital, India

***Correspondence:**
Yongkang Ou
ouyk@mail.sysu.edu.cn
Yiqing Zheng
yiqingzheng@hotmail.com

†These authors have contributed equally to this work and are co-first authors

Specialty section:
This article was submitted to Neuro-Otology, a section of the journal Frontiers in Neurology

Received: *06 December 2018*
Accepted: *15 March 2019*
Published: *09 April 2019*

Citation:
Tang X, Huang Q, Chen L, Liu P, Feng T, Ou Y and Zheng Y (2019) Clinical Findings in Patients With Persistent Positional Nystagmus: The Designation of "Heavy and Light Cupula". Front. Neurol. 10:326. doi: 10.3389/fneur.2019.00326

Objective: Direction-changing positional nystagmus (DCPN) had been observed as persistent horizontal apogeotropic and was considered as "cupulolithiasis or heavy cupula. " Recently, the concept of "light cupula" exhibiting persistent geotropic DCPN has been introduced. However, the light cupula is not systematically described, while the identification and diagnosis of "light cupula" should be improved. Here we investigated the underlying characteristics and therapeutic options designed to the "light" and "heavy" cupula, respectively; and summarized the clinical characteristics and therapeutic effect in the two groups.

Methods: A total of 359 cases with vertigo and bilateral DCPN were found in the supine roll test. Only 25 patients with persistent DCPN were enrolled and followed up. According to the direction of nystagmus, we further divided the patients into "heavy cupula" (apogeotropic) and "light cupula" (geotropic) groups. We compared the incidence, characteristics of nystagmus and the efficacy of repositioning maneuver in the two groups.

Results: Nine patients with persistent horizontal geotropic DCPN were confirmed as "light cupula," other 16 patients with persistent horizontal ageotropic DCPN were confirmed as heavy cupula. All 25 patients had null plane; the mean value and standard deviation of the null plane in light cupula and heavy cupula was 25.67 ± 9.31° and 27.06 ± 6.29°, respectively. The mean value and standard deviation of the termination plane in light cupula was 28.78 ± 10.00°, and 30.25 ± 6.53° in heavy cupula. There was no statistical significance between the two groups. We found that the direction of evoked nystagmus in the supine position was toward the intact side in light cupula, while in heavy

cupula, it was toward the lesion side. The null plane appeared on the lesion side. For light cupula patients, the effect was not obvious at Day-7 after the treatment, however, treatment for most heavy cupula patients were effective. All patients recovered after 30 days of treatment.

Conclusion: The null plane is crucial in determining the lesion side for light or heavy cupula. Although the short-term therapeutic effect of the light cupula is not as promising as the effect seen in heavy cupula, the long-term prognosis in both groups is comparable; with all patients recovered after 30 days of treatment.

Study design: This is a retrospective cohort study.

Keywords: DCPN, light cupula, heavy cupula, null plane, reposition maneuver

INTRODUCTION

Benign Paroxysmal Positional Vertigo (BPPV) is the most frequent episodic vestibular disorder. The BPPV horizontal semicircular canal recognizes two variants, conductolitiasis and cupulolithiasis, with the former being more frequently diagnosed (1). It has been reported that approximately 10–30% of BPPV originate from the horizontal semicircular canal (2). For patients with LSCC BPPV, direction-changing positional nystagmus (DCPN) is typically observed in a supine roll test. Moreover, LSCC BPPV can be divided into horizontal apogeotropic DCPN and geotropic DCPN. Generally, if the apogeotropic DCPN is persistent and lasts for more than 1 min, it is considered as cupulolithiasis or heavy cupula where the otolith debris may attach onto the cupula. In the clinics, the duration of the most of evoked geotropic nystagmus was less than 35 s and relatively gradually weakened or disappeared after positional examination, which is commonly considered as canalithiasis.

However, recently, a new concept of "light cupula" exhibiting persistent geotropic DCPN has emerged (3). "Light cupula" accounts for special geotropic positional vertigo where the geotropic DCPN is always persistent and lasts for more than 1 min but lacks latency or fatigability. Although the positional vertigo and nystagmus of light cupula manifests similarly to BPPV, whether or not it is a special type of BPPV is yet to be determined, and its pathogenesis is still unclear and is generally considered as a vestibular pathological phenomenon and theoretical hypothesis corresponding to clinic (4). In light cupula, the specific gravity of the cupula is lower than that of the surrounding endolymph, which either activates or inhibits hair cells under the cupula according to the head position in the gravitational plane (3, 5). Ichijo et al. hypothesized that the buoyancy traction migration of the ampulla ridge was caused when the low-density debris adhered to the ventral ridge of the affected side of the ampulla (6).

More interestingly, in both light cupula and heavy cupula, symptoms of patients with static DCPN disappeared on a certain plane when the head was rotated to a certain degree from the supine position. Therefore, this point is fixed as the null plane(7). The null plane, also known as "zero plane," refers to the certain plane where the nystagmus disappeared during the head turning from side to side.

The null plane is the most important characteristic for the diagnosis of light cupula. However, to date, the underlying pathogenesis of light cupula is unknown, and the standard of diagnosis and identification of this disease are confusing in clinical practice, with no available effective treatment options.

In this paper, we intend to explore the possibility in exacting the null plane in precise diagnosis of the two types of DCPN in order to suggest a standardized diagnosis and treatment option for both heavy and light cupula.

PATIENTS AND METHODS

Patients

In this study, a total of 359 cases of bilateral DCPN were found in the supine roll test in patients with vertigo who visited the outpatient department of Sun Yat-sen Memorial Hospital, Sun Yat-sen University from July 2016 to May 2017. All the patients' symptoms were recorded by Vesticon system 2000 infrared video ophthalmogram recording analyzer Videonystagmography (VNG) during the supine roll test. Spontaneous nystagmus was recorded in the sitting position both with and without visual fixation. Gaze-evoked nystagmus, and horizontal saccades and smooth pursuit were also evaluated.

From the 359 cases of bilateral DCPN, we analyzed the "heavy cupula" and "light cupula" patients according to the following parameters of nystagmus (**Tables 1**, **2**).

All patients had audiology and imaging examination. Audiology examination showed no obvious abnormality in all patients. Brain MRI was supplemented in all patients to exclude other vestibular and neurological diseases (8). The Dix-Hallpike test was routinely performed simultaneously to exclude

TABLE 1 | Inclusion criteria of light cupula.

(1) No nystagmus observed in the sitting position
(2) Presence of horizontal persistent nystagmus in the supine position
(3) Horizontal geotropic DCPN in the Supine Roll test
(4) The duration of DCPN is more than 1 min
(5) No latency or fatigability observed
(6) Presence of null plane

TABLE 2 | Inclusion criteria of heavy cupula.

(1) No nystagmus observed in the sitting position
(2) Presence of horizontal persistent nystagmus in the supine position
(3) Horizontal apogeotropic DCPN in the Supine Roll test
(4) The duration of DCPN is more than one min
(5) No latency or fatigability observed
(6) Presence of null plane

other positional nystagmus. No drugs affecting central nervous system excitability or inhibition was taken at least 24 h prior to examination.

All patients agreed to participate in the study were given a thorough explanation of the study and have given their written consent. The patients were followed up until the completion of the study. This study was approved by the Ethics Committee of Sun Yat-sen Memorial Hospital, Sun Yat-sen University.

METHOD

Examination Procedure and Nystagmus Analysis

The presence of horizontal DCPN was analyzed during the running of a series of head positions using Epley Omniax360, which is designed as automatic rotary instrument for the positional test and repositional maneuvers. The instrument can be used for head and body fixation of 360°. The software simulates the deflection angle of the head- semicircular canal on different planes for measuring and recording (**Figure 1**).

A series of head positions were done in the following order: U (sitting, head in normal position and straight forward); S (supine position, head elevated 30°); SL (supine position and then head turned max to the left); SR (supine position and then head turned max to the right); DHL (hanging head 45° to left); DHR (hanging head 45° to right); The evoked nystagmus were recorded using EPLEY OMNIAX360, and digitally stored in degrees per second. Spontaneous, positional, latency and duration of position-induced nystagmus were recorded. The nystagmus was observed for at least 2 min at each position, the maximal SPV was compared between turning to the right and left during the supine roll test.

Null plane: by slowly rotating the subject's head in the S position from left ear down to right ear down, a plane was sought where there was no vertigo and nystagmus and beyond which the nystagmus changed direction.

Treatment

The repositioning maneuvers to treat the patients with light cupula was done using the Barbecue method. In brief, Barbecue was performed as: (1) lie flat on the back from an upright position (2) turn to the left (or right) along the longitudinal axis body turn 90° (3) continue to turn to the same direction of 90 °(4) continue to turn again to the same direction of 90°(5) sit upright (**Figure 2A**).

The patients with heavy cupula were successfully converted to geotropic nystagmus by the Gufoni method. Gufoni was performed as: (1) the patient is sitting, rapidly lying on his or her affected side (2) head is quickly turned to the contralateral rotation 45° (3) sit upright, and then continue with by Barbecue method (**Figure 2B**).

Position tests were re-evaluated weekly after the repositioning maneuver. If positional vertigo still persisted in patients 1 week after treatment, the Barbecue method was performed again, with the supplementation of the Gufoni method if necessary. All patients were followed up every week and followed up for more than 1 month. The therapeutic effect of the repositioning maneuvers was evaluated at Day-7 and Day-30.

Statistical Analysis

SPSS19.0 statistical software was used for all data analysis. *T*-test was used for the comparison between two groups. All data were considered statistically significant if $p < 0.05$.

RESULTS

Characteristics of Nystagmus

From 359 patients, after considering the inclusion and exclusion criteria, we finally recruited 25 patients with persistent horizontal DCPN (25/359, 4.6%). The course of the patients lasted 1 to 13 weeks, among which 21 cases were primary and 4 cases were secondary, including three cases of sudden deafness and one case of Meniere's disease. Gender wise, 7 patients were male with the average age of 50.4 ± 14.7, and 18 female patients with the average age of 47.9 ± 7.

Of the 25 patients, 9 (3 males and 6 females) showed persistent geotropic DCPN with a null plane during the supine roll test and were diagnosed with light cupula; 16 (4 males and 12 females) showed persistent apogeotropic DCPN with a null plane and were diagnosed with heavy cupula. The mean value and standard deviation of the occurrence and termination angle of the null plane were recorded and shown in **Table 3**.

In our study, we found that the rotational angle from the ceasing of nystagmus to re-appearance was about 2° (**Figure 3**) and was designated as null plane. Vertigo and nystagmus also disappeared when the head was rotated to 180° from the null plane.

In the group of light cupula diagnosis, the stronger side of geotropic nystagmus (lesion side) on supine roll test was identified in 6 of 9 patients (67%). The null plane of the 6 patients all appeared on the side of the lesion. We were unable to identify the lesion side with supine roll test in the remaining 3 cases. In the group of heavy cupula diagnosis, the weaker side of apogeotropic nystagmus (lesion side) on supine head roll test was identified in 12 of 16 patients (75%). The null plane of the 12 patients were all on the side of the lesion. We were unable to identify the lesion side with supine roll test in the remaining 4 cases.

Molina, MI (9) reported that Canal paresis (CP) was observed in 25% (16/64) of cases with BPPV. In our study, vestibular function examination: Due to the requirements of patients' wishes, 15 in 25 patients underwent caloric testing after the

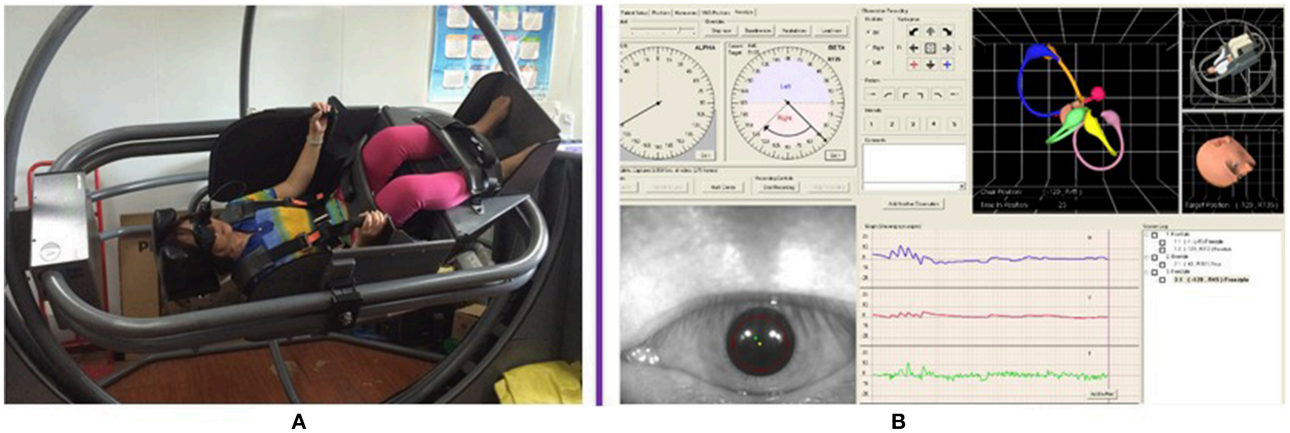

FIGURE 1 | Automatic rotary instrument Epley Omniax360 showed the position of the patient and the exact angle when body rotation. **(A)** The position of the patient. **(B)** The exact angle when body rotating from one plane to another as seen on the computer software.

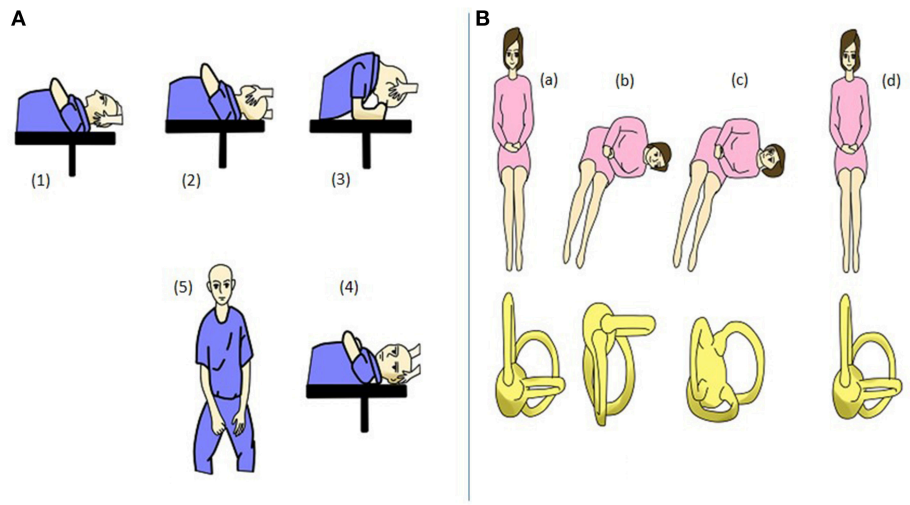

FIGURE 2 | Repositional maneuvers. **(A)** Barbecue maneuver. **(1)** Lie flat on back from an upright position. **(2)** Turn 90° to left (or right) along the longitudinal axis body. **(3)** Continue to turn 90° in the same direction. **(4)** Continue to turn 90° in the same direction. **(5)** Sit upright. **(B)** Gufoni maneuver. **(a,b).** Lie on affected side rapidly from upright position. **(c)** Rotate the head 45° quickly to the contralateral side. **(d)** Sit upright.

complete disappearance of positional nystagmus (5 cases with heavy cupula and 10 cases with light cupula). The results showed that 0 of 5 cases with heavy cupula had CP, while 2 of 10 cases with light cupula (20%) had CP, which was the same result reported by Hiroaki Ichijo (10).

In addition, we found that the direction of evoked nystagmus in the supine position in light cupula was toward the intact side, while in heavy cupula, the direction of evoked nystagmus in the supine position was toward to the lesion side. We also observed that direction of evoked nystagmus in the supine position in light cupula was in the contralateral side of the null plane location, while the direction of evoked nystagmus in the supine position in heavy cupula was at the same side of null plane. Therefore, another simple yet reliable method of differentiating these two groups is to determine the location of the affected area with a reference to the null plane.

TABLE 3 | Null plane occurrence and termination angle of 25 patients with horizontal DCPN(°).

Null plane	Light cupula	Heavy cupula	t	P^*
Occurrence angle	25.67 ± 9.31 (θ_1)	28.78 ± 10.00 ($\beta 1$)	0.109	2.782
Termination angle	27.06 ± 6.29 ($\theta_1 + \theta_2$)	30.25 ± 6.53 ($\beta 1 + \beta 2$)	0.086	3.226

**No statistically significance between the two groups(P > 0.05).*

Efficacy of Repositioning Maneuver Therapy

According to the intensity of nystagmus, the side of affected ear was determined. In the light cupula group: 2 cases were

on the left; 4 cases were on the right; and in heavy cupula group: 5 cases were on the left and 7 cases were on the right. The patients in both groups were treated with repositioning maneuver (using Barbecue, Gufoni and Barbecue method as described above). The therapeutic efficacy of this method was determined at Day-7 and Day-30 (**Figure 4**). The outcome was categorized as either complete resolution, partial/no resolution, or canal conversion. For those who were categorized as partial/no resolution or canal conversion, a follow up visit was arranged within 7 days, and these patients were treated with another cycle of appropriate procedure (as mentioned in Methodology). Successful repositioning was defined as complete resolution (CR) of any positional nystagmus. Residual dizziness (RD) was defined as a subjective report of partial or no response despite successful repositioning. Treatment failure (TF) was defined as partial/no resolution after four or more cycles of repositioning (11).

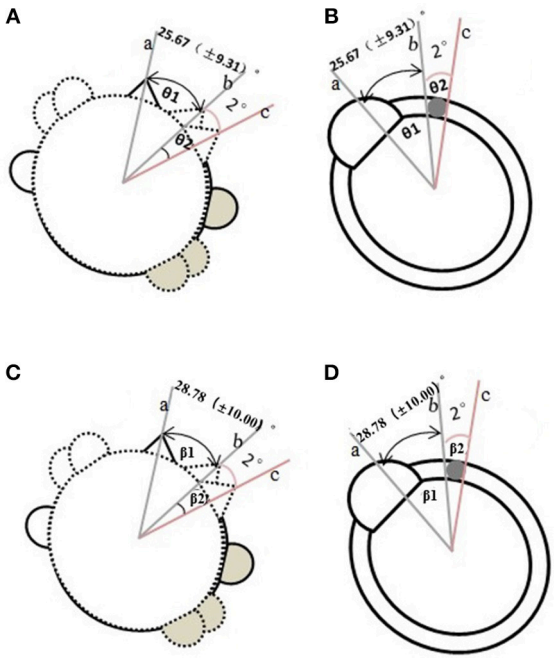

FIGURE 3 | Determination of the null plane in light cupula and heavy cupula. **(A)** The method in determining the null plane in the light cupula (view of head rotation). (A-a) the supine position. (A-b) the plane from the supine position turning to the affected side when the evoked-DCPN disappeared. (A-c) another plane that continued turning the head to the affected side when the evoked- DCPN re-appeared. (θ1 was the angle from line a to b. θ2 was the angle from b to c, termed as the null plane). **(B)** The view of semicircular canal corresponding to **(A)**. **(C)** The method in determining the null plane in the heavy cupula (view of head rotation). (C-a) The supine position. (C-b) the plane from the supine position turning to the affected side when the evoked-DCPN disappeared. (C-c) Another plane that continued turning the head to the affected side when the evoked-DCPN re-appeared. (θ3 was the angle from line a to b. θ4 was the angle from b to c, termed as the null plane). **(D)** The view of semicircular canal corresponding to **(C)**.

Since the intensity of nystagmus could not be used to determine the lesion side for some cases, t, the side of null plane was used to determine the side of lesion. The results showed that in light cupula group 2 cases were on the left, 1 case was on the right; and in heavy cupula group 3 cases were on the left and 1 case was on the right.

Seven days after the repositioning maneuvers of the light cupula, only 2 cases showed improvement (2/9; 22.2%), and the other 7 patients still complained of nystagmus and vertigo. 30 days after the repositioning maneuvers, all the light cupula patients were fully cured. Whereas, in the heavy cupula group, 81% (13/16) showed improvement 7 days after the repositioning maneuvers, with disappearance of vertigo and nystagmus. Position test were re-evaluated after 30 days, and the results indicated that only 1 case (6.3%) reported no improvement (**Table 4**), which indicated that the repositioning maneuvers were effective for the treatment of heavy cupula, while affirming the fact that the side of lesion could be correctly determined by using the null plane. The treatment effect of light and heavy cupula is consistent with the report by Hiruma et al. (12). Therefore, with this method, patients with cupulopathy would now have a better long-term prognosis.

DISCUSSION

Cupulolithiasis or "heavy cupula" was diagnosed when the duration of position-induced horizontal apogeotropic DCPN is persistent for more than 1 min. As the otolith debris is attached onto the cupula, the sensitivity of the cupula increases

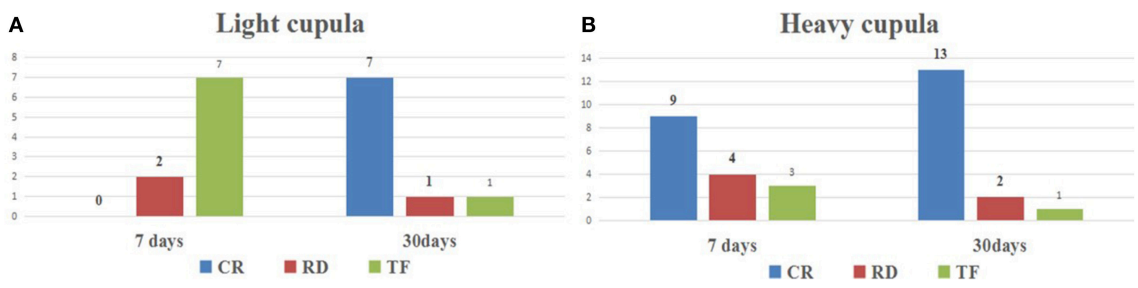

FIGURE 4 | The therapeutic effect of repositioning maneuver in the light cupula and heavy cupula. **(A)** The effect was evaluated at Day-7 days and Day-30 after repositioning maneuver in heavy cupula. **(B)** The effect was evaluated at Day-7 days and Day-30 after repositioning maneuver in light cupula. (CR, complete resolution; RD, residual dizziness; TF, treatment failure).

TABLE 4 | The therapeutic effect of repositioning maneuver in the light cupula and heavy cupula during follow-up after 7 days and 30 days.

	CR	RD	TF
7 DAYS-FOLLOW UP			
Light cupula	0	2	7
heavy cupula	9	4	3
30 DAYS-FOLLOW UP			
Light cupula	7	1	1
Heavy cupula	13	2	1

CR, complete resolution; RD, Residual dizziness; TF, Treatment failure.

when gravity changes. The formation of "heavy cupula" (7) was relative to the endolymphatic density. In a few of patients with apogeotropic DCPN, persistence within 1 min was thought to be caused by otolith flow to the anterior part of semicircular canal of the ampulla, which is also considered to be canalithiasis (13). However, canalithiasis was most commonly seen as geotropic DCPN for no more than 35 s, which the otolith debris may be located in the long arm of LSC. Recently, we found another type of persistent horizontal geotropic DCPN in the clinics, with more than 1 min persistence without latency or fatigability, which is defined as "light cupula." In 1956, Aschan et al. (14) described the nystagmus, which was called alcoholic nystagmus, a symptom appearing after drinking. It was found that this type of positional vertigo was similar to the horizontal semicircular cupulolithiasis, but it could not be explained by the theory of canalithiasis. Bergenius et al. (3) further proposed that the name "light cupula nystagmus" and further described its characteristics. The present study suggests that light cupula is not a disease but is a vestibular pathological phenomenon and theoretical hypothesis corresponding to BPPV pathogenesis.

The common characteristics observed in patients with light or heavy cupula where head position-induced persistent horizontal DPCN in the Supine roll test (2) are (i) Persistent horizontal nystagmus with fixed orientation in either lying, supine or prone position; (ii) symptoms that last for more than 1 min; (iii) no latency and fatigue observed; and (iv) the presence of null planes (15). We found that not all horizontal semicircular canal BPPV patients in supine position will have sustained fixed nystagmus and null plane. Whether this result is dependent on the location of otolith adhesion or not remains to be further studied. On the basis of a morphological study of squirrel monkeys and computed tomography (CT) of the human inner ear (7), the top of the horizontal canal cupula is leaning toward the lateral side, and therefore we can estimate that the angle between the sagittal plane and the horizontal canal cupula is approximately 20°. When the head is in bowing or leaning position, it further deflects the head toward the lesion side. This would lead to the formation of a parallel axis of the plane of gravity and the ampulla of the lesion. When the ampulla no longer deviates from the utricle, the nystagmus stops. This point is dictated as the null plane.

Previously, Kim et al. (16) and Ichijo et al. (7) reported that Supine roll test based on the head deflecting can be used to determine the null plane. Furthermore, Kim (15) reported that the head bending and elevation also could be used, which was similar to the Bow and Lean Test (BLT). He hypothesized that the nystagmus was evoked when the patient was sitting upright both in heavy and light cupula. The first null plane is determined when the nystagmus disappeared on the certain position when the head was bowed or leaned at a certain angle. Choi et al. (17) reported that the BLT were observed in 65% (48 of 74) of patients with LSCC canalolithiasis. In his study bowing nystagmus (BN) and leaning nystagmus (LN) were in the opposite direction in 38 (out of 48) patients and in the same direction in 10 (out of 48) patients. In our current study, the direction of BN by BLT was opposite to the LN in all patients. In the heavy cupula patients, BN was directed toward the intact side, and that LN was directed toward the lesion side. Vice versa, in the light cupula patients, BN beat toward the lesion side,and that LN beat toward the intact side.

When the head was supine and hanged 60°, then the nystagmus was evoked, while nystagmus symptom disappeared when the head was turned either to the left or right at 20°-30°. This is determined to be the second null plane. In our study, we did not find the evoked horizontal nystagmus that was previously reported by Kim et al. (16) in the sitting upright position, which was pseudo spontaneous nystagmus. It is speculated that there is a 30° difference between the upright head LSC and the horizontal plane, putting the ampullary at a higher position than the other semicircular canals, which in turn cause the light or heavy cupula to either deviate or move closer to the utricle (2). We also found that it was more difficult to find the null plane with the BLT method in clinical practice than that with the Supine Roll test, and it was hard to accurately measure the angle of head bend forward and backward. In this study, we found that nystagmus could be evoked in all the 25 patients on the supine position (Although in light cupula, the nystagmus was directed to the intact side, while in heavy cupula, the nystagmus was directed to the lesion side), while continued turning of the head at a 10°-38° to the lesion side could relieve the nystagmus syndrome. This null plane agrees with the angle reported by Kim et al. (13).

Kiyoshi Hiruma et al. (12) used infrared photogrammetry or Frenzel glasses and a protractor to measure the null plane angle in the heavy cupula or light cupula. Although this method was comparatively easy, the correct posture of patient was too difficult to control. Here we used the EPLEY OMNIAX automatic positional vertigo diagnosis instrument (Vesticon company, USA), the angle is directly displayed on the computer software along the angle of the head—body axis plane, which can be displayed and measured accurately by the computer. Our results showed that there was no significant difference in the occurrence and termination angle of null plane between the light cupula and the heavy cupula.

According to the Committee of the Bárány Society in 2017 (2), the diagnostic criteria for BPPV are as follows: In the supine roll test, patients with geotropic nystagmus usually display stronger intensity—when the head turned to the affected ear, while in patients with apogeotropic nystagmusis, stronger intensity was observed when the head turned away from the lesion ear. In this study, we had 25 patients with persistent

DCPN. Among them, there were 9 cases with light cupula and 16 cases with heavy cupula. In the light cupula group, the remaining 3 cases were unable to identify the lesion side with supine head-roll test, while in the heavy cupula group, there were 4 cases. In the process of null plane detection, we found that if nystagmus direction in the supine position was consistent with the null plane side, which was heavy cupula, and on the contrary, was light cupula. The null planes all appeared on the lesion side—this can be mutually authenticated with Supine roll test. In the vestibular function examination, CP did not appear in the heavy cupula group during the caloric testing, while 20% of the light cupula group had CP on the lesion side.

The patients with heavy cupula were treated with repositioning maneuvers. After Gufoni maneuvers (10 cases), 62% cases were converted into geotropic nystagmus, and then were further treated with the Barbecue method. The efficacy rate of short-term (1 week) and long-term (1 month) were 75 and 94% respectively. Otoliths in the cases with heavy cupula successfully converted may adhered to the ampulla rather than the utricle. Therefore, we thought that null plane can help the light and heavy cupula to determine the lesion side. Accurate localization depends on the efficacy of repositioning maneuvers.

The success rate of light cupula repositioning maneuvers is low, which corresponds to the result reported by previous studies (12, 15). Park et al. (18) reported that intratympanic steroid injection can be used in light cupula, however, there was no significant different at 1 week follow-up when comparing to the other treatment, perhaps due to the unclear pathophysiology of the light cupula. To date, there are three major hypotheses of the above phenomenon: (1) a light cupula is caused by a decrease in the density of the cupula (14) (2) an increase in the specific gravity of the endolymph leads to a decrease in the relative density of the cupula (6, 12) (3) light debris attached to the cupula gives rise to a light cupula (3). In support of the last hypothesis, Kim et al. (16) suggested the possibility that light debris were water-soluble macromolecules, such as proteoglycans, in the endolymph (16).

LIMITATIONS

Caloric tests were only performed in 10 patients due to the wishes of patients. Although the video impulse test is known to be more sensitive to define vestibular function, we could not carry out this experiment due to the lack of instrument.

CONCLUSION

Taken together, this study elucidated a simple yet accurate method in determining light and heavy cupula; depending on the side of supine position and null plane. Same-side supine position and null plane indicated heavy cupula while opposite-side supine position and null plane indicated light cupula. Although it is known that the side of null plane is always located on the side of lesion, in some cases, the lesion side may not be easy to determine, as it is difficult to be detected via nystagmus intensity. In this situation, the null plane is a very effective method to identify the lesion side of light cupula or heavy cupula. Moreover, the caloric testing is also another way for light cupula to identify the lesion side.

AUTHOR CONTRIBUTIONS

XT and QH analyzed the data and drafted the manuscript. LC, PL, and TF collected candidate information. YO and YZ edited the manuscript.

FUNDING

This work was supported by a grant from the National Natural Science Foundation of China (81400456) to QH and Guangdong Province Science and Technology Project (2014A020212097) to YO.

REFERENCES

1. Perez-Vazquez P, Franco-Gutiérrez V, Soto-Varela A, Amor-Dorado JC, Martín-Sanz E, Oliva-Domínguez M, et al. Practice guidelines for the diagnosis and management of benign paroxysmal positional vertigo otoneurology committee of Spanish otorhinolaryngology and head and neck surgery consensus document. *Acta Otorrinolaringol Esp.* (2018) 69:345–66. doi: 10.1016/j.otoeng.2018.10.002
2. von Brevern M, Bertholon P, Brandt T, Fife T, Imai T, Nuti D, et al. Benign paroxysmal positional vertigo: diagnostic criteria consensus document of the committee for the classification of vestibular disorders of the barany society. *Acta Otorrinolaringol Esp.* (2017) 68:349–60. doi: 10.1016/j.otorri.2017.02.007
3. Bergenius, J, Tomanovic T. Persistent geotropic nystagmus–a different kind of cupular pathology and its localizing signs. *Acta Otolaryngol.* (2006) 126:698–704. doi: 10.1080/00016480500475609
4. Imai T, Matsuda K, Takeda N, Uno A, Kitahara T, Horii A, et al. Light cupula: the pathophysiological basis of persistent geotropic positional nystagmus. *BMJ Open.* (2015) 5:e006607. doi: 10.1136/bmjopen-2014-006607
5. Hiruma K, Numata T. Positional nystagmus showing neutral points. *Otorhinolaryngol Relat Spec.* (2004) 66:46–50. doi: 10.1159/000077234
6. Ichijo H. Persistent direction-changing geotropic positional nystagmus. *Eur Arch Otorhinolaryngol.* (2012) 269:747–51. doi: 10.1007/s00405-011-1700-1
7. Ichijo H. Neutral position of persistent direction-changing positional nystagmus. *Eur Arch Otorhinolaryngol.* (2016) 273:311–6. doi: 10.1007/s00405-014-3487-3
8. Huh YE, Kim JS. Patterns of spontaneous and head-shaking nystagmus in cerebellar infarction: imaging correlations. *Brain.* (2011) 134(Pt 12):3662–71. doi: 10.1093/brain/awr269
9. Molina MI, López-Escámez JA, Zapata C, Vergara L. Monitoring of caloric response and outcome in patients with benign paroxysmal positional vertigo. *Otol Neurotol.* (2007) 28:798–800. doi: 10.1097/MAO.0b013e318067e322
10. Ichijo H. Caloric testing in patients with heavy or light cupula of the lateral semicircular canal. *Laryngoscope Investig Otolaryngol.* (2016) 1:163–8. doi: 10.1002/lio2.39
11. Chen CC, Cho HS, Lee HH, Hu CJ. Efficacy of repositioning therapy in patients with benign paroxysmal positional vertigo and preexisting central neurologic disorders. *Front Neurol.* (2018) 9:486. doi: 10.3389/fneur.2018.00486
12. Hiruma K, Numata T, Mitsuhashi T, Tomemori T, Watanabe R, Okamoto Y. Two types of direction-changing positional nystagmus with neutral points. *Auris Nasus Larynx.* (2011) 38:46–51. doi: 10.1016/j.anl.2010.07.004

13. Kim CH, Choi JM, Jung HV, Park HJ, Shin JE. Sudden sensorineural hearing loss with simultaneous positional vertigo showing persistent geotropic direction-changing positional nystagmus. *Otol Neurotol.* (2014) 35:1626–32. doi: 10.1097/MAO.0000000000000457
14. Aschan G, Bergstedt M, Goldberg L, Laurell L. Positional nystagmus in man during and after alcohol intoxication. *Q J Stud Alcohol.* (1956) 17:381–405.
15. Kim CH, Shin JE, Kim YW. A new method for evaluating lateral semicircular canal cupulopathy. *Laryngoscope.* (2015) 125:1921–5. doi: 10.1002/lary.25181
16. Kim CH, Kim MB, Ban JH. Persistent geotropic direction-changing positional nystagmus with a null plane: the light cupula. *Laryngoscope.* (2014) 124:E15–9. doi: 10.1002/lary.24048
17. Choi S, Choi HR, Nahm H, Han K, Shin JE, Kim CH. Utility of the bow and lean test in predicting subtype of benign paroxysmal positional vertigo. *Laryngoscope.* (2018) 128:2600–4. doi: 10.1002/lary.27142
18. Park JS, Kim SY, Kim MB. Effect of intratympanic steroid injection in light cupula. *Acta Otolaryngol.* (2018) 138:769–74. doi: 10.1080/00016489.2018.1467135

Conflict of Interest Statement: The authors declare that the research was conducted in the absence of any commercial or financial relationships that could be construed as a potential conflict of interest.

frontiers in Neurology

ORIGINAL RESEARCH
published: 13 November 2019
doi: 10.3389/fneur.2019.01190

Clinical Characteristics and Risk Factors for the Recurrence of Benign Paroxysmal Positional Vertigo

Cui Ting Zhu[1,2,3], *Xing Qquan Zhao*[1,2,3]*, *Yi Ju*[1,2,3]*, *Yan Wang*[1,2,3], *Mei Mei Chen*[1,2,3] and *Yu Cui*[1,2,3]

[1] Department of Neurology, Beijing Tiantan Hospital, Capital Medical University, Beijing, China, [2] China National Clinical Research Center for Neurological Diseases, Beijing, China, [3] Center of Stroke, Beijing Institute for Brain Disorders, Beijing, China

OPEN ACCESS

Edited by:
Toshihisa Murofushi,
Teikyo University, Japan

Reviewed by:
Tjasse Bruintjes,
Gelre Hospitals, Netherlands
Andrés Soto-Varela,
Complejo Hospitalario Universitario de Santiago, Spain

***Correspondence:**
Xing Qquan Zhao
zxq@vip.163.com
Yi Ju
juyi1226@vip.163.com

Specialty section:
This article was submitted to Neuro-Otology, a section of the journal Frontiers in Neurology

Received: 07 July 2019
Accepted: 25 October 2019
Published: 13 November 2019

Citation:
Zhu CT, Zhao XQ, Ju Y, Wang Y, Chen MM and Cui Y (2019) Clinical Characteristics and Risk Factors for the Recurrence of Benign Paroxysmal Positional Vertigo. Front. Neurol. 10:1190. doi: 10.3389/fneur.2019.01190

Benign paroxysmal positional vertigo (BPPV) manifests itself as a paroxysm of vertigo and nystagmus lasting several seconds, which is self-limiting. The clinical characteristics and risk factors for the recurrence of BPPV in different ages have not yet been investigated.

Materials and Methods: A retrospective observational study was conducted in the Department of Neurology in Beijing Tiantan Hospital from July 2009 to June 2015. The study included 1,012 patients aged 18–93 years. All patients received the definitive diagnosis and canalith repositioning maneuvers treatment and finally accomplished follow-up. Demographic variables, potential recurrence risk factors, neurological examination, and laboratory indexes were assessed.

Data Analyses: The *t*-test or chi-squared test was first performed for group comparison, then logistic regression analysis was used to investigate the risk factors of BPPV recurrence.

Results: The 1-year recurrence rates of BPPV patients after reposition maneuvers were, respectively, 22.79% (aged 18–45 years), 23.92% (aged 45–60 years), 28.89% (over 60 years). The recurrence rates among the three groups have no statistically significant difference. Logistic regression analysis shows that women BPPV patients have more recurrence risks than do men. Ménière's disease (odds ratio = 6.009, 95% confidence interval: 2.489–14.507, $p < 0.001$), hypertension (odds ratio = 1.510, 95% confidence interval: 1.095–2.084, $p = 0.012$), migraine (odds ratio = 2.534, 95% confidence interval: 1.164–5.516, $p = 0.019$), and hyperlipemia (odds ratio = 1.419, 95% confidence interval: 1.024–1.968, $p = 0.036$) were risk factors for the recurrence of BPPV in patients.

Conclusion: We conclude that Ménière's disease, hypertension, migraine, and hyperlipemia may be independent risk factors for the recurrence of BPPV in patients, but aging does not increase the recurrence risk.

Keywords: benign paroxysmal positional vertigo, cerebrovascular risk factors, recurrence rate, young, older

INTRODUCTION

The objective of this study was to investigate the clinical characteristics and risk factors for the recurrence of benign paroxysml positional vertigo (BPPV) in young, middle-aged, and older patients to provide a guideline for developing effective prevention strategies for BPPV.

BPPV, a common peripheral vestibular disorder, occurs in nearly 17% of patients with dizziness or vertigo (1). It is caused by abnormal stimulation of the cupula in any of the three semicircular canals. Typically, BPPV manifests itself as a paroxysm of vertigo and nystagmus lasting several seconds, which is self-limiting (2). Currently, canalith repositioning maneuvers (CRM) are the mainstream treatment for BPPV, which have been successful in improving symptoms. The recurrence rate of BPPV after treatment is high, which results in anxiety and poor quality of life in patients. Vertigo and dizziness increase the risk of falls because of the imbalance caused by impaired movement and space-directed damage. Therefore, understanding the risk factors for the recurrence of BPPV is imperative for better symptom and relapse prevention.

Previous studies showed that cerebrovascular risk factors influenced BPPV recurrence and severity of symptoms (3). In Taiwan (4), a nationwide population study found that BPPV increased the risk of ischemic stroke. It was also reported that BPPV patients with hypertension and hyperlipidemia were at a higher risk of symptom recurrence (5). One observational study reported that patients with BPPV had a higher prevalence of hypertension and coronary artery disease (4). Another study showed that carotid plaque was a risk factor of the peripheral vestibular disorder (6). It has also been found that hyperglycemia and hyperinsulinemia are risk factors for the recurrence of BPPV (7). Normal aging is accompanied by vascular changes, such as the formation of utriculus that causes hypoperfusion of inner circulation, giving rise to otolith formation. The internal auditory artery and anterior vestibular artery are branches of the anterior inferior cerebellar artery. An ischemic attack of the transitory artery is likely to cause peripheral vestibulopathy (8). However, these risk factors are highly heterogeneous and thus not clearly understood. Therefore, further studies are required to explore how cerebrovascular risk factors influence the recurrence of BPPV.

In addition, studies have shown that symptoms and prognosis differ between young and old BPPV patients. A population study in Germany revealed that almost 1.1 million adults suffered from BPPV each year (9). It was reported that the prevalence of BPPV in the young adults was 9% (10). One study found that older BPPV patients receiving treatment experience residual dizziness, characterized by subjective dizziness and imbalance without episodic nystagmus (11). Residual dizziness may lead to nervousness, panic, or insomnia and negatively affect the quality of life of patients (12). The incidence of psychogenic disorder is influenced by age, being prevalent in individuals over 65 years old. It is well-known that old age is accompanied by a combination of comorbidities. So far, the risk factors for recurrence of BPPV in young patients have not been sufficiently characterized. BPPV is largely a secondary outcome of inner ear disorders such as Ménière's disease, migraine, and sudden deafness (13). Therefore, in this retrospective study, we aimed to (1) investigate the risk factors for BPPV in young, middle-aged, and older patients separately; and (2) explore the association between cerebrovascular risk factors and BPPV recurrence. We hypothesized that the recurrence of BPPV in young, middle-aged, and older BPPV patients may be modulated by different cerebrovascular risk factors.

MATERIALS AND METHODS

Patients and Procedures

The study was performed according to the Declaration of Helsinki guidelines, and written informed consent was obtained from all participants. The patients in our study only underwent standard treatment without additional interventions for research purposes, so no formal ethics approval was required. In total, 1,046 patients were retrospectively enrolled in this study. The patients received the definitive diagnosis and CRM treatment, and finally got cured. Finally, 1,012 patients accomplished follow-up in the Department of Neurology, Beijing Tiantan Hospital from July 2009 to June 2015, with 3.3% lost rate of follow-up (Details in **Supplementary Figure 1**). After enrollment, the patients were divided into the young group (aged 18–45 years), middle-aged group (aged 45–60 years), and the older group (over 60 years). The patients who met the criteria were enrolled: (1) Vertigo attack due to changes in head position, with a positive Dix-Hallpike or Roll test; (2) Patients were suitable for CRM treatment and finally got cured; (3) Patients who signed the informed consent and accepted a telephone follow-up. Those with the following conditions were excluded: (1) Patients who did not complete position test and CRM; (2) Patient information was incomplete; (3) Patients who did not complete follow-up.

Treatment and Follow-Up

Following the clinical practice guideline of BPPV established by the American Academy of Otolaryngology-Head and Neck Surgery Foundation (14), the patients were treated with the CRM. The Dix-Hallpike and roll tests were conducted on patients. Patients with abnormal test results were diagnosed with BPPV. Patients with posterior semicircular canal otolith were treated with Epley or Semont maneuver. The Lempert or Barbecue maneuver and the Gufoni method (to the healthy side) were performed for horizontal geotropic nystagmus. The calcium carbonate debris was located in the long arm of the semicircular canal. Horizontal apogeotropic nystagmus: Gufoni maneuver (to the affected side) or modified Semont maneuver was also used. The calcium carbonate debris was attached to the cupulolithiasis. The treatments for multiple BPPV were chosen on the basis of severity of vertigo and nytagmus, and different semicircular canal-type maneuvers were applied. The success of the treatment was defined as the absence of vertigo and nystagmus on positional testing (15). One week after CRM treatment, the BPPV patients returned to the hospital for efficacy evaluation. Recurrence was defined as: After successful treatment for 1 week; (1) The patients had similar positional vertigo as the primary attack; (2) a positive positional nystagmus test was confirmed.

Measurement Indexes

The patients were assessed in terms of demographic variables, potential recurrent risk factors, neurological examination, and laboratory indexes. A questionnaire was used to record gender, recurrence times (one, two, or more than three), Ménière's disease, sudden deafness, migraine, cerebrovascular risk factors (hypertension, hyperlipemia, diabetes, coronary heart disease, arterial plaque) and cerebral infarction as related data. We identified the etiology of BPPV as idiopathic, various disorders of the inner ear, vestibular neuronitis (patients with a history of acute vestibulopathy on the affected side), prolonged recumbent position, or traumatic. Patients were followed up 1 year after the treatment to record the recurrence data via telephone, which was carried out by a postgraduate clinician. During the assessment, hypertension (ICD-10 code E10.X01), hyperlipemia (ICD-10 code E78.501), diabetes (ICD-10 code E11.951), and coronary heart disease (ICD-10 code I 25.101) were defined according to International Classification of Diseases 10 (ICD-10) (16). Secondary BPPV was defined as the presence of a history of acute or chronic inner ear disease or unilateral vestibular loss within 1 year prior to this study (13). Ménière's disease was defined according to the American Academy of Otolaryngology-Head and Neck Surgery Foundation (1995) guideline (17). Migraine was diagnosed on the basis of the International Headache Society (IHS) criteria (18). Sudden deafness was defined as a history of unilateral sensorineural hearing loss with sudden onset, without other prior otological histories (19).

Data Analysis

Patients were divided into three different age groups (young patients 18–45 years; middle-aged patients 45–60 years; older patients over 60 years). Statistical significance between the young, middle-aged, and older BPPV patients was determined using a *t*-test, chi-squared test, or Fisher's exact test. When $p < 0.05$, the differences between the three groups were deemed to be statistically significant. Multivariable logistic regression was performed to identify the recurrence risk factors in all of the patients. All statistical analyses were performed using the IBM SPSS statistical software version 22.0.

RESULTS

Demographic Profile

In total, 1,012 BPPV patients accepted definitive diagnosis, CRM treatment, and finally accomplished follow-up in the Department of Neurology, Beijing Tiantan Hospital from July 2009 to June 2015. There were 208 young patients (80 male and 128 female), 489 middle-aged patients (146 male and 343 female), and 315 older patients (90 male and 225 female). The average ages of the three groups of patients were 37.10 ± 6.47, 53.63 ± 4.18, and 67.70 ± 5.88 years, respectively (**Table 1**). The sex ratio difference between the three groups was not statistically significant. The median disease duration of BPPV in the young group was 23.93 ± 46.21 days, in the middle-aged group 40.38 ± 20.78 days, and in the older group 30.90 ± 57.66 days, with no statistically significant difference ($p = 0.158$) (Details in **Supplementary Figure 1**). We collected the differential type of semicircular canal: posterior canal 155 young patients, 368 middle-aged patients, and 248 older patients; horizontal canal 53 young patients, 121 middle-aged patients, and 67 older patients. Multiple semicircular canal BPPV in the three groups respectively was 9, 21, and 12 patients. In the young group, 47 patients recurred 1 year after CRM treatment, and 28 patients (59.57%) suffered one episode of recurrence; six patients (12.76%) suffered two episodes of recurrence; and 13 patients (27.67%) suffered more than three episodes. In the middle-aged group, 117 patients recurred 1 year after CRM treatment, and 61 patients (52.13%) suffered one episode of recurrence; 17 patients

TABLE 1 | Baseline characteristics of the three groups ($N = 1,012$).

Variables	18–45 years ($n = 208$)		45–60 years ($n = 489$)		Over 60 years ($n = 315$)		*p*-value
	Total (*N*)	Column (%)	Total (*N*)	Column (%)	Total (*N*)	Column (%)	
Age, years (mean ± SD)	37.10 ± 6.47		53.63 ± 4.18		67.70 ± 5.88		–
Disease duration (mean ± SD)	23.93 ± 46.21		40.38 ± 20.78		30.90 ± 57.66		0.158
Male	80	38.64	146	29.85	106	33.65	0.074
1-year recurrence	47	22.79	117	23.92	91	28.89	0.195
MD	1	0.04	10	2.04	13	4.12	0.024
Sudden deafness	0	0.00	4	2.22	7	0.08	0.045
Migraine	9	0.43	15	3.06	5	1.58	0.187
Hypertension	20	9.61	130	26.58	126	40.00	<0.001
Hyperlipemia	20	9.61	135	27.60	111	35.23	<0.001
Diabetes	11	5.28	36	7.36	40	12.69	0.005
CHD	0	0.00	22	4.49	35	11.11	<0.001
Arterial plaque	8	3.84	109	22.29	141	44.76	<0.001
CI	3	1.44	10	2.04	30	9.52	<0.001

SD, standard deviation; MD, Ménière's disease; CHD, coronary heart disease; CI, cerebral infarction.

(14.52%) suffered two episodes of recurrence; and 39 patients (33.35%) suffered more than three episodes. In the older group, 91 patients recurred 1 year after CRM treatment, and 53 patients (58.24%) suffered one episode of recurrence; 12 patients (13.18%) suffered two episodes of recurrence; and 26 patients (28.58%) suffered more than three episodes. The recurrence rate of BPPV 1 year after CRM treatment was 22.79% in young patients, 23.92% in middle-aged patients, and 28.57% in older patients, showing no statistically significant difference ($p = 0.195$). The prevalence of Ménière's disease, sudden deafness, hypertension, hyperlipemia, coronary heart disease, diabetes, arterial plaque, and cerebral infarction in young group was significantly lower than middle-aged and older aged group.

Recurrence Risk Factor Analysis

There was no statistically significant difference of recurrence rate in the three groups. We performed both univariate and multivariable analyses to identify the possible recurrence risk factors for BPPV in all of the patients. The results were shown in **Table 2**. We chose gender, sudden deafness, Ménière's disease, migraine, and cerebrovascular risk factors as recurrence-related variables. It showed that BPPV recurrence was associated with gender, Ménière's disease, migraine, sudden deafness, hyperlipemia, and hypertension (**Table 2**). Multivariable logistic regression revealed that Ménière's disease (odds ratio = 6.009, 95% confidence interval: 2.489–14.507, $p < 0.001$), hypertension (odds ratio = 1.510, 95% confidence interval: 1.095–2.084, $p = 0.012$), migraine (odds ratio = 2.534, 95% confidence interval: 1.164–5.516, $p = 0.019$), and hyperlipemia (odds ratio = 1.419, 95% confidence interval: 1.024–1.968, $p = 0.036$) may be risk factors for the recurrence of BPPV (**Table 3**).

TABLE 2 | Univariate analysis of BPPV recurrence-related risk factors.

Variables	Recurrence		Odds ratio	95% CI	*p*-value
	Yes	No			
	N (%)	*N* (%)			
Gender			0.679	0.495–0.931	0.016
Male	68 (26.67)	264 (34.87)			
Female	187 (73.33)	493 (65.13)			
Ménière's disease			6.268	2.649–14.828	<0.001
Yes	16 (6.27)	8 (1.05)			
No	239 (93.73)	749 (98.95)			
Migraine			2.874	1.367–6.039	0.005
Yes	14 (5.49)	15 (1.98)			
No	241 (94.51)	742 (98.02)			
Sudden deafness			3.619	1.095–11.962	0.035
Yes	6 (2.35)	5 (0.66)			
No	249 (97.65)	752 (99.34)			
Hypertension			1.631	1.201–2.215	0.002
Yes	89 (34.90)	187 (24.70)			
No	166 (65.10)	570 (75.30)			
Hyperlipemia			1.549	1.136–2.112	0.006
Yes	84 (32.94)	182 (24.04)			
No	171 (67.06)	575 (75.96)			
Diabetes			1.143	0.698–1.871	0.596
Yes	24 (9.41)	63 (8.32)			
No	231 (90.59)	694 (91.68)			
CHD			1.167	0.643–2.119	0.611
Yes	16 (6.27)	41 (5.41)			
No	239 (93.73)	716 (94.59)			
Arterial plaque			0.728	0.531–0.997	0.142
Yes	77 (30.19)	181 (23.91)			
No	178 (69.81)	575 (76.09)			
CI			1.118	0.543–2.302	0.762
Yes	10 (3.92)	33 (4.35)			
No	245 (96.08)	724 (95.65)			

CHD, coronary heart disease; CI, cerebral infarction.

DISCUSSION

This study shows that BPPV patients with Ménière's disease have 6.009-fold higher risk of recurrence compared to those without Ménière's disease. BPPV patients with hypertension have a 1.510-fold higher risk of recurrence compared to those without hypertension. The analysis also reveals that BPPV patients with migraine have a 2.534-fold higher risk of recurrence compared to those without migraine. Previous studies found that comorbidity with hypertension increased the risk of BPPV recurrence (20). Another study showed that the occurrence of hypertension and diabetes in BPPV patients influenced the prognosis of the residual symptoms (21). A recent meta-analysis reported that Ménière's disease was a risk factor for the recurrence of BPPV after otolith reduction (22). This is in agreement with the findings of this study. The prevalence of vertigo increases with age, being higher in individuals over 60 years old (23). The function of semicircular canals and otoconia gradually decreases due to age-related demineralization. This may cause blood vessel and circulation abnormalities leading to obstruction of inner ear circulation. Vascular stress of the anterior vestibular artery may reduce blood flow to the labyrinth and hence cause serious damage to the macula and otoconia detachment (24). Ballester reported that vertigo in BPPV patients with Ménière's disease required longer time to recover (25). This phenomenon may also be influenced by the balance disorder between endolymphatic absorption and utricle (26). This study shows that 10.3% of BPPV occurred as a secondary effect of impaired inner ear function, 50.7% due to sudden deafness, and 28.9% due to Ménière's disease (13).

Studies have reported that cerebrovascular disease is a risk factor for the recurrence of BPPV. In the present study, analysis of cerebrovascular disease risk factors in BPPV patients reveals that patients with hyperlipemia and hypertension may have a higher recurrence rate. A study found that the recurrence

TABLE 3 | Multivariate analysis of BPPV patients during 1-year follow-up.

Variables	Odds ratio	95% Confidence interval	*p*-value
Gender	0.714	0.517–0.986	0.041
Ménière's diseases	6.009	2.489–14.507	<0.001
Sudden deafness	1.858	0.511–6.760	0.347
Hypertension	1.510	1.095–2.084	0.012
Migraine	2.534	1.164–5.516	0.019
Hyperlipemia	1.419	1.024–1.968	0.036

rate increased with the number of comorbidities of BPPV (27). Multiple systemic diseases can cause the labyrinth disorder leading to more frequent otolith detachment, which prolongs the recovery (28). Hyperinsulinism may disrupt inner ear hemostasis and alter the ionic and metabolic characteristics of the stria vascularis (7). On the other hand, hyperglycemia increases vascular resistance by inhibiting nitric oxide-related vasodilation. Therefore, a combination of hypertension and diabetes may lead to tissue hypoxia and cochleovestibular degeneration (5). Arterial plaque indicates early atherosclerosis. This may trigger intravascular thrombosis and cause hypoperfusion of the inner circulation (6). Previously, it was reported that residual symptoms in BPPV patients suffering from hypertension, diabetes, heart disease, and ischemic encephalopathy did not heal without treatment. Frequent recurrence episodes of BPPV may affect patients' quality of life. Therefore, early recognition and prompt management of BPPV are important in resolving further discomforts.

This study shows that the 1 year recurrence rate in young patients is 22.79%. There may be some unrecognized symptoms in young adults. Previous research has not largely focused on exploring the risk factors in a young population. Here, we divided the patients into young, middle-aged, and older patients and compared their features. Although the recurrence rate among the three groups was not statistically different, the older patients with a combination of cerebrovascular comorbidities need more attention.

Our study indicates that the 1-year recurrence rate in older BPPV patients is 28.89%. This suggests that the incidence rate of residual dizziness is 61%, which persists beyond 2 weeks even after successful treatment of BPPV with CRM. This may increase unsteadiness and risk of falls (11). The severest damage caused by BPPV is falls-related injuries and disability. Falls may lead to high morbidity and mortality in older patients, and the morbidity rate ranges from 13 to 38% (29). BPPV is the most common cause of vertigo disorders and is a well-recognized risk factor for falls. The proportion of aging population has been increasing in many countries. Therefore, prevention of falls in older people requires the development of more effective strategies. A timed Get-up-and-Go test which can be performed in <10 s has been recommended (30). Therefore, considering the benefits and harms caused by falls risk screening in older BPPV patients, it is necessary to implement early detection, diagnosis, and treatment. Otherwise, exercise and physical therapies can facilitate timely prevention and clinical intervention.

This study has the following limitations. First, our study reviewed recovery patients that may omit refractory cases, especially those with anterior semicircular canal BPPV. Second, some potential risk factors such as vestibular migraine, osteoporosis, or psychological factors were not available in this database. Due to incompleteness of patients' information, the occurrence of head trauma was not assessed in this study. In addition, we grouped BPPV patients into three groups according to age, which may cause comparison bias. We advocate for further studies to provide further detailed insight into the mechanisms of BPPV recurrence.

CONCLUSION

In conclusion, we find that Ménière's disease, migraine, hyperlipemia, and hypertension exhibit a higher risk of recurrence compared to age-matched patients without these diseases. This retrospective study indicates the association of BPPV recurrence and cerebrovascular risk factors and provides some insight into the falls risk evaluation and early prevention of older patients with BPPV.

DATA AVAILABILITY STATEMENT

The datasets generated for this study are available on request to the corresponding author.

ETHICS STATEMENT

Ethical review and approval was not required for the study on human participants in accordance with the local legislation and institutional requirements. The patients/participants provided their written informed consent to participate in this study.

AUTHOR'S NOTE

The abstract of this paper was presented at the XXX Bárány meeting in Uppsala as a poster presentation with interim findings.

AUTHOR CONTRIBUTIONS

CZ conceived the study and design, conducted the experiment, and wrote the manuscript. XZ provided the data analysis, preparation of manuscript, and revised this manuscript. YJ conceived the study and design and edited the manuscript. YW, MC, and YC conducted acquisition of subjects and interpretation of data.

FUNDING

This work was supported by Accuracy and Refinement of Evaluation of Oculomotor System in Posterior Circulation Ischemia based on HINTS (2016-2-2042) from Beijing Tiantan Hospital.

ACKNOWLEDGMENTS

We thank all of the members of the Department of Neurology, Beijing Tiantan Hospital, Capital Medical University.

SUPPLEMENTARY MATERIAL

The Supplementary Material for this article can be found online at: https://www.frontiersin.org/articles/10.3389/fneur.2019.01190/full#supplementary-material

Supplementary Figure 1 | The flow chart.

REFERENCES

1. Parnes LS, Agrawal SK, Jason A. Diagnosis and management of benign paroxysmal positional vertigo (BPPV). *CMAJ*. (2003) 169:681–93. doi: 10.1620/tjem.201.127
2. Ferber-Viart C, Dubreuil C, Vidal PP. Effects of acetyl-DL-leucine in vestibular patients: a clinical study following neurotomy and labyrinthectomy. *Audiol Neurotol*. (2009) 14:17–25. doi: 10.1159/000148206
3. Chan KC, Tsai YT, Yang YH, Chen PC, Chang PH. Osteoporosis is associated with increased risk for benign paroxysmal positional vertigo: a nationwide population-based study. *Arch Osteopor*. (2017) 12:106. doi: 10.1007/s11657-017-0403-7
4. Kao CL, Cheng YY, Leu HB, Chen TJ, Ma HI, Chen JW, et al. Increased risk of ischemic stroke in patients with benign paroxysmal positional vertigo: a 9-year follow-up nationwide population study in Taiwan. *Front Aging Neurosci*. (2014) 6:108. doi: 10.3389/fnagi.2014.00108
5. D'Silva LJ, Staecker H, Lin J, Sykes KJ, Phadnis MA, McMahon TM, et al. Retrospective data suggests that the higher prevalence of benign paroxysmal positional vertigo in Individuals with type 2 diabetes is mediated by hypertension. *J Vestib Res*. (2016) 25:223–39. doi: 10.3233/VES-150563
6. Wada M, Takeshima T, Nakamura Y, Nagasaka S, Kamesaki T, Kajii E. Carotid plaque is a new risk factor for peripheral vestibular disorder: a retrospective cohort study. *Medicine*. (2016) 95:e4510. doi: 10.1097/MD.0000000000004510
7. Webster G, Sens PM, Salmito MC, Cavalcante JD, Santos PR, Silva AL, et al. Hyperinsulinemia and hyperglycemia: risk factors for recurrence of benign paroxysmal positional vertigo. *Braz J Otorhinolaryngol*. (2015) 81:374–51. doi: 10.1016/j.bjorl.2014.09.008
8. Amarenco P, Rosengart A, Dewitt L, Pessin M, Caplan L. Anterior inferior cerebellar artery territory infarcts. Mechanisms and clinical features. *Arch Neurol*. (1993) 50:154–61. doi: 10.1002/ana.410330222
9. von Brevern M, Radtke A, Lezius F, Feldmann M, Ziese T, Lempert T, et al. Epidemiology of benign paroxysmal positional vertigo: a population based study. *J Neurol Neurosurg Psychiatry*. (2007) 78:710–5. doi: 10.1136/jnnp.2006.100420
10. Kerrigan MA, Costigan MF, Blatt KJ, Mathiason MA, Domroese ME. Prevalence of benign paroxysmal positional vertigo in the young adult population. *Pm R*. (2013) 5:778–85. doi: 10.1016/j.pmrj.2013.05.010
11. Seok JI, Lee HM, Yoo JH, Lee DK. Residual dizziness after successful repositioning treatment in patients with benign paroxysmal positional vertigo. *J Clin Neurol*. (2008) 4:107–10. doi: 10.3988/jcn.2008.4.3.107
12. Wan TJ, Yu YC, Zhao XG, Tang P, Gong YS. Efficacy of betahistine plus cognitive behavioral therapy on residual dizziness after successful canalith repositioning procedure for benign paroxysmal positional vertigo. *Neuropsychiatr Dis Treat*. (2018) 14:2965–71. doi: 10.2147/ndt.s182809
13. Lee NH, Ban JH, Lee KC, Kim SM. Benign paroxysmal positional vertigo secondary to inner ear disease. *Otolaryngology*. (2010) 143:413–7. doi: 10.1016/j.otohns.2010.06.905
14. Bhattacharyya N, Baugh RF, Orvidas L, Barrs D, Bronston LJ, Cass S, et al. Clinical practice guideline: benign paroxysmal positional vertigo. *Otolaryngol Head Neck Surg*. (2008) 139:S47–81. doi: 10.1016/j.otohns.2008.08.022
15. Herdman SJ, Tusa RJ, Zee DS, Proctor LR, Mattox DE. Single treatment approaches to benign paroxysmal positional vertigo. *Arch Otolaryngol Head Neck Surg*. (1993) 119:450–4. doi: 10.1001/archotol.1993.01880160098015
16. Disantostefano J. International Classification of Diseases 10th Revision (ICD-10). *J Nurse Pract*. (2009) 5:56–7. doi: 10.1016/j.nurpra.2008.09.020
17. Listed NA. Committee on hearing and equilibrium guidelines for the evaluation of results of treatment of conductive hearing loss. AmericanAcademy of Otolaryngology-Head and Neck Surgery Ffoundation, Inc. *Otolaryngol Head Neck Surg*. (1995) 113:186–7. doi: 10.1016/s0194-5998(95)70103-6
18. Olesen J. The international classification of headache disorders. 2nd edition (ICHD-II). *Cephalalgia*. (2005) 161:689–91. doi: 10.1016/S0035-3787(05)85119-7
19. Plaza G, Durio E, Herráiz C, Rivera T, García-Berrocal JR. Consensus on diagnosis and treatment of sudden hearing loss. *Acta Otorrinolaringol*. (2011) 62:144–57. doi: 10.1016/s2173-5735(11)70025-4
20. Tan J, Deng Y, Zhang T, Wang M. Clinical characteristics and treatment outcomes for benign paroxysmal positional vertigo comorbid with hypertension. *Acta Otolaryngol*. (2016) 137:482–4. doi: 10.1080/00016489.2016.1247985
21. Zhou F, Fu M, Zhang N, Xu Y, Ge Y. Investigation of the relationship between chronic diseases and residual symptoms of benign paroxysmal positional vertigo. *J Clin Otorhinolaryngol Head Neck Surg*. (2015) 29:1627–9. doi: 10.13201/j.issn.1001-1781.2015.18.010
22. Wang CX, Wang JM. Risk factors for recurrence of benign paroxysmal positional vertigo: a Meta analysis. *J Clin Otorhinolaryngol Head Neck Surg*. (2018) 32:1298–303. doi: 10.13201/j.issn.1001-1781.2018.17.003
23. Rubin DI, Cheshire WP. Evaluation of "dizziness" in the neurology office. *Semin Neurol*. (2011) 31:029–41. doi: 10.1055/s-0031-1271306
24. Babac S, Djeric D, Petrovic-Lazic M, Arsovic N, Mikic A. Why do treatment failure and recurrences of benign paroxysmal positional vertigo occur? *Otol Neurotol*. (2014) 35:1105–10. doi: 10.1097/MAO.0000000000000417
25. Kasse CA, Santana GG, Scharlach RC, Gazzola JM, Branco FC, Doná F. Results from the balance rehabilitation unit in benign paroxysmal positional vertigo. *Braz J Otorhinolaryngol*. (2010) 76:623–9. doi: 10.1590/S1808-86942010000500015
26. Karlberg M, Hall K, Quickert N, Hinson J, Halmagyi GM. What inner ear diseases cause benign paroxysmal positional vertigo? *Acta Otolaryngol*. (2000)120:380–5. doi: 10.1080/000164800750000603
27. Parham K, Kuchel GA. A geriatric perspective on benign paroxysmal positional vertigo. *J Am Geriatr Soc*. (2016) 64:378–85. doi: 10.1111/jgs.13926
28. De Stefano A, Dispenza F, Suarez H, Perez-Fernandez N, Manrique-Huarte R, Ban JH, et al. A multicenter observational study on the role of comorbidities in the recurrent episodes of benign paroxysmal positional vertigo. *Auris Nasus Larynx*. (2014) 41:31–6. doi: 10.1016/j.anl.2013.07.007
29. Alrwaily M, Whitney S. Vestibular rehabilitation of older adults with dizziness. *Otolaryngol Clin North Am*. (2011) 44:473–96. doi: 10.1016/j.otc.2011.01.015
30. U.S. Preventive Services Task Force. Interventions to prevent falls in community-dwelling older adults: recommendation statement. *Am Fam Phys*. (2018) 319:1696–1704. doi: 10.1001/jama.2018.3097

Conflict of Interest: The authors declare that the research was conducted in the absence of any commercial or financial relationships that could be construed as a potential conflict of interest.

frontiers in Neurology

ORIGINAL RESEARCH
published: 09 January 2020
doi: 10.3389/fneur.2019.01361

Spatial Navigation Is Distinctively Impaired in Persistent Postural Perceptual Dizziness

Hayo A. Breinbauer[1,2,3], Maria Daniela Contreras[3], Juan P. Lira[3], Claudia Guevara[3], Leslie Castillo[3], Katherine Ruëdlinger[3], Daniel Muñoz[1] and Paul H. Delano[1,2]*

[1] Department of Otolaryngology, Facultad de Medicina, Universidad de Chile, Santiago, Chile, [2] Department of Neurocience, Facultad de Medicina, Universidad de Chile, Santiago, Chile, [3] Department of Otolaryngology, Facultad de Medicina Clínica Alemana, Universidad del Desarrollo, Santiago, Chile

Objective: To determine whether performance in a virtual spatial navigational task is poorer in persistent postural perceptual dizziness (PPPD) patients than in healthy volunteers and patients suffering other vestibular disorders.

Methods: Subjects were asked to perform three virtual Morris water maze spatial navigational tasks: (i) with a visible target, (ii) then with an invisible target and a fixed starting position, and finally (iii) with an invisible target and random initial position. Data were analyzed using the cumulative search error (CSE) index.

Results: While all subjects performed equally well with a visible target, the patients with PPPD ($n = 19$) performed poorer ($p < 0.004$) in the invisible target/navigationally demanding tasks (CSE median of 8) than did the healthy controls ($n = 18$; CSE: 3) and vestibular controls ($n = 19$; CSE: 4). Navigational performance in the most challenging setting allowed us to discriminate PPPD patients from controls with an area under the receiver operating characteristic curve of 0.83 (sensitivity 78.1%; specificity 83.3%). PPPD patients manifested more chaotic and disorganized search strategies, with more dispersion in the navigational pool than those of the non-PPPD groups (standard distance deviation of 0.97 vs. 0.46 in vestibular controls and 0.20 in healthy controls; $p < 0.001$).

Conclusions: While all patients suffering a vestibular disorder had poorer navigational abilities than healthy controls did, patients with PPPD showed the worst performance, to the point that this variable allowed the discrimination of PPPD from non-PPPD patients. This distinct impairment in spatial navigation abilities offers new insights into PPPD pathophysiology and may also represent a new biomarker for diagnosing this entity.

Keywords: dizziness, functional dizziness, persistent postural perceptual dizziness, spatial navigation, morris water maze

OPEN ACCESS

Edited by:
Iole Indovina,
Saint Camillus International University of Health and Medical Sciences, Italy

Reviewed by:
Viviana Mucci,
Swiss Concussion Center, Switzerland
Jeffrey P. Staab,
Mayo Clinic, United States

****Correspondence:***
Hayo A. Breinbauer
hbreinbauer@uchile.cl

Specialty section:
This article was submitted to Neuro-Otology, a section of the journal Frontiers in Neurology

Received: *29 October 2019*
Accepted: *10 December 2019*
Published: *09 January 2020*

Citation:
Breinbauer HA, Contreras MD, Lira JP, Guevara C, Castillo L, Ruëdlinger K, Muñoz D and Delano PH (2020) Spatial Navigation Is Distinctively Impaired in Persistent Postural Perceptual Dizziness. Front. Neurol. 10:1361. doi: 10.3389/fneur.2019.01361

INTRODUCTION

Persistent postural perceptual dizziness (PPPD) is a clinical entity that comprises different types of non-vertiginous dizziness and represents the most common cause of chronic vestibular syndromes (1, 2). There are no objective biomarkers for PPPD, and its diagnosis depends entirely on clinical criteria (1).

The physiopathology of PPPD remains unclear (2–5). One theoretical approach focuses on errors in visual, proprioceptive, and vestibular integration (6–8) and the reduced cortical integration of spatial orientation cues as a pathological response to a triggering event (9, 10). These disturbed computations of multimodal inputs can generate an inappropriate inner spatial model of the environment and of the patient's position in it. It has been proposed that the discrepancies between the inner spatial model and reality are responsible for PPPD symptomatology (2, 4, 11). This framework is particularly interesting, as it offers a better understanding of visual induced dizziness and symptoms reported in PPPD, particularly in regard to the response of complex visual stimuli or the difficulty these patient refer when being in crowed spaces, such as a mall or in a subway station, with multiple objects moving rapidly in different directions (which could be understood as an overload of multimodal information to be processed, and a subsequent difficulty on constructing an accurate and properly timed inner model).

However, whether an altered internal cognitive map of the spatial environment is distinctively impaired in PPPD patients compared with individuals with other non-PPPD vestibular pathologies remains unknown (6, 12, 13).

We hypothesize that an important feature of PPPD is a disturbance in the mechanisms necessary to maintain an internal spatial map of the environment, which can impact individuals' performance in a navigational task.

Spatial navigation, an ability that emerges from the proper management of an internal spatial map, can be tested by means of the Morris water maze (MWM) experimental paradigm (14), in which the subject (originally a rodent) swims freely in a round pool that has visual cues installed around it. A transparent glass platform, which the subject cannot initially see, is located in the pool. The subject must find the platform to rest. He must also remember its location in relation to the visual cues to reach it faster on subsequent trials of the test by following a more direct route. Subjects with impaired memory or spatial navigation abilities (such as hippocampal lesions) fail to locate the platform and wander erratically around for a long period of time, even after having found the platform in previous trials. For human testing, virtual versions of the MWM paradigm have been validated and proved for use in identifying memory impairments, such as those found in individuals with Alzheimer's disease (15–18).

Navigational abilities have been explored in vestibular research, having found decreased performance in navigation in bilateral peripheral vestibular loss (12, 19). Nevertheless, the interpretation of these findings has been questioned due to methodological issues and revisited (13, 20), suggesting that there might be confounding variables involved, regarding cognitive and emotional aspects of patients. We believe that the confounding variable might indeed be the presence of PPPD.

Here, we studied spatial navigation in patients with PPPD, vestibular patients without PPPD and controls. We found worse performance in the virtual MWM spatial navigation test (12, 15–17) in patients presenting with PPPD than in both healthy subjects and patients suffering from other vestibular disorders but not presenting with PPPD.

MATERIALS AND METHODS

A cross-sectional study was conducted in which three groups of age-matched subjects were recruited: (i) patients suffering from PPPD, (ii) patients suffering from vestibular disorders other than PPPD, and (iii) healthy volunteers. Non-PPPD vestibular disorders included benign paroxysmal positional vertigo (BPPV), acute unilateral vestibulopathy, vestibular migraine and Ménière's disease. We chose to include these pathologies as representatives of the most common non-PPPD disorders in neuro-otology, producing different types of vestibular disfunctions. BPPV patients were analyzed before repositioning maneuvers. Ménière's and migraine patients were assessed during inter-ictal periods. Patients with acute vestibulopathy were assessed at least 3 months after onset, and only in patients who did no longer had spontaneous nystagmus, and that had not begun vestibular rehabilitation at the time of the procedures related to this research.

All subjects were assessed by means of a virtual version of the MWM task. Additionally, the Montreal Cognitive Assessment (MoCA) test was performed to exclude patients with cognitive impairment, which can affect the navigation assessment.

Patients being treated in an outpatient neurotology–otolaryngology unit at Clínica Alemana de Santiago medical center in Chile were invited to participate in the study. The study was performed in accordance with the Helsinki declaration. Written informed consent was obtained. This study is part of the "Characterization of Patients with Vestibular Disorders," a larger research endeavor, which has been approved by Clínica Alemana de Santiago's Scientific Ethical Committee. We set the inclusion criteria to be participants aged between 18 and 65. This upper limit was particularly relevant to diminish the possibility of cognitive impairment affecting the navigation assessment. The exclusion criteria were patients with known psychiatric or neurological conditions in their medical records and patients with a MoCA score of <25 points.

Patients were assessed during the initial medical consultation for PPPD (1), as well as for other vestibular diseases, following the most recent Bárány Society diagnostic criteria for the definitive forms of the diseases (21–25). *Ad hoc* audiological and vestibular tests were administered, including pure tone audiometry, video-nystagmography, video head impulse, and vestibular evoked myogenic potential tests. During these tests, the virtual MWM test was conducted by an audiologist blinded to the current diagnosis of the patient, who also conducted MoCA.

All virtual MWM tests were conducted in front of the same 24-inch desktop computer, and the subjects used a gaming joystick to navigate the virtual scenario (**Figure 1**). This scenario was presented in a full screen by means of the software "Computer Generated Arena Software" (26) and consisted of a square room measuring 1×1 virtual units of distance in the "North–South" and "East–West" dimensions. Regarding the visual cues, in three of the four walls of the room, pictures that covered 0.4 virtual units of each wall were always centrally placed in the same relative order: the northern wall was empty, the eastern wall displayed a flower, the southern wall displayed a turtle and the western wall

displayed an airplane. In the middle of the room, a round pool measuring 0.8 virtual units in diameter was placed (**Figure 2**).

The virtual MWM testing protocol consisted of 18 trials divided into three Blocks. Before each trial, patients could practice moving inside the round pool for as long as they needed in order to feel comfortable using the joystick to move in this virtual scenario; this practice session lasted between 2 and 5 min for all subjects.

In Block A (four trials), patients started at a fixed location, nearest to the northern end of the pool, facing southward. A fixed and visible blue square target area measuring 0.09 × 0.09 virtual units was placed on the ground in the southeast quadrant (**Figure 2**). Patients were instructed to navigate toward the blue target. When they arrived at the target, a rewarding sound was emitted, and the trial ended (each trial had a maximum duration of 1 min, even if the target was not reached). This first Block was designed to allow patients to become familiar with the virtual scenario and the testing protocol. Given the "training" nature of this Block, only four trials were conducted in this Block.

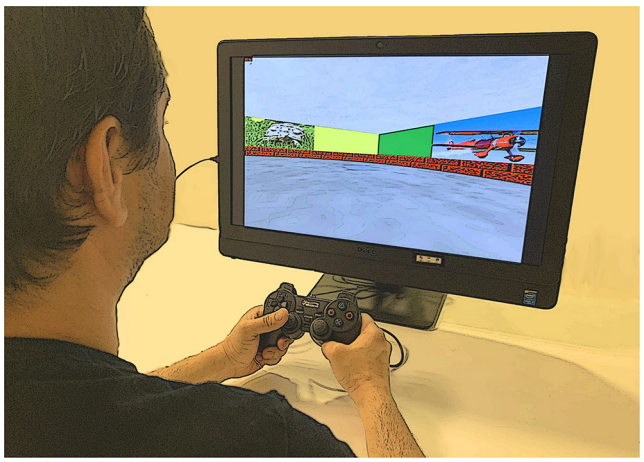

FIGURE 1 | Experimental setting. All virtual Morris Water Maze tests were conducted in front of the same 24-inch desktop computer, and the subjects used a gaming joystick to navigate the virtual scenario.

In Block B (seven trials), patients started at the same fixed location in the northern end of the pool. The square target was placed at a different fixed location (on the southwest quadrant) and was invisible. The target only turned visible when the patients stepped over it while navigating (and the rewarding sound was also emitted). Patients were instructed to navigate through the virtual pool to find the hidden target, and when they found the target, they had to remember its location to find it faster in subsequent trials. This process was repeated for seven trials.

In Block C (seven trials), patients started at a random location anywhere in the pool, facing toward a random direction. The square target was placed on a third different fixed location (in the east quadrant, slightly to the south) and was again invisible. The same instructions as those provided in Block B were given.

There are many ways to measure navigational performance in the MWM paradigm, including total path length traveled from the starting point to the target (measured in terms of "pool diameters," which is equivalent to 0.8 virtual units in our study), latency or time spent navigating before reaching the target, and time spent in the quadrant where the target was located. Nevertheless, one of the most sensible metrics is Gallagher's proximity, or cumulative search error (CSE) (27–30). CSE is the sum of the average distance between the subject and the target at every second the subject is navigating during a single trial (28). Even when a subject is navigating in the vicinity of the target, if he or she does not find the target, he or she receives a lower CSE score than a subject who navigates far away from the target.

In addition, with the MWM paradigm, it is possible to assess not only the performance in a given trial but also spatial learning

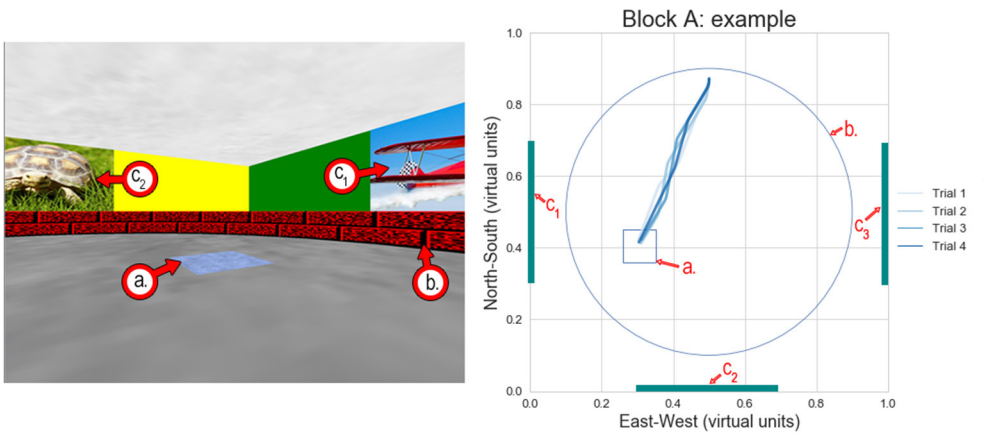

FIGURE 2 | Example of the virtual Morris water maze test—Block A (fixed starting position/visible target). **(Left)** Screenshot of the virtual environment where the subjects were instructed to navigate toward the blue square on the ground. In the screenshot, the subject was in the northern half of the pool, looking southwards and slightly eastwards. **(Right)** Diagram showing the entire virtual environment from above. The four blue lines indicate the path the subject took from his starting point toward the target in each of the four replicate trials. The light blue line shows the first trial, and the dark blue line shows the last trial. In this case, the paths in every trial were almost identical, as the target was visible (a.) Square target—visible in this block. (b.) Boundary of the round pool in which the subjects were allowed to navigate. (c.) Visual cues on three of the four walls of the virtual environment. In all cases, C_1 was an airplane, C_2 was a turtle, and C_3 was a flower.

by analyzing performance across sequential trials. In the first trial (always depicted in the lightest blue color in the figures), the subjects navigated with the intent of locating the target. After the subjects found the target in one of the early trials of a given Block, they were expected to remember the target location and navigate more directly toward it in later trials, thus achieving better performance scores in later trials (darker blue routes on our diagrams).

Based on data in studies using a similar methodology (31, 32) and considering a minimal significant difference between groups of 4 pool diameters in terms of the CSE score, a statistical power of 80% and an alpha error of 5%, a sample size of 18 subjects per group was calculated. Given the small sample size, non-parametric tests were preferred in the comparative analysis between groups; the Kruskal–Wallis test was used to summarize the data within a distinct scenario, and the Friedman test was used when data of sequential trials in a given Block were assessed as repeated measurements. Receiver operating characteristic (ROC) curves were calculated with the clinical criteria for a PPPD diagnosis as the gold standard and CSE scores as discriminating values. Normalized kernel density estimation plots with standard distance deviations were calculated to reveal the areas of the pool most visited during navigation. All analyses and spatial drawings were conducted and constructed, respectively, with Python 3.6 statistical and graphical packages.

Data Availability Statement

Data analyzed in this study is available at Dryad open repository.

RESULTS

Fifty-two patients were invited to participate in the study (2 declined, 50 accepted). A total of 19 patients fulfilling criteria for PPPD [as can be found on (1)] were recruited for the "PPPD" group, while 19 patients who did not meet the PPPD criteria but had other vestibular diagnoses were recruited for the "Vestibular" group (seven patients with PPPD, and five patients who could have joined the Vestibular group were excluded due to low MoCA results). BPPV, Ménières disease, vestibular migraine, and acute vestibulopathy were present in similar quantities in both (PPPD and non-PPPD) groups (**Table 1**). Eighteen healthy volunteers were included in the "Control" group. No significant differences were found in terms of age, sex, or MoCA results between groups. **Table 1** summarizes the main characteristics of all subjects.

In terms of path length, latency/time taken to reach the target, and CSE scores (considering all trials and blocks), the PPPD group performed worse than the patients in the vestibular and control groups did ($p < 0.05$, Kruskal–Wallis, Dunn's *post-hoc* test, see **Table 2**). We also found that the vestibular group performed worse than the healthy controls did in terms of the CSE scores. **Figure 3** (upper left panel) shows the difference in the average CSE scores, including all trials between groups.

When the CSE was analyzed within each block, all subjects, regardless of their group, performed equally well in Block A (fixed initial position and target visible). **Figure 3** (upper right panel) shows this similarity between groups in each of the four trials in Block A (no significant difference was observed). In all cases, subjects navigated in a straight line from the starting point toward the target (as seen in **Figure 2**). Higher CSE scores were recorded only in trial 1 (the first time all subject attempted to complete the task of navigating toward the target).

On the other hand, an important difference was observed in Block B (starting position fixed, invisible target) and Block C (starting position random, invisible target). On both blocks, the PPPD group performed worse than the vestibular and control groups did, and the vestibular group performed worse than the control group did [Friedman test ($p < 0.001$), with Bonferroni *post-hoc* testing confirming that all groups were different from each other]. Moreover, in both navigationally challenging settings, the control, and vestibular groups showed successful spatial learning, as their CSE scores decreased across trials, while the PPPD group showed a lack of improvement in CSE scores in the later trials. **Figure 3** (lower panels) presents these data graphically.

Figure 4 shows examples of the navigational performance during Blocks B and C of three individuals from the three different groups. In each diagram, all seven trials for each block are drawn. These plots illustrate how subjects from the vestibular and control groups learned these spatial tasks: once they found the hidden target, usually during the first three trials, they quickly learned its location and navigated in an almost straight line toward the target, even if the initial position was randomly set (Block C, diagrams to the right). The main difference between the control and vestibular groups is that the vestibular non-PPPD patients had slightly more difficulty in finding the target, as shown by the poorer CSE scores of this

TABLE 1 | Demographic summary of the PPPD, vestibular, and control groups.

		Group		
		PPPD	**Vestibular**	**Control**
Number of patients		19	19	18
Age	Median	47	46	43
	IQR*	32–58	28–53	34–56
	Range	22–65	23–62	29–60
Sex	Male/female	47.4/52.6%	42.1/57.9%	45/55%
MoCA	Median	26	27	28
	IQR	24–27	26–29	27–29
Diagnosis number [percentage of group]	BPPV**	3 [15.8%]	2 [10.5%]	–
	Vestibular migraine	6 [31.6%]	4 [21.1%]	–
	Menière's disease	5 [26.3%]	6 [31.6%]	–
	Acute unilateral vestibulopathy***	6 [31.6%]	8 [42.1%]	–

IQR, Interquartile range.
**BPPV, Benign paroxysmal positional vertigo.*
***Vestibular neuritis. More than 3 months after onset.*
The sum of the diagnosis percentages is >100%, as some patients in both the PPPD and the vestibular groups presented more than one of the listed diagnoses. There were no differences in age, sex, or cognition between the three studied groups.

TABLE 2 | Navigation performance after averaging all trials in the three blocks.

	Group				
	PPPD	**Vestibular**	**Control**	**Kruskal–Wallis *F*-value *p*-value**	***Post-hoc* Dunn's test ($p < 0.05$)**
Path length (pool diameters)	**2** Mean = 1.9 (SD = 1.4)	**1** Mean = 0.8 (SD = 1.4)	**1** Mean = 0.6 (SD = 0.9)	7.45 0.015	PPPD > Vestibular PPPD > Control
Time (seconds)	**20** (IQR = 16–35)	**14** (IQR = 12–21)	**10** (IQR = 9–17)	7.64 0.011	PPPD > Vestibular PPPD > Control
CSE (pool diameters)	**7** (IQR = 5–11)	**4** (IQR = 4–7)	**3** (IQR = 2–6)	9.21 0.004	PPPD > Vestibular PPPD > Control Vestibular > Control

SD, standard deviation; IQR, interquartile range; CSE, cumulative search error.
Medians are shown in bold. In path length, means and SDs are added to better assess the differences among groups.

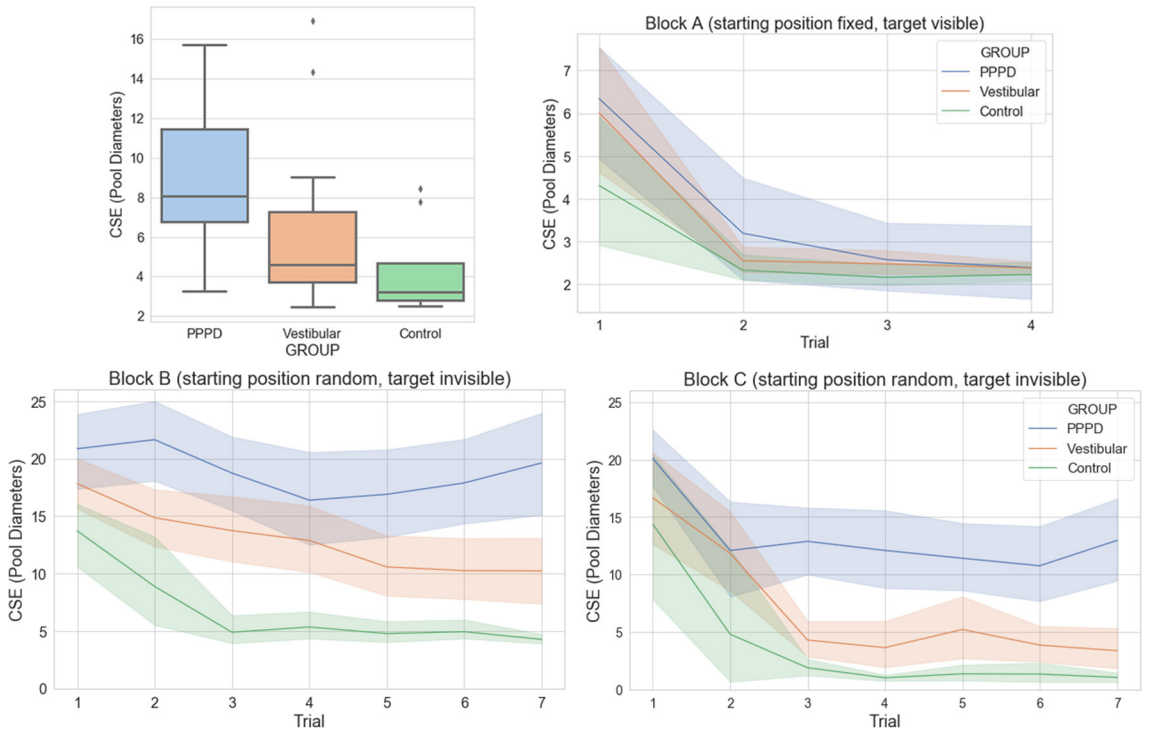

FIGURE 3 | Cumulative search error (CSE) performance during MWM navigation in the PPPD, vestibular, and control groups. In all panels, a larger CSE reflects poorer performance in spatial navigation. **(Upper-left)** Boxplot of CSE performance for each group (PPPD group in blue, vestibular group in orange, controls in green), summarizing all 18 trials/three blocks. The difference between each group was significant (Kruskal–Wallis, $p < 0.004$; Dunn's *post-hoc* testing confirming the difference between every pair of groups). **(Upper-right)** Mean and standard error are shown for the CSE scores for each of the four trials in Block A (visible target) for each group. There were no significant differences between groups. **(Lower)** Mean and standard error are shown for the CSE scores for each of the seven trials in Block B **(lower-left)** and block C **(lower-right)** for each group. The Friedman test showed significant differences between each group across the seven trials in blocks B and C ($p < 0.001$).

group depicted in **Figure 3** (lower panels). On the other hand, subjects in the PPPD group behaved qualitatively differently. They explored the pool in a more disorganized fashion. While the PPPD group explored the pool by following many different routes, they failed to navigate the pool systematically; they neglected parts of the pool and left them unexplored. The PPPD group also tended to stay close to or continuously hit the wall of the pool and ventured less toward the center of the pool. Reaching the target in one of the trials did not improve the PPPD group's routes in subsequent attempts, showing that spatial learning is impaired in these individuals. Another repeatedly observed behavior was the tendency in many PPPD subjects to make circular movements, perhaps in an attempt to become familiar with the virtual scenario. These

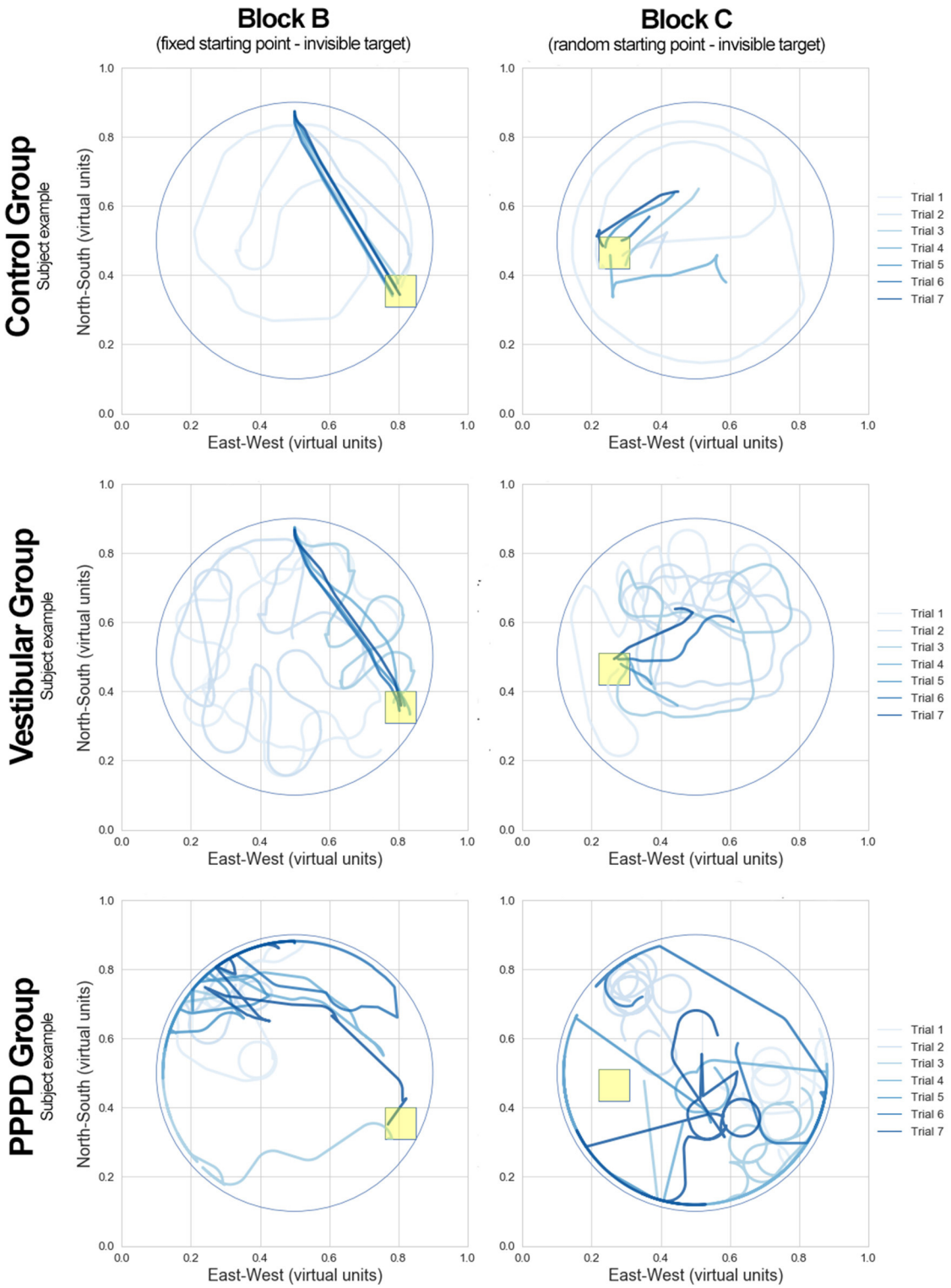

FIGURE 4 | Examples of MWM navigation paths in the PPPD, vestibular, and control groups. Three individuals from each of the corresponding groups (control, vestibular, and PPPD) illustrating MWM performance in blocks B and C. All seven trials of a given block are drawn in the same diagram. Lines in a lighter blue color represent the early trials in each block, while the darker blue color represents the final trials. The yellow square box represents the target position in each block.

patterns were observed in at least half of the subjects in the PPPD group.

While the examples in **Figure 4** are qualitatively striking, we sought to assess this difference in behavior at the group level (and not in individual cases). Therefore, to quantify the behavioral pathways in the MWM paradigm, we constructed density plots from kernel estimations (with normalization to 1 in each virtual pool and 50 distinct levels of probability), which described the position of the subjects from each group at every given moment in all trials in blocks A–C. **Figure 5** shows these plots, where the red areas represent the portions of the pool with higher location probability (where the subjects spent more time), and the blue areas represent places where the subjects did not visit often or never visited. The white squares represent the target in each block. For each group/block pool, the standard distance deviation (the equivalent to standard deviation

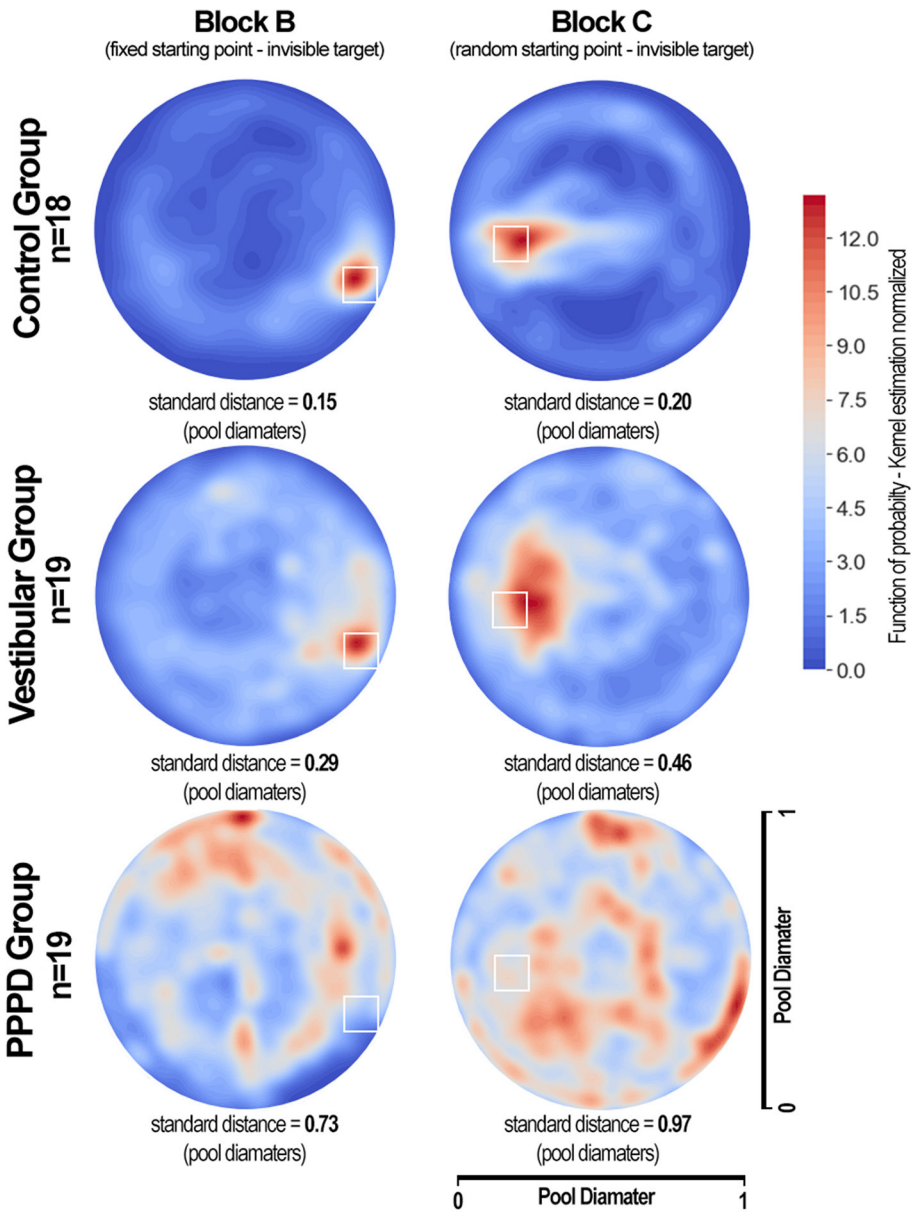

FIGURE 5 | Density plots showing the areas that were most visited during MWM navigation in the PPPD, vestibular, and control groups. Each density plot presents data from all subjects in a given group in all seven trials of blocks B and C. The colored bar shows normalized values of density function (kernel estimation), with 50 levels of density colors (the sum of all values in the entire plot is equal to 1). The standard distance deviation for each group/block is shown. The areas in red represent the locations most visited during navigation, while the areas in blue represent the areas where subjects spent less time. The white squares represent the target in each block. Healthy volunteers in the control group navigated very close to the targets. Subjects in the vestibular group also concentrated their movements toward the targets, but with more dispersion. The PPPD group showed an inconsistent, more chaotically distributed density plot with a tendency to travel around the wall limits of the pool.

for two-dimensional spatial data) is shown as a numerical value of the amount of dispersion/concentration of the navigation patterns (higher values represent higher dispersion). Levene's test indicated the standard distance deviation to be significantly different between groups (W = 345.5; $p < 0.001$ for block B. W = 423.7; $p < 0.001$ for block C). Additionally, in the vestibular and PPPD patients, standard distance deviations were larger in block C than those in block B (W = 92.2, $p = 0.21$ for control; W = 198.2, $p = 0.04$ for vestibular; W = 339.2, $p < 0.001$ for PPPD).

Finally, **Figure 6** shows the receiver operating characteristic (ROC) curves we plotted to assess whether the mean CSE scores could discriminate between PPPD and non-PPPD patients. Five distinct curves were calculated. The solid yellow line represents all 18 trials of the three blocks merged together, with an area-under-the curve (AUC) of 0.70. The dashed lines show curves for the mean CSE score of all four training trials with a visible target in Block A (in green, AUC = 0.51), all seven trials with invisible targets and fixed initial positions in Block B (in red, AUC = 0.75), and all seven trials with invisible targets and random initial positions in Block C (in purple, AUC = 0.83). The solid blue line represents the mean CSE performance of all trials where the target was invisible (Block B + C, non-training trials), with an AUC of 0.83.

In summary, we found that (i) in a non-navigationally challenging setting, i.e., that of Block A, all subjects performed equally well in terms of CSE (**Figure 3**—upper right panel); (ii) in navigationally challenging settings, vestibular patients performed worse than controls did, but PPPD patients performed even worse (**Figure 3**—upper left and lower panels); (iii) while the non-PPPD groups showed successful spatial learning, the PPPD patients showed a lack of change in the CSE scores across trials (**Figure 3**—lower panels); (iv) assessing all patients together—and not only individual examples—showed that the control and vestibular subjects focused their navigational movements near the target, while PPPD patients wandered all over the pool without a clear focus point (the amount of dispersion in this navigational pattern was larger in vestibular subjects than in controls, but it was even larger in PPPD patients); and (v) the CSE scores were able to distinguish PPPD patients from non-PPPD patients, particularly in the Block C setting, which yielded high AUCs in the ROC curves.

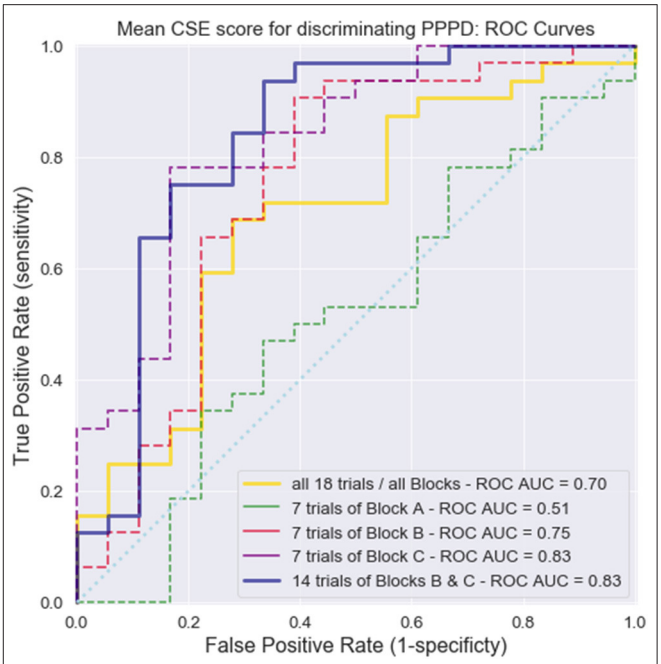

FIGURE 6 | Receiver operating characteristics (ROC) curves for the diagnosis of PPPD using the MWM navigation task. Five ROC curves were calculated considering mean CSE scores as discriminating values and the presence of PPPD as the gold standard. Solid yellow line, all trials and all blocks together; dashed green line, Block A; dashed red line, Block B; dashed purple line, Block C; and solid blue line, Blocks B and C together (trials where the target was invisible, thus representing a navigational challenge). The area under the curve (AUC) values for each curve are shown.

DISCUSSION

Groups Did Not Differ in Performance When the Target Was Visible

Regardless of their group, all subjects performed equally well when asked to navigate toward a visible target (**Figure 3**—upper right panel). In MWM research, this kind of experimental setting that does not present a navigational challenge is intended to account for gross motor issues or problems with the handling of the computer elements of a virtual scenario task itself. Therefore, it is not surprising that CSE scores did not have sufficient power to discriminate between patients in block A and yielded an AUC of 0.51 (equal to chance), which is represented by the dashed green curve in **Figure 6**.

Groups Performed Differently When Target Was Invisible. The PPPD Group Performed Worse Than the Non-PPPD Groups Did

The three groups in our study behaved differently in the navigationally challenging settings in Blocks B and C. In terms of total path length, latency (time), and particularly the CSE scores, PPPD patients showed a much worse performance in the MWM navigational task than did the age-matched vestibular patients and healthy controls. This finding can be clearly seen in **Figure 3**. Vestibular patients, particularly the PPPD patients, evidenced a significant impairment in spatial navigational abilities.

The PPPD Group Showed Less Spatial Learning Than the Non-PPPD Groups Did

Spatial learning in an MWM setting includes the ability of subjects to identify a target in relation to environmental cues, retain this information in the form of a navigational map, and use this information to find more direct routes to the target in subsequent attempts. PPPD patients not only had lower CSE scores than the non-PPPD patients (control and vestibular groups) but also showed little spatial learning. As seen in **Figure 3** (lower panels), the controls and vestibular subjects managed to improve their CSE scores in later trials, showing steep decreasing curves of the CSE scores. After the third or fourth trial, subjects showed a low "minimal" route, evidencing good spatial learning

(particularly clear on Block C, presumably revealing cumulative learning of the whole experimental setting). The visual examples of individual performance shown in **Figure 4** reinforce this idea. Routes in darker blue show how the selected control and vestibular subjects retained the location of the target and found a more direct path in subsequent trials. In contrast, PPPD patients showed less improvement or even no improvement in navigational performance across trials, as evidenced by the nearly flat curves in the lower panels of **Figure 3**. A selected case shown in **Figure 4** helps us understand the behavior of PPPD subjects. Even after finding the target in an early trial, the subject did not navigate near that point and focused rather aimlessly in other parts of the pool, showing no evidence of remembering the location of the target. While **Figure 4** presents a single case, the consistently high CSE scores across trials of the PPPD group reflects a lack of spatial learning in the group as a whole.

It remains to be seen in further studies if spatial learning remains impaired in PPPD in repetitions of such an experimental MWM testing over time (assessing how much navigation can be trained after repeating the task), or if this learning recovers after PPPD treatment.

The PPPD Group Not Only Showed Worse Performance Than the Non-PPPD Groups Did but Also Showed Qualitatively Different Navigational Behavior

These results acquire much richer meaning after analyzing **Figure 3** (individual examples) and **Figure 4** (grand average) together. In contrast to healthy controls, vestibular patients not presenting PPPD had slightly more difficulties completing the task of navigating effectively to a hidden target. However, both healthy controls and non-PPPD vestibular patients explored the virtual pool with reasonable strategies, covering as much ground as possible, and when they find the target, they managed to locate it again in the later trials. This behavior is well-reflected by the concentration of subjects' movements near the target area in both non-PPPD groups, as shown in **Figure 5**.

PPPD patients not only wandered around far more than the non-PPPD subjects did while trying to find the target but also wandered in a very disorganized, non-strategic and disoriented fashion. This behavior can be observed in the selected PPPD examples in **Figure 4**, and it can be observed even more clearly in the widespread non-localized distribution of the grand average location probability of PPPD patients across the pool but not around the target, as shown in **Figure 5**, with significantly larger dispersion values.

Spatial Navigation Impairment May Be a Key Feature of PPPD

Altogether, these findings suggest that navigation performance is impaired at some degree in all patients with vestibular impairment [which has been postulated in previous research (12, 13, 20)] and that this impairment is more severe in PPPD patients, to the point that it can be identified at the individual level and differentiate PPPD subjects from non-PPPD subjects (**Figure 6**). This ability of CSE scores to discriminate subjects was the highest in Block C (the most challenging navigational task in our experimental protocol, and thus the most sensitive task for identifying navigational impairment).

Again, this phenomenon appears to reflect not only the degree but also the quality of navigation in these patients. **Figure 5** is particularly relevant for illustrating this point. While vestibular patients show significantly more disperse navigational patterns than controls do, both groups focus their navigational movements around the target. On the other hand, PPPD patients do not focus their movements around the target but rather move aimlessly around the pool, with much larger dispersion and more movements at the walls. This dispersion increases when the navigational setting is more demanding. This wandering without a clear effective navigational strategy or evidence of spatial learning can be further corroborated when reviewing individual cases such as those in **Figure 4**. Therefore, we believe the impairment or dysfunction of navigational abilities in PPPD patients to be a distinct one, different in degree and in qualitative features, in contrast to the lower-degree of impairment (and qualitatively normal navigational movements) presented in patients suffering from other vestibular disorders other than PPPD.

Navigation Impairment Could Explain PPPD Symptomatology

We believe our finding raises the question of whether navigation-related functions in the brain represent a key feature in PPPD. We do not propose that PPPD patients have specifically and clinically relevant difficulties in navigating their everyday spaces and environments; instead, we propose that this disruption in the ability to construct, maintain and manage an internal map/model of the patients' spatial environment leads to an inappropriate and erroneous perception of the environment and therefore leads to the symptoms of PPPD. From this hypothesis, the latest definition of dizziness by the Bárány Society, which is "the sensation of disturbed or impaired spatial orientation without a false or distorted sense of motion," gains new meaning (33).

While the relevance of vestibular input in the hippocampal navigational network has been studied, particularly its interaction with head direction cells (maintaining an internal "compass" of the direction relative to a determined "north" in the spatial environment), recent findings suggest that this computation is actually multimodal and fed strongly from extravestibular cues (visual, somatosensory, and efference copy computations) (34, 35).

From this perspective, it is easy to understand how a decrease in the quality of vestibular inputs (which can be supposed to have occurred in our vestibular group) can impair navigational performance. However, our findings of worse performance in the PPPD group can be interpreted as a disturbance not of the directly driven vestibular computations but rather of the extravestibular multimodal integrations, particularly given that head rotations are not used to aid navigation in our MWM setting. Future research should include comparisons of navigational performance in PPPD patients between a head-static setting (such as the one used in the present study) and an immersive virtual reality setting, where "real-life" head rotations contribute to orientation in the virtual space. We hypothesize

that such a study would highlight PPPD disfunction as one of the computations of extravestibular cues.

Brain Changes in PPPD: Is the Navigational Network Altered?

Following this line of thought, it would be very interesting to assess morphological changes in gray matter volume and connectivity—particularly in the hippocampus, entorhinal cortex, cerebellum and parietal regions—in these patients and the correlation between these changes and navigational performance. Recent imaging *has* found evidence of decreased volume and connectivity in many of these cerebral regions, as well as other regions, in PPPD patients (5, 36, 37). However, these changes have not been correlated with functional performance, such as navigation.

If our hypothesis that spatial navigation impairment is the core of PPPD is correct, one should expect to find worse spatial navigation performance in patients with less gray matter volume and connectivity in cortical areas specific to spatial navigation.

A Diagnostic Tool?

From a more clinical and practical perspective, virtual MWM testing could eventually serve as a diagnostic tool, given that there are currently no biological markers for PPPD, and it remains an entity of pure clinical diagnosis. In our experimental setting, with a threshold of 8.16 pool diameters as the mean score of seven subsequent trials in the block C experimental setting, PPPD patients can be discriminated from non-PPPD patients with a sensitivity of 78.1% and a specificity of 83.3% (positive predictive value of 66%, negative predictive value of 88%). Such findings, particularly in patients with no other better explanation for a chronic vestibular syndrome (such as bilateral vestibulopathy, among others), could be strong objective indicators of PPPD. Nevertheless, this was not a study designed for testing a new diagnostic tool. Following diagnostic tests research (38), at the moment MWM could be considered as being in phase 1 (of 4) of becoming a reliable test.

Limitations

Regarding the limitations of our study, we acknowledge that our findings must be confirmed in future research studies with larger sample sizes. Also, and given our present results, we believe necessary to compare PPPD navigational performance not with an "other vestibular disorders" group, but to every distinct neuro-otological disease by itself. If MWM could serve as diagnostic tool, it is very important to assess this test's behavior in patients presenting syndromes which can be easily confused in some cases with PPPD, such as Mal de Debarquement, visual induced dizziness, bilateral vestibulopathy, and vestibular migraine.

Follow-up or test-retest reliability would have also been of great assistance in determining the robustness of our findings. As has been commented further above, imaging techniques could have helped in understanding our findings more thoroughly, but also would have contribute to their validity by discarding any underlying neuroanatomical abnormalities.

Additionally, factors which could affect MWM performance could be even more rigorously controlled, including the use of more comprehensive neuro-psychological assessments for different degrees of cognitive impairment in addition to the MoCA, as tests assessing different psychological states, such as anxiety, which could be of influence at the time of testing. Given the high comorbidity rate of psychiatric and psychological disorders with PPPD, we acknowledge that this issue should be address in future research.

CONCLUSIONS

Our findings suggest that while vestibular non-PPPD patients show poorer outcomes than healthy controls do in the navigational scores, PPPD patients perform significantly worse than both groups of individuals. PPPD navigational impairment is not only larger in magnitude when compared to that of non-PPPD subjects (vestibular and controls) but is apparently poorer in quality, showing disorganized and disoriented navigational patterns.

If confirmed in future studies, these findings highlight the relevance of a disturbance in navigation-related networks in the brain as a relevant feature in PPPD pathophysiology. Moreover, this distinctive spatial impairment in PPPD subjects might have a role as a biomarker for PPPD diagnosis.

DATA AVAILABILITY STATEMENT

The datasets generated for this study are available on request to the corresponding author.

ETHICS STATEMENT

The studies involving human participants were reviewed and approved by Clínica Alemana de Santiago's Scientific Ethical Committee. The patients/participants provided their written informed consent to participate in this study.

AUTHOR CONTRIBUTIONS

HB designed and guided the study. HB, MC, JL, CG, LC, and KR contributed to patient's recruitment and assessment. HB and DM conducted statistical analysis. HB and PD wrote the manuscript.

FUNDING

PD was funded by AC3E, CONICYT BASAL FB008, and BNI, Proyecto ICM P09-015F. There were no direct funding supporting this specific study.

ACKNOWLEDGMENTS

We would like to thank Jose Luis Valdes, at the Department of Neuroscience in Universidad de Chile, for his invaluable ideas and experience regarding the MWM setting, and also for introducing us to the virtual navigation software used in this research.

REFERENCES

1. Staab JP, Eckhardt-Henn A, Horii A, Jacob R, Strupp M, Brandt T, et al. Diagnostic criteria for persistent postural-perceptual dizziness (PPPD): consensus document of the committee for the Classification of Vestibular Disorders of the Bárány Society. *J Vestib Res*. (2017) 27:191–208. doi: 10.3233/VES-170622
2. Trinidade A, Goebel JA. Persistent postural-perceptual dizziness—a systematic review of the literature for the balance specialist. *Otol Neurotol*. (2018) 39:1291–303. doi: 10.1097/MAO.0000000000002010
3. Popkirov S, Stone J, Holle-Lee D. Treatment of persistent postural-perceptual dizziness (PPPD) and related disorders. *Curr Treat Options Neurol*. (2018) 20:50. doi: 10.1007/s11940-018-0535-0
4. Passamonti L, Riccelli R, Lacquaniti F, Staab JP, Indovina I. Brain responses to virtual reality visual motion stimulation are affected by neurotic personality traits in patients with persistent postural-perceptual dizziness. *J Vestib Res Equilib Orientat*. (2019) 28:369–78. doi: 10.3233/VES-190653
5. Nigro S, Indovina I, Riccelli R, Chiarella G, Petrolo C, Lacquaniti F, et al. Reduced cortical folding in multi-modal vestibular regions in persistent postural perceptual dizziness. *Brain Imaging Behav*. (2019) 13:798–809. doi: 10.1007/s11682-018-9900-6
6. Indovina I, Riccelli R, Chiarella G, Petrolo C, Augimeri A, Giofrè L, et al. Role of the insula and vestibular system in patients with chronic subjective dizziness: an fMRI study using sound-evoked vestibular stimulation. *Front Behav Neurosci*. (2015) 9:334. doi: 10.3389/fnbeh.2015.00334
7. Cousins S, Kaski D, Cutfield N, Arshad Q, Ahmad H, Gresty MA, et al. Predictors of clinical recovery from vestibular neuritis: a prospective study. *Ann Clin Transl Neurol*. (2017) 4:340–6. doi: 10.1002/acn3.386
8. Riccelli R, Indovina I, Staab JP, Nigro S, Augimeri A, Lacquaniti F, et al. Neuroticism modulates brain visuo-vestibular and anxiety systems during a virtual rollercoaster task. *Hum Brain Mapp*. (2017) 38:715–26. doi: 10.1002/hbm.23411
9. Best C, Tschan R, Eckhardt-Henn A, Dieterich M. Who is at risk for ongoing dizziness and psychological strain after a vestibular disorder? *Neuroscience*. (2009). 164:1579–87. doi: 10.1016/j.neuroscience.2009.09.034
10. Holmberg J, Tjernström F, Karlberg M, Fransson PA, Magnusson M. Reduced postural differences between phobic postural vertigo patients and healthy subjects during a postural threat. *J Neurol*. (2009) 256:1258–62. doi: 10.1007/s00415-009-5110-x
11. Dieterich M, Staab JP. Functional dizziness: from phobic postural vertigo and chronic subjective dizziness to persistent postural-perceptual dizziness. *Curr Opin Neurol*. (2017). 30:107–13. doi: 10.1097/WCO.0000000000000417
12. Kremmyda O, Hüfner K, Flanagin VL, Hamilton DA, Linn J, Strupp M, et al. Beyond dizziness: virtual navigation, spatial anxiety and hippocampal volume in bilateral vestibulopathy. *Front Hum Neurosci*. (2016) 10:139. doi: 10.3389/fnhum.2016.00139
13. Bigelow RT, Agrawal Y. Vestibular involvement in cognition: visuospatial ability, attention, executive function, and memory. *J Vestib Res Equilib Orientat*. (2015) 25:73–89. doi: 10.3233/VES-150544
14. Morris R. Developments of a water-maze procedure for studying spatial learning in the rat. *J Neurosci Methods*. (1984). 11:47–60. doi: 10.1016/0165-0270(84)90007-4
15. Hamilton DA, Driscoll I, Sutherland RJ. Human place learning in a virtual Morris water task: some important constraints on the flexibility of place navigation. *Behav Brain Res*. (2002). 129:159–70. doi: 10.1016/S0166-4328(01)00343-6
16. Wood H. A virtual Morris maze to assess cognitive impairment in Alzheimer disease. *Nat Rev Neurol*. (2016) 12:126. doi: 10.1038/nrneurol.2016.16
17. Harrison FE, Hosseini AH, McDonald MP. Endogenous anxiety and stress responses in water maze and Barnes maze spatial memory tasks. *Behav Brain Res*. (2009) 198:247–51. doi: 10.1016/j.bbr.2008.10.015
18. Wei EX, Oh ES, Harun A, Ehrenburg M, Agrawal Y. Vestibular loss predicts poorer spatial cognition in patients with Alzheimer's Disease. *J Alzheimer's Dis*. (2018) 61:995–1003. doi: 10.3233/JAD-170751
19. Brandt T, Schautzer F, Hamilton DA, Brüning R, Markowitsch HJ, Kalla R, et al. Vestibular loss causes hippocampal atrophy and impaired spatial memory in humans. *Brain*. (2005) 128:2732–41. doi: 10.1093/brain/awh617
20. Harun A, Oh ES, Bigelow RT, Studenski S, Agrawal Y. Vestibular impairment in dementia. *Otol Neurotol*. (2016) 37:1137–42. doi: 10.1097/MAO.0000000000001157
21. Lempert T, Olesen J, Furman J, Waterston J, Seemungal B, Carey J, et al. Vestibular migraine: diagnostic criteria. *J Vestib Res*. (2012) 22:167–72. doi: 10.3233/VES-2012-0453
22. Bisdorff AR, Staab JP, Newman-Toker DE. Overview of the international classification of vestibular disorders. *Neurol Clin*. (2015) 33:541–50. doi: 10.1016/j.ncl.2015.04.010
23. von Brevern M, Bertholon P, Brandt T, Fife T, Imai T, Nuti D, et al. Benign paroxysmal positional vertigo: diagnostic criteria. *J Vestib Res*. (2015) 25:105–17. doi: 10.3233/VES-150553
24. Kim HA, Bisdorff A, Bronstein AM, Lempert T, Rossi-Izquierdo M, Staab JP, et al. Hemodynamic orthostatic dizziness/vertigo: diagnostic criteria. *J Vestib Res*. (2019) 29:1–12. doi: 10.3233/VES-190655
25. Lopez-Escamez JA, Carey J, Chung WH, Goebel JA, Magnusson M, Mandalà M, et al. Diagnostic criteria for Meniere's disease. *J Vestib Res*. (2015) 25:1–7. doi: 10.3233/VES-150549
26. Kallai J, Makany T, Karadi K, Jacobs WJ. Spatial orientation strategies in Morris-type virtual water task for humans. *Behav Brain Res*. (2005) 159:187–96. doi: 10.1016/j.bbr.2004.10.015
27. Possin KL, Sanchez PE, Anderson-Bergman C, Fernandez R, Kerchner GA, Johnson ET, et al. Cross-species translation of the Morris maze for Alzheimer's disease. *J Clin Invest*. (2016) 126:779–83. doi: 10.1172/JCI 78464
28. Pereira IT, Burwell RD. Using the spatial learning index to evaluate performance on the water maze. *Behav Neurosci*. (2015) 129:533–9. doi: 10.1037/bne0000078
29. Maei HR. What is the most sensitive measure of water maze probe test performance? *Front Integr Neurosci*. (2009) 3:4. doi: 10.3389/neuro.07.004.2009
30. Maei H. Development and validation of a sensitive entropy-based measure for the water maze. *Front Integr Neurosci*. (2009) 3:33. doi: 10.3389/neuro.07.033.2009
31. Daugherty AM, Yuan P, Dahle CL, Bender AR, Yang Y, Raz N. Path complexity in virtual water maze navigation: differential associations with age, sex, and regional brain volume. *Cereb Cortex*. (2015) 25:3122–31. doi: 10.1093/cercor/bhu107
32. Epstein RA, Patai EZ, Julian JB, Spiers HJ. The cognitive map in humans: spatial navigation and beyond. *Nat Neurosci*. (2017) 20:1504–13. doi: 10.1038/nn.4656
33. Bisdorff A, Von Brevern M, Lempert T, Newman-Toker DE. Classification of vestibular symptoms: towards an international classification of vestibular disorders. *J Vestib Res*. (2009) 19:1–13. doi: 10.3233/VES-2009-0343
34. Cullen KE, Taube JS. Our sense of direction: progress, controversies and challenges. *Nat Neurosci*. (2017) 20:1465–73. doi: 10.1038/nn.4658
35. Dale A, Cullen KE. The ventral posterior lateral thalamus preferentially encodes externally applied versus active movement: implications for self-motion perception. *Cereb Cortex*. (2019) 29:305–18. doi: 10.1093/cercor/bhx325
36. Lee JO, Lee ES, Kim JS, Lee YB, Jeong Y, Choi BS, et al. Altered brain function in persistent postural perceptual dizziness: a study on resting state functional connectivity. *Hum Brain Mapp*. (2018) 39:3340–53. doi: 10.1002/hbm.24080
37. Wurthmann S, Naegel S, Schulte Steinberg B, Theysohn N, Diener HC, Kleinschnitz C, et al. Cerebral gray matter changes in persistent postural perceptual dizziness. *J Psychosom Res*. (2017) 103:95–101. doi: 10.1016/j.jpsychores.2017.10.007
38. Sackett DL, Haynes RB. The architecture of diagnostic research. *BMJ*. (2002) 324:539–41. doi: 10.1136/bmj.324.7336.539

Conflict of Interest: The authors declare that the research was conducted in the absence of any commercial or financial relationships that could be construed as a potential conflict of interest.

frontiers in Neurology

ORIGINAL RESEARCH
published: 05 February 2020
doi: 10.3389/fneur.2020.00007

Prediction of Vestibular Dysfunction by Applying Machine Learning Algorithms to Postural Instability

*Teru Kamogashira, Chisato Fujimoto, Makoto Kinoshita, Yayoi Kikkawa, Tatsuya Yamasoba and Shinichi Iwasaki**

Department of Otolaryngology and Head and Neck Surgery, University of Tokyo, Tokyo, Japan

Objective: To evaluate various machine learning algorithms in predicting peripheral vestibular dysfunction using the dataset of the center of pressure (COP) sway during foam posturography measured from patients with dizziness.

Study Design: Retrospective study.

Setting: Tertiary referral center.

Patients: Seventy-five patients with vestibular dysfunction and 163 healthy controls were retrospectively recruited. The dataset included the velocity, the envelopment area, the power spectrum of the COP for three frequency ranges and the presence of peripheral vestibular dysfunction evaluated by caloric testing in 75 patients with vestibular dysfunction and 163 healthy controls.

Main Outcome Measures: Various forms of machine learning algorithms including the Gradient Boosting Decision Tree, Bagging Classifier, and Logistic Regression were trained. Validation and comparison were performed using the area under the curve (AUC) of the receiver operating characteristic curve (ROC) and the recall of each algorithm using K-fold cross-validation.

Results: The AUC (0.90 ± 0.06) and the recall (0.84 ± 0.07) of the Gradient Boosting Decision Tree were the highest among the algorithms tested, and both of them were significantly higher than those of the logistic regression (AUC: 0.85 ± 0.08, recall: 0.78 ± 0.07). The recall of the Bagging Classifier (0.82 ± 0.07) was also significantly higher than that of logistic regression.

Conclusion: Machine learning algorithms can be successfully used to predict vestibular dysfunction as identified using caloric testing with the dataset of the COP sway during posturography. The multiple algorithms should be evaluated in each clinical dataset since specific algorithm does not always fit to any dataset. Optimization of the hyperparameters in each algorithm are necessary to obtain the highest accuracy.

Keywords: posturography tests, machine learning (artificial intelligence), vestibular dysfunction, Gradient Boosting Decision Tree (GBDT), hyperparameter

OPEN ACCESS

Edited by:
Joel Alan Goebel, Washington University School of Medicine in St. Louis, United States

Reviewed by:
Juan Carlos Amor-Dorado, Hospital Can Misses, Spain
Erin Gillikin Piker, James Madison University, United States

****Correspondence:***
Shinichi Iwasaki
iwashin-tky@umin.ac.jp

Specialty section:
This article was submitted to Neuro-Otology, a section of the journal Frontiers in Neurology

Received: *10 November 2019*
Accepted: *07 January 2020*
Published: *05 February 2020*

Citation:
Kamogashira T, Fujimoto C, Kinoshita M, Kikkawa Y, Yamasoba T and Iwasaki S (2020) Prediction of Vestibular Dysfunction by Applying Machine Learning Algorithms to Postural Instability. Front. Neurol. 11:7. doi: 10.3389/fneur.2020.00007

INTRODUCTION

The postural control system in humans is maintained by muscular actions governed by the central nervous system, which integrates information from vestibular, visual, and somatosensory inputs. Posturography is a clinical technique used to measure the movement of the center of foot pressure (COP) during sway in order to analyze postural control performance in detail (1). In this posturography system, various parameters of the COP have been used to investigate vestibular disorders, central nervous system disorders and orthopedic disorders (2–4). These parameters include the velocity, path length, envelopment area, movements in the medial-lateral and/or anterior-posterior direction, amplitude of displacement, power frequency, and Romberg's ratio, which is the ratio of parameters in eyes-closed to eyes-open conditions. To statistically analyze these parameters obtained from the COP measurements, a generalized linear model has often been utilized (3).

Recently, machine learning, which is a set of computational methods that learn patterns in data without being explicitly programmed, has been utilized in the field of medicine (5). Machine learning algorithms can be roughly divided into two algorithms: a method for predicting an answer for a new case based on a dataset whose correct answer is known, and a method for classifying a dataset into multiple groups. In clinical research, the former method has frequently been adopted, and many studies have been undertaken to try to predict diseases from medical images based on an algorithm learned from a dataset corresponding multiple images with diseases (6, 7). Among various algorithms of machine learning, a convolutional neural network has been widely used as a suitable method for predicting the disease from the image, although the type of effective machine learning algorithms may differ depending on the nature of the dataset and the number of datasets to be studied.

Among the machine learning algorithms, an artificial neural network has been applied to process the parameters obtained from posturography to assess fall risk and to diagnose various balance disorders (8–10). However, the efficacy of the many other machine learning algorithms have not been evaluated in detail with regard to posturography parameters.

The current study aimed to evaluate multiple machine learning algorithms and traditional statistical algorithms to predict the presence of peripheral vestibular dysfunction from posturography parameters. We evaluated various machine learning algorithms in predicting vestibular dysfunction using a dataset of the center of pressure (COP) sway during foam posturography obtained from patients with dizziness.

SUBJECTS AND METHODS

Patients were recruited between January 2017 and November 2018 at the Balance Disorder Clinic, Department of Otolaryngology, The University of Tokyo Hospital. The study was approved by the regional ethical standards committee in the Faculty of Medicine at the University of Tokyo. The study was conducted according to the tenets of the Declaration of Helsinki, and informed consent was obtained from each participant. Patients were scheduled to undergo caloric testing before posturography. Both tests were performed on the same day. The posturography test has been taken 1 h or over after the caloric test to prevent the effect of dizziness. Caloric testing was performed in a darkened room by irrigating the external auditory canal with 2 mL ice water (4°C) for 20 s followed by aspiration of water. This method of caloric stimulation is easier to perform than bithermal irrigation with water at 30 and 44°C, and has been shown to have a high sensitivity and specificity for detecting canal paresis (CP) based on Jongkees' formula (11). Caloric nystagmus was recorded using an electronystagmograph. An abnormal caloric response was defined by either of the following criteria: (1) CP percentage >20% (12); or (2) maximum slow phase eye velocity <10°/s bilaterally (13). A total of 99 consecutive patients showed abnormal caloric responses. We excluded 14 patients who had non-vestibular diseases that could cause postural instability: brainstem hemangioma ($n = 2$), migraine ($n = 2$), psychogenic disorder ($n = 2$), meningitis ($n = 1$), multiple neuropathy ($n = 1$), neurosarcoidosis ($n = 1$), orthostatic disturbance ($n = 1$) and disturbance of deep sensation ($n = 1$). Thus, 85 patients (41 men, 44 women) were enrolled in this study. The mean age (±standard deviation), the mean height, and the mean weight of the 85 patients were 52.6 (±15.4) years, 161.7 (±7.7) cm and 59.7 (±15.3) kg, respectively.

Of the 85 patients, 50 patients were diagnosed as having unilateral peripheral vestibulopathy, with etiologies of Meniere's disease ($n = 13$), acoustic tumor ($n = 12$), vestibular neuritis ($n = 8$), benign paroxysmal positional vertigo ($n = 6$), Ramsay-Hunt syndrome ($n = 3$), cholesteatoma ($n = 2$), delayed endolymphatic hydrops ($n = 2$), sudden deafness with vestibular dysfunction ($n = 2$), otosclerosis ($n = 1$), and temporal bone fracture ($n = 1$). The other 31 patients with unilateral peripheral vestibulopathy could not be diagnosed as having an established clinical entity. Four patients showed bilateral abnormal caloric responses, with an etiology of idiopathic bilateral vestibulopathy ($n = 2$) or another etiology ($n = 2$). The CP percentage ranged from 20 to 100, and the average (±standard deviation) was 54.0 (±27.5).

We enrolled 163 healthy control subjects (84 men, 79 women) in the present study. Subjects in the control group have no symptoms of dizziness, no dizziness in the past, and no problem with walking. The mean age (±standard deviation), the mean height, and the mean weight of the 163 healthy control subjects were 48.7 (±22.5) years, 160.6 (±11.9) cm, and 59.4 (±11.7) kg, respectively.

We used a Gravicorder G-5500 (Anima Co. Ltd., Tokyo, Japan) with/without a foam rubber layer on the posture platform (Nagashima Medical Instruments, Tokyo, Japan). The posture platform contains vertical force transducers to determine instantaneous fluctuations in the COP at a sampling frequency of 20 Hz. The sway path of the COP was obtained from these data. The foam rubber material was made of natural rubber, with a tensile strength of 2.1 Kgf/cm^2, an elongation stretch percentage of 110%, a density of 0.06 g/cm^3, and a thickness of 3.5 cm. Two-legged stance tasks were performed with both arms at the subject's side under four conditions: eyes open or eyes closed, with or without the foam rubber. The distal ends of the big toes were positioned 45 degrees apart with the heels of both feet close

to each other. The recording time was 60 s or until the subject required assistance to prevent falling. In the eyes-open condition, the subjects were asked to watch a small red circle 2 m away from where they were standing in a quiet, well-lit room. We measured the mean velocity of movement of the COP for 60 s, which was termed "the velocity," and the envelopment area traced by the movement of the COP, which was termed "the area." These parameters can indirectly reflect the function of the peripheral and central vestibular system due to the reduction of visual and somatosensory inputs.

We estimated the power spectrum of the acceleration signal for the anterior-posterior (AP) and the medial-lateral (ML) axes by using the maximum entropy method (MEM), which is superior to a fast Fourier transform for analyzing relatively short samples. Frequency resolution was set at 0.001 Hz, and the lag value was set at 120. The area under the curve (AUC) of the power spectral density (PSD) of the COP were calculated for each axis across three frequency ranges: between 0.02 and 0.1 Hz (low-frequency range, LF-AUC), between 0.1 and 1 Hz (middle-frequency range, MF-AUC) and between 1 and 10 Hz (high-frequency range, HF-AUC). The sum of these individual AUCs was also calculated (total AUC) (14).

The dataset included the presence of peripheral vestibular dysfunction (VD) evaluated with the method above, the subject's age and the posturography parameters, which were the velocity, the area, the MF-AUC of the AP and ML axes and the total AUC of the AP and ML axes.

Training and analysis were completed using Python 3.5 with scipy 0.18 and scikit-learn 0.18, and R version 3.4.4 (15). The applied supervised machine learning algorithms were ensemble methods (adaptive boosting classifier, bagging classifier, extra trees classifier, gradient boosting classifier, random forest classifier), support vector classification (SVC) [c-support vector classification (SVC), nu-support vector classification (Nu SVC)], decision trees (decision tree classifier, extra tree classifier), multi-layer perceptron classifier (MLPClassifier, neural network, deep learning) and generalized linear models [logistic regression, stochastic gradient descent (SGD) classifier]. The dataset was separated into the training dataset and the validation dataset with the split ratio of 80 and 20%. Then each machine learning algorithm was trained with the training dataset, and vestibular dysfunction in the validation dataset was predicted using trained algorithms from the validation dataset. The recall and the AUC of ROC were calculated (**Figure 1**). The validation and comparison of the algorithms were performed using K-fold cross-validation with the Wilcoxon signed-rank test, and $p < 0.05$ was considered to be significant (16, 17).

RESULTS

All of the healthy control subjects were able to complete posturography tests. The 10 patients were unable to stand for 60 s in eyes closed/foam rubber condition and to complete the exam. Eight of them were patients with unilateral peripheral vestibulopathy, and the other two were patients with bilateral peripheral vestibulopathy. We analyzed the data obtained from the remaining 75 patients. The basic physical parameters and posturography results of 75 patients with peripheral vestibular dysfunction and 163 healthy controls are shown in **Table 1** and **Figure 2**. There were no significant differences in age, height, or body weight between the patients and the healthy controls ($p > 0.05$, respectively). On the other hand, the velocity and the area in the eyes-closed condition on the foam rubber were significantly greater in patients compared to controls ($p < 0.0001$).

TABLE 1 | The basic physical parameters and posturography results.

Parameters	Average ± standard deviation		Significant difference
	Healthy subjects	Patients with CP	
Age	48.7 ± 22.5	52.6 ± 15.4	$p > 0.05$
Height	160.6 ± 11.9 cm	161.7 ± 7.7 cm	$p > 0.05$
Body weight	59.4 ± 11.7 k	59.7 ± 15.3 k	$p > 0.05$
MF-AUC of AP axis with eyes closed and with rubber	0.6 ± 0.3 cm^2	1.5 ± 1.0 cm^2	$p < 0.0001$
MF-AUC of LR axis with eyes closed and with rubber	0.5 ± 0.3 cm^2	1.2 ± 0.9 cm^2	$p < 0.0001$
Total AUC of AP axis with eyes closed and with rubber	1.0 ± 0.6 cm^2	1.9 ± 1.2 cm^2	$p < 0.0001$
Total AUC of LR with eyes closed and with rubber	0.7 ± 0.5 cm^2	1.6 ± 1.1 cm^2	$p < 0.0001$
Velocity with eyes closed and with rubber	3.7 ± 1.8 cm/s	5.6 ± 2.1 cm/s	$p < 0.0001$
Area with eyes closed and with rubber	13.6 ± 7.8 cm^2	28.9 ± 20.7 cm^2	$p < 0.0001$

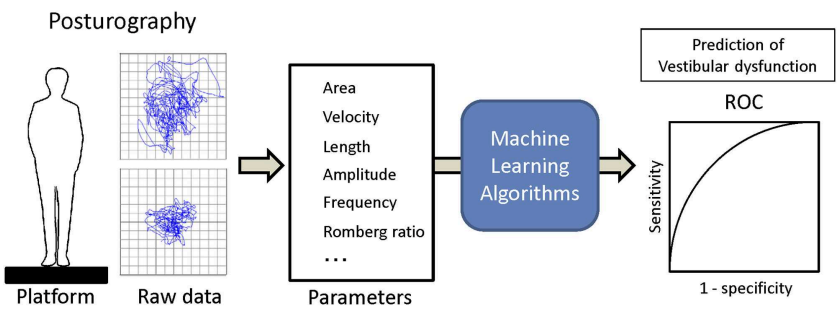

FIGURE 1 | Overview of the machine learning analysis from posturography data.

First, we fed the age and the posturography data into the various machine-learning algorithms, and compared the AUC and the recall regarding the presence of peripheral vestibular dysfunction (**Figure 3**). Among the algorithms tested, the gradient boosting classifier showed the highest AUC (0.89 ± 0.05) as well as the highest recall (0.82 ± 0.06). Both the AUC and the recall were significantly higher in the gradient boosting classifier than those of the logistic regression (AUC: 0.85 ± 0.06; recall: 0.78 ± 0.06). The AUC and the recall of the SVC (AUC: 0.81; recall: 0.73) and MLPClassifier (AUC: 0.76; recall: 0.73) were significantly lower than those of the logistic regression ($p < 0.05$). The recall of the bagging classifier (0.81 ± 0.05) and random forest classifier (0.81 ± 0.05) were also significantly higher compared to the logistic regression ($p < 0.05$). The comparisons of the AUC and the recall of all algorithms tested are shown in **Supplementary Table 1**. The ROC curves of the Gradient boosting classifier, Bagging classifier, logistic regression, and MLPClassifier are shown in **Figure 4**. The ROC curves of the all algorithms tested are shown in **Supplementary Figure 2**, and the ROC curve of logistic regression using typical posturography parameter are shown in **Supplementary Figure 3**. The sensitivity as well as the specificity of the gradient boosting classifier, the bagging classifier and the MLPClassifier were higher than those of the logistic regression.

Then, we evaluated the learning curve of the Gradient Boosting Classifier, which showed the best performance (**Figure 5A**). The training accuracy of the gradient boosting classifier was almost 1, and the validating accuracy tended to improve up to 0.85 over 100 training instances. This result indicates that higher predictability could be expected in the gradient boosting classifier if the dataset is much larger.

In utilizing machine learning algorithms, it is important to pay attention to the risk of overfitting. Changes in accuracy during the optimization process must be carefully evaluated for each hyperparameter. In ensemble learning algorithms including the gradient boosting classifier, some models are built from multiple decision trees (**Supplementary Figure 1**). We evaluated how the accuracy changes as the size and the depth of the decision trees were adjusted in the gradient boosting classifier. Regarding the number of decision trees, the validating accuracy was the highest when the number was about 50, while it tended to decrease when the number was more than 100 (**Figure 5B**). The training accuracy was 1 when the number was more than 100, and the gradient boosting classifier algorithm was the most efficient model to predict peripheral vestibular dysfunction in this dataset. Regarding the depth of the decision tree, the validating accuracy was the highest at around 3, and the accuracy tended to decline as the tree became deeper (**Figure 5C**). The training

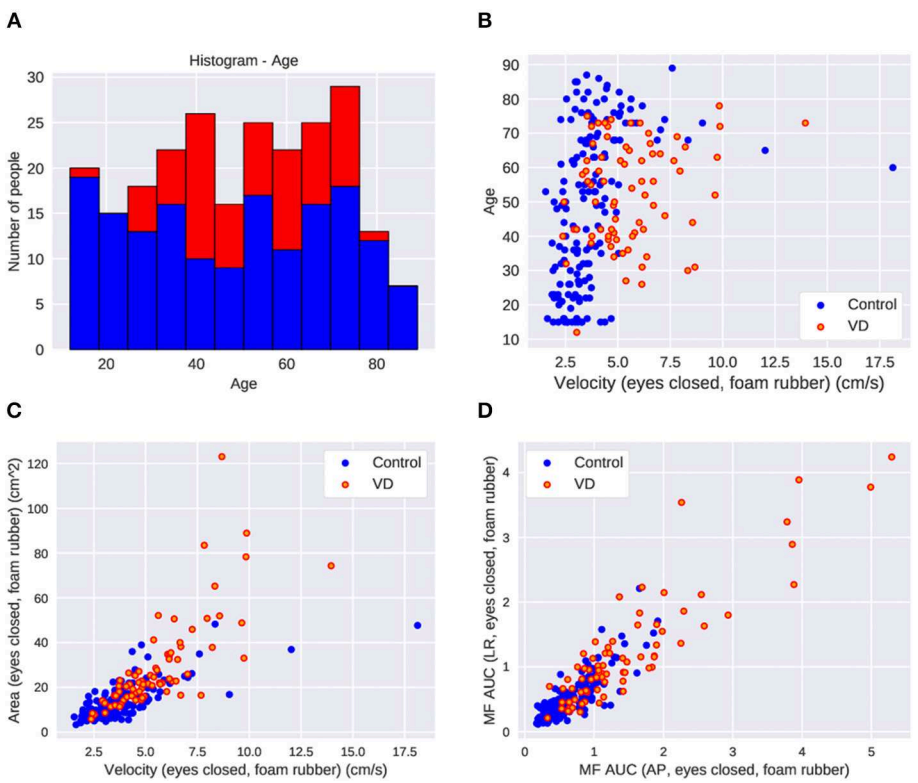

FIGURE 2 | The parameter distribution of the dataset in control and patients with vestibular dysfunction (VD). **(A)** Histogram of age. **(B)** Scatter plot of age and velocity of COP in the eyes-closed foam rubber condition. Greater VD cases at higher velocities. **(C)** Scatter plot of area and velocity in the eyes-closed foam rubber condition. More VD cases where the area and velocity are large. **(D)** Scatter plot of middle frequency AUC in the back and forth direction and middle frequency AUC in the left and right direction in the eyes-closed foam rubber condition. There are more VD patients in cases where each parameter is large.

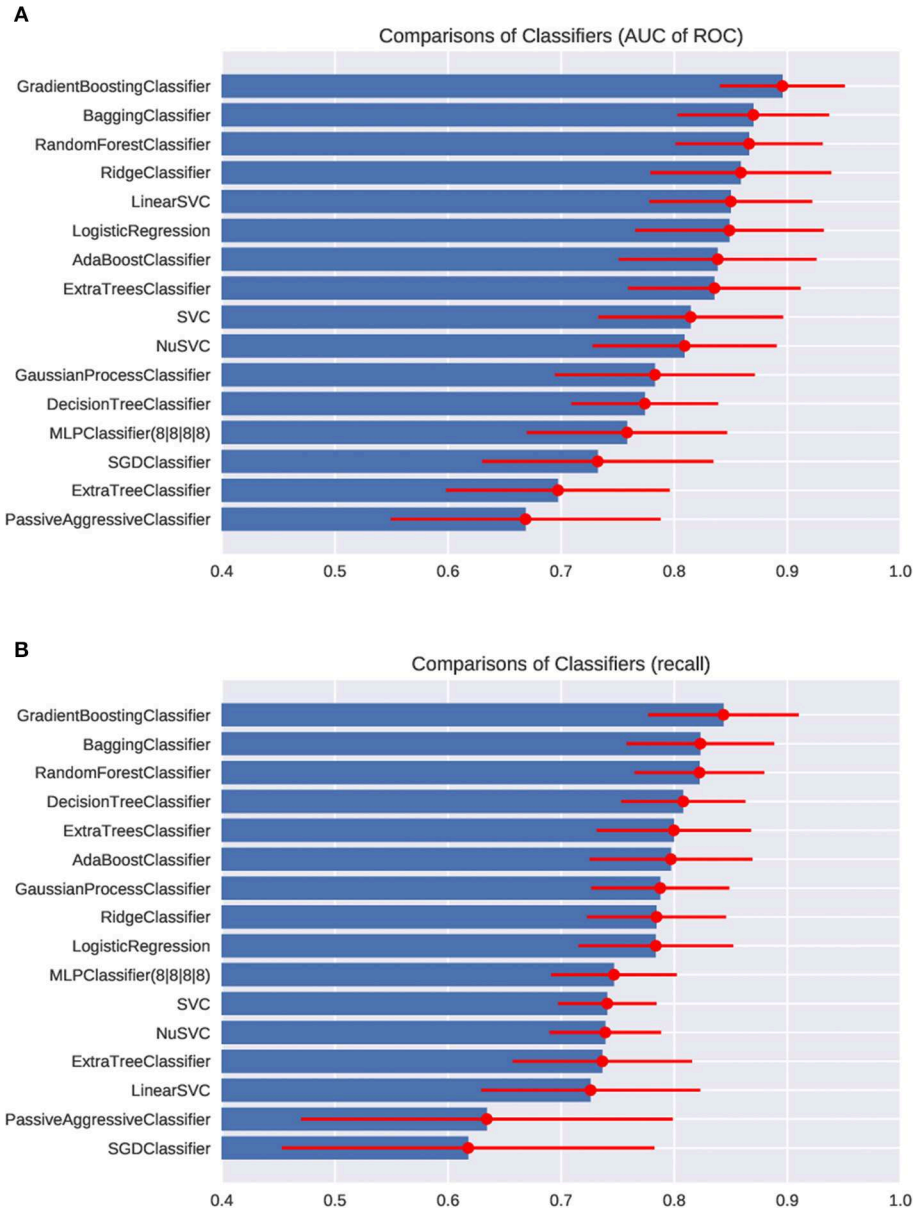

FIGURE 3 | Comparisons of classifiers in the AUC of ROC **(A)** and the recall **(B)**.

accuracy was 1 when the depth was more than 5, and the gradient boosting classifier algorithm was the most efficient model to predict peripheral vestibular dysfunction in this dataset. In the optimum parameter search of this dataset, the accuracy was the highest when depth was 2 and the number of decision trees was 45. These results suggest that selecting optimal hyperparameters is an important process in utilizing machine learning algorithms.

DISCUSSION

In the present study, we have evaluated multiple machine learning algorithms to predict vestibular dysfunction from datasets obtained from posturography. We have shown that the ensemble learning algorithms such as the gradient boosting classifier and bagging classifier can predict vestibular dysfunction better than the generalized linear models. The prediction ability of these ensemble learning algorithms are expected to be higher than that of traditional statistical models.

Machine learning has recently become utilized in the field of medicine (5, 18), including for the detection of hepatocellular carcinoma (19), the prediction of urinary tract infections in the emergency department (20), the prediction of hip fractures (21), the diagnosis of diabetic retinopathy (22), and the prediction of heart failure (23). Machine learning is also applied in the field of neurotology where it has been evaluated for use as a new diagnostic posturographic tool for disorders of stance, with an overall sensitivity and specificity of about 0.9 (8).

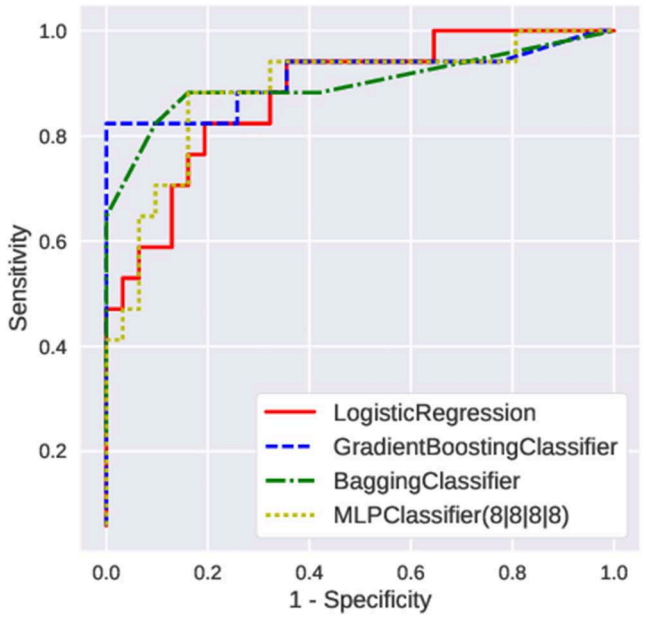

FIGURE 4 | The ROC curve of typical machine learning algorithms.

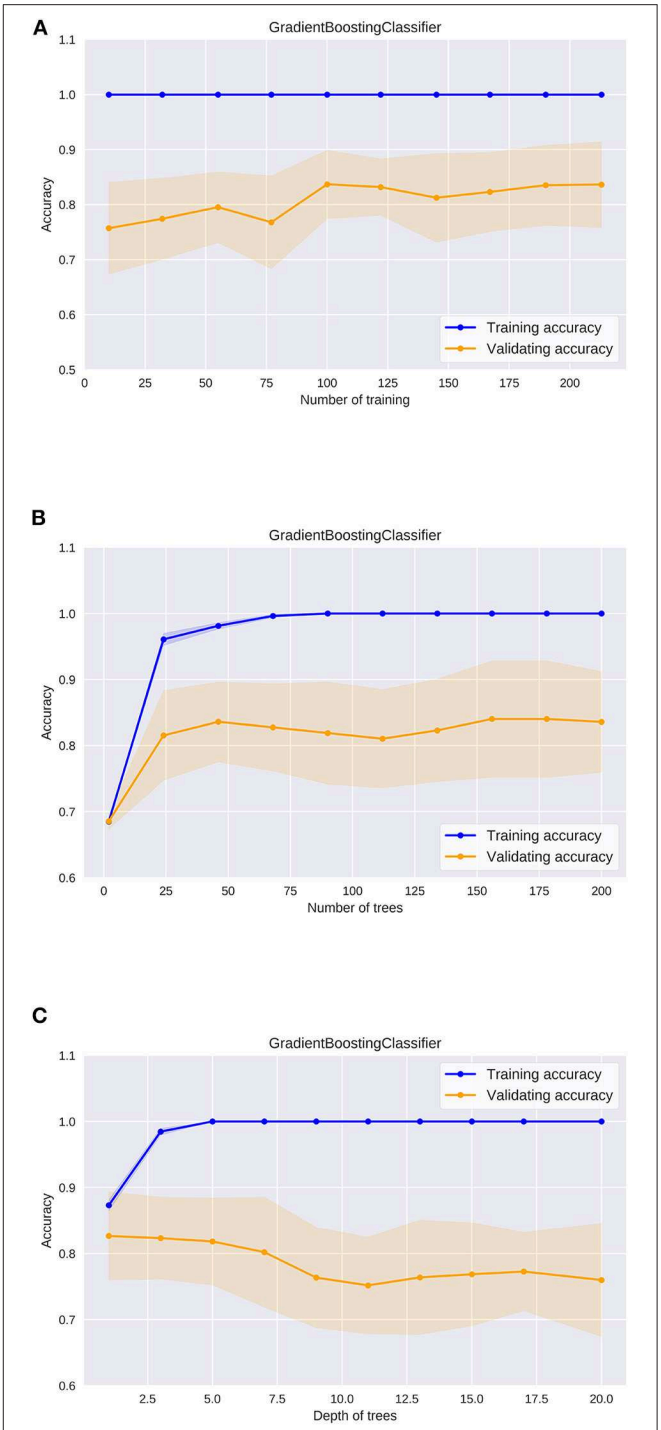

FIGURE 5 | The learning curve of the gradient boosting classifier **(A)**, the validation curve of the number of trees in the gradient boosting classifier **(B)**, the validation curve of the depth of trees in the gradient boosting classifier **(C)**.

The vestibulo-ocular reflex rotational test has been evaluated using machine learning for the assessment of vestibular function and the accuracy was 93.4% (24). Machine learning is a promising diagnostic tool for neurological disorders.

The gradient boosting classifier was the best algorithm in our datasets. This algorithm has recently been studied in varied medical fields (20, 21, 25, 26), and has shown highly predictive performance. Other algorithms including SVC (24, 27–29), decision trees (30), genetics-based algorithms (31), and the multi-layer perceptron classifier (32) did not show the best predictive performance in our datasets. The reason for the high predictive score of the gradient boosting classifier is that this classifier identifies the shortcomings of weak learners (multiple decision trees) in the loss function (which measures the fitting of the data to the model) to optimize the model. The neural network algorithm which has been widely adopted in the research of image-based diagnosis (6, 7) was not an effective method. The reason for this was that the number of cases in our dataset was not big enough to sufficiently train the model (33). The multiple algorithms should be evaluated individually with each clinical dataset because a specific algorithm does not necessarily fit any dataset (34, 35).

The hyperparameters of the machine-learning algorithms are set values which can greatly affect the performance of the prediction model (34–36). Thus, optimization of the hyperparameters is important for achieving the best prediction results from machine learning algorithms. Because there is no mathematical expression to calculate the optimum hyperparameters, the calculation of the optimum hyperparameters is simply based on the empirical method or the exploratory method, in which various values are applied to numerous model hyperparameters to obtain the maximum prediction rate. The AUC of ROC and the recall vary depending on the hyperparameters of the algorithm, and thus it is important to search for the optimum hyperparameters. Each machine learning algorithm has multiple hyperparameters that can be adjusted to obtain better prediction performance.

Some clinical parameters which have not been determined to be effective for disease prediction by conventional statistical methods may be effective for disease prediction by bundling them with other data and processing with machine learning algorithms.

There are some limitations in our study. First, the main explanatory variables that were used to predict vestibular dysfunction may change depending on the feature of the datasets, and we need to prepare every parameter in each evaluation. Second, the study was limited to the size of the datasets. The optimum algorithm will differ depending on the numerous aspects of the datasets. Third, not all hyperparameters were evaluated in this study because calculation of all hyperparameters is extremely resource consuming. Other advanced methods of searching for the optimum hyperparameters are needed to evaluate more types of algorithms.

In this study, the vestibular function was evaluated by caloric test only because other reliable vestibular function tests including video Head Impulse Test (vHIT) was not available. The database including further vestibular functional studies will provide more clinically useful tools for vestibular diagnosis.

CONCLUSION

The ensemble learning algorithms including the gradient boosting classifier and bagging classifier can predict vestibular dysfunction as identified using caloric testing from the datasets better than traditional regression algorithms.

Because the human being is a complex biological system, machine learning algorithms can build better classifiers than traditional linear classifiers to predict diagnostic values from clinical data and can be a useful tool to investigate the information in the datasets.

DATA AVAILABILITY STATEMENT

The datasets generated for this study are available on request to the corresponding author.

ETHICS STATEMENT

The studies involving human participants were reviewed and approved by the regional ethical standards committee in the Faculty of Medicine at the University of Tokyo. Written informed consent to participate in this study was provided by the participants' legal guardian/next of kin.

AUTHOR CONTRIBUTIONS

TK, CF, and SI conceived of the study, conducted the experiments, wrote the manuscript, and edited the manuscript for content. MK conducted the experiments and edited the manuscript for content. YK provided statistical advice, performed statistical analysis, and edited the manuscript for content. TY conceived of the study, supervised interpretation of data, and edited the manuscript for content.

FUNDING

This study was supported by grants from the Japan Agency for Medical Research and Development.

SUPPLEMENTARY MATERIAL

The Supplementary Material for this article can be found online at: https://www.frontiersin.org/articles/10.3389/fneur.2020.00007/full#supplementary-material

Supplementary Figure 1 | Examples of decision trees constituting the ensemble learning algorithm.

Supplementary Figure 2 | The ROC curve of each machine learning algorithms.

Supplementary Figure 3 | The ROC curve of logistic regression using single posturography parameter. The velocity (eyes closed, foam rubber) and the area (eyes closed, foam rubber) were analyzed.

Supplementary Table 1 | The comparison of each machine learning algorithms ($^*p < 0.05$).

REFERENCES

1. Paillard T, Noé F. Techniques and methods for testing the postural function in healthy and pathological subjects. *Biomed Res Int.* (2015) 2015:891390. doi: 10.1155/2015/891390
2. Golomer E, Dupui P, Bessou P. Spectral frequency analysis of dynamic balance in healthy and injured athletes. *Arch Int Physiol Biochim Biophys.* (1994) 102:225–9. doi: 10.3109/13813459409007543
3. Fujimoto C, Murofushi T, Chihara Y, Ushio M, Sugasawa K, Yamaguchi T, et al. Assessment of diagnostic accuracy of foam posturography for peripheral vestibular disorders: analysis of parameters related to visual and somatosensory dependence. *Clin Neurophysiol.* (2009) 120:1408–14. doi: 10.1016/j.clinph.2009.05.002
4. Furman JM. Role of posturography in the management of vestibular patients. *Otolaryngol Head Neck Surg.* (1995) 112:8–15. doi: 10.1016/S0194-5998(95)70300-4
5. Deo RC. Machine learning in medicine. *Circulation.* (2015) 132:1920–30. doi: 10.1161/CIRCULATIONAHA.115.001593
6. Anwar SM, Majid M, Qayyum A, Awais M, Alnowami M, Khan MK. Medical image analysis using convolutional neural networks: a review. *J Med Syst.* (2018) 42:226. doi: 10.1007/s10916-018-1088-1
7. Yasaka K, Akai H, Kunimatsu A, Kiryu S, Abe O. Deep learning with convolutional neural network in radiology. *Jpn J Radiol.* (2018) 36:257–72. doi: 10.1007/s11604-018-0726-3
8. Krafczyk S, Tietze S, Swoboda W, Valkovic P, Brandt T. Artificial neural network: a new diagnostic posturographic tool for disorders of stance. *Clin Neurophysiol.* (2006) 117:1692–8. doi: 10.1016/j.clinph.2006.04.022
9. Brandt T, Strupp M, Novozhilov S, Krafczyk S. Artificial neural network posturography detects the transition of vestibular neuritis to phobic postural vertigo. *J. Neurol.*. (2012) 259:182–4. doi: 10.1007/s00415-011-6124-8
10. Giansanti D, Maccioni G, Cesinaro S, Benvenuti F, Macellari V. Assessment of fall-risk by means of a neural network based on parameters assessed by a wearable device during posturography. *Med Eng Phys.* (2008) 30:367–72. doi: 10.1016/j.medengphy.2007.04.006
11. Schmäl F, Lübben B, Weiberg K, Stoll W. The minimal ice water caloric test compared with established vestibular caloric test procedures. *J Vestib Res.* (2005) 15:215–24.

12. Iwasaki S, Takai Y, Ozeki H, Ito K, Karino S, Murofushi T. Extent of lesions in idiopathic sudden hearing loss with vertigo: study using click and galvanic vestibular evoked myogenic potentials. *Arch Otolaryngol Head Neck Surg.* (2005) 131:857–62. doi: 10.1001/archotol.131.10.857
13. Fujimoto C, Murofushi T, Chihara Y, Suzuki M, Yamasoba T, Iwasaki S. Novel subtype of idiopathic bilateral vestibulopathy: bilateral absence of vestibular evoked myogenic potentials in the presence of normal caloric responses. *J Neurol.* (2009) 256:1488–92. doi: 10.1007/s00415-009-5147-x
14. Fujimoto C, Kamogashira T, Kinoshita M, Egami N, Sugasawa K, Demura S, et al. Power spectral analysis of postural sway during foam posturography in patients with peripheral vestibular dysfunction. *Otol Neurotol.* (2014) 35:e317–23. doi: 10.1097/MAO.0000000000000554
15. R Core Team. *R: A Language and Environment for Statistical Computing*. Vienna: R Foundation for Statistical Computing (2018). Available online at: http://www.r-project.org/
16. Raschka S, Mirjalili V. *Python Machine Learning: Machine Learning and Deep Learning with Python, Scikit-Learn, and TensorFlow*. Expert Insight, Birmingham: Packt Publishing.
17. Chollet F. *Deep Learning with Python*. New York, NY: Manning Publications
18. Rajkomar A, Dean J, Kohane I. Machine Learning in medicine. *N Engl J Med*. (2019) 380:1347–58. doi: 10.1056/NEJMra1814259
19. Sato M, Morimoto K, Kajihara S, Tateishi R, Shiina S, Koike K, et al. Machine-learning approach for the development of a novel predictive model for the diagnosis of hepatocellular carcinoma. *Sci Rep*. (2019) 9:7704. doi: 10.1038/s41598-019-44022-8
20. Taylor RA, Moore CL, Cheung KH, Brandt C. Predicting urinary tract infections in the emergency department with machine learning. *PLoS ONE.* (2018) 13:e0194085. doi: 10.1371/journal.pone.0194085
21. Kruse C, Eiken P, Vestergaard P. Machine learning principles can improve hip fracture prediction. *Calcif Tissue Int.* (2017) 100:348–60. doi: 10.1007/s00223-017-0238-7
22. Gulshan V, Peng L, Coram M, Stumpe MC, Wu D, Narayanaswamy A, et al. Development and validation of a deep learning algorithm for detection of diabetic retinopathy in retinal fundus photographs. *JAMA*. (2016) 316:2402–10. doi: 10.1001/jama.2016.17216
23. Weng SF, Reps J, Kai J, Garibaldi JM, Qureshi N. Can machine-learning improve cardiovascular risk prediction using routine clinical data? *PLoS ONE.* (2017) 12:e0174944. doi: 10.1371/journal.pone.0174944
24. Priesol AJ, Cao M, Brodley CE, Lewis RF. Clinical vestibular testing assessed with machine-learning algorithms. *JAMA Otolaryngol Head Neck Surg.* (2015) 141:364–72. doi: 10.1001/jamaoto.2014.3519
25. Chiew CJ, Liu N, Tagami T, Wong TH, Koh ZX, Ong MEH. Heart rate variability based machine learning models for risk prediction of suspected sepsis patients in the emergency department. *Medicine.* (2019) 98:e14197. doi: 10.1097/MD.0000000000014197
26. Babajide Mustapha I, Saeed F. Bioactive molecule prediction using extreme gradient boosting. *Molecules.* (2016) 21:983. doi: 10.3390/molecules21080983
27. Yeh SC, Huang MC, Wang PC, Fang TY, Su MC, Tsai PY, et al. Machine learning-based assessment tool for imbalance and vestibular dysfunction with virtual reality rehabilitation system. *Comput Methods Programs Biomed.* (2014) 116:311–8. doi: 10.1016/j.cmpb.2014.04.014
28. Lee JO, Lee ES, Kim JS, Lee YB, Jeong Y, Choi BS, et al. Altered brain function in persistent postural perceptual dizziness: a study on resting state functional connectivity. *Hum Brain Mapp.* (2018) 39:3340–53. doi: 10.1002/hbm.24080
29. Walther LE, Repik I, Schnupp T, Sommer D, Hörmann K, Golz M. The use of artificial neural networks in evaluation of posturographic data. *Laryngorhinootologie.* (2011) 90:211–7. doi: 10.1055/s-0030-1267980
30. Viikki K, Kentala E, Juhola M, Pyykkö I. Decision tree induction in the diagnosis of otoneurological diseases. *Med Inform Internet Med.* (1999) 24:277–89. doi: 10.1080/146392399298302
31. Laurikkala JP, Kentala EL, Juhola M, Pyvkkö IV. A novel machine learning program applied to discover otological diagnoses. *Scand Audiol Suppl.* (2001) 30:100–102. doi: 10.1080/010503901300007218
32. Juhola M. On machine learning classification of otoneurological data. *Stud Health Technol Inform.* (2008) 136:211–6. doi: 10.3233/978-1-58603-864-9-211
33. Zacksenhouse M, Braun S, Feldman M, Sidahmed M. Toward helicopter gearbox diagnostics from a small number of examples. *Mech Syst Signal Process.* (2000) 14:523–43. doi: 10.1006/mssp.2000.1297
34. Beunza JJ, Puertas E, García-Ovejero E, Villalba G, Condes E, Koleva G, et al. Comparison of machine learning algorithms for clinical event prediction (risk of coronary heart disease). *J Biomed Inform.* (2019) 97:103257. doi: 10.1016/j.jbi.2019.103257
35. Cao Y, Fang X, Ottosson J, Näslund E, Stenberg E. A comparative study of machine learning algorithms in predicting severe complications after bariatric surgery. *J Clin Med.* (2019) 8:E668. doi: 10.3390/jcm8050668
36. Meiring C, Dixit A, Harris S, MacCallum NS, Brealey DA, Watkinson PJ, et al. Optimal intensive care outcome prediction over time using machine learning. *PLoS ONE.* (2018) 13:e0206862. doi: 10.1371/journal.pone.0206862

Conflict of Interest: The authors declare that the research was conducted in the absence of any commercial or financial relationships that could be construed as a potential conflict of interest.

frontiers in Neurology

ORIGINAL RESEARCH
published: 21 April 2020
doi: 10.3389/fneur.2020.00289

Computing Endolymph Hydrodynamics During Head Impulse Test on Normal and Hydropic Vestibular Labyrinth Models

Jorge Rey-Martinez[1†], Xabier Altuna[1†], Kai Cheng[2], Ann M. Burgess[2] and Ian S. Curthoys[2†]*

[1] Neurotology Unit, ENT Department, Hospital Universitario Donostia, San Sebastián - Donostia, Spain, [2] Vestibular Research Laboratory, School of Psychology, The University of Sydney, Sydney, NSW, Australia

OPEN ACCESS

Edited by:
Herman Kingma,
Maastricht University, Netherlands

Reviewed by:
Erich Schneider,
Brandenburg University of Technology Cottbus-Senftenberg, Germany
Konrad P. Weber,
University of Zurich, Switzerland

***Correspondence:**
Jorge Rey-Martinez
bendermh@hotmail.com

†ORCID:
Jorge Rey-Martinez
orcid.org/0000-0001-7649-3823
Xabier Altuna
orcid.org/0000-0002-3453-5017
Ian S. Curthoys
orcid.org/0000-0002-9416-5038

Specialty section:
This article was submitted to Neuro-Otology, a section of the journal Frontiers in Neurology

Received: 02 December 2019
Accepted: 26 March 2020
Published: 21 April 2020

Citation:
Rey-Martinez J, Altuna X, Cheng K, Burgess AM and Curthoys IS (2020) Computing Endolymph Hydrodynamics During Head Impulse Test on Normal and Hydropic Vestibular Labyrinth Models. Front. Neurol. 11:289. doi: 10.3389/fneur.2020.00289

Hypothesis: Build a biologic geometry based computational model to test the hypothesis that, in some circumstances, endolymphatic hydrops can mechanically cause enhanced eye velocity responses during clinical conditions of the head impulse test.

Background: Some recent clinical and experimental findings had suggested that enhanced eye velocity responses measured with the video head impulse test could not only be caused by recording artifacts or central disfunction but also could be directly caused by the mechanical effect of endolymphatic hydrops on horizontal semicircular canal receptor.

Methods: Data from clinical video head impulse test was computed in three biologic-based geometry models governed by Navier-Stokes equations; six head impulses of incrementally increasing peak head velocity were computed in each one of the three different geometric models, depending on absence, canal or utricular hydrops.

Results: For all computed head impulses an increased endolymphatic pressure was measured at the ampullar region of the horizontal semicircular canal on both canal and utricular hydrops models. The mean of aVOR gain was 1.01 ± 0.008 for the no-hydrops model, 1.14 ± 0.010 for the canal hydrops model was, and 1.10 ± 0.007 for the utricular hydrops model.

Conclusion: The results of the physical computation models support-the hypothesis that in endolymphatic hydrops conditions, which are affecting horizontal semicircular canal and utricular region on moderate dilatations, the eye velocity responses output-by the aVOR will be enhanced by a 1.14 factor and aVOR gain values will be enhanced by over 1.1 for impulses to the right side.

Keywords: menière disease, endolymphatic hydrops, vHIT, VOR, clinical sign, enhanced eye velocity, CFD

INTRODUCTION

The video head impulse test (vHIT) is a computer-quantified clinical test of semicircular canal function that has a wide clinical application for vestibular and central pathologies in which the angular vestibulo-ocular reflex (aVOR) is affected (1, 2). vHIT has two main quantified outputs that are used in clinical practice. The first is the quotient between eye and head velocity during the slow

phase period (1) known as the gain of the aVOR (3) and the second is the timing, velocity and synchronicity of the saccadic eye responses produced during slow- or fast-phase periods (4).

About the gain of aVOR parameter it is also widely accepted that the presence of a lower value of aVOR gain—corresponding to situations where the slow-phase eye velocity is lower than head velocity most of the time—is a direct indicator of vestibular hypofunction (1), but recently published case reports have suggested that enhanced eye velocity responses during the head impulse test could be a quantified sign of endolymphatic hydrops (5). Enhanced aVOR responses are characterized by an enhanced eye velocity in response to head velocity. This enhanced eye velocity is reflected as a slight increase of the aVOR gain parameter, usually measured in a gain range between 1.1 and 1.3 (5). In this previously published case report we suggest that although enhanced eye velocity responses could be related with central vestibular disorders or vHIT goggle slippage due to an inadequate acquisition technique, there are some cases in which the most probable cause of the enhanced eye velocity responses is the endolymphatic hydrops.

Based on previous investigations (6), we suggest that the increase of volume and pressure on the horizontal semicircular canal will provoke an increased (transcupular) pressure on the cupula receptor that will also increase the vestibular afferent signal.

Because direct experimentation of this hypothesis on humans will cause loss of vestibular and auditive functions, researchers classically returned to experimental animal models to explore vestibular function tests (7) under different normal or pathologic biologic conditions. As an alternative to experiments, mathematical, and physical models supporting vestibular physiology do not cause any loss of biologic function, and they give strong evidence that modeled hypotheses are plausible from a physical and mathematical point of view. But these models are sometimes difficult to solve because of the complex mathematical methods required, making the physical-based predictions of the models very basic and imprecise.

Despite computer science has many outstanding figures who has significantly contributed to its development, it's probably since Alan Turing introduced the possibility of complex mathematical function computation by using recursive algorithms based on simple mathematical operations that could be automatically computed by a (theoretical) machine (8), that the use of computational models has grown significantly, with robust methods to develop realistic computer models to explain complex physical and biological phenomena. In the vestibular research field, these complex computational methods have recently been successfully used to model and predict vestibular caloric test responses in normal and endolymphatic hydrops on simplified anatomic models (9) or to reach a better understanding of the Tullio Phenomenon (10).

The main purpose of this research is to develop an anatomical model of the membranous vestibular labyrinth to compute and simulate endolymph hydrodynamics during real clinical head impulse test movement for models of both normal endolymph volume, and of endolymph volume increased by hydrops. With these models we will try to test the hypothesis that, in some circumstances, endolymphatic hydrops can mechanically cause enhanced eye velocity responses during head impulse testing in clinical conditions.

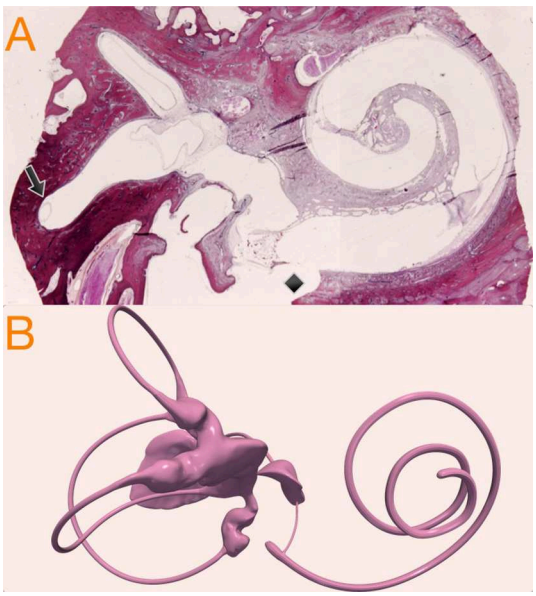

FIGURE 1 | (A) Temporal bone histologic (hematoxylin-eosin) preparation showing cochlear and vestibular structures on a parasagittal plane. The black arrow indicates the relation of endolymph horizontal duct inside the osseous space. The black diamond shows post-mortem promontorial cochleostomy with endosteal layer injury and *scala tympani* traumatic penetration. **(B)** Micro-CT volumetric of the endolymphatic spaces of the membranous labyrinth reconstruction used in this study as original 3D model of the inner ear.

MATERIALS AND METHODS

Development of Geometric Models of the Vestibular Organ for Normal and Hydropic Endolymph Volumes

The anatomic model used in this study was obtained from an intact *ex vivo* temporal bone using micro-computer tomography (microCT) scan; a Skyscan 1,172 (Bruker, DKSH Management Ltd, Zurich, Switzerland) microCT desktop scanner device was used in this study. Multiple images obtained using x-ray transmission were saved as uncompressed True Image File Format (TIFF) files.

The TIFF image sequence of the temporal bone was then loaded, processed, combined and exported as a single file in Nearly Raw Raster Data (NRRD) file format. The NRRD file was loaded into 3D Slicer (https://www.slicer.org) reconstruction software where a final 3D reconstructed anatomic model surface of the endolymphatic spaces of the membranous labyrinth model was created as seen in **Figure 1B**. The reconstructed 3D model was finally exported as standard triangle language (STL) file format that was used in computations as the anatomic model, and was also used as the base model to develop the hydrops models.

To develop the hydrops model we considered as McGarvie et al. had previously published (11) that, in human anatomy, the horizontal semicircular duct can be expanded to six times its normal diameter, because of the relative space distribution between endolymph duct and semicircular bone canal (**Figure 1A**): these authors describe an endolymph duct of 0.23 mm inside a osseous canal of 1.53 mm.

Based on this, because our 3D model duct has a diameter of 0.45 mm, we therefore allowed it to be uniformly increased x3 to reach a plausible 1.3 mm hydropic diameter, that still fit inside the osseous canal frame. Because utricular hydrops is not so well-defined in the literature, we decided to develop the hydrops model with a uniform expansion similar to the model of canal hydrops. Normal, canal hydrops and utricular hydrops are presented in **Figure 2**. The two hydrops models were designed using 3D computer design software Blender 2.8 (Blender—a 3D modeling and rendering package, Blender Foundation, Amsterdam, Netherlands; www.blender.org).

Computer Fluid Dynamics Simulations

All developed 3D models were exported in STL file format to the computational fluid dynamics (CFD) software: fully licensed SimFlow 3.1 (SIMFLOW technologies, Warsaw, Poland; https://sim-flow.com) CFD software was used to perform the model simulations to explore the endolymph hydrodynamics during the head impulse test. Once the 3-D models were imported into SimFlow a high-resolution mesh was created using the STL geometric models, defining the outer surfaces of the volumetric model.

The next step in the computer simulation was to select the solver, the mathematic algorithms used to compute the fluid dynamics during head impulses. The transient state with dynamic mesh capability "*PimpleDyMFoam*" (OpenFOAM documentation, The OpenFOAM Foundation Ltd, London, England; https://www.openfoam.org) solver was used on parallel running for our head impulse test computations. "*PympleDyMFoam*" algorithm's governing equation is based on the Navier-Stokes equations (12) for incompressible fluids, considering the vestibular labyrinth as the rotating absolute velocity frame. According to the solver's algorithm developer (OpenFOAM documentation, The OpenFOAM Foundation Ltd, London, England; https://www.openfoam.org) these governing equations are:

$$\begin{cases} \nabla \bullet \left(\overrightarrow{u_{\mathcal{R}}} \otimes \overrightarrow{u_{\mathcal{I}}}\right) + \overrightarrow{\Omega} \times \overrightarrow{u_{\mathcal{I}}} = -\nabla\left(p/\rho\right) + \upsilon \nabla \bullet \nabla\left(\overrightarrow{u_{\mathcal{I}}}\right) \\ \nabla \bullet \overrightarrow{u_{\mathcal{I}}} = 0 \end{cases}$$

Where $\overrightarrow{\Omega}$ is the acceleration of the rotating frame, $\mathcal{I}$ is notation for inertial movement, $\mathcal{R}$ is notation for rotating movement, $\overrightarrow{u}$ is (endolymph) velocity vector, ρ is the endolymph viscosity and p is the pressure. The $\otimes$ operator is used to denote the tensor product between velocity vectors.

For the external (vestibular labyrinth) rotational head velocity input vector we used head velocity data from a video head impulse test database at Royal Prince Alfred Hospital, Sydney. These impulses were all from the same participant and testing session and operator, and were selected to have values of peak head velocity ranging from 102.62°/s to 249.47°/s (**Appendix Figure 1**). The head impulses were recorded with a prototype ICS Impulse (GN Otometrics, Taastrup, Denmark) vHIT device with a sampling time of 0.004 s per frame, i.e., with an acquisition frequency of 250 Hz. The total duration recorded for each head impulse was 0.7 s.

The recorded head velocity data of the six impulses were lowpass-filtered and exported to the SimFlow software to be computed each one with so that each impulse could be applied to all of the three 3D models: normal, canal hydrops and utricular hydrops. For initial conditions endolymph and vestibular organ rotation velocities were set to 0 °/s, and the thermodynamic properties of endolymph were directly extrapolated from water thermodynamic properties: for the present research endolymph kinematic viscosity was 1 e-06 m^2/s.

All computation step was recorded, step duration was set to 0.004 s and simulation total time was set to 0.7, to exactly agree with vHIT sampling frequency and impulse recording duration.

Accordingly, a total of eighteen head impulses were computed in three geometric biologic-based models governed by Navier-Stokes equations; six incremental peak velocity head impulses were computed in each one of the three different geometric models depending on absence, canal or utricular hydrops. CSV head impulse velocity data, STL vestibular geometric models and CFD configuration files for each geometric model are available at **Appendix Datasheet 1–5**.

Computer Fluid Dynamics Simulations Postprocessing and Analysis

Computed head impulses were analyzed and postprocessed with Paraview 5.7.0 (Sandia National Laboratories, Albuquerque & Kitware Inc, New York, USA; https://www.paraview.org) software. Pressure and velocity 3D spaces and endolymph steam lines were the main outputs measured and visualized using Paraview; **Appendix Videos 1–3** supplementary files shows the Paraview exported videos of the normal and canal hydrops models for the head impulse test VI. The main pressure outcome was measured by selecting as pressure receptors the middle and superior points of the internal wall of the ampullar region; the mean pressure measures over time were exported to be analyzed using MATLAB R2019B (The MathWorks, Inc, Natick, Massachusetts, USA; https://www.mathworks.com).

As was described by Grant and Curthoys, the ampullar crista receptor was considered as an highly overdamped pressure—accelerometer sensor that directly responds to endolymph displacement velocity (13) that is directly proportional to angular head velocity (14) and according to Ramat (15), the neural discharge of vestibular afferents for high frequency head movements, in the range of physiological movements, is also a transduction of head angular velocity.

But in our developed geometric model the cupula was modeled as a rigid wall and it was not possible to directly measure the cupula deflection that occurs on biological semicircular canal. As an approach, cupular volume displacement can be estimated from the variation over time of transcupular pressure, that was the main variable measured in our CFD model.

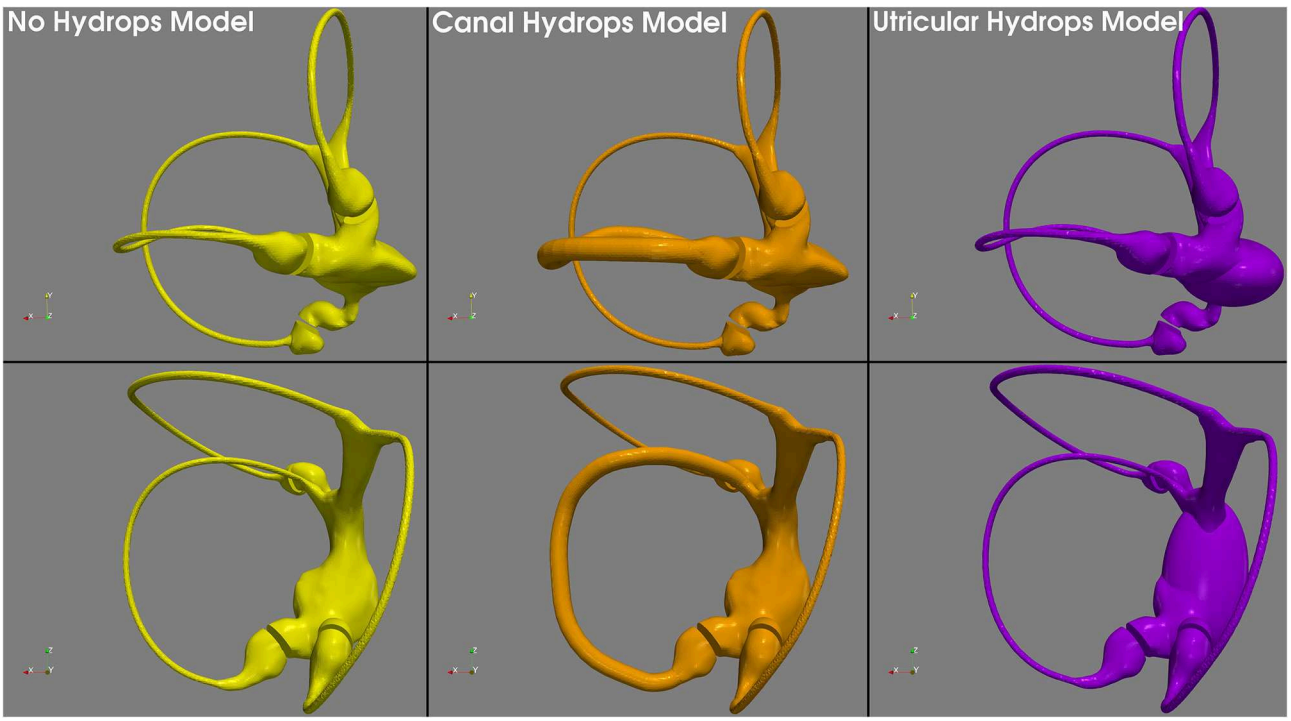

FIGURE 2 | 3D geometric models used in this research. The no hydrops model **(left)** obtained with conservative postprocessing from micro-CT scan, the canal hydrops model **(center)** with a uniform x3 horizontal endolymph duct dilatation, and the utricular hydrops model **(right)** with a similar to canal hydrops model expansion applied to the utricular region.

According to Squires et al. cupular volume displacement $V_c\,(t)$ is in relation to the applied pressure variation $\Delta P_c\left(t'\right)$ by the equation (16):

$$V_c\,(t) = \frac{1}{\gamma}\int_{-\infty}^{t} \Delta P_c\left(t'\right) e^{\frac{-(t-t')}{\tau_c}}\,dt'$$

Where τ_c, cupular time constant, is given by the equation (16):

$$\tau_c = \frac{8\mu\beta_d R}{\pi\, b_d^4 K}$$

And γ is given by the equation (16):

$$\gamma = \frac{8\mu\beta_d R}{\pi\, b_d^4}$$

Where μ is the endolymph viscosity, β_d is the angle subtended by semicircular duct, R is the major radius of semicircular canal, b_d is the duct radius and K the cupular elastic constant.

Finally, head movement Ω_0 is related with cupular volume displacement V_c by the expression, for human beings (16):

$$\frac{\Omega_0}{V_c} \approx 5.6 \times 10^{-2}\ \left(\frac{^\circ}{pL\ s}\right)$$

With the computed cupular displacement V_c approximated from the measured ΔP_c on the CFD simulations for each (hydropic and not hydropic) models we obtained the theoretical head movement measured by the cupula in both normal and hydropic semicircular canal for each one of the six head impulses. Assuming that because the unique perturbation introduced in our models was the hydrops of the duct or utricle regions, keeping intact all the other structures from cupula to eye that participates on the aVOR response, we predicted the eye responses by applying a (normofunctional) aVOR gain of ∼1 between eye and head responses. Using this approach, we predicted the final eye response based on the obtained head velocity by computing the measured ΔP_c.

To calculate the gain of the aVOR response on the computer simulation results, the obtained eye velocity values for each head impulse computation area under curve value were divided by the area under the curve of the head impulse velocity data for the corresponding simulation. To measure the area under the curve from both real head velocity and computed eye velocity, the HITCal (4) open source calculus tool (https://github.com/bendermh/HITCal/releases) was used under a MATLAB computational environment.

RESULTS

Vestibular model computations with CFD software were successfully performed with a residuals level under 0.01 during the head impulse movement for all cases. None of the variables, grouped by geometric model, showed statistical differences from a normal distribution on Kolmogorov-Smirnov normality test ($p > 0.5$).

TABLE 1 | Main outputs of the model's computation.

Impulse	Hydrops model	Increment of ampular pressure (Pa)	Predicted eye velocity peak (°/s)	Head velocity peak (°/s)
I	No Hydrops	0.054	102.33	102.62
II	No Hydrops	0.081	137.06	137.46
III	No Hydrops	0.089	141.22	140.50
IV	No Hydrops	0.100	173.22	173.81
V	No Hydrops	0.126	210.97	209.11
VI	No Hydrops	0.125	248.06	249.47
I	Canal Hydrops	0.061	115.79	102.62
II	Canal Hydrops	0.091	155.16	137.46
III	Canal Hydrops	0.101	159.74	140.50
IV	Canal Hydrops	0.113	195.53	173.81
V	Canal Hydrops	0.142	238.64	209.11
VI	Canal Hydrops	0.137	282.98	249.47
I	Utricular Hydrops	0.058	111.40	102.62
II	Utricular Hydrops	0.088	148.58	137.46
III	Utricular Hydrops	0.097	152.82	140.50
IV	Utricular Hydrops	0.109	184.43	173.81
V	Utricular Hydrops	0.136	229.01	209.11
VI	Utricular Hydrops	0.131	272.03	249.47

Computationally measured increment of pressure on the internal wall of the ampulla, and predicted eye velocity values according to measured pressure levels for all the six head impulses on each three anatomical hydrops models.

The main results of computations are presented in **Table 1** and are also plotted in **Figure 3**. For measured ampullar pressure values (**Table 1**, **Figure 3A** and **Appendix Figure 2**) higher peak pressure was measured in canal hydrops model with a mean pressure between impulses of 0.107 ± 0.030 Pa, followed by utricular hydrops model with a mean pressure of 0.103 ± 0.028 Pa. Lowest peak pressure levels were measured in no-hydrops model with a mean pressure of 0.095 ± 0.027.

Predicted eye velocity peak values (**Table 1**, **Figure 3B** and **Appendix Figure 3**) were also highest in canal hydrops model, with a mean peak eye velocity of 191.355 ± 61.10 °/s, followed by peak velocity values from utricular hydrops model of 183.61 ± 58.79 °/s. Lowest peak eye velocity values were also measured in no-hydrops model with a mean velocity of 168.82 ± 53.51 °/s.

For all models highest peak pressure and peak eye velocity were measured on V and VI impulses (209.11 °/s and 249.47 °/s head peak velocity values, respectively) while lowest predicted peak eye velocity and peak pressure vales were measured on impulse I (102.62 °/s).

The computed aVOR gain values using area under the curve method (**Table 2**, **Figure 4**) did show a mean aVOR gain of 1.01 ± 0.008 for the no-hydrops model, a mean gain of 1.14 ± 0.014 for the canal hydrops model, and a mean gain of 1.10 ± 0.007 for the utricular hydrops model.

DISCUSSION

In this study we predicted the endolymph hydrodynamics in geometric models of both normal and hydropic vestibular membranous labyrinths, using computer fluid dynamics software during the movement condition of the head impulse test.

Probably the most important question before discussing the computations performed in this research itself is about the actual evidence of the presence of vestibular hydrops affecting utriculus and semicircular canals in Menière disease and near spectrum human pathologies.

Although there are published cases of utricular and canal hydrops observation on 3 Tesla magnetic resonance imaging (MRI) with specific endolymph sequences (17), most actual imaging sequences of Menière disease and endolymphatic hydrops show cochlear and saccular hydrops, but not utricular or canal hydrops, which are rare findings in the published literature. It is not clear if this absence of MRI hydrops is related to a real lack of hydrops in these structures or other factors could be underlie these "anecdotal" cases of hydrops location. Probably, as suggested by Lopez-Escamez on a recent systematic review of the published papers on hydrops detection on 3 Tesla MRI sequences, actual MRI methods to adequate evaluate the endolymphatic hydrops are too novel and heterogenous to be considered as mature and reproducible techniques, especially in patients with early Menière disease (18).

On the other hand, despite the fact that most histologic published papers are focused on cochlear hydrops there are some histologic studies that strongly support the idea that utricular and canal hydrops may be also (relatively) frequent in the Menière disease population. Okuno and Sando (19) described the histopathological findings in 22 temporal bones from Menière's disease patients. Regarding vestibular organ hydrops, these authors found that saccular hydrops was present in 19 of 22 (86%) temporal bones, but also 11 of 22 (50%) temporal bones showed evident hydrops signals in the utricle region and 5–8 (23–36%) showed hydrops on at least one of the semicircular canals, the posterior canal being the most often affected (8/22) 36%. Concerning the severity of hydrops, these authors also described that saccular hydrops is less conservative with the original vestibular organ anatomy than utricular and semicircular canal hydrops are. Considering the histologic evidences published by Okuno and Sando, utricular hydrops could not be considered as infrequent, because it was present in 50% of temporal bones; also, canal hydrops should not be considered as a rare event, with a 23–35% of prevalence on temporal bones from Menière's disease patients.

The lack of an actual descriptive geometric model of the vestibular organ hydrops developed from radiological or histological findings forced us to develop a hydrops models based on McGarvie (11) descriptions but also inside the real measurements published by Okundo and Sando (19). Unfortunately, at the present moment, we were not able to find a more precise source to develop our vestibular hydrops models. This limitation in our models could be solved with future histological and radiological data or performing new CFD simulations, based on the here presented, where the hydrops geometry will be the main parameter to be tested.

In the developed models we only considered one volumetric dilatation ratio for each model. The effect of other dilatation ratios and its influence on VOR gain values should be evaluated

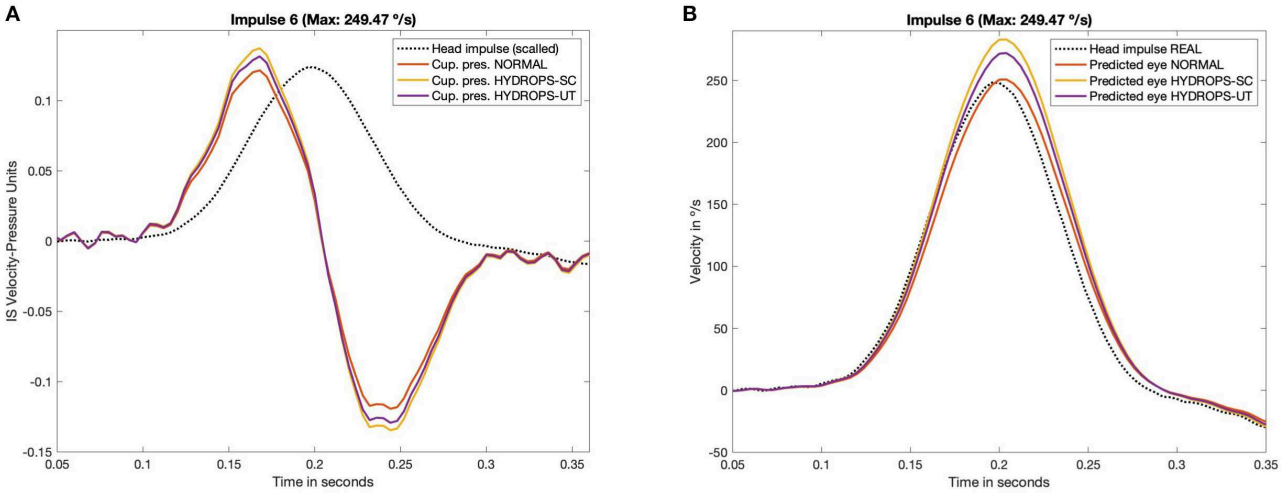

FIGURE 3 | Measured pressure **(A)** on CFD simulation and predicted eye velocity responses **(B)** of the three hydrops models (non-hydrops, utricular hydrops and semicircular canal hydrops), for the head impulse with the highest peak velocity included in this study (249.47 °/s). The pressure and velocity plots obtained from all the others impulses included in this study are available in **Appendix Figures 2**, **3**.

on further studies, this will be of particular interest to determine how will be the eye velocity enhancement at different Menière disease clinical stages.

Obviously, despite computer simulations being plausible from a physical point of view, they are not the strongest scientific evidence and also have limitations. In our computations we used anatomic 3D models from microCT reconstruction (**Figure 1B**), that have never before been used with this purpose in vestibular physiopathology research. In our model we considered the membranous labyrinth to consist of rigid walls, when really, they are elastic, and this elasticity could influence the endolymph flow during the head impulse test (20).

In our model cupula region was represented as a rigid wall. Goyens et al. (21) has recently evaluated the effect of different cupula designs and its biophysical effects on main variables that could affect to the VOR responses, concluding that the use of simplified models where the cupula is represented as a rigid wall, the same as we used in our model, are also adequate and valid models to evaluate the vestibular system biomechanics. Also, other vestibular models, like the model developed by Grieser et al. (6) that includes an elastic cupula in a simplified vestibular model has outputted similar enhancement of eye velocity responses reported by here.

The evidence of the concordance between models supports the mathematical approach used in our model to predict the (hypothetical) cupula deflection from a given variation of transcupular pressure over time which appears to be an acceptable approximation to overcome the lack of an anatomical and elastic cupula in our model. Other limitation about this research is that we build a model where only the information of ipsilateral afference vestibular signal was computed and the contralateral vestibular organ was not included on our model. To reach a better understanding of hydrops effect on vestibular system a more complete vestibular model, including contralateral vestibular organ signal should be considered on further researches.

Also, although microCT reconstruction of the vestibular labyrinth has a high resolution, the anatomic details of the ampullar receptor were not included in our models, and the cupula region was modeled as a simple wall, not including other geometric and elastic details. With the obtained computations we suggest that micro-CT geometric models using CFD software to

TABLE 2 | Gain (aVOR) values computed using area-under-curve method for predicted eye velocity values and real measured head velocity values for the six head impulse tests included and the three hydrops models included in this study.

Impulse	Hydrops Model	Predicted aVOR gain
I	No Hydrops	1.014
II	No Hydrops	1.010
III	No Hydrops	1.024
IV	No Hydrops	1.000
V	No Hydrops	1.019
VI	No Hydrops	1.019
I	Canal Hydrops	1.149
II	Canal Hydrops	1.148
III	Canal Hydrops	1.158
IV	Canal Hydrops	1.122
V	Canal Hydrops	1.159
VI	Canal Hydrops	1.149
I	Utricular Hydrops	1.104
II	Utricular Hydrops	1.095
III	Utricular Hydrops	1.109
IV	Utricular Hydrops	1.091
V	Utricular Hydrops	1.104
VI	Utricular Hydrops	1.111

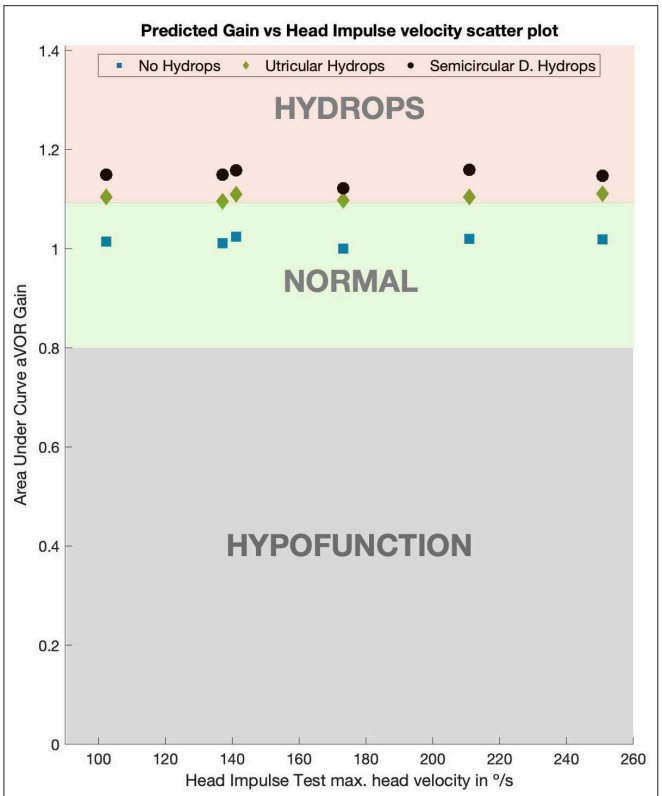

FIGURE 4 | Predicted values of aVOR gain for normal, utricular and canal hydrops models. For both (utricular and canal) hydrops models aVOR gains were always >1.09 on all the tested head impulse velocities. Gains for the utricular model were slightly lower than for the canal model, but always over 0.1 more than the normal model gain values, which had gain value of 1.

predict endolymph flow appear to be a very strong experimental method that could be applied to other vestibular function tests and other models of vestibular pathology.

As similar experimental research that partially supports the results obtained in this study, Yamauchi et al. (22) found that in animal models of horizontal canal hydrops that afferent vestibular nerve discharge is increased by the experimental induction of a hydropic environment, for both during static conditions and during sinusoidal (not impulsive) head movements. Nevertheless, Yamauchi et al. (22) describes that the static increase of discharge is adapted by the system along time and the dynamic (sinusoidal) response is variable depending on stimulus frequency. A very interesting point in this research is that Yamauchi et al. also describes that the increased vestibular discharges observed due the hydrops are not sustained over time. To explain this, the authors suggests that the vestibular system adaptation circuits will decrease these increased responses along time. If this vestibular adaptation mechanism is also applied to our human vestibular model it is probable that the enhanced eye responses will be more evident on the nearest time to the hydrops attack and probably will be decreased (due vestibular system adaptation) over time.

In this research results, we found that for head impulses of all head velocities, the velocities of the eye response are amplified by a 1.14 factor; for the canal hydrops model this was also in concordance with the aVOR gain values obtained in the canal hydrops model (**Figure 4**). With a slightly lower magnitude, aVOR gain was also significantly enhanced in the utricular hydrops model. These predicted enhanced eye velocities and aVOR gains were observed in the same proportion on all the head impulses included in this study. Because we obtained a 1.01 mean value for aVOR gain on non-hydrops models, the gain enhancement predicted by this study can be only directly extrapolated to right-side head impulse tests, in which the vHIT camera records responses of the right eye. This is because a gain value of 1 is only observed on the right side impulses of vHIT device with right-side mounted camera, and left-side impulses have a slightly lower than 1 aVOR gain value (23). But probably x1.14 enhancement of velocity data could be applied to left-side impulses.

Histopathological findings have also pointed a possible vestibular labyrinth structural alteration that, owing to the effect of hydrops, could affect to the pressure on ampullar receptors of horizontal semicircular canal. In the temporal bone series presented by Okuno and Sando (19) severe saccular hydrops had caused in 7 of 22 (31%) temporal bones a herniation of part of the saccular dilated structure into non-ampullar side of the horizontal side of this semicircular canal. Although our models did not compute the effect on ampullar pressure of this saccular herniation into the posterior region of the horizontal canal, it is probable that this herniation will also provoke an enhanced eye velocity response, probably greater than the observed in our models.

From a more hypothetical point of view, but based on findings of this study and the actual evidence of utricular or semicircular hydrops incidence in Menière disease patients (17–19), the enhanced eye velocity sign should appear in no more than half of Menière's disease patients, according to the described prevalence of canal and utricular hydrops (19). But there is a second factor that should be considered in addition to hydrops location: the time of evolution of the Menière disease. It has been described that for longstanding Menière disease patients type II hair cell vestibular receptors number is decreased and also an even more significant loss of cells on Scarpa's ganglion (24). These two histopathological findings present in patient with well-defined Menière disease could predict that the (related to hydrops) enhanced eye velocity will decrease to a normal or reduced eye velocity response due to the loss of sensitivity of vestibular receptors. Because this cellular damage depends on the time of evolution of the Menière disease, the initial prevalence of enhanced eye responses will also decrease with time. Considering these factors, it is probable that enhanced eye velocities will be only observed only in a fraction of Menière disease patients, and should be more prevalent in patients in the (relatively) early stage of the disease.

This theoretical prevalence of enhanced eye velocity responses in early Menière patients could suggest that enhanced velocity on head impulse test will be a very specific sign for

early stages of Menière disease, but with a limited clinical sensibility due to the relatively low incidence of utricular or semicircular hydrops.

We conclude that, with the described limitations, the results of our physical computation model support the hypothesis that in endolymphatic hydrops conditions, when they are affecting horizontal semicircular canal and utricular region on moderate dilatations, the eye velocity responses output by the aVOR will be enhanced by an 1.14 factor, and aVOR gain values will be over 1.1 for right-sided impulses. These predictions must be confirmed by clinical trials, but should be considered in clinical practice, especially when cases of early Menière disease are suspected.

DATA AVAILABILITY STATEMENT

All datasets generated for this study are included in the article/**Supplementary Material**.

ETHICS STATEMENT

This study was designed and performed in accordance with the ethical guidelines of the 1975 Declaration of Helsinki.

AUTHOR CONTRIBUTIONS

JR-M designed the computation model, performed the computer simulations and redacted the manuscript. XA co-designed the computation model and redacted the manuscript. KC developed the 3D geometric model and redacted the manuscript. AB submitted the clinical data, reviewed and redacted the manuscript. IC co-designed the computation model, redacted the manuscript and reviewed and supervised this research.

FUNDING

IC was receipt of a conjoint grant from the Garnett Passe and Rodney Williams Memorial Foundation; that grant pays the salary of AB.

ACKNOWLEDGMENTS

First author wants to thank to Michal Sajkowski and SIMFLOW Technologies (www.sim-flow.com) that very kindly contributed to this research by giving a full license of SimFlow computational fluid dynamics software. We thank L. A. McGarvie of Royal Prince Alfred Hospital, Sydney, for the data for six head impulses.

SUPPLEMENTARY MATERIAL

The Supplementary Material for this article can be found online at: https://www.frontiersin.org/articles/10.3389/fneur.2020.00289/full#supplementary-material

Appendix Videos 1–3 | Paraview software exported videos of the normal (**Video S1**), canal hydrops (**Video S2**) and utricular hydrops (**Video S3**) models for the raw head impulse test VI.

Appendix Figure 1 | Video head impulse tests used in the simulations. Traces of head velocity versus time for the set 6 head impulses, obtained from a real vHIT measurement database after lowpass filter postprocess, with peak head velocity varying in approximately equal steps from 102.62 °/s to 249.47 °/s.

Appendix Figure 2 | Increase of ampullar pressure during the head impulse test for the six progressive velocity head impulses computed on the three hydrops models. Higher pressure values were measured in both the models of canal hydrops, and those of utricular hydrops.

Appendix Figure 3 | Predicted eye velocity values during head impulse test for the six progressive velocity head impulses computed on the four hydrops models, showing the pressure values measured, assuming semicircular receptors to be highly overdamped accelerometer sensors. Higher velocity values were measured in both the models of canal hydrops, and those of utricular hydrops.

Appendix Simulation Files (Datasheet 1–5) | Compressed in this folder the reader can find: The anatomic 3D models folder, where the STL files used in this research can be found, these models are also automatically incorporated to the simulations folders. The head impulses folder, where the CSV files containing the head velocity real data used in this research can be found, these files are ready to be imported to the simulation software. In the "Dynamic mesh" section of the software, reader should select rigid type and rotating motion with omega from table, selecting the impulse of interest to be used as simulated head impulse and also setting the origin on movement to a medial point of the utricular region. In the Hydrops_SC, Hydrops_UC and NoHydrops folders configuration files ready to be open by the SimFlow 3.1 version simulation software are provided for each 3D STL model of the vestibular labyrinth. See methods section for detailed info about simulation software reference.

REFERENCES

1. Halmagyi G, Chen L, MacDougall H, Weber K, McGarvie L, Curthoys I. The video head impulse test. *Front Neurol.* (2017) 8:258. doi: 10.3389/fneur.2017.00258
2. Curthoys I, Halmagyi G. What does head impulse testing really test? *JAMA Otolaryngol Head Neck Surg.* (2019) 145:1080–1. doi: 10.1001/jamaoto.2019.2779
3. Aw S, Haslwanter T, Halmagyi G, Curthoys I, Yavor R, Todd M. Three dimensional vector analysis of the human vestibuloocular reflex in response to high-acceleration head rotations. I. responses in normal subjects. *J Neurophysiol.* (1996) 76: 4009–20. doi: 10.1152/jn.1996.76.6.4021
4. Rey-Martinez J, Batuecas-Caletrio A, Matiño E, Perez Fernandez N. HITCal: a software tool for analysis of video head impulse test responses. *Acta Otolaryngol.* (2015) 135:886–94. doi: 10.3109/00016489.2015.1035401
5. Rey-Martinez J, Burgess A, Curthoys I. Enhanced vestibulo-ocular reflex responses on vHIT. is it a casual finding or a sign of vestibular dysfunction? *Front Neurol.* (2018) 15:866. doi: 10.3389/fneur.2018.00866
6. Grieser B, McGarvie L, Kleiser L, Manzari L, Obrist D, Curthoys I. Numerical investigations of the effects of endolymphatic hydrops on the VOR response. Presented as poster presentation P-Q-4 at XXVIII bárány society meeting. buenos aires, Argentina. *J Vestib Res.* (2014) 24:219. doi: 10.3233/VES-140517
7. Valli P, Buizza A, Botta L, Zucca G, Ghezzi L, Valli S. Convection, buoyancy or endolymph expansion: what is the actual mechanism responsible for the caloric response of semi- circular canals? *J Vestib Res.* (2002) 12:155–65.
8. Turing AM. On Computable numbers, with an application to the entscheidungsproblem. *Proc Lond Math Soc.* (1937) s2–42:230–65. doi: 10.1112/plms/s2-42.1.230
9. Rey-Martinez J, McGarvie L, Perez-Fernandez N. Computing simulated endolymphatic flow thermodynamics during the caloric test using normal and hydropic duct models. *Acta*

Otolaryngol. (2017) 137:270–4. doi: 10.1080/00016489.2016.1242775
10. Grieser B, Kleiser L, Obrist D. Identifying mechanisms behind the tullio phenomenon: a computational study based on first principles. *J Assoc Res Otolaryngol.* (2016) 17:103–18. doi: 10.1007/s10162-016-0553-0
11. McGarvie L, Curthoys I, MacDougall H, Halmagyi G. What does the dissociation between the results of video head impulse versus caloric testing reveal about the vestibular dysfunction in Ménière's disease? *Acta Otolaryngol.* (2015) 135:859–65. doi: 10.3109/00016489.2015.1015606
12. Wesseling P. *Principles of Computational Fluid Dynamics*. Berlin, Heidelberg: Springer-Verlag (2001). doi: 10.1007/978-3-642-05146-3
13. Grant W, Curthoys I. Otoliths - accelerometer and seismometer; implications in Vestibular Evoked Myogenic Potential (VEMP). *Hear Res.* (2017) 253:26–35. doi: 10.1016/j.heares.2017.07.012
14. Wilson VJ, Jones GM. Biophysics of the peripheral end organs. In: VJ. Wilson, ed *Mammalian Vestibular Physiology*. Boston: Springer (1979). doi: 10.1007/978-1-4757-5702-6_3
15. Ramat S. Understanding the rotational vestibular ocular reflex: from differential equations to laplace transforms. *Prog Brain Res.* (2019) 248:29–44. doi: 10.1016/bs.pbr.2019.04.030
16. Squires T, Weidman M, Hain T, Stone H. A mathematical model for top-shelf vertigo: the role of sedimenting otoconia in BPPV. *J Biomech.* (2004) 37:1137–46. doi: 10.1016/j.jbiomech.2003.12.014
17. Gürkov R, Flatz W, Ertl-Wagner B, Krause E. Endolymphatic hydrops in the horizontal semicircular canal: a morphologic correlate for canal paresis in Ménière's disease. *Laryngoscope.* (2012) 123:503–6. doi: 10.1002/lary.23395
18. Lopez-Escamez J, Attyé A. Systematic review of magnetic resonance imaging for diagnosis of meniere disease. *J Vestib Res.* (2019) 29:121–9. doi: 10.3233/VES-180646
19. Okuno T, Sando I. Localization, frequency, and severity of endolymphatic hydrops and the pathology of the labyrinthine membrane in Menière's disease. *Ann Otol Rhinol Laryngol.* (1987) 96:438–45. doi: 10.1177/000348948709600418
20. Rabbitt R. Semicircular canal biomechanics in health and disease. *J Neurophysiol.* (2019) 121:732–55. doi: 10.1152/jn.00708.2018
21. Goyens J, Pourquie M, Poelma C, Westerweel J. Asymmetric cupula displacement due to endolymph vortex in the human semicircular canal. *Biomech Model Mechanobiol.* (2019) 18:1577–90. doi: 10.1007/s10237-019-01160-2
22. Yamauchi A, Rabbitt R, Boyle R, Highstein S. Relationship between inner-ear fluid pressure and semicircular canal afferent nerve discharge. *J Assoc Res Otolaryngol.* (2002) 3:26–44. doi: 10.1007/s1016200 10088
23. Rey-Martinez J, Thomas-Arrizabalaga I, Espinosa-Sanchez J, Batuecas-Caletrio A, Trinidad-Ruiz G, Matiño-Soler E, et al. Vestibulo-ocular reflex gain values in the suppression head impulse test of healthy subjects. *Laryngoscope.* (2018) 128:2383–9. doi: 10.1002/lary.27107
24. Tsuji K, Velázquez-Villaseñor L, Rauch S, Glynn R, Wall C III, Merchant S. Temporal bone studies of the human peripheral vestibular system. Meniere's disease. *Ann Otol Rhinol Laryngol Suppl.* (2000) 181:26–31. doi: 10.1177/00034894001090S505

Conflict of Interest: The authors declare that the research was conducted in the absence of any commercial or financial relationships that could be construed as a potential conflict of interest.

frontiers in Neurology

ORIGINAL RESEARCH
published: 14 May 2020
doi: 10.3389/fneur.2020.00332

Somatosensory Influence on Platform-Induced Translational Vestibulo-Ocular Reflex in Vertical Direction in Humans

Dieter F. Kutz[1†], Florian P. Kolb[2], Stefan Glasauer[3] and Hans Straka[4]*

[1] Institute of Human Movement Sciences, Faculty of Behavioral and Social Sciences, Chemnitz University of Technology, Chemnitz, Germany, [2] Department of Physiological Genomics, Institute of Physiology, Ludwig-Maximilian-University Munich, Munich, Germany, [3] Computational Neuroscience, Institute of Medical Technology, Brandenburg University of Technology Cottbus-Senftenberg, Cottbus, Germany, [4] Department of Biology II, Ludwig-Maximilians-University Munich, Munich, Germany

OPEN ACCESS

Edited by:
Dominik Straumann,
University of Zurich, Switzerland

Reviewed by:
Christoph Helmchen,
Luebeck University of Applied Sciences, Germany
Takeshi Tsutsumi,
Tokyo Medical and Dental University, Japan

***Correspondence:**
Dieter F. Kutz
dieter.kutz@uni-muenster.de

†Present address:
Dieter F. Kutz,
Institute of Sport and Exercise Sciences, University of Münster, Münster, Germany

Specialty section:
This article was submitted to Neuro-Otology, a section of the journal Frontiers in Neurology

Received: 16 January 2020
Accepted: 07 April 2020
Published: 14 May 2020

Citation:
Kutz DF, Kolb FP, Glasauer S and Straka H (2020) Somatosensory Influence on Platform-Induced Translational Vestibulo-Ocular Reflex in Vertical Direction in Humans. Front. Neurol. 11:332. doi: 10.3389/fneur.2020.00332

The vestibulo-ocular reflex (VOR) consists of two components, the rotational VOR (rVOR) elicited by semicircular canal signals and the translational VOR (tVOR) elicited by otolith signals. Given the relevant role of the vertical tVOR in human walking, this study aimed at measuring the time delay of eye movements in relation to whole-body vertical translations in natural standing position. Twenty (13 females and 7 males) healthy, young subjects (mean 25 years) stood upright on a motor-driven platform and were exposed to sinusoidal movements while fixating a LED, positioned at a distance of 50 cm in front of the eyes. The platform motion induced a vertical translation of 2.6 cm that provoked counteracting eye movements similar to self-paced walking. The time differences between platform and eye movements indicated that the subject's timing of the extraocular motor reaction depended on stimulus frequency and number of repetitions. At low stimulus frequencies (<0.8 Hz) and small numbers of repetitions (<3), eye movements were phase advanced or in synchrony with platform movements. At higher stimulus frequencies or continuous stimulation, eye movements were phase lagged by ∼40 ms. Interestingly, the timing of eye movements depended on the initial platform inclination. Starting with both feet in dorsiflexion, eye movements preceded platform movements by 137 ms, whereas starting with both feet in plantar flexion eye movement precession was only 19 ms. This suggests a remarkable influence of foot proprioceptive signals on the timing of eye movements, indicating that the dynamics of the vertical tVOR is controlled by somatosensory signals.

Keywords: locomotion, moving platform, retinal slip, bob, heave

INTRODUCTION

Vision is the dominant sensory modality in primates and humans that allows precise mapping and actively exploring the environment. However, during bipedal locomotion, the world cyclically shifts in the vertical direction and would thus impair optical image exploration. During everyday activities, visuo-vestibular reflexes induce counteracting eye/head movements that stabilize gaze on particular objects of interest (1). The VOR is the dominant motor reaction that provides fast compensation of retinal image motion during both translational and rotational head/body

movements. Both reflex components work in concert and ensure optimal image stabilization during passive and active motions (2).

The rotational VOR could completely compensate visual perturbations such that the entire visual scene is stabilized on the retina. In contrast, during translational motion, the respective VOR is unable to stabilize the overall retinal image but only the image in the fixation plane (1, 3). Objects in front of the fixation plane will virtually move in the opposite direction to the translation, whereas objects behind the fixation plane will move in the direction of the translation [e.g., Figure 2 in (1)]. Accordingly, images of near and distant objects cannot be simultaneously stabilized on the retina during head translations. One solution is that the brain deliberately chooses a set point that minimizes relative image motion of the object of interest with respect to the background (4–8). Thus, the brain must decide whether to stabilize a particular image of a near object on the fovea or to minimize image motion relative to the background. Apparently, the brain chooses a compromise set point for the gain of the translational VOR that is optimal for the overall visual performance during locomotion (9). Thus, the translational VOR decreases conjugate retinal image slip and minimizes binocular disparities during self-induced motion or passive displacements. These vestibular-driven eye movements, which are vital for visual acuity, complement and work synergistically with visuo-motor reflexes (e.g., ocular following reflex) and depend on a decoding of either optic flow patterns or depth and binocular disparity cues [for review see Angelaki (2)].

During locomotion, the erect, straight-legged gait of humans induces substantial head translations in the vertical plane as well as side-to-side head translations (8, 10). These head perturbations have a predominant frequency range of 0.5–5.0 Hz (11–13). The rotational VOR counteracts head motion by inducing image stabilizing eye rotations during locomotion with latencies as short as 14–18 ms (14, 15). In contrast, cortical visual processing is too slow to contribute to gaze stabilization during locomotion-induced head perturbations [latency $<$ 85 ms, Table 1 in (1)]. However, some cortical areas are involved in visuo-motor procession of egomotion that aim at guiding locomotion (16). In the event that these reflexes are functionally incomplete, the resulting retinal image slip activates visual tracking mechanisms that operate as closed-loop negative feedback systems to produce eye movements that reduce the retinal image slip (3). Studies of gaze stability with subjects walking on a treadmill report a large retinal image slip (7–14°/s) and oscillopsia—illusory motion of a near target (17, 18). This suggests that the translational VOR minimizes the relative retinal vertical image slip of far and near objects, which optimizes the ability of the visual system to use motion parallax as a cue for navigation (6, 19).

This study thus aimed at a systematical determination of the time delays of vertical eye movements during vertical whole-body translations in natural upright position. The employed frequency range complied with that of normal locomotion. To evaluate the influence of somatosensory signals on the timing, the foot position at start was systematically altered.

METHODS

Subjects and Ethics Statement

The study was performed with the permission of the ethics committee of the Ludwig-Maximilians-University Munich (#354-06) and was carried out in accordance with *The Code of Ethics of the World Medical Association* (*Declaration of Helsinki*). Twenty (13 females and 7 males) paid, healthy, young subjects [age 25.2 ± 0.6 years, mean ± standard error of mean (SEM)] participated in the study after having given written informed consent. Anthropomorphic characteristics of all participants are listed in **Table 1**. As a particularly important parameter, the length of the head–neck segment was calculated as the difference of the height of the eyes and the cervical vertebra C7. The mass of the head–neck segment was calculated by the formula given by (20) and (21):

$$head - neck\ mass = total\ body - weight * factor \tag{1}$$

$$with\ factor = \begin{cases} 0.08\ for\ women \\ 0.0826\ for\ men \end{cases}$$

Platform and Video-Oculography

Subjects were asked to stand barefoot on a computer-controlled, motor-driven platform with a separate unit for each leg (Stopper, Burladingen, Germany), which was described elsewhere (22). Subjects were instructed to position each foot at the end of each half-platform with a distance of the ankles ∼12.5 cm from the axis of the platform and to stand motionless on the platform (**Figure 1A**). The resultant distance between the heel centers was 23 cm, with the feet forming a slight V-shape. Platform movements were digitally, controlled, and recorded at 200 Hz/channel using a 12-bit A/D recording system (Micro Link 1000, WES, Germany) using custom-made software.

Eye movements were recorded with a mobile video-oculography system (EyeSeeCam, EyeSeeTec GmbH, Munich, Germany) at a sampling rate of 220 Hz. The spatial resolution of the eye-tracking device was 0.02° and the precision (relative error) on the order of 0.1° (23). Platform movements were synchronized to the start of the video-oculography by means of a specialized piece of equipment (Infrared SYNC Receiver for EyeSeeCam, EyeSeeTec GmbH, Munich, Germany).

Experimental Procedure and Analysis

Subjects stood motionless at the rear end of the platform under room illumination with the instruction to fixate a LED at 50-cm distance (**Figure 1A**). The LED was positioned at the level of the eyes at horizontal platform position (i.e., 0°) at the midline of the subjects. All test persons confirmed to see the LED. Some of them wore contact lenses. Nevertheless, visual acuity was not specifically measured. Subjects were exposed to two different stimulus conditions for vertical whole-body movements (experiments A and B in natural upright position). To achieve this goal, neither the head was fixed relative to the body nor body segments were fixed to each other. The movement amplitude of the platform was ± 6° with respect to the horizontal plane and resulted in a vertical translation of ± 1.3 cm of the

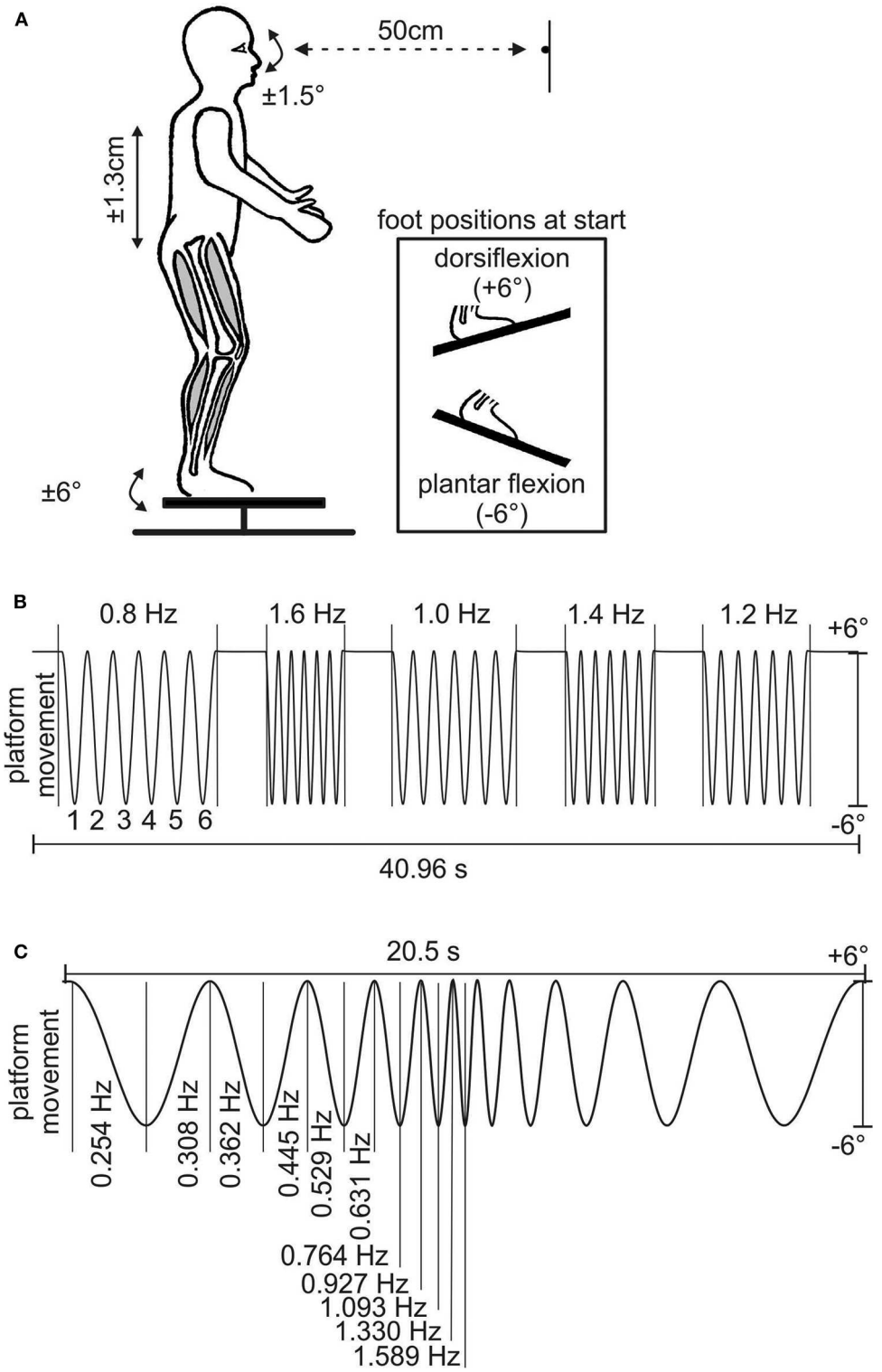

FIGURE 1 | Experimental setup and stimulus paradigms. **(A)** Schematic of human subject on the motion platform with the LED positioned at the level of the eyes; the inset shows the different foot positions at the start of experiment B. **(B)** Stimulus sequence of experiment A; *y*-axis indicates ± 6° of platform movement, which resulted in a vertical translation of the head of ± 1.3 cm. Owing to the proximity of the LED, an eye movement amplitude of ± 1.5° is required for complete compensation of the head translation. The numbers above and below the sinusoids indicate stimulus frequency and number of stimulus cycle, respectively. **(C)** Stimulus sequence of experiment B depicting the 11 cycles of ascending–descending stimulus frequency profile of the platform motion; *y*-axis is the same as in B.

TABLE 1 | Mean values and standard deviations (sd) of anthropometric parameters of all subjects ($N = 20$).

	Weight (kg)	Height above ground (cm)						Head–neck segment	
		Total	Eye	C7	Hip	Knee	Ankle	Length (cm)	Mass (kg)
Mean	67.4	170.4	160.0	145.0	96.9	47.8	8.0	25.5	5.5
sd	11.0	9.2	9.0	7.9	5.8	4.7	0.8	2.7	0.9
Range	53–92	158–188	147–178	134–161	88–111	41–58	6–9	21–30	4.4–7.6

The mass of the head–neck segment was calculated following Equation 1 [for references, see (20, 21)].

subject's body. This is similar to the vertical translation during self-paced walking (24, 25). To maintain fixation, subjects had to compensate the vertical translation by oppositely directed vertical eye movements. Owing to the proximity of the LED, the amplitude of the eye movements for complete compensation of the head translation must be ± 1.5° with respect to the straight-ahead position.

In experiment A, subjects were exposed to a stimulus consisting of five different frequencies (0.8, 1.6, 1.0, 1.4, and 1.2 Hz; see **Figure 1B**). The sequence consisted of six cycles at each frequency, separated by a 2-s interval of steady position. The total duration of a single trial was 40.96 s (**Figure 1B**). Subjects always started with feet in dorsiflexion (**Figure 1A**). Accordingly, the platform starting position was +6°. The sequence was presented to the subjects once for familiarization followed by five successive repetitions that were used for the analysis.

In experiment B, subjects were exposed to a stimulus of 22 up and down movements of the platform with logarithmically changing frequencies (26) at each change of movement direction (**Figure 1C**). Each trial was divided into two parts with the first half consisting of continuously increasing frequencies (0.254, 0.308, 0.362, 0.445, 0.529, 0.631, 0.764, 0.927, 1.093, 1.330, and 1.589 Hz) and the second half in reverse order. Initially, the sequence was presented to the subjects once with feet in plantar flexion for familiarization followed by five successive repetitions that were used for the analysis. For this purpose, the platform starting position was −6°. Immediately afterwards, the experiment was repeated starting with feet in dorsiflexion (**Figure 1A**), and five trials were recorded.

After the experiments, individual stride frequency during self-paced walking was determined to measure the time required to walk through an indoor corridor. The track was about 27 m long and was passed twice to count at least 40 strides.

Data and Statistical Analysis

Data and statistical analysis were carried out using the language for statistical computing "R" (27). Vertical eye movements were down sampled to 200 Hz. Blinks were removed and substituted in three steps. First, all intervals with eye velocities exceeding 25°/s were detected. Second, start and end of such an interval were defined by a preceding and following value of velocity below 10°/s. The coherence between vertical eye movements and platform movements was analyzed using the R-package "WaveletComp, version 1.1" (28). For coherency analyses, the platform data were inverted such that a coherency of +1 indicates a phase of 0° and −1 a phase of 180°. Examples of coherence analyses are provided in the (**Supplement Figures S1, S2**). For significant coherence ($p < 0.01$, Bonferroni corrected), time differences between eye and platform movement were taken into account as phase. For the same interval, the gain was calculated as the amplitude of the eye movement divided by the amplitude of the theoretically necessary eye movement to compensate the platform movement. The vertical head angle in the pitch plane was calculated by integration of the head velocity obtained by the video-oculography system. The calculations of phase and gain were performed in experiment A separately for each of the six cycles of the five stimulus frequencies. For experiment B, the calculations were done separately for each half cycle of stimulation frequency, half-trial (increasing frequency and decreasing frequency), and foot position at start (dorsiflexion and plantar flexion). Differences between stimulus frequency and cycle in experiment A and between stimulus frequency, half-trial, and foot position at start in experiment B were analyzed by ANOVA with mixed design and multiple repetitions using the R-package "ez," version 4.4-0 (29). Effect size η^2_G is given to provide comparability (30). *p*-values were corrected following Greenhouse–Geisser, where appropriate.

RESULTS

A total of 20 subjects, aged 25.2 ± 0.6 years (mean ± SEM, 13 females), participated in both sets of experiments. For the experiments, participants were asked to stand on a motion platform that allowed applying vertical body translations. During the experiments, subjects had to fixate a white LED (**Figure 1A**), which, during vertical translations, provoked counteracting eye movements to maintain gaze on the target. In experiment A, five sequences of distinct platform motion frequencies between 0.8 and 1.6 Hz were tested (see **Figure 1B**). Experiment B consisted of sinusoidal platform motion with logarithmically ascending–descending stimulus frequency profile that ranged from 0.25 to 1.59 Hz (**Figure 1C**).

Experiment A

In general, subjects were able to compensate the cyclic vertical body translations by dynamically adequate counteracting eye movements, however, with two limitations: first, eye movement magnitudes were smaller than required for complete motion compensation (**Figure 2A**; note that platform movement is inverted); second, the eye position in the orbital cavity was not stable but oscillated around the horizontal straight ahead position (0° in **Figure 2A**). Interestingly, the head angle in the

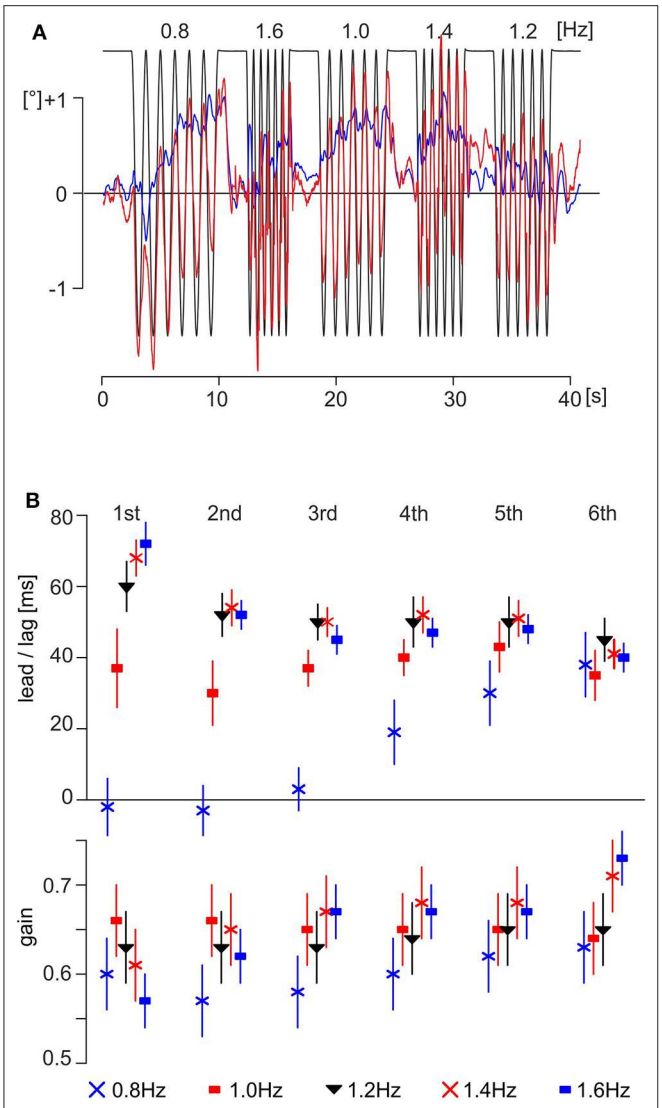

FIGURE 2 | Data and results of experiment A. **(A)** Exemplary traces of one subject (male, 26.1 years); the eye motion is shown as a thick red line and the head angle in the pitch plane as a thin blue line. The theoretically necessary eye movement to fully compensate for the platform movement is shown as a thin black line. Note that the platform motion is shown inverted, scaled to overlap with eye position when the movement is compensatory. **(B)** Time delays (upper part) and gain (lower part) of evoked eye movements of all subjects (mean ± SEM; $N = 20$) in experiment A with respect to stimulus cycle.

pitch plane describes an envelope of the eye movement maxima (**Figure 2A**, blue and red lines), with a tendency of the head pointing upwards. The original position is reached again and again during the stimulation pauses. This is an indication that the participant is changing his posture slightly by lowering the body. It seems that the participant tries to attenuate the stimulation by allowing relative movements of joints (e.g., vertebrae, hip, knee, and ankle). This changed posture is compensated by an inclination in the pitch plane. During the pauses, he or she stretches again and the pitch angle returns to zero.

The time delays of the eye movements with respect to the vertical body motion differed depending on stimulus frequency and cycle number (**Figure 2B**, upper part). The fastest reactive eye movements were observed for the first and second cycles of the motion sequence at 0.8 Hz with a lag of 2 ± 6 ms (mean ± SEM) and a lead of −4 ± 5 ms, respectively (**Figure 2B**, upper part, blue X at the first and second cycles). Interestingly, the time delays at 0.8 Hz increased over the following four cycles to reach a steady state of 37 ± 7 ms for the sixth cycle (**Figure 2B**, upper part, blue X at sixth cycle). The longest latency of 72 ± 4 ms was observed for the first cycle of the motion sequence at 1.6 Hz (**Figure 2B**, upper part, filled blue squares at the first cycle) that, however, decreased during the following five cycles to 40 ± 2 ms for the sixth cycle (**Figure 2B**, upper part, filled blue squares at the sixth cycle). A similar behavior was encountered for the sequences with vertical motion stimulus frequencies of 1.2 and 1.4 Hz. At both stimulus frequencies, the time delays decreased from the first to sixth cycle (**Figure 2B**, upper part, filled black triangles and red X for 1.2 and 1.4 Hz, respectively). Interestingly, however, during stimulation with a motion frequency of 1.0 Hz, the time delays remained relatively constant over all cycles with a mean of 37 ± 2 ms (**Figure 2B**, upper part, filled red squares). This suggests that platform motion at 1.0 Hz appears to resonate with a particular intrinsic temporal feature at variance with higher or lower stimulus frequencies. ANOVA with mixed design and multiple repetitions confirmed the significant effects ($\alpha = 0.001$, Bonferroni corrected) for the main effect *frequency* and for the interaction *frequency* × *number of cycle* (**Table 2**). The gain was similar for all frequencies and cycles (**Figure 2B**, lower part), with a range from 0.57 to 0.73 (first and sixth cycles for a stimulation at 1.6 Hz, filled blue squares in **Figure 2B**, lower part) and a total mean value of 0.64. ANOVA with mixed design and multiple repetitions showed a significant effect only for the interaction *frequency* × *number of cycle* ($\alpha = 0.001$, Bonferroni corrected, **Table 2**). This interaction is mainly driven by the increasing gain for stimulation frequencies 1.4 and 1.6 Hz during repetitions (**Figure 2B**, lower part, red X and filled blue squares, respectively).

In order to allow a comparison of vertical eye motion dynamics during passive perturbations with those during locomotion, we determined individual stride parameters during self-paced walking for each subject. The mean stride frequency was 0.99 ± 0.02 strides/s (mean ± SEM), the mean length of the head–neck segment was 25.5 ± 2.7 cm, and the mean mass of the head–neck segment was 5.5 ± 0.9 kg (**Table 1**). Interestingly, stride frequency decreases significantly with increasing length of the head–neck segment [$F_{(1,12)} = 7.17$, $p = 0.020$, $\eta^2_G = 0.374$] and with increasing mass [$F_{(1,12)} = 5.53$, $p = 0.037$, $\eta^2_G = 0.316$] (**Figure 3**, adj. $R^2 = 0.369$). Assuming that the head–neck segment is an inverted version of a simple gravity pendulum with a pendulum length of 25.5 cm, the swing period approximates to 1.01 s, which corresponds to stride frequency. Hence, subjects prefer a stride frequency that matches the physical characteristics of their head–neck system. These results potentially explain the phase advance of counteracting eye movements during vertical motion platform oscillations when the stimulus frequency is lower than the individual stride frequency. This assumption was

TABLE 2 | Statistical parameters of the ANOVA of experiment A.

Experiment A	Effect	Degree of freedom (nominator)	Degree of freedom (denominator)	*F*	*P*	η^2_G
Timing	Frequency	4	76	22.10	$\mathbf{5.12 * 10^{-8}}$	0.21
	Cycle	5	95	4.21	$2.68 * 10^{-2}$	0.02
	Frequency × cycle	20	380	10.78	$\mathbf{1.09 * 10^{-5}}$	0.09
Gain	Frequency	4	76	1.92	$1.64 * 10^{-1}$	0.02
	Cycle	5	95	7.61	$5.02 * 10^{-3}$	0.01
	Frequency × cycle	20	380	6.75	$\mathbf{1.15 * 10^{-5}}$	0.02

p-values were corrected following Greenhouse–Geisser, where appropriate. Significant p-values after Bonferroni correction at a level of α = 0.001 are indicated in bold.

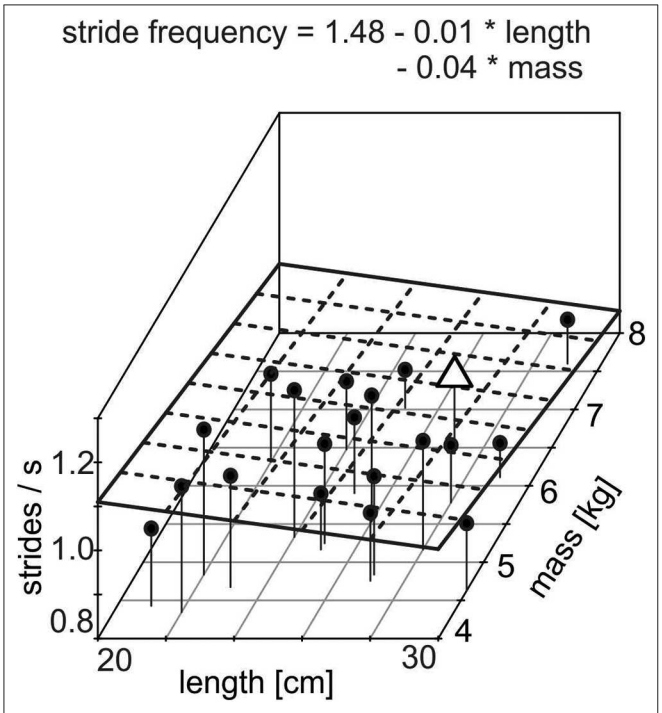

FIGURE 3 | Three-dimensional scatterplot of individual stride frequency with respect to length and mass of the individual head–neck segment of all subjects ($N = 20$); individual values are shown as black dots; the plane given by the dashed lines shows the regression plane given by the equation. The data of the subject, shown in **Figures 2A**, **4A**, are indicated by an open triangle. Note the significant decrease in stride frequency with increasing length and mass (adjusted $R^2 = 0.369$).

further tested in experiment B, where a stimulus sequence with lower frequencies was used.

Experiment B

Application of sinusoidal platform motion with a logarithmically ascending–descending stimulus frequency profile (**Figures 1C**, **4A**) provoked counteracting eye movements with corresponding dynamics. As in experiment A, the eye motion did not completely offset the vertical head/body translation, neither at low nor at higher stimulus frequencies (**Figure 4A**). During the initial part of the stimulus, subjects often anticipated or phase-timed the eye movements (see interval of 0–5 s in **Figure 4A**). In contrast, eye movements during later stimulus cycles were often phase lagged with respect to the vertical head/body perturbation (see interval of 12–17 s in **Figure 4A**). The head angle in the pitch plane rises slowly until 9.2 s, then tilts slowly until 13.4 s, and finally rises again (**Figure 4A**, blue line). A correlation between head position and eye position is not visible (**Figure 4A**, blue line and red line). Again, the participant tries to attenuate the stimulation by a slight change in his posture, which resulted by allowing relative movements of corresponding joints. As this stimulation is continuous and there is no pause time, the inclination of the head reaches a value that is perceived as to great and a counteracting movement of the head is initiated (e.g., **Figure 4A**, blue line approximately at 9.2 s). Overall, subjects appeared to be unable to predict the forthcoming stimulus cycle on the basis of the prior cycle.

In general, the time delays differed owing to the continuously increasing or decreasing stimulus frequencies and owing to the foot position at start (**Figure 4B**, upper part). During increasing frequencies up to 0.76 Hz, eye movements were phase leading or in phase with the platform movements. Note that during this interval the mean time delay of the response with feet starting in dorsiflexion was significantly shorter than the corresponding time delay with feet starting in plantar flexion (**Figure 4B**, upper part, red and orange thick lines). At higher stimulus frequencies, that is, from 0.97 to 1.59 Hz, eye movements were phase lagged relative to the platform movements and independent of foot position, with a mean lag of 40 ± 2 ms (mean ± SEM) at 1.59 Hz. During the subsequent stimulus sequence with decreasing frequencies, eye movements remained phase lagging independent of stimulus frequency and foot position (**Figure 4B**, upper part, blue and cyan thick lines for dorsiflexion and plantar flexion, respectively) with a mean time delay of 41 ± 11 ms. ANOVA with mixed design and multiple repetitions confirmed the significance ($\alpha = 0.001$, Bonferroni corrected) for the main effects *frequency* and *half-trial*, and for the interaction *frequency* × *half-trial*, *frequency* × *foot position at start*, half-*trial* × *foot position at start*, and *frequency* × *half-trial* × *foot position at start*. The significance of the main effect *foot position at start* reached after Bonferroni correction only the value of a trend (**Table 3**). The gain was similar for all frequencies and position of the feet (**Figure 4B**, lower part) with a range from 0.58 (increasing frequencies, dorsiflexion at 0.362 Hz) to 0.89 (increasing frequencies, plantar flexion at 1.093 Hz) and a total

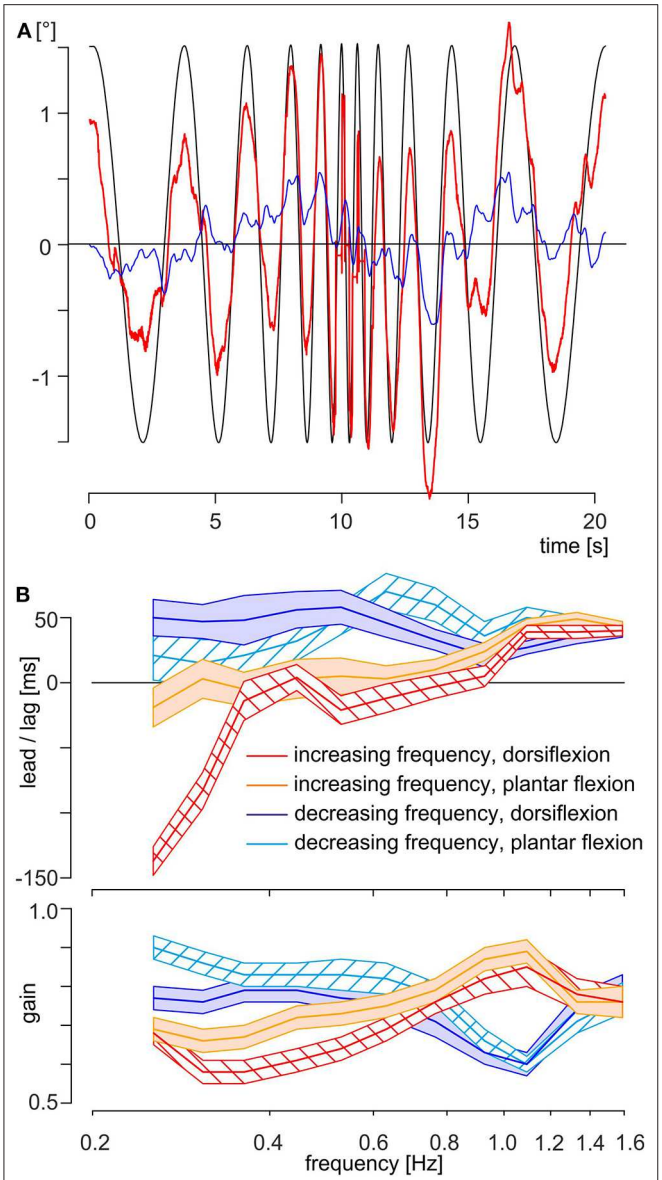

FIGURE 4 | Data and results of experiment B. **(A)** Exemplary traces of the same subject as shown in **Figure 2**; the eye motion is indicated as a thick red line and the head angle in the pitch plane as a thin blue line. The theoretically necessary eye movement to fully compensate for the platform movement is shown as a thin black line. Note that the platform motion is shown inverted, scaled to overlap with eye position when the movement is compensatory. **(B)** Time delays (upper part) and gain (lower part) of evoked eye movements of all subjects ($N = 20$) in experiment B with respect to stimulus frequency and separated by half-trial and position of the feet at start. The mean is shown as a colored thick line and SEM as a colored area with, red line and red left oblique hatched area: increasing frequency with feet in dorsiflexion, orange line and orange filled area: increasing frequency with feet in plantar flexion, blue line and blue filled area: decreasing frequency with feet in dorsiflexion, cyan line and cyan right oblique hatched area: decreasing frequency with feet in plantar flexion.

mean value of 0.74. ANOVA with mixed design and multiple repetitions showed a significant effect only for the interaction *frequency* × *half-trial* ($\alpha = 0.001$, Bonferroni corrected, **Table 3**). This interaction is mainly driven by the higher gain for the stimulus sequence with decreasing frequencies below 0.764 Hz (**Figure 4B**, lower part, red and orange thick lines vs. blue and cyan thick lines).

DISCUSSION

This study aimed at determining the time delays of counteracting vertical eye movements induced during cyclic vertical body movements. Eye movements preceded body movements during the first cycle of stimulus frequencies < 1 Hz but lagged body motion at stimulus frequencies > 1 Hz. During continuous stimulation, the time delays of eye movements reached a steady-state value of ∼40 ms. For frequencies between 1.9 and 2.3 Hz, latencies from 20 ms (6, 31) up to 50 ms (32) and 70 ms (33) were reported. For stimulation frequencies below 1 Hz, lagging behavior was reported [38 ms at 0.73 Hz, (33)]. In this case, the reported value was calculated over a period of more than 20 s during stimulation with a sum-of-sines waveform. Hence, the reported value refers to steady state and is similar to our value. Comparable observations were also reported for horizontal translational motion stimulation on a sled. Phase-advanced eye movements with 111 and 56 ms were reported for stimulation frequencies of 0.25 and 0.5 Hz, respectively (34), whereas eye movements lagged body translation for 8 ms at a stimulus frequency of 0.5 Hz (35). Independent of stimulus frequency, the gain of the eye movements was lower than necessary for compensation with a total mean value of 0.64 and 0.74 for experiments A and B, respectively. This is consistent with the reported gain spectrum (0.42–0.75) of earlier reports (6, 31–33). Interestingly, the mean time lag of 40 ms in the current study is maintained during an experimental sequence even when stimulus frequency decreased below 1 Hz. This suggests that this magnitude is the preferred frequency for this reactive motor behavior, which perfectly matches the value (mean: 0.99 strides/s) for self-paced stride frequency. Moreover, this coincidence extends to normal walking at a speed of 4–5 km/h, equivalent to a stride frequency of ∼1 stride/s in normal subjects at which the energy costs are the best compromise between movement effort and muscle efficiency (25).

During vertical body movements at a frequency < 1 Hz, the time delays of the eye movements depended on the starting position. For the first two stimulation frequencies, eye movements started earlier when feet at start were in dorsiflexion than in plantar flexion (**Figure 4B**, upper part, red and orange thick lines). This might derive from the fact that during vertical body movements, the LED elicits an optokinetic reaction or pursuit eye movement. This assumption complies with a larger influence of vision up to stimulus frequencies of 0.4 Hz as the response gains are close to 1, whereas gains decrease significantly at higher visual motion stimulus frequencies (36–40). Different results have been reported regarding the directional symmetry of the gain. Symmetrical responses were reported on a group level by (36) and (40), whereas individual subjects could either have higher gains for downward directed (39, 40) or upward movements (36). The later behavior was also

TABLE 3 | Statistical parameters of the ANOVA of experiment B.

Experiment B	Effect	Degree of freedom (nominator)	Degree of freedom (denominator)	*F*	*p*	η^2_G
Timing	Frequency	10	190	12.78	$\mathbf{1.79 * 10^{-5}}$	0.12
	Half-trial	1	19	52.59	$\mathbf{6.99 * 10^{-7}}$	0.14
	Foot position at start	1	19	7.99	$1.08 * 10^{-2}$	0.02
	Frequency × half-trial	10	190	21.27	$\mathbf{9.26 * 10^{-10}}$	0.11
	Frequency × foot position at start	10	190	4.58	$\mathbf{2.86 * 10^{-3}}$	0.02
	Half-trial × foot position at start	1	19	22.78	$\mathbf{1.32 * 10^{-4}}$	0.02
	Frequency × half-trial × foot position at start	10	190	14.81	$\mathbf{2.76 * 10^{-7}}$	0.06
Gain	Frequency	10	190	0.75	0.48	0.01
	Half-trial	1	19	7.74	$1.19 * 10^{-2}$	0.01
	Foot position at start	1	19	6.98	$1.61 * 10^{-2}$	0.03
	Frequency × half-trial	10	190	55.18	$\mathbf{2.98 * 10^{-15}}$	0.21
	Frequency × foot position at start	10	190	3.40	$2.63 * 10^{-2}$	0.02
	Half-trial × foot position at start	1	19	0.10	0.76	0.00
	Frequency × half-trial × foot position at start	10	190	2.43	$7.44 * 10^{-2}$	0.01

p-values were corrected following Greenhouse–Geisser, where appropriate. Significant p-values after Bonferroni correction at a level of α = 0.001 are indicated in bold. For the effect "half-trial," the frequency increased continuously during the first half and decreased continuously during the second half. The foot position at start was dorsiflexion or plantar flexion.

described by (39). A prevalence of the upward direction on group level was reported by (37) and by (38). It must be noted, however, that in our experiment the platform direction and, hence, the stimulus direction reverses after every half wave and, second, that the direction of the visual field motion depends on the point of fixation (1, 3). Assuming that the direction of stimulation of the visual field behind the LED would have a stronger influence on the time delays, the results must be reordered. The sequence for upward direction would be 0.254 Hz/dorsiflexion, 0.308 Hz/plantar flexion, 0.362 Hz/dorsiflexion, and so forth, and for the downward direction 0.254 Hz/plantar flexion, 0.308 Hz/dorsiflexion, 0.362 Hz/plantar flexion, and so forth (**Supplementary Table S1**). ANOVA with mixed design and multiple repetitions showed no significant result for the main effect *direction* and the interaction *direction* × *half-trial*. The only significant effect was for *half-trial* demonstrating that the system reached a steady state during the first half of the trial (**Figure 4B**, upper part). Hence, the differences in time delays with respect to the starting position of the feet cannot be exclusively explained by visuo-motor contributions.

At the start, the test person is in an upright position in both forms of stimulation (dorsiflexion and plantar flexion). Therefore, the signals of the otolith system are comparable. It can be assumed that the test person tries to maintain the original posture and orientation during the stimulation. Therefore, he or she is dependent on somato-sensory signals as a replacement for the otolith system. This is important because it indicates the likelihood of proprioceptive influences on eye movement behavior. Mullick et al. (41) studied electromyographic activity of three lower limb muscles (*musculus gastrocnemius*, *m. soleus*, and *m. tibialis anterior*) in human standing quietly on a inclined surface similar to our experiments. They show that the *m. gastrocnemius* and the *m. soleus* are more active when standing on a descending platform (plantar flexion) compared to an ascending to ascending platform (dorsiflexion) whereas the *m. tibialis* anterior does not show significant differences (see **Figure 2A** of that paper). The latter one is co-activated with the former during posture stabilization after perturbation [e.g., Kolb et al., (42)]. The different muscle activation during the initial situations is accompanied by corresponding gamma-motoneuron activity, which in turn is associated with a different sensitivity of the muscle spindle. Because the *m. tibialis* does not contribute significantly in both initial situations, proprioceptive perception is driven by the different activation of the *m. gastrocnemius* and *m. soleus*. We are convinced that this influences extraocular motor function and thus the different response behaviors. Thus, this extraocular motor behavior can be appropriated to the responses of the ankle extensor.

In addition, recordings of the *m. gastrocnemius*-innervating tibial nerve [e.g., Jones and Small (43), Riffel and Stohr (44), and Tinazzi et al., (45)] indicated that the average latency from the ankle to the brainstem is ∼29 ms, somewhat longer than the shortest latency for eye muscle activation in humans (11–16 ms) or following step-like head translation [16 ms; (5)]. A value of 10–15 ms therefore appears to be the typical delay for motion-induced eye movements as suggested from recordings of single motor unit activity of the *inferior oblique* and *inferior rectus* eye muscles following skull vibration and sound application in human subjects (46). Following arithmetic addition of the latencies from the ankle to the brainstem and from the brainstem to the eye muscles, it is likely that ankle movements could in fact evoke eye muscle activity within 40–46 ms.

Subjects apparently learn to counteract gaze changes induced by vertical body movements using sensory information from

the feet and/or other parts of the leg. Altered gravity—by unloading body weight or by exposition to hypogravity and hypergravity during parabolic flights—is able to change head and eye movements (47–51). For example, head pitch amplitude increases ∼1° with respect to normal walking when subjects perform a 30-min unloaded locomotor training while watching a movie on a computer screen as gaze task. During the post-training phase, subjects return to normal behavior after just four walking trials of 30 s each (51). In addition, upright-standing subjects during parabolic flights produce a sustained downbeat nystagmus during sudden hypogravity and a sustained upbeat nystagmus during sudden hypergravity (47–50). Recent studies have shown that a positional nystagmus is common in healthy subjects under normal gravity depending on the subject's position (52, 53) and can be explained by the effect of gravity on otolith pathways for static eye position (54). Following (50), the results of these different experiments lead to a set of important conclusions: "(1) sustained downbeat or upbeat nystagmus in altered gravity unmasks a fundamental, permanent influence of normal gravity on vertical eye position, which is maximal in the upright position and minimal in the horizontal position of the head; (2) consequently, to stabilize vertical eye position in erect positions of the head, a neuronal system is required to counteract gravity permanently." Nevertheless, human subjects are able to adapt to prolonged changes in gravity (50, 51), suggesting that peripheral somatosensory signals converge with otolith signals. During unloaded locomotor training, the central nervous system must adapt motor behavior to reduced somatosensory signals from the foot plantar sole as well as from other parts of the body. Hence, a fast mechanism to readapt vestibular signals by somatosensory signals must therefore exist. A putative structure for such adaptive computations is the cerebellum (54–57). Thus, in conclusion, during walking, eye movements are coupled to the somatosensory system through a modulation of the vestibulo-ocular reflex.

DATA AVAILABILITY STATEMENT

The datasets generated for this study will not be made publicly available due to local law restrictions.

ETHICS STATEMENT

The studies involving human participants were reviewed and approved by Ludwig-Maximilians-University Munich, Faculty of Medicine. The patients/participants provided their written informed consent to participate in this study.

AUTHOR CONTRIBUTIONS

DK and FK performed data collection and analysis. The manuscript was written in sections by the different authors and was compiled by DK. All authors read and approved the final manuscript and contributed to the study conception and design.

FUNDING

The authors acknowledge financial support from the Bernstein Center for Computational Neuroscience Munich (BT-1) and the Deutsche Forschungsgemeinschaft (GL 342/2-1).

ACKNOWLEDGMENTS

We are indebted to all subjects for participating so willingly in our study.

SUPPLEMENTARY MATERIAL

The Supplementary Material for this article can be found online at: https://www.frontiersin.org/articles/10.3389/fneur.2020.00332/full#supplementary-material

REFERENCES

1. Miles FA. The neural processing of 3-D visual information: evidence from eye movements. *Eur J Neurosci*. (1998) 10:811–22. doi: 10.1046/j.1460-9568.1998.00112.x
2. Angelaki DE. Eyes on target: what neurons must do for the vestibuloocular reflex during linear motion. *J Neurophysiol*. (2004) 92:20–35. doi: 10.1152/jn.00047.2004
3. Miles FA. Visual stabilization of the eyes in primates. *Curr Opin Neurobiol*. (1997) 7:867–71. doi: 10.1016/S0959-4388(97)80148-1
4. Rushton DN. Geometrical optics of the retinal image stabilisation device. *J Neurol Neurosurg Psychiatr*. (1989) 52:137–8. doi: 10.1136/jnnp.52.1.137
5. Ramat S, Straumann D, Zee DS. Interaural translational VOR: suppression, enhancement, and cognitive control. *J Neurophysiol*. (2005) 94:2391–402. doi: 10.1152/jn.01328.2004
6. Liao K, Walker MF, Joshi A, Reschke M, Leigh RJ. Vestibulo-ocular responses to vertical translation in normal human subjects. *Exp Brain Res*. (2008) 185:553–62. doi: 10.1007/s00221-007-1181-z
7. Liao K, Walker MF, Joshi A, Reschke M, Wang Z, Leigh RJ. A reinterpretation of the purpose of the translational vestibulo-ocular reflex in human subjects. In: Kennard C, Leigh RJ, editors. *Progress in Brain Research*. Oxford: Elsevier (2008). p. 295–302.
8. Liao K, Schneider RM, Yaniglos SS, Bertolini G, Glendinning P, Sawyer J, et al. Visual and vestibular determinants of the translational vestibulo-ocular reflex. *Ann NY Acad Sci*. (2011) 1233:263–70. doi: 10.1111/j.1749-6632.2011.06148.x
9. Zee DS, Jareonsettasin P, Leigh RJ. Ocular stability and set-point adaptation. *Philos Trans R Soc B Biol Sci*. (2017) 372:20160199. doi: 10.1098/rstb.2016.0199
10. MacNeilage PR, Glasauer S. Quantification of head movement predictability and implications for suppression of vestibular input during locomotion. *Front Comput Neurosci*. (2017) 11:47. doi: 10.3389/fncom.2017.00047
11. Grossman GE, Leigh RJ, Abel LA, Lanska DJ, Thurston SE. Frequency and velocity of rotational head perturbations during locomotion. *Exp Brain Res*. (1988) 70:470–6. doi: 10.1007/BF00247595
12. Pozzo T, Berthoz A, Lefort L. Head stabilization during various locomotor tasks in humans. *Exp Brain Res*. (1990) 82:97–106. doi: 10.1007/BF00230842
13. Hausamann P, Daumer M, Macneilage PR, Glasauer S. Ecological momentary assessment of head motion: toward normative data of head stabilization. *Front Human Neurosci*. 13:179. doi: 10.3389/fnhum.2019.00179
14. Lisberger S. The latency of pathways containing the site of motor learning in the monkey vestibulo-ocular reflex. *Science*. (1984) 225:74–6. doi: 10.1126/science.6610214
15. Bush GA, Miles FA. Short-latency compensatory eye movements associated with a brief period of free fall. *Exp Brain Res*. (1996) 108:337–40. doi: 10.1007/BF00228107

16. Serra C, Galletti C, Di Marco S, Fattori P, Galati G, Sulpizio V, et al. Egomotion-related visual areas respond to active leg movements. *Hum Brain Mapp*. (2019) 40:3174–91. doi: 10.1002/hbm.24589
17. Crane BT, Demer JL. Human gaze stabilization during natural activities: translation, rotation, magnification, and target distance effects. *J Neurophysiol*. (1997) 78:2129–44. doi: 10.1152/jn.1997.78.4.2129
18. Moore ST, Hirasaki E, Cohen B, Raphan T. Effect of viewing distance on the generation of vertical eye movements during locomotion. *Exp Brain Res*. (1999) 129:347–61. doi: 10.1007/s002210050903
19. Liao K, Walker MF, Joshi AC, Reschke M, Strupp M, Wagner J, et al. The linear vestibulo-ocular reflex, locomotion and falls in neurological disorders. *Restor Neurol Neurosci*. (2010) 10:91–103. doi: 10.3233/RNN-2010-0507
20. Plagenhoef S, Evans FG, Abdelnour T. Anatomical data for analyzing human motion. *Res Quart Exercise Sport*. (1983) 54:169–78. doi: 10.1080/02701367.1983.10605290
21. Tierny RT, Sitler MR, Swanik CB, Swanik KA, Higgins M, Torg J. Gender differences in head-neck segment dynamic stabilization during head acceleration. *Med Sci Sports Exercise*. (2005) 37:272–9. doi: 10.1249/01.MSS.0000152734.47516.AA
22. Baldinotti I, Timmann D, Kolb FP, Kutz DF. Jerk analysis of active body-weight-transfer. *Gait Posture*. (2010) 32:667–72. doi: 10.1016/j.gaitpost.2010.08.011
23. Schneider E, Villgrattner T, Vockeroth J, Bartl K, Kohlbecher S, Bardins S, et al. EyeSeeCam: an eye movement–driven head camera for the examination of natural visual exploration. *Ann NY Acad Sci*. (2009) 1164:461–7. doi: 10.1111/j.1749-6632.2009.03858.x
24. Mamoto Y, Yamamoto K, Imai T, Tamura M, Kubo T. Three-dimensional analysis of human locomotion in normal subjects and patients with vestibular deficiency. *Acta Oto-Laryngol*. (2002) 122:495–500. doi: 10.1080/00016480260092282
25. Massaad F, Lejeune TM, Detrembleur C. The up and down bobbing of human walking: a compromise between muscle work and efficiency. *J Physiol*. (2007) 582:789–99. doi: 10.1113/jphysiol.2007.127969
26. Kolb FP, Rubia FJ. Information about peripheral events conveyed to the cerebellum via the climbing fiber system in the decerebrate cat. *Exp Brain Res*. (1980) 38:363–73. doi: 10.1007/BF00237516
27. R-Coreteam. *R: A Language and Environment for Statistical Computing*. Vienna: R Foundation for Statistical Computing (2018).
28. Roesch A, Schmidbauer H. *WaveletComp: Computational Wavelet Analysis*. R package version 1.1 ed. (2018). Available online at: https://CRAN.R-project.org/package=WaveletComp
29. Lawrence MA. *ez: Easy Analysis and Visualization of Factorial Experiments*. R package version 4.4-0 ed. (2016). Available online at: https://CRAN.R-project.org/package=ez
30. Bakeman R. Recommended effect size statistics for repeated measures designs. *Behav Res Methods*. (2005) 37:379–84. doi: 10.3758/BF03192707
31. Demer JL, Viirre ES. Visual-vestibular interaction during standing, walking, and running. *J Vestibular Res Equil Orient*. (1996) 6:295–313. doi: 10.3233/VES-1996-6407
32. Schneider R, Walker MF. Amplitude and frequency prediction in the translational vestibulo-ocular reflex. *J Vestib Res*. (2014) 24:357–64. doi: 10.3233/VES-140528
33. Walker M, Liao K. The human translational vestibulo-ocular reflex in response to complex motion. *Ann NY Acad Sci*. (2011) 1233:242–8. doi: 10.1111/j.1749-6632.2011.06167.x
34. Seidman SH, Yong NA, Paige GD. The perception of translational motion. *Ann NY Acad Sci*. (2009) 1164:222–8. doi: 10.1111/j.1749-6632.2009.03771.x
35. Shelhamer M, Roberts DC, Zee DS. Dynamics of the human linear vestibulo-ocular reflex at medium frequency and modification by short-term training. *J Vestib Res Equilib Orient*. (2000) 10:271–82.
36. Baloh RW, Honrubia V, Yee RD, Jacobson K. Vertical visual-vestibular interaction in normal human subjects. *Exp Brain Res*. (1986) 64:400–6. doi: 10.1007/BF00340476
37. Van Den Berg AV, Collewijn H. Directional asymmetries of human optokinetic nystagmus. *Exp Brain Res*. (1988) 70:597–604. doi: 10.1007/BF00247608
38. Murasugi CM, Howard IP. Up-down asymmetry in human vertical optokinetic nystagmus and afternystagmus - contributions of the central and peripheral retinae. *Exp Brain Res*. (1989) 77:183–92. doi: 10.1007/BF00250580
39. Böhmer A, Baloh RW. Vertical optokinetic nystagmus and optokinetic afternystagmus in humans. *J Vestib Res*. (1990) 1:309–15.
40. Demer JL. Mechanisms of human vertical visual-vestibular interaction. *J Neurophysiol*. (1992) 68:2128–46. doi: 10.1152/jn.1992.68.6.2128
41. Mullick AA, Turpin NA, Hsu S-C, Subramanian SK, Feldman AG, Levin MF. Referent control of the orientation of posture and movement in the gravitational field. *Exp Brain Res*. (2018) 236:381–98. doi: 10.1007/s00221-017-5133-y
42. Kolb FP, Lachauer S, Maschke M, Timmann D. Classical conditioning of postural reflexes. *Pflugers Archiv-Eur J Physiol*. (2002) 445:224–37. doi: 10.1007/s00424-002-0892-z
43. Jones SJ, Small DG. Spinal and sub-cortical evoked-potentials following stimulation of posterior tibial nerve in man. *Electroencephal Clin Neurophysiol*. (1978) 44:299–306. doi: 10.1016/0013-4694(78)90305-X
44. Riffel B, Stohr M. Spinal and subcortical somatosensory evoked-potentials after stimulation of the tibial nerve. *Archiv Fur Psychiatr Nervenkrankheiten*. (1982) 232:251–63. doi: 10.1007/BF02141785
45. Tinazzi M, Zanette G, Polo A, Bonato C, Manganotti P, Fiaschi A, et al. Subcortical P30 potential following tibial nerve stimulation: detection and normative data. *Italian J Neurol Sci*. (1995) 16:623–8. doi: 10.1007/BF02230912
46. Weber KP, Rosengren SM, Michels R, Sturm V, Straumann D, Landau K. Single motor unit activity in human extraocular muscles during the vestibulo-ocular reflex. *J Physiol*. (2012) 590:3091–101. doi: 10.1113/jphysiol.2011.226225
47. Von Baumgarten RJ, Baldrighi G, Vogel H, Thumler R. Physiological-response to hypergravity and hypogravity during rollercoaster flight. *Aviation Space Environ Med*. (1980) 51:145–54.
48. Clément G, Andredeshays C, Lathan CE. Effects of gravitoinertial force variations on vertical gaze direction during oculomotor reflexes and visual fixation. *Aviation Space Environ Med*. (1989) 60:1194–8.
49. Cheung BS, Money KE, Howard IP. Human gaze instability during brief exposure to reduced gravity. *J Vestib Res*. (1994) 4:17–27.
50. Pierrot-Deseilligny C. Effect of gravity on vertical eye position. *Ann NY Acad Sci*. (2009) 1164:155–65. doi: 10.1111/j.1749-6632.2009.03864.x
51. Mulavara AP, Ruttley T, Cohen HS, Peters BT, Miller C, Brady R, et al. Vestibular-somatosensory convergence in head movement control during locomotion after long-duration space flight. *J Vestib Res*. (2012) 22:153–66. doi: 10.3233/VES-2011-0435
52. Bisdorff AR, Sancovic S, Debatisse D, Bentley C, Gresty MA, Bronstein AM. Positional nystagmus in the dark in normal subjects. *Neuro-Ophthalmology*. (2000) 24:283–90. doi: 10.1076/0165-8107(200008)2411-VFT283
53. Martens C, Goplen FK, Nordfalk KF, Aasen T, Nordahl SHG. Prevalence and characteristics of positional nystagmus in normal subjects. *Otolaryngol-Head Neck Surg*. (2016) 154:861–7. doi: 10.1177/0194599816629640
54. Marti S, Straumann D, Büttner U, Glasauer S. A model-based theory on the origin of downbeat nystagmus. *Exp Brain Res*. (2008) 188:613–31. doi: 10.1007/s00221-008-1396-7
55. Bodranghien F, Bastian A, Casali C, Hallett M, Louis E, Manto M, et al. Consensus paper: revisiting the symptoms and signs of cerebellar syndrome. *Cerebellum*. (2016) 15:369–91. doi: 10.1007/s12311-015-0687-3
56. Ilg W, Branscheidt M, Butala A, Celnik P, De Paola L, Horak FB, et al. Consensus paper: neurophysiological assessments of ataxias in daily practice. *Cerebellum*. (2018) 17:628–53. doi: 10.1007/s12311-018-0937-2
57. MacNeilage PR, Glasauer S. Gravity perception: the role of the cerebellum. *Curr Biol*. (2018) 28:R1296–8. doi: 10.1016/j.cub.2018.09.053

Conflict of Interest: The authors declare that the research was conducted in the absence of any commercial or financial relationships that could be construed as a potential conflict of interest.

frontiers in Neurology

ORIGINAL RESEARCH
published: 22 May 2020
doi: 10.3389/fneur.2020.00441

Modeling Vestibular Compensation: Neural Plasticity Upon Thalamic Lesion

Stefan Reuss[1†], Elena Siebrecht[2‡], Ulla Stier[2], Hans-Georg Buchholz[1], Nicole Bausbacher[1], Nadine Schabbach[2], Andrea Kronfeld[3], Marianne Dieterich[4,5] and Mathias Schreckenberger[1*]*

[1] Department of Nuclear Medicine, University Medical Center, Johannes Gutenberg-University, Mainz, Germany, [2] Department of Anatomy and Cell Biology, University Medical Center, Johannes Gutenberg-University, Mainz, Germany, [3] Department of Neuroradiology, University Medical Center, Johannes Gutenberg-University, Mainz, Germany, [4] Department of Neurology and German Center for Vertigo and Balance Disorders, Ludwig Maximilians-University München, Munich, Germany, [5] Cluster of Systems Neurology, SyNergy, München, Germany

OPEN ACCESS

Edited by:
Carey David Balaban,
University of Pittsburgh, United States

Reviewed by:
Paul Smith,
University of Otago, New Zealand
Vincenzo Marcelli,
Local Health Authority Naples 1 Center, Italy

***Correspondence:**
Stefan Reuss
reuss@uni-mainz.de
Mathias Schreckenberger
mathias.schreckenberger@unimedizin-mainz.de

†ORCID:
Stefan Reuss
orcid.org/0000-0003-1064-5067

‡Present address:
Elena Siebrecht,
Geisenheim University, Geisenheim, Germany

Specialty section:
This article was submitted to Neuro-Otology, a section of the journal Frontiers in Neurology

Received: 25 February 2020
Accepted: 24 April 2020
Published: 22 May 2020

Citation:
Reuss S, Siebrecht E, Stier U, Buchholz H-G, Bausbacher N, Schabbach N, Kronfeld A, Dieterich M and Schreckenberger M (2020) Modeling Vestibular Compensation: Neural Plasticity Upon Thalamic Lesion. Front. Neurol. 11:441. doi: 10.3389/fneur.2020.00441

The present study in rats was conducted to identify brain regions affected by the interruption of vestibular transmission and to explore selected aspects of their functional connections. We analyzed, by positron emission tomography (PET), the regional cerebral glucose metabolism (rCGM) of cortical, and subcortical cerebral regions processing vestibular signals after an experimental lesion of the left laterodorsal thalamic nucleus, a relay station for vestibular input en route to the cortical circuitry. PET scans upon galvanic vestibular stimulation (GVS) were conducted in each animal prior to lesion and at post-lesion days (PLD) 1, 3, 7, and 20, and voxel-wise statistical analysis of rCGM at each PLD compared to pre-lesion status were performed. After lesion, augmented metabolic activation by GVS was detected in cerebellum, mainly contralateral, and in contralateral subcortical structures such as superior colliculus, while diminished activation was observed in ipsilateral visual, entorhinal, and somatosensory cortices, indicating compensatory processes in the non-affected sensory systems of the unlesioned side. The changes in rCGM observed after lesion resembled alterations observed in patients suffering from unilateral thalamic infarction and may be interpreted as brain plasticity mechanisms associated with vestibular compensation and substitution. The second set of experiments aimed at the connections between cortical and subcortical vestibular regions and their neurotransmitter systems. Neuronal tracers were injected in regions processing vestibular and somatosensory information. Injections into the anterior cingulate cortex (ACC) or the primary somatosensory cortex (S1) retrogradely labeled neuronal somata in ventral posteromedial (VPM), posterolateral (VPL), ventrolateral (VL), posterior (Po), and laterodorsal nucleus, dorsomedial part (LDDM), locus coeruleus, and contralateral S1 area. Injections into the parafascicular nucleus (PaF), VPM/VPL, or LDDM anterogradely labeled terminal fields in S1, ACC, insular cortex, hippocampal CA1 region, and amygdala. Immunohistochemistry showed tracer-labeled terminal fields contacting cortical neurons expressing the μ-opioid receptor. Antibodies to tyrosine hydroxylase, serotonin, substance P, or neuronal nitric oxide-synthase did not label any of the traced structures. These findings provide evidence for opioidergic transmission in thalamo-cortical transduction.

Keywords: PET-imaging, lesion, cerebral cortex, thalamus, neuronal tracing, immunofluorescence

INTRODUCTION

The bilateral central vestibular system provides an excellent paradigm to study mechanisms of brain plasticity, since it is able to compensate a certain loss of function by reorganizing its neurotransmission parameters ("vestibular compensation," VC). Patients suffering from an acute deficit of vestibular function caused by unilateral peripheral or central lesions show symptoms such as vertigo, dizziness, nystagmus, or body and perceptual tilts that may, however, be relieved or disappear completely in the course of the lesion. This is thought to be due to the compensation of unilateral functional loss by changes in neurotransmission such as up- or down-regulation of transmitter and/or receptor synthesis or affinity, to the shift of transmission to other brain regions in the same or other hemisphere and to reactive neuro- and gliogenesis [cf. (1–3)].

Our knowledge of vestibular processing in cortical and subcortical cerebral regions, however, is restricted. Some studies describe functional aspects of these regions during VC, based on neuroanatomical, physiological, and imaging studies in animal models and on patient studies investigating changes in cerebral metabolism after vestibular lesions (4–14).

In animals, neuronal plasticity underlying VC include changes in the physiological properties of afferents in the end-organ, mediated through the efferent system, as well as changes in the function of the vestibulocerebellum and its projection to the brainstem vestibular nuclei [VN; (15–17)]. These involve functional changes in neurotransmitter systems using ɣ-amino-butyric acid (GABA), acetylcholine (ACh), glutamate and, in particular, dopamine, and their receptors [cf. (18–20)]. These effects were observed in the VN, the target structure of the vestibular organ, in studies focusing on intact central processing structures and compensation following experimental labyrinthectomy in animal models (6, 14, 18–25) or in acquired peripheral lesions in patients (11, 13, 14, 26, 27).

It is, however, open so far as to which aspects of VC occur when the end-organ is left intact and instead the VN-cortical stream is experimentally interrupted (corresponding to a thalamic stroke in patients). There is evidence that "multiple, parallel plastic processes at various sites in the brain" including cerebellum, entorhinal cortex, and hippocampus, are involved in vestibular compensation of central lesions [cf. (14)].

Only a few studies have utilized an *in vivo*-approach to vestibular processing in animals, and most of these were electrophysiological studies. Less is known about processing of vestibular input after lesion of subcortical vestibular regions in animals, and functional brain imaging such as PET was so far used only in clinical studies. A distinct pattern of activation and inactivation of cerebro-cortical and subcortical regions has been observed in patients suffering from vestibular neuritis (10, 12), unilateral medullary and midbrain strokes (28, 29) or from unilateral infarction of the posterolateral thalamus (a relay-station for vestibular input to the vestibular cortex). The latter caused a significant reduction of the activity within the multisensory vestibular cortex areas in the hemisphere ipsilateral, and to a lesser extent also contralateral, to the thalamic lesion (11).

Our previous study was the first to use functional brain imaging (positron emission tomography, PET) upon galvanic vestibular stimulation (GVS) in rats to identify brain regions involved in vestibular processing (30). Cortical and subcortical clusters of augmented rCGM were observed in primary and secondary somatosensory cortex, auditory cortical areas, cingulate gyrus, dorsal intermediate entorhinal cortex, granular insular cortex (to minor extent), hippocampus, and amygdala in the left hemisphere upon either left or right vestibular stimulation. Bilateral activation was found in the cerebellar crus 1 and within the laterodorsal thalamic nucleus in both its dorsomedial and ventrolateral parts (LDDM, LDVL). Our data revealed that these thalamic structures possess major functions such as to collect, filter, integrate, and send vestibular information to cortical regions and combine it with other sensory modalities. To affect the major relay station of the thalamo-cortical vestibular network, these thalamic subnuclei were lesioned unilaterally in the present study.

The availability of pre-lesion testing and well-defined lesions that may later be characterized by histology are major benefits of functional brain imaging in experimental animals. Thalamic lesions, as conducted here, have the advantage over peripheral lesions that they do not affect the peripheral auditory system in a way labyrinthectomy does. They reduce respective artifacts and, in particular, they mimic the situation of thalamic infarction in patients.

The aim of the present study therefore was in a first part to investigate the processing and compensatory mechanisms at the cerebro-cortical and subcortical level after a defined central vestibular lesion and during the recovery phase in rats.

A second series of experiments was conducted to further investigate the connections between subcortical and cortical regions known from imaging studies to process vestibular information. We selected the somatosensory (S1) region and the anterior cingulate cortex (ACC) for injection of a *retrograde*

Abbreviations: ^{18}F-FDG, ^{18}F-Fluorodesoxyglucose; ACC, anterior cingulate cortex; ACh, acetylcholine; Amyg, amygdala; AuC1/AuC2, primary/secondary auditory cortex; PBS, Phosphate-buffered saline; CA, cornu ammonis; CbN, cerebellar nuclei; Cop, copula pyramis; CPu, caudate putamen (striatum); EC, entorhinal cortex; FOV, central field of view; FG, Fluoro-Gold; FR, Fluoro-Ruby; GABA, gamma-aminobutyric acid; GVS, galvanic vestibular stimulation; Hip, hippocampus; IC, inferior colliculus; IHC, immunohistochemistry; In, insular cortex; isRt, isthmic reticular formation; LC, locus coeruleus; LDDM, dorsomedial part of laterodorsal thalamic nucleus; LDVL, ventrolateral part of laterodorsal thalamic nucleus; M1, primary motor cortex; Me5, mesencephalic trigeminal nucleus; MGB, medial geniculate body; MGBv, ventral aspect of medial geniculate body; MOR, μ-opioid receptor; MRI, magnetic resonance imaging; MVe, medial vestibular nucleus; PaF, parafascicular nucleus of the thalamus; PET, positron emission tomography; Pha-L, Phaseolus vulgaris-leucoagglutinin; PIVC, parieto-insular vestibular cortex; PLD, post-lesion day; Po, posterior nucleus of the thalamus; PP, peripeduncular nucleus; PrCnF, precuneiform area; rCGM, regional cerebral glucose metabolism; S1/S2, primary/secondary somatosensory cortex; SC, superior colliculus; SL, Sham-lesion; SN, substantia nigra; TeA, temporal association cortex; TH, tyrosine hydroxylase; V1M, primary visual area, monocular region; V1, primary visual cortex; V2, secondary visual cortex; VC, vestibular compensation; VeCb, vestibular cerebellar nucleus; VL, ventrolateral nucleus of the thalamus; VN, vestibular nuclei; VPL, ventral posterolateral nucleus of the thalamus; VPM, ventral posteromedial nucleus of the thalamus.

neuronal tracer to label afferent subcortical neurons. We then injected *anterograde* tracer substances into thalamic nuclei (parafascicular, ventral posterolateral/-medial, laterodorsal) to label cortical target sites. Selected sections exhibiting anterograde or retrograde labeling were processed for immunohistochemistry to test for the possible presence of tyrosine-hydroxylase, serotonin, neuronal nitric oxide-synthase, substance *P*, or the μ-opioidergic receptor in or adjacent to tracer-labeled structures.

MATERIALS AND METHODS

The procedures concerning animals reported in this study complied with German and European laws for the protection of animals and were approved by the county-government office (Bezirksregierung Rheinhessen-Pfalz). All efforts were made to minimize the number of animals and their suffering.

Anesthesia

Galvanic stimulation and PET-scans, electrolytic thalamic lesions, magnetic resonance imaging, and intracerebral injections of neuronal tracers in rats were conducted at day time under general anesthesia. This was initiated by isoflurane inhalation and then maintained by 5 mg/kg b.wt. of a mixture of 55% ketamine (Ketavet, Pfizer, Berlin, Germany) and 45% xylazine (Rompun, Bayer, Leverkusen, Germany) given intraperitoneal (i.p.). After 25 min, rats received 30% of the initial dose to continue anesthesia. Animals were placed under a red light to keep body temperature constant.

First Experimental Series: PET Study

Animals

Nineteen adult male Sprague-Dawley rats (Harlan-Winkelmann, Borchen, Germany) were maintained under constant conditions (light:dark 12:12 h, room temperature 21 ± 1°C) with food and water available *ad-libitum*. Body weights were 286 ± 57 g (mean ± SD, range 230–400 g) at first experimental day, and 429 ± 37 g (range 340–470) at the final experimental day.

Galvanic Vestibular Stimulation

Galvanic vestibular stimulation (GVS) was used to stimulate the vestibular system. This method, a variant of transcranial direct current stimulation, is well-established for vestibular stimulation in animal models (31) and for vestibular diagnosis and therapy in men (32–34).

As described in detail in our previous paper (30), the stimulation (cathodal) electrode was placed subcutaneously in the midline, and the anodal electrode was placed at the left external auditory meatal cartilage. The electric stimulus, generated by a custom-built battery-driven stimulator, consisted of square-wave pulses (1 Hz; 0.2 mA, 500 ms duration, 3,000 stimuli). The effectiveness of GVS was evaluated by the presence or absence of a resulting nystagmus in the animals. Immediately before the 50 min stimulation period, the tracer ^{18}F-FDG was injected.

Thalamic Lesions

The animals were divided into two groups. One group consisted of eight rats receiving a thalamic lesion, i.e., damage of the left dorsomedial (LDDM) and ventrolateral (LDVL) parts of the laterodorsal thalamic nucleus. The stereotactic coordinates for LDDM/LDVL lesion (centered at Bregma−3 mm, 2 mm lateral to midline, 4.5 mm below surface) were taken from the rat brain atlas (35). The animal's head was fixed in a prone position in a stereotaxic unit. A little hole was drilled into the skull using a dental drill. The electrode was inserted stereotactically and a current of 1.5 mA lasting 10 s was applied. After replacing the electrode, the animals received adequate medical treatment. Four sham-lesioned (SL) control animals underwent the same procedure without applying a current.

Immediately after surgical intervention, (sham-) lesion sites were verified by magnetic resonance imaging (MRI) using a Siemens Magnetom 3.0 Tesla (Siemens, Erlangen, Germany). For this purpose, a 3D-gradient echo data set with TR = 50 ms, TE = 43 ms, FA = 25° and an isotropic resolution of 0.3 mm was acquired. The puncture was observed as a hypo-intense, elongated volume, and was marked in a copy of each 3D-data set. After normalization of each original data set, transformations were transferred to the copies, which were then averaged.

After the final PET-scan, animals were killed by cervical dislocation. The brains were removed and deep-frozen, cut on a cryostat in the frontal plane and stained with hematoxylin-eosin for lesion verification.

PET-Scans

The data were acquired with the small-animal PET-scanner micro-PET Focus 120 (Siemens, Erlangen, Germany). The scanning procedure was the same as described in our previous study (30). Animals were deprived of food in the evening prior to scanning. Listmode acquisition started at 60 min after tracer injection and data were collected for 30 min. A transmission scan was performed using a ^{57}cobalt source to correct for radiation attenuation of tissues of different densities. A 3D maximum a posteriori (MAP) algorithm with 18 iterations and a regularization parameter of 0.05 within a 256 × 256 matrix was used to reconstruct images with scatter and attenuation correction. The PET-scanner consisted of 168 lutetium-oxyorthosilicate detectors ordered in four contiguous rings of 25.8 cm in diameter and 7.6 cm axial length resulting in an intrinsic spatial resolution of 1.4 mm at central field of view (CFOV) and a slice thickness of 0.8 mm (36).

To examine the chronic course of metabolism after lesion, each animal was scanned upon vestibular stimulation 1 day before the thalamic lesion and four times after lesion (i.e., at post-lesion-days one, three, seven, and twenty, see **Figure 1**). Brain activity was evaluated using the radiopharmaceutical tracer ^{18}Fluorodesoxyglucose (^{18}F-FDG), a glucose-analog containing the positron-emitting radioactive isotope fluorine 18. Animals received i.p. injections of 25–35 MBq FDG prior to each stimulation. The tracer was taken up and accumulated in brain regions relative to their metabolic rates.

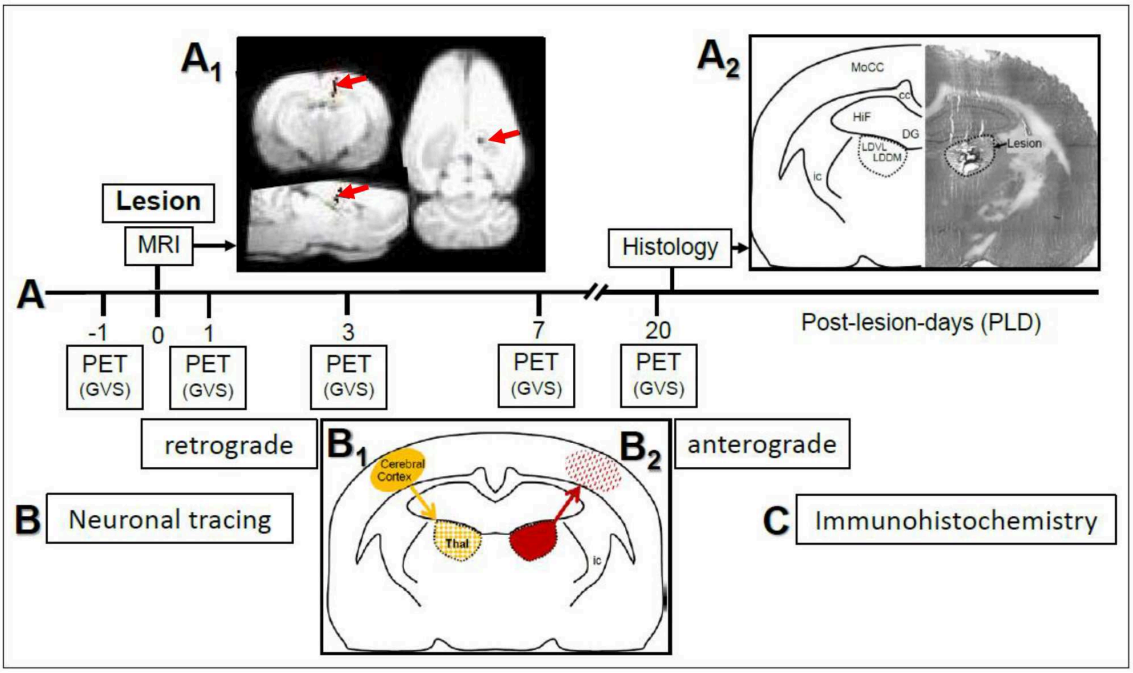

FIGURE 1 | (A) Study design and time course of μPET-scans in rats upon galvanic vestibular stimulation (GVS). An electrolytic lesion was conducted in the thalamus (dorsomedial and ventrolateral parts of laterodorsal thalamic nucleus, LDDM, LDVL), followed by magnetic resonance imaging (MRI) scan to control for lesion site (red arrows in $\mathbf{A_1}$). Control animals received sham-lesions. PET-scans were conducted 1 day before the lesion and on post-lesion days 1, 3, 7, and 20. After the final scan, brains were processed for lesion histology. The approximate level exhibiting the lesion site is Bregma−3 mm, according to Figure 58 of the rat brain atlas (35). All procedures were carried out under deep anesthesia. Details of the GVS paradigm were given in Best et al. (30). **(B)** Neuronal tracing; retrograde labeling of thalamic neurons upon cortical injections **($\mathbf{B_1}$)** and anterograde labeling of cortical afferents upon thalamic injections **($\mathbf{B_2}$)**. **(C)** Selected sections were exposed to immunohistochemical incubations for transmitter and receptor molecules. cc, corpus callosum; DG, dentate gyrus; HiF, hippocampal formation; ic, internal capsule; MoCC, motor regions of cerebral cortex.

PET-Data Analysis

From the 19 rats used in this experimental series, seven were excluded from analysis since they were used for lesion testing prior to the experiments or were not scanned at all time-points for technical reasons. Data from eight lesioned and four sham-lesioned animals were analyzed as follows.

Spatial normalization into the in-house FDG-template in Paxinos space and statistical analyses of rat brain images were performed with a tailored version of SPM5 (Wellcome Department of Cognitive Neurology, London, UK, http://www.fil.ion.ucl.ac.uk/spm), as described by Best et al. (30). A three-dimensional Gaussian filter using 8 mm full width at half-maximum kernel (voxel size, $2 \times 2 \times 2$ mm^3) was used for smoothening.

Two different comparisons were analyzed: first, paired T-tests between each PLD (1, 3, 7, or 20 days after surgery) and the pre-lesion status and the two-samples T-tests between the lesion and the sham-group at each PLD. Statistical thresholds were initially set to $P < 0.001$ (uncorrected). Multiple comparison correction of the clusters at $P < 0.001$ was performed using the small volume correction (SVC) method implemented in SPM. Clusters were considered as significant if P (SVC-corrected) < 0.05.

For illustrating purposes, the activations and deactivations, respectively, were superimposed on standard MRI-templates in Paxinos-space.

Second Experimental Series: Neuroanatomical Study

Animals

Twenty-five rats (five groups of five animals each) were used in this part of the study. Each animal of a given group received a single application of one of the neuronal tracer substances into one of the injection sites (see below and **Table 2**).

Neuronal Tracing and Tissue Fixation

Animals were anesthetized as described above and fixed in a stereotaxic frame. After a medial incision of the scalp, a small hole was drilled into the skull with a dental drill. After cutting the dura mater, a glass capillary (tip diameter < 1 μm) was inserted and the tracer was slowly pressure-injected. The injection methods were optimized in our laboratory and used in a number of anterograde and retrograde tracing studies [e.g., (37–40)]. This included backfilling of the capillary, the careful cleaning of the tip, and pulling back a small amount of fluid before insertion. The injection coordinates were taken from the rat brain atlas (35), and are given in **Table 2**.

The *retrograde* tracer Fluoro-Gold [FG, 150 nl, 5 % in distilled water, Fluorochrome, Englewood, CO, USA, (41)] was injected into either the primary somatosensory (S1) cortex or the anterior cingulate cortex.

The *anterograde* tracer Phaseolus vulgaris-leucoagglutinin (Pha-L, 200 nl, 2.5% diluted in 0.1 M phosphate-buffered physiological saline (PBS), Vector, Burlingame, CA, USA) was injected into either the parafascicular nucleus (PaF), or the posteromedial/posterolateral ventral nuclei of the thalamus (VPM/VPL). The anterograde tracer Fluoro-Ruby (FR, 100 nl, 10% in PBS; Fluorochrome) was injected into the dorsomedial part of the laterodorsal thalamic nucleus (LDDM).

After 5–7 days, the animals were killed by anesthesia overdose and immediately perfused transcardially with PBS containing 15,000 IU heparin/l followed by 300 ml of ice-cold PLP solution (4% paraformaldehyde, 1.37% L-lysine, 0.21% sodium-periodate in PBS); according to McLean and Nakane (42) at a constant rate of 25 ml/min. The brains were removed and postfixed overnight in PLP, then cryoprotected in phosphate-buffered 30 % sucrose. They were marked on one side and sectioned serially at 30 mm thickness on a freezing microtome in the frontal plane, and collected in PBS into four parallel sets of sections. One set was directly mounted in order of appearance on gelatinized glass slides, dried, cleared in xylene, and coverslipped with Merckoglas (Merck, Darmstadt, Germany) for injection site verification. It was found that the tracer destination site was hit in at least three of five animals of each of the five injection groups. Sections stemming from these rats were analyzed further.

To visualize tracing, sections of one set were incubated free-floating with primary antibodies directed against Pha-L (1:1000 in PBS, raised in rabbit; Vector), while the autofluorescent substances Fluoro-Ruby and Fluoro-Gold do not require detection by antibody. Selected sections containing injection or target sites were counterstained with hematoxylin-eosin.

At least 10 sections per set from each of three rats of either injection group were used for immunohistochemistry. Further brain sections were used for antigen distribution and antibody specificity tests.

Immunohistochemistry

Sections exhibiting labeling of terminal fields in cortical regions upon application of an anterograde tracer into the thalamic nuclei were incubated with an antibody directed against the μ-opioidergic receptor (guinea pig-anti-MOR-1, 1:2500, Chemicon, Temecula, CA, USA).

Sections from thalamic regions which exhibited labeling of neuronal perikarya after retrograde tracing from cortical regions were incubated with primary antibodies directed against either tyrosine-hydroxylase (mouse-anti-TH, 1:1000, Chemicon), serotonin (rat anti-SER, 1:200, Chemicon), neuronal nitric oxide-synthase (rabbit anti-nNOS, 1:1000, Progen, Heidelberg, Germany), or substance P (rat anti-SP, 1:200, Abcam, Cambridgeshire, England). Sections were incubated in primary antibodies diluted in PBS to which 0.1% Triton X-100 and 3% normal donkey serum were added. Immunoreactions were visualized with Cy2- or Cy3-conjugated $F(ab)_2$-fragment of IgG directed against the host species of the primary antibody (1:200–1:400 in PBS, Jackson ImmunoResearch, Newmarket, Suffolk, England). Immunohistochemical specificity studies, carried out by omitting primary or secondary antibodies or by absorbing the primary antibody with the immunogen, showed the absence of the immunofluorescent signal. The antibodies had been used earlier in our laboratory and were characterized previously. Further details are given in Reuss et al. (43).

All sections were analyzed using an Olympus BX51 research microscope equipped with epifluorescence unit, highly specific single and dual band filter sets allowing the single or simultaneous excitation and observation of dyes without overlapping-artifacts (Olympus fluorescence monochromatic and dichromatic mirror cubes, maximal excitation/maximal emission, Cy2: 489/506 nm, Cy3: 552/565 nm). Photomicrographs were taken with a digital color camera employing the Analysis Software (Soft Imaging System, Münster, Germany). The Adobe Photoshop and Powerpoint programs were used to arrange images, to adjust image contrast and brightness, and to add labels.

RESULTS

Design and time course of the present study are given in **Figure 1**. In the first part (**Figure 1A**), rats with either thalamic lesions or sham-lesions were subjected to five PET-scans in the course of 21 days. MRI (**Figure $1A_1$**) and histology (**Figure $1A_2$**) verified lesions. In the second part (**Figure 1B**), neuronal tracing was used to identify connections between thalamic and cerebro-cortical regions. Immunohistochemistry was used for the detection of selected neuroactive substances in these regions. Delineations, nomenclature and abbreviations of thalamic nuclei, subcortical and cortical regions were adopted from the stereotactic rat brain atlas by Paxinos and Watson (35).

First Experimental Series: PET Study

The effects of GVS in the unlesioned animals closely resembled those found in our previous study on the vestibular activation pattern in the two cerebral hemispheres (30). We then compared the effects of GVS in lesioned animals with those in sham-lesioned animals by two-sample-*T*-test and found time-after-lesion-dependent activations of distinct regions in lesioned animals (see **Figure S1** and **Table S1**).

Group Analyses; Intact Vestibular Stimulation vs. Lesion Time Frames (Paired *T*-Tests)

Scans before lesion were compared with post-lesion scans at different post-lesion days (PLD) upon vestibular stimulation of all animals of the lesion group. Brain areas with augmented metabolism after lesions as well as areas with diminished metabolism were identified (**Table 1**; **Figures 2**, **3**).

At PLD 1, activity was detected in the cerebellum bilaterally, with a contralateral dominance in the paramedian lobe and in the ipsilateral crus 2. The major cluster, located contralateral, also includes the copula of the pyramis, and parts of the vermis (lobules 8–10) (**Figure 2**). The area containing the electrode tract

TABLE 1 | Regions showing more ("activation," positive Z-score) or less ("deactivation," negative Z-score) rCGM augmentation upon galvanic vestibular stimulation at post-lesion days (PLD) 1–20, compared to pre-lesion levels (paired *T*-test).

PLD	Brain region	Center of cluster coordinates (X/Y/Z)	Cluster size	*Z*-score	Figures
Activations					
1	Inferior colliculus, contra	−2.6 / −9.8 / −2.6	273	+ 3.97	2
	Cerebellum, contra	−2.0 / −13.6 / −5.8	2019	+ 4.44	
3	Superior colliculus, contra	−1.4 / −7.0 / −3.6	150	+ 3.96	2
7	Me5 / PrCnF / isRt, ipsi Superior colliculus,	1.2 / −7.4 / −5.4	67	+ 3.85	2
	contra	−1.2 / −7.2 / −4.0	214	+ 3.71	
20	Cerebellum, contra	−3.4 / −13.6 / −5.4	522	+ 4.74	2
Deactivations					
1	Needle track/lesioned area	1.8 / −2.4 / −0.6	123	− 3.67	3
3	Entorhinal cortex, ipsi	6.2 / −4.0 / −8.2	162	− 4.47	3
7	Visual cortex, ipsi	4.8 / −7.2 / −1.0	51	− 3.48	3
20	Visual cortex, ipsi	5.2 / −3.4 / −1.6	200	− 3.73	3
	Somatosensory cortex, ipsi				
Activability loss at PLD 20					
1–20	Ventral medial geniculate body / Peripeduncular nucleus, contra	− 3.2/− 5.8/− 6.6	138	+ 4.7	4
1–20	Somatosensory cortex, contra	2.8/− 0.6/− 2.0	1635	+ 5.17	4

Cluster size > 50 vx. Coordinates relate to Paxinos and Watson (35). X, lateral to midline; Y, anterior or posterior to Bregma; Z, below surface, in mm. Listed are clusters with high Z-scores, as depicted in ***Figures 2–4****. Z-score is the position of a raw score in terms of its distance from the mean, measured in standard deviation units. Ipsi and contra refers to laterality with respect to lesion and stimulation. Me5, mesencephalic trigeminal nucleus; PrCnF, precuneiform area; isRt isthmic reticular formation. See results for more details.*

and the lesion, as well as the secondary visual area (V2), exhibited decreased activity (**Figure 3**).

At PLD 3, activity was augmented contralateral to the lesion in the superior colliculus, in the copula pyramis mainly contralateral and the contralateral retrosplenial primary visual cortex (V1, monocular area). It was diminished ipsilateral in the V1 area and in a cluster centered in the entorhinal cortex and partly covering aspects of ventral perirhinal and dorsal piriform cortices, as well as dorsal endopiriform and lateral amygdaloid nuclei.

At PLD 7, increased activation upon GVS was detected in the superior colliculus contralateral, in the bilateral cerebellar copula, and an activation cluster containing the closely located vestibular cerebellar nucleus and medial vestibular nucleus of the brainstem. Ipsilateral, the substantia nigra and a smaller mesencephalic cluster apparently including trigeminal nucleus, precuneiform area and isthmic reticular formation (**Figure 2**). Less activation was observed in the ipsilateral visual cortex and temporal association cortex (**Figure 3**).

At PLD 20, a similar activation cluster as at PLD 1 appeared in the cerebellum, again with a clear contralateral predominance and smaller clusters ipsilateral. Deactivations upon GVS were present in ipsilateral somatosensory and visual cortical area. These results are summarized in **Figure 5**.

In the parasagittal images of PLD 1-20 (**Figure 2**), an "activation band" was observed as an artifact dorsal to the cortical surface, mainly outside brain issue, that most probably is due to disturbed blood flow following lesion surgery (see discussion).

The subtraction of activation patterns of PLD 20 from PLD 1 demonstrated higher activity 1 day after lesion in the contralateral ventral aspect of the medial geniculate body and peripeduncular nucleus, as well as primary somatosensory and primary motor cortical area bilaterally, with an ipsilateral predominance (**Figure 4**). In addition, cerebellar nuclei showed a small activation cluster. Clusters of lower activity upon GVS were not apparent.

Lesion Verification

Upon magnetic resonance imaging (MRI), pixels representing the needle track were visualized by a superposition of the images to a T1-weighted data set. The analysis of the lesion setting revealed the stereotactically correct insertion of the electrodes (**Figure 1A$_1$**). The histological control of lesions, conducted after the final PET-scan (**Figure 1A$_2$**) to confirm MRI-findings, showed that the main part of the LDDM and the dorsal and medially located aspects of the LDVL were damaged.

Second Experimental Series: Neuroanatomical Study

Neuronal Tracing

Sections from 15 rats exhibiting successful injection of the neuronal tracers were analyzed. The results (consistent between all investigated rats) are summarized in **Table 2**, and examples are given in **Figures 6**, **7**. We did not observe any spilling of the tracers into ventricular cerebrospinal fluid.

The *retrograde* neuronal tracer Fluoro-Gold (FG) was used to label cell bodies of neurons projecting to distinct cortical regions such as the primary somatosensory cortex (S1) or anterior cingulate cortex (ACC) (**Figure 1B$_1$**). After injection of FG into S1 (**Figures 6A,B**), distinct labeling of neuronal perikarya was

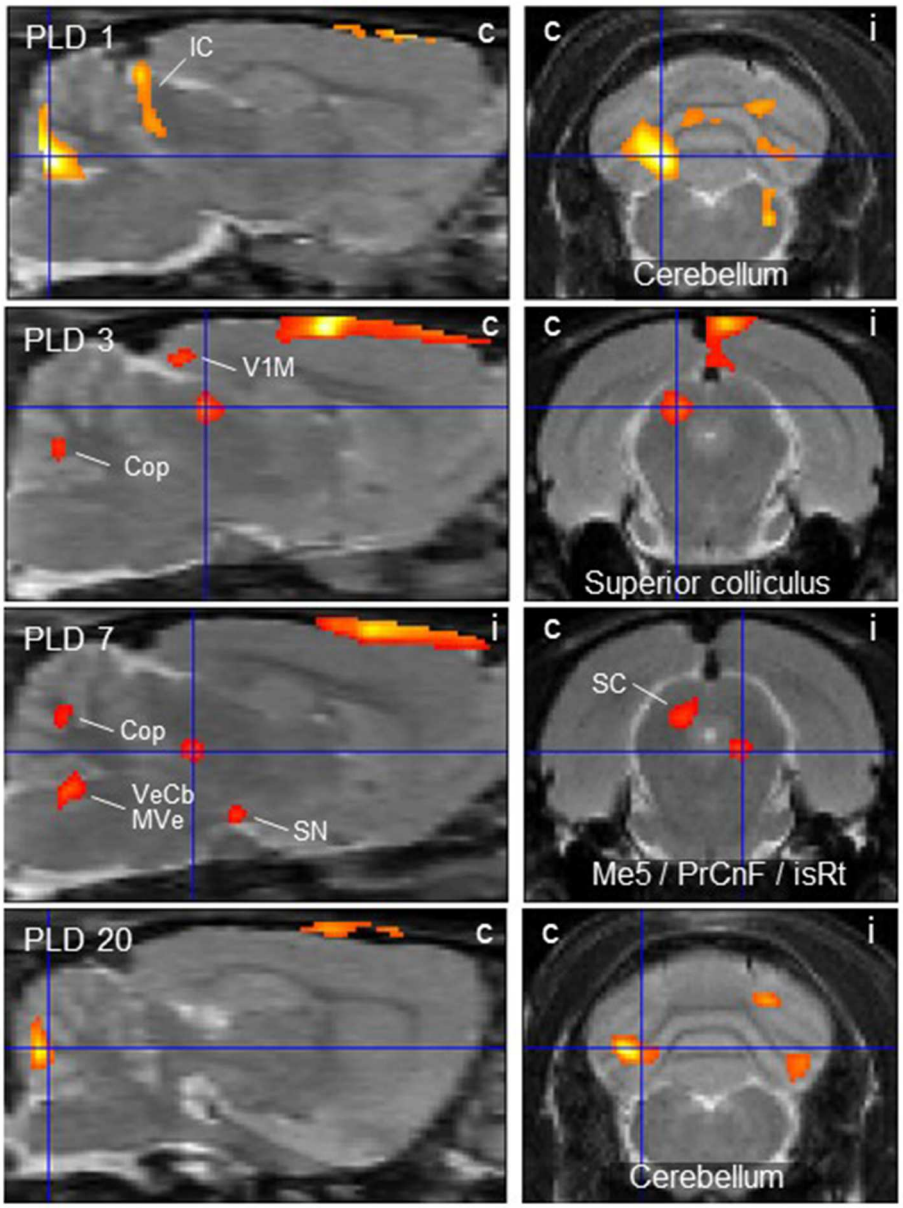

FIGURE 2 | Thalamic lesion activates vestibular stimulation-induced glucose consumption in distinct brain regions. Clusters of higher metabolism upon galvanic vestibular stimulation after thalamic lesion compared to pre-lesion (paired *T*-test), at post-lesion days (PLD) 1–20. Shown are parasagittal (left) and coronal (right) sections. Orientation (i/c) = ipsi-/contralateral to lesion and GVS site. Cluster parameters are given in **Table 1**. Cop, copula pyramis; IC/SC, inferior/superior colliculus; isRt, isthmic reticular formation; Me5, mesencephalic trigeminal nucleus; MVe medial vestibular nucleus; PrCnF, precuneiform area; SN, substantia nigra; V1M primary visual area, monocular region; VeCb, vestibular cerebellar nucleus. The dorsalmost signal mainly outside brain parenchyma is an artifact related to lesion-surgery.

found. They were located in groups with clear-cut borders. The comparison with Nissl-sections stained subsequently to fluorescence shooting and/or with those from the stereotactic rat atlas (35), revealed that they were located in the ipsilateral ventral posteromedial and posterolateral (VPM / VPL; **Figures 6C,D,F**), posterior (Po; **Figures 6E,F**), and ventrolateral (VL; **Figure 6G**) thalamic nuclei. While labeled neurons were densely packed in the VPM, they were more scattered in the VPL. We also found labeled neuronal somata in the ipsilateral granular, agranular, and disgranular insular cortical regions, in the locus coeruleus (LC; **Figures 6I,J**), and in the secondary auditory cortex. Some labeled somata were also found in the contralateral S1-region.

The injection of FG into the ACC resulted in retrogradely labeled neuronal perikarya in ipsilateral granular/disgranular insular cortex and in the thalamic LDDM/LDVL (**Figure 6H**).

The *anterograde* neuronal tracers Phaseolus vulgaris-Leucoagglutinin (Pha-L) and Fluoro-Ruby (FR) were used to label axonal projections to the cerebral cortex originating in

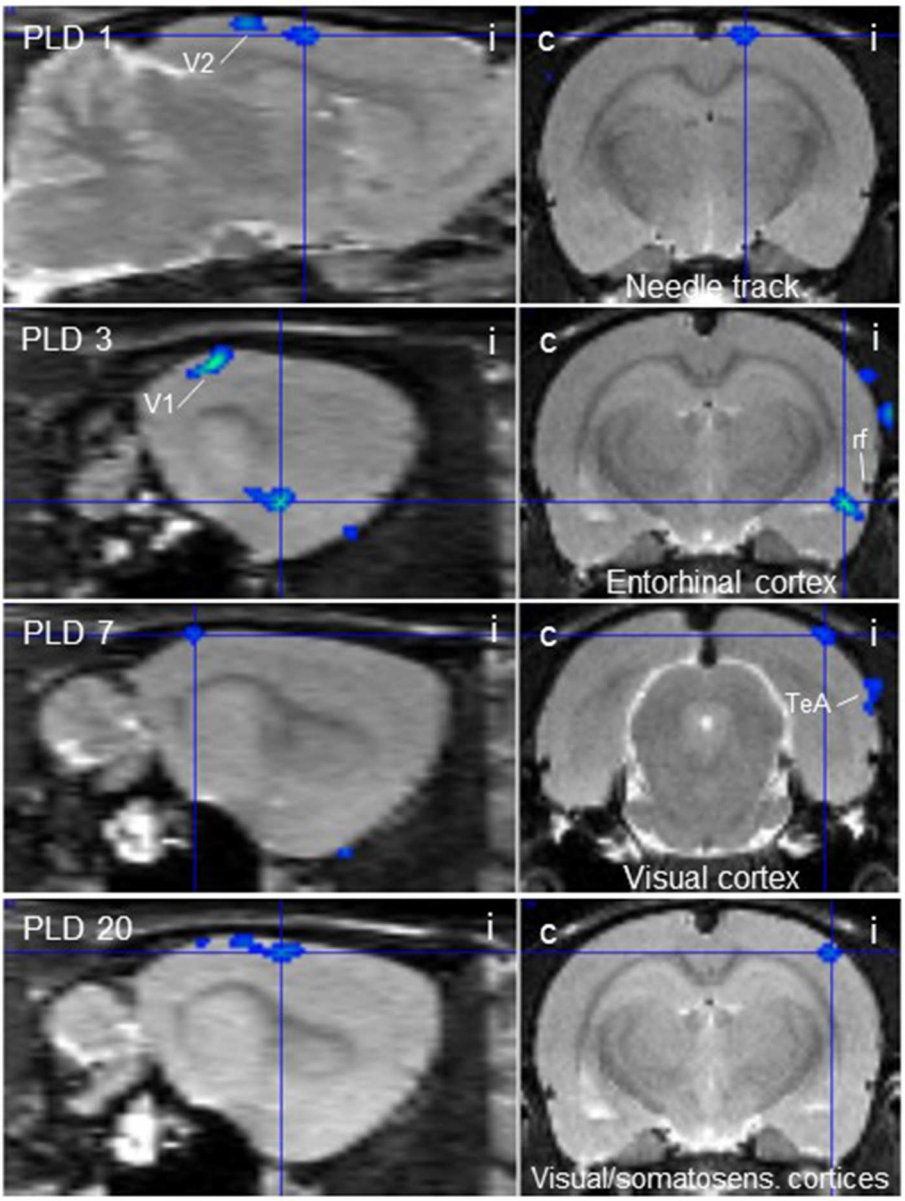

FIGURE 3 | Thalamic lesion inhibits vestibular stimulation-induced glucose consumption in distinct brain regions. Clusters of decreased metabolism upon galvanic vestibular stimulation after thalamic lesion compared to pre-lesion (paired *T*-test), at post-lesion days (PLD) 1–20, as seen in parasagittal (left) and coronal (right) sections. i/c = ipsi-/contralateral to lesion and stimulation site. TeA, temporal association cortex; V1, primary visual cortex; V2, secondary visual cortex. Cluster parameters are given in **Table 1**.

thalamic nuclei (**Figure 1B$_2$**). Prior experiments showed that thalamo-cortical tracing results were similar regardless of the anterograde tracer substance used. Injections were directed to either the PaF, VPM/VPL, or LDDM. Results of PaF-injections are given in **Table 2** and depicted in **Figures 7A–D** and **Figure S2**. Fiber and/or terminal labeling was found in ipsilateral cerebro-cortical regions such as entorhinal cortex (**Figure 7A**), amygdala (**Figure 7B**), and primary somatosensory cortex (S1) (**Figures 7C,D**), as well as in ACC, hippocampal CA2 region and posterior agranular insular cortex (**Figures 7A–D**, **Figure S2**). The injection of FR into the LDDM caused labeling of fibers and terminal fields in the ACC. The injection of Pha-L into the posteromedial and posterolateral ventral thalamic nuclei (VPM/VPL) resulted in labeling of terminal fields in the primary somatosensory cortex, ACC, insular and auditory cortex.

Immunohistochemistry on Labeled Structures

Sections showing successful neuronal tracing of perikarya or terminal fields, respectively, were subjected to

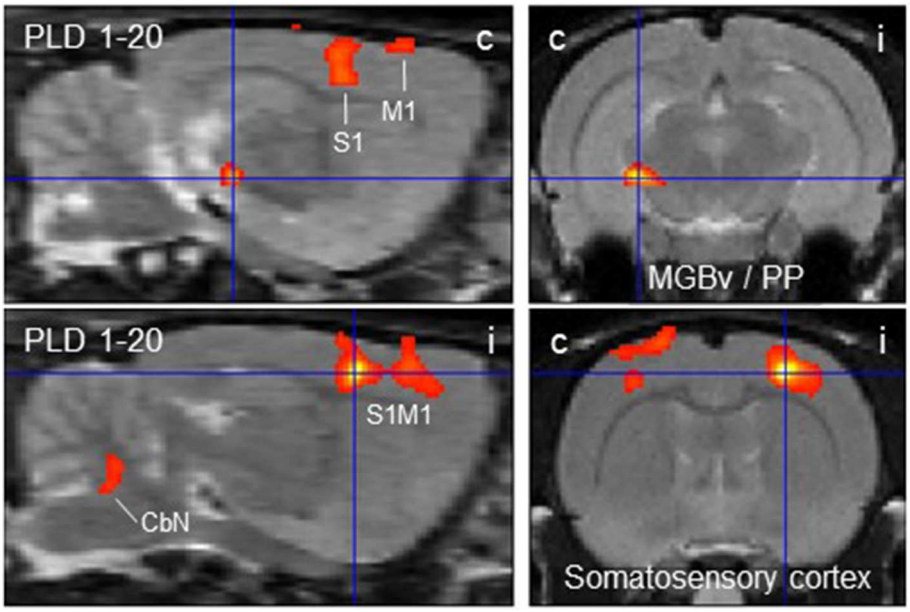

FIGURE 4 | Distinct brain regions that were more activated upon galvanic vestibular stimulation at post-lesion day 1 (PLD 1) than at PLD 20. Clusters of higher metabolism at PLD 1 compared to PLD 1 (paired *T*-test) were found contralaterally in the ventral part of the medial geniculate nucleus/peripeduncular nucleus and bilaterally in the somatosensory cortex, as demonstrated in parasagittal (left) and coronal (right) sections. Deactivations were not observed under these conditions. i/c = ipsi-/contralateral to lesion and stimulation site. CbN, cerebellar nuclei; M1, primary motor cortex; PP, peripeduncular nucleus; S1, primary somatosensory cortex; MGBv, ventral aspect of medial geniculate body.

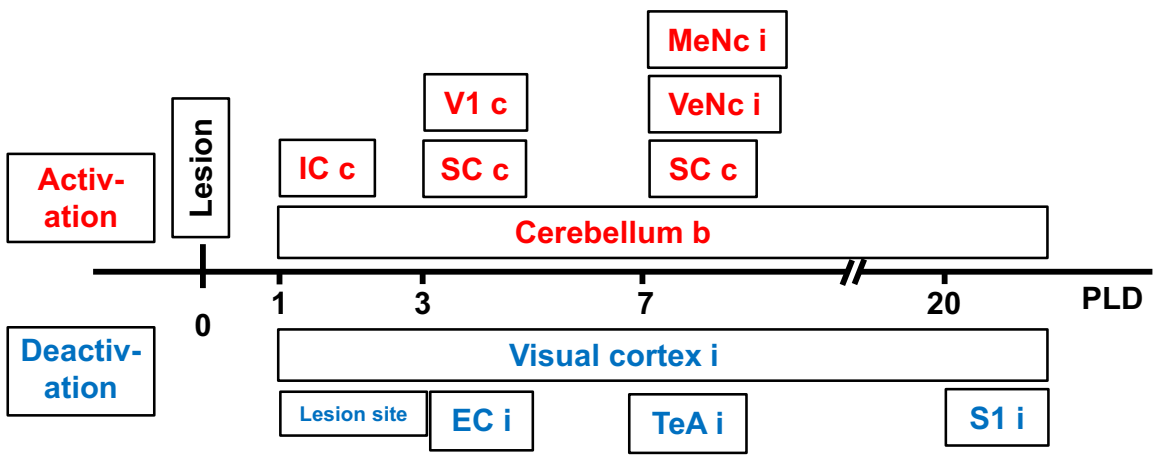

FIGURE 5 | Time-course of augmented or reduced activation of metabolic activity in rat brain upon galvanic vestibular stimulation (GVS), at postlesion (PLD) days 1–20 compared to prelesion. EC, entorhinal cortex; IC, inferior colliculus; MeNc mesencephalic nuclei; SC superior colliculus; S1 primary somatosensory cortex; VTeA, temporal association cortex; V1, primary visual cortex; VeNc, vestibular nuclei; b, bilateral, c, contralateral, i, ipsilateral to lesion and stimulation.

immunohistochemical incubations in order to identify putative neurotransmitter systems (**Figure 1C**). The immunofluorescent detection of the μ-opioid receptor (MOR) resulted in labeled neuronal perikarya in cerebrocortical regions such as the entorhinal cortex (**Figure 7A**), amygdala (**Figure 7B**), and primary somatosensory cortex (**Figure 7C**) in each of the animals investigated. In this region, we observed terminal boutons anterogradely traced upon Pha-L-injection into the PaF in close vicinity to and covering MOR-positive neuronal somata (**Figures 7C,D**).

From the antibodies used, those directed against serotonin, TH, nNOS, or SP did not identify any structures labeled by antero- or retrograde tracing. The presence of respective immunofluorescence in the same section or in adjacent regions, however, validated our methodical approach. An example is given in **Figures 7E,F** showing the absence

TABLE 2 | Labeled brain regions upon neuronal tracing.

Tracing type	Tracer substance	Injection site (center coordinates, X/Y/Z)	Tracer target site	IHC	Figures
Retrograde	FG	S1 (4.8/−2.5/3)	VPL, VPM, VL, Po, PaF, In, LC, AuC2, S1 contra	TH-neg. somata	7
	FG	ACC (0.5/−1.5/1.7)	In, LDDM, LDVL		6
Anterograde	Pha-L	PaF (1.4/−4/5.7)	In, Hip (CA1), Amyg, EC, ACC S1	MOR-pos. somata	7, Suppl.2
	Pha-L	VPM/VPL (3/−3/5.8)	S1, ACC In, AuC		
	FR	LDDM (2/−2.5/4.5)	ACC		

For abbreviations, see list. Injection site coordinates relate to Paxinos and Watson (35). X, lateral to midline; Y, anterior or posterior to Bregma; Z, below surface, in mm.

of TH-immunofluorescence in PaF thalamic neuronal perikarya retrogradely labeled upon FG-injection into S1, while immunoreactive neurons were present in subcortical regions in the same brain section (**Figure 7G**).

DISCUSSION

This rat study is the first to use functional brain imaging for the investigation of vestibular processing in the acute and subacute course following unilateral experimental lesion of a central vestibular site in the dorsolateral thalamus. It aimed at the processes underlying the clinical phenomenon known as "vestibular compensation (VC)" that includes a behavioral recovery after acute unilateral peripheral or central lesions within the vestibular system in patients [for reviews, see (15, 44, 45)]. For that purpose, we conducted PET-scans of the rat brain after lesion of the laterodorsal thalamic subnuclei (LDDM, LDVL). We also sought to add further knowledge to the subcortical-cortical pathways known to process vestibular information by bidirectional neuronal tracing of thalamo-cortical connections upon injections into involved sites.

In the first experimental series, we scanned rat brains by FDG-PET at five time-points. After the first scan, animals were subjected to an electrolytic lesion of the thalamus to interrupt the relay station of the inner ear-vestibular cortex chain. The PET-scans were conducted employing the galvanic vestibular stimulation (GVS) paradigm as used in our previous study (30). In intact animals, it widely mimics the physiological situation of vestibular challenge in anesthetized animals (31).

Thalamic lesions have the advantage that they leave the peripheral vestibular organ intact. They avoid tympanic membrane and ossicle removal as well as lymphatic breakdown and render the auditory system operating, also minimizing respective artifacts. This paradigm serves as a model for human thalamic infarcts, which often cause acute vestibular symptoms and thus are a major object of clinical therapy [cf. (11, 46, 47)]. Since we previously found in rats that vestibular processing was primarily resident in the left hemisphere regardless of the side of GVS (30), thalamic lesions were conducted at the left side in the present study.

We observed altered metabolism upon GVS in distinct brain regions after the lesion. That these effects were not a by-product of surgery was revealed by the comparison of lesioned animals to the group of sham-lesioned rats, which showed clear-cut differences under otherwise identical surgical procedures (see **Supplementary Material**). It should be emphasized here that we did not aim at the effects of GVS on the activation pattern in both hemispheres as in our previous study (30) but rather sought to identify structures that were altered in metabolism, and the time-course of these changes, by the experimental thalamic lesion. This lesion site represents an important relay and integration area of vestibular projections en route to the cortical vestibular circuitry that was characterized by diffusion tensor imaging and connectivity MRI studies in healthy participants more recently (48, 49). We will discuss the different findings in their context in the following.

Vestibular Stimulation Pre- vs. Post-Lesion (Paired *T*-Test)

The most important findings of our PET-scan analysis were based on paired *T*-tests comparing brain metabolic activity after the unilateral lesion with pre-lesion data in single animals, in each case upon GVS. The differences at a given PLD were then averaged over all animals of the group. As summarized in **Table 1** and shown in **Figure 2**, we found major clusters of augmented metabolism, at different times after lesion, in the cerebellum and superior colliculus, either bilaterally or particularly contralateral to the lesion site. We also found activation after lesion in the visual cortex, inferior colliculus, and vestibular nuclei, although to minor degrees. These regions are part of the multisensory vestibular network [cf. (45, 50, 51)]. Diminished metabolism was found in ipsilateral entorhinal, visual, and somatosensory cortical areas. This is in line with the concept of a reciprocal inhibitory interaction between the sensory systems, i.e., activation of the vestibular system by GVS and downregulation of the visual and somatosensory systems (52), and was recently supported by imaging data on multiple central vestibular pathways that exert "large-scale modulatory effects of the vestibular system on sensory processing" (53).

The cerebellum showed activated metabolism during the period of study, with decreasing magnitude from PLD 1 to

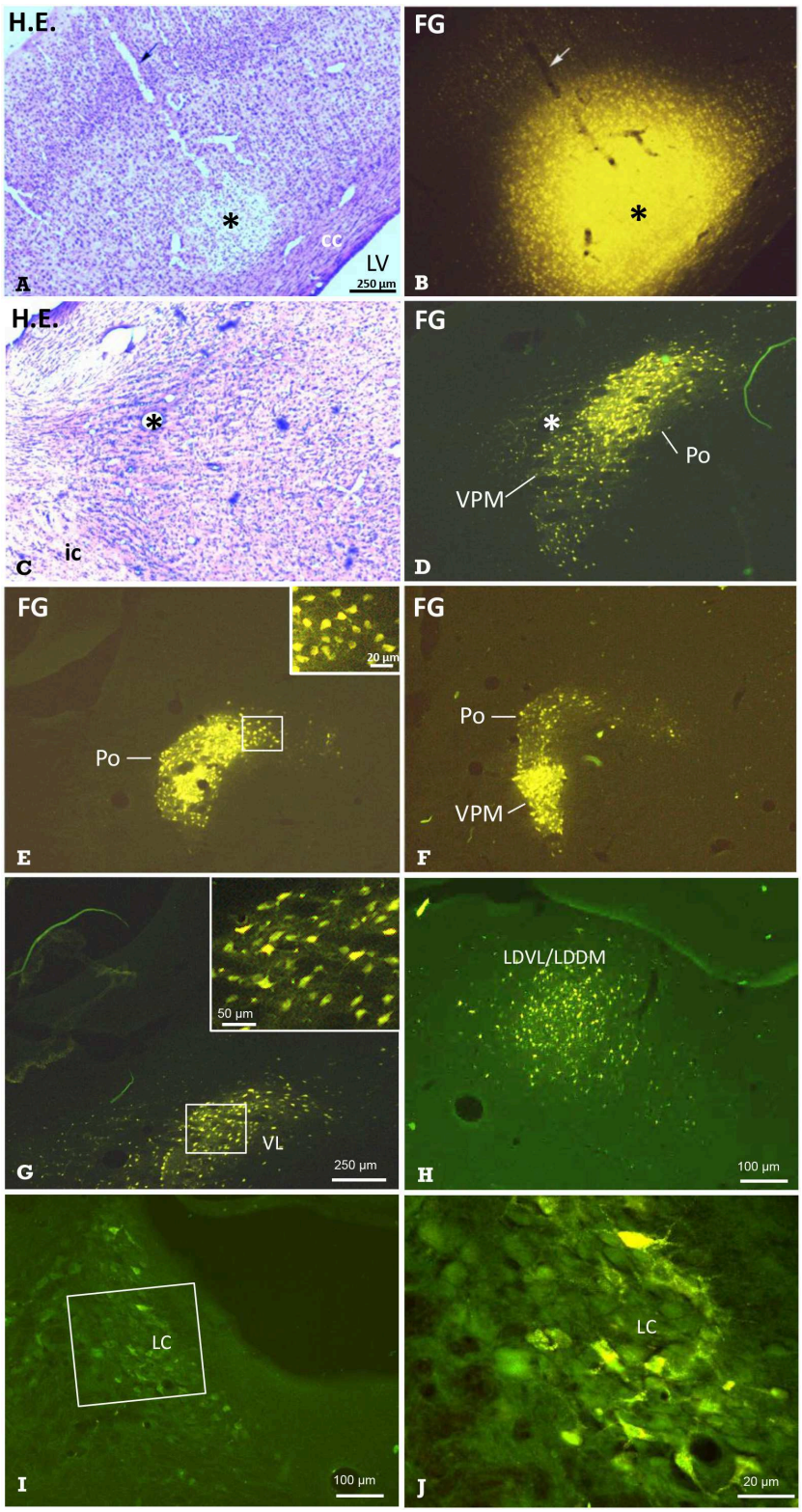

FIGURE 6 | Identification of thalamic nuclei projecting to the cerebral cortex by retrograde labeling. Frontal sections showing the site of FG-injection and retrogradely labeled neurons in thalamic nuclei. **(A)** Hematoxylin-eosin-(H.E.) staining and **(B)** FG fluorescence imaging of the same section demonstrating a typical injection into S1. Arrows point to the pipette track. In the same animal, retrogradely labeled neuronal somata were observed in the **(C,D)** ventral posteromedial thalamus and

(Continued)

FIGURE 6 | posterior thalamic nucleus (VPM/Po). E Labeled neuronal somata in Po, and F in Po and VPM of the same animal, as well as in the ventrolateral thalamic nucleus (VL in **G**), ventrolateral and dorsomedial parts of the laterodorsal thalamic nucleus (LDVL/LDDM upon injection into ACC, in **H**), and in the locus coeruleus (**I**; boxed area is shown in higher magnification in **J**). Dorsal is up, lateral is left **(A–J)**. All labeled neurons were seen ipsilateral to the injection site. Marker bar in A applies to **(A–F)**. The insert in E enlarges labeled neuronal somata from the medial aspect of the Po. Asterisks in **(A–D)** mark the same structures. Approximate levels with regard to Bregma are: **(A,B)** −2.5 mm [according to Figure 54 of the rat stereotactic atlas (35)], **(C,D)** −3 mm (Figure 58), **(E)** −2.5 mm (Figure 54) and **(F)** −4.4 (Figure 70), **(G)** −2 mm (Figure 50), **(H)** −2.7 mm (Figure 56), **(I,J)** −9.7 mm (Figure 114). See also **Table 2** for details. cc, corpus callosum; ic, internal capsule; LV, lateral ventricle.

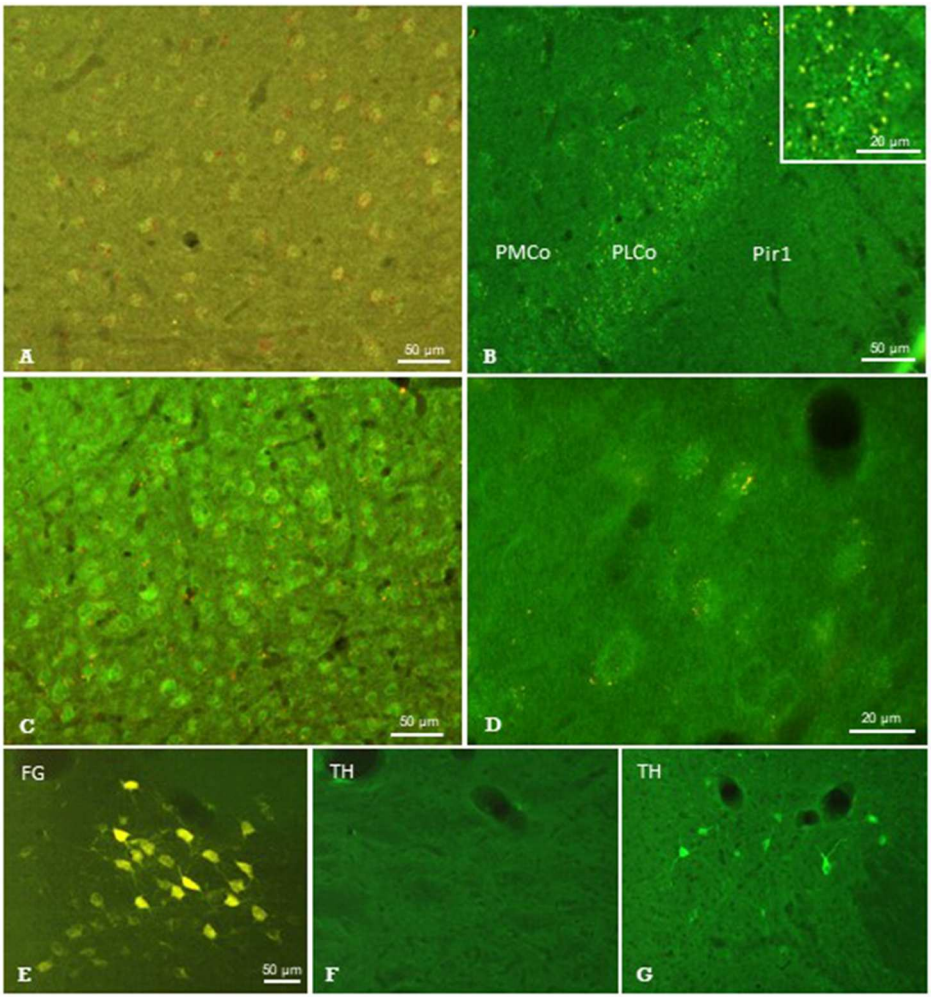

FIGURE 7 | Results of neuronal tracing combined with immunohistochemistry. Injection of Pha-L into the thalamic parafascicular nucleus (PaF) resulted in anterogradely labeled axonal terminals (yellow-red) at neuronal somata exhibiting faint μ-opioidergic receptor-immunoreaction (green fluorescence) in the ipsilateral entorhinal cortex **(A)**, amygdala **(B)** and primary somatosensory cortex **(C,D)**. Retrogradely labeled PaF neurons upon FG injection into S1 **(E)**. These neurons did not show immunolabeling for tyrosine-hydroxylase (TH; **F**), which was, however, present in the hypothalamus in the same section **(G)**. FG, Fluoro-gold; Pir1, piriform cortex layer 1; PLCo/PMCo, posterolateral/posteromedial cortical amygdaloid nucleus. Brain surface is up.

PLD 20. A major cluster was located contralateral, while smaller clusters were activated in the ipsilateral copula pyramis and lobules 8–10 of the vermis, thus covering regions known as part of the vestibulocerebellum [cf. (54)]. This brain structure is a major relay in the processing of vestibular input to control and fine-tune stabilization of the eyes, head, and body during motion. The vestibulocerebellum is a direct target of primary or secondary vestibular input in mammals including man [cf. (45, 55)], and it projects back to the brainstem vestibular nuclei and to the cerebellar fastigial nuclei, an output relay station, where units respond to GVS (56). There is also evidence that the cerebellum is important in compensation of vestibular deficits (57), which was supported, inter alia, by the finding that mice lacking cerebellar Purkinje (output) neurons recovered less efficiently from vestibular lesions than wild-type mice (58). The vestibulocerebellum, notably, was also

among the structures exhibiting increased rCGM contralateral to labyrinthectomy in rats (22). Enhanced cerebellar activations were in parallel also found in patients with unilateral infarctions of the medulla affecting the VN (28) and of the midbrain (29). Augmented cerebellar metabolic activity in the present study may be attributed to increased processing effort due to incongruent vestibular inputs in both hemispheres, i.e., intact input via vestibular nerve and pathways in one hemisphere and interrupted input via the lesioned thalamic pathway in the other.

The second structure activated by GVS in lesioned animals, the superior colliculus, is strongly involved in the control of eye movements during vestibular processing. In the comparison lesion vs. sham-lesion (see **Supplementary Material**), it showed decreased metabolic activity at day 1 and, in the pre- vs. post-lesion analysis, at days 3 and 7. These results may indicate a compensatory shift to visual signaling due to the damage of vestibular signaling. Such a substitution by one sensory system in case of a lesion in another is known from acute as well as chronic vestibular disorders (27, 59) in several systems. This is further supported by our present finding that the ipsilateral visual V1/V2 regions were deactivated at PLD 1 to 20, while the contralateral (monocular) primary visual area was activated.

In addition, the ipsilateral entorhinal, somatosensory, and temporal association cortices exhibited diminished activation upon GVS in the post-lesion period which may be explained by reduced vestibular (and putatively other esp. somatosensory) input upon thalamic lesion and therefore reduced intersensory interaction within the hemisphere. Moreover, the thalamic damage not only affects vestibular, but also somatosensory and visual thalamo-cortical afferents directly. This reduced activation was not observed contralateral to the lesion where the pathway was not interrupted. It appeared that, in most regions, the activation by GVS was reduced at the side of lesion, while it was rather augmented contralateral. There were, however, a few ipsilateral regions activated by GVS, but these are integrated "upstream" to the lesion in the pathway under investigation. They include a relatively small mesencephalic cluster covering the trigeminal nucleus, precuneiform area and isthmic reticular formation, which provide functional features such as intrathalamic relay, midbrain locomotion center, and reticulocortical projections, respectively (60). Further activated were the ipsilateral substantia nigra and, notably, vestibular nuclei of cerebellum and brainstem.

With regard to the "activation band" dorsal to the cortical surface, mainly outside brain tissue, as visible in the parasagittal images of PLD 1-20 (**Figure 2**), it should be pointed out that this is most probably an artifact that is due to disturbed blood flow and respective regeneration processes following lesion surgery involving craniotomy and cutting of the dura mater. The "signal" was not seen in prelesion-PET presently and in our previous paper (30), which did not include surgery.

It is believed that these cortical sites belong to the network of cortical regions involved in vestibular processing. In rats, they include primary and secondary somatosensory, infralimbic and cingulate cortices (30, 61). In monkeys, important sites are area 7 as well as the parieto-insular vestibular cortex (PIVC) (7, 8, 62, 63). In humans, the posterior insular cortex, retroinsular region, parietal operculum, somatosensory Brodmann areas 2 and 3a, superior temporal gyrus, inferior-parietal gyrus, anterior cingulate cortex, and the hippocampus belong to this network (1, 9, 64, 65). Metaanalyses of human imaging studies support the view that the posterior insula, retroinsular region, and parietal operculum may represent the core region PIVC in monkeys (66, 67).

This above-mentioned network shows functional dichotomy as (1) vestibular projections diverge into a network of several cortical regions and (2) multisensory information converges in distinct cerebral areas such as the vestibular nuclei and thalamus. This implies also that respective brain regions such as vestibular cerebellum, thalamus, and cortex are not exclusively in charge for vestibular processing but are multisensory and handle also extravestibular inputs [cf. (45, 68)]. Based on previous and actual findings, we used neuroanatomical methods to add further knowledge on the connections of involved structures.

Neuronal Tract Tracing

Since the S1 region was the most dominant structure upon GVS in our previous PET-study (30), we conducted retrograde neuronal tracing upon unilateral injection of FG into this region and thereby labeled neuronal perikarya in several thalamic nuclei. We then performed anterograde tracing upon unilateral Pha-L or FR injections into the thalamic VPL/VPM or PaF, and observed labeled terminals in several cortical regions.

Clear corticopetal projections to S1 originating in thalamic regions VPL, VPM, VL, Po, and LDDM were observed upon retrograde tracing presently. The scattered distribution of labeled neurons in the anterior VPM, VPL, and posterior Po and their rather dense appearance in anterior Po and posterior VPM suggest that the latter contribute stronger to S1-directed projections. Anterograde tracing confirmed the findings of retrograde tracing as labeled terminals were observed in S1 upon injection into VPM/VPL or PaF. Our findings support and extend thalamo-somatosensory cortical projections described previously upon lesion studies in monkeys (69) and upon anterograde neuronal tracing in rats (70). It is agreed to that the thalamus represents a subcortical site of multisensory integration. Many of its neurons (e.g., in laterodorsal nucleus, VPM, VPL, MGB) respond to vestibular, visual, proprioceptive, and somatosensory stimuli, and project to vestibular and non-vestibular cortical regions (71). Parenthetically, similar mechanisms of vestibular and extravestibular integration have been identified in the VN that provide projections to the thalamus. Ascending and descending in- and outputs of various cell branches account for the complexity of the vestibular network at this level, where the sensory input of location and motion depends on various other information such as gaze control, head-neck motion, and stabilization as well as fear, memory, and viscerosensory information (50, 72).

The characteristic of thalamic nuclei as vestibular relay station was also revealed previously by demonstration of connections from the VN to thalamic nuclei such as VPM (73, 74) and PaF (75–77), from the thalamus to somatosensory cortical regions, and by somatosensory backprojections to the thalamus (78) in rats. Several studies using functional brain imaging in man and

rat showed the vestibular association of these connections (11, 30, 65). Functional connectivity MRI in healthy participants found two parts of the thalamus involved in vestibular processing, the paramedian subnuclei and the dorsolateral subnuclei (48, 49). These two regions processing vestibular information were also found to be causative in those patients with acute thalamic infarctions presenting with symptoms of an acute vestibular imbalance, i.e., either ipsilateral or contralateral tilts of the subjective visual vertical (79).

We also found projections to the S1-region originating from locus coeruleus as well as from secondary auditory and insular cortical regions. There is evidence that the LC is involved in vestibular processing since projections from VN to LC and vice versa have been shown previously (80, 81).

In addition to S1, the ACC is a target of parallel vestibular-related pathways. It receives projections from VPM/VPL and LDDM (our present retro- and anterograde tracings), and is activated by saccular or caloric stimulation (82, 83). The LDDM, part of the lateral thalamic complex, was previously identified by GVS as part of the vestibular network (30). Its neurons are directly innervated by medial vestibular nuclei neurons (75), to which the ACC in turn sends backprojections (84). Furthermore, recent tract tracing in mice revealed that the laterodorsal thalamus relays cerebellar projections to the hippocampus (85).

Finally, our injections into the PaF resulted in anterograde labeling of fibers and putative terminals in hippocampus, amygdala and entorhinal and insular cortices, which all showed altered metabolism upon GVS (30). Since entorhinal cortex and hippocampal CA1 harbor so-called place-cells and head-direction-cells coding a subject's location within the environment, it is likely that the vestibular input contributes to spatial information processing (86). The loss of this vestibular input resulted in hippocampal atrophy in patients with bilateral vestibular failure and deficits in spatial memory (87). In addition, effects upon experimental alterations of gravity revealed the involvement of the amygdala in vestibular processing (88, 89).

Special attention should be given to the insular cortex, the core region of the vestibular cortical network. Neurophysiological studies in animals (8, 90–92) and functional brain imaging in rat (30) and man (64, 65, 83, 93), imaging meta-analyses (66, 67) as well as functional connectivity studies in men (94) underline the importance of the insular-opercular area for vestibular processing, particularly in primates. A comparison of vestibular spatio-temporal tuning in macaque cortical areas PIVC, VIP, and MSTd showed a gradual transformation of temporal responses that suggest a hierarchy in cortical vestibular processing, with PIVC being most proximal to the vestibular periphery and MSTd being most distal (92). In line, neurons in the insular cortex were labeled upon retrograde tracer injections into the ACC in the present study demonstrating this tight connection. In humans, anterior and posterior insula, dorsolateral thalamus, ACC and cerebellum were activated by GVS, while visual and somatosensory cortices were simultaneously deactivated (65). Similar activations and deactivations were found in patients with vestibular neuritis predominantly in the contralateral hemisphere (95). Patients suffering from acute unilateral infarction of the posterolateral thalamic nuclei exhibited stronger activation of the inferior insula and reduced activation in the ipsilateral temporo-parietal cortex upon caloric stimulation, whereas the activation pattern was normal during caloric stimulation of the ear contralateral to the lesioned side (11). This affection of thalamo-cortical pathways within the lesioned hemisphere was now worked-up in more detail by retro-and anterograde tracer labeling in the current study.

However, the cortical aspects of metabolic alterations following thalamic lesion had not been in the focus of experimental studies yet. Recently, the time-course of rGCM upon surgical labyrinthectomy in rats was studied by PET-imaging (22). In the acute phase, VN, cerebellum, thalamus, hippocampus and amygdala were affected, while at post-lesion day 2 thalamus and cortex were inconspicuous, and glucose metabolism increased in vestibulocerebellum, amygdala, and hippocampus.

The present study combining brain PET-imaging upon thalamic lesions and retro- and anterograde neuronal tracing thus supports and extends earlier neuroanatomical and electrophysiological findings on the vestibular network.

Immunohistochemistry Suggests Involvement of Opioids

Neuroactive substances found in the vestibular system belong to three chemical groups, i.e., amino acids, monoamines, and ACh, and neuropeptides. Their distribution was studied predominantly in the end organ, in Scarpa's ganglion and in VN, structures that are well-defined with respect to their functional identity. Studies of "central vestibular transmission" actually identified dopaminergic, serotonergic, nitrergic, and amino-acidergic transmitter systems of the VN [cf. (96–98)] while subcortical and cortical structures of the pathways upstream to the VN are less well-defined in terms of neurochemistry. However, many thalamic and cortical regions are multisensory and multimodal and thus may use various neuroactive substances for transmission.

Dopaminergic involvement in vestibular pathways was described previously. In the rat VN, D2-receptors are present, and there is evidence for noradrenergic input from locus coeruleus neurons [cf. (96)]. Notably, dopamine-receptor availability was reduced in temporo-parieto-occipital cortex, striatum and thalamus in patients with chronic bilateral vestibular failure, suggesting that lacking peripheral vestibular input led to receptor down-regulation in these regions (99). However, respective immunohistochemical data demonstrating the presence of these aminergic substances are missing. Our findings that thalamic neurons projecting to S1 did not exhibit immunoreactivity to TH, a marker enzyme of dopaminergic/noradrenergic synthesis, reveal that this part of the vestibular pathway is not dopaminergic. It should be noted that, similarly, serotonin, nNOS, and SP were not detected in structures identified by neuronal labeling in our study.

Several lines of evidence, on the other hand, suggest the presence of opioidergic mechanisms in vestibular pathways. The presence of enkephalins in vestibular efferent neurons (100) suggests that the end-organ is under opioidergic influence, probably via kappa-opioid receptors expressed in hair cells and μ-opioidergic receptors (MOR) in afferent synapses (101). There is further evidence for the involvement of enkephalins in the medial VN in vestibular processing and in compensational mechanisms (21), probably mediated by delta-opioid receptors on MVe neurons (102). Our finding that terminals of thalamic neurons were present at cerebrocortical neuronal cell bodies expressing MOR fits well to the modulation of opioid receptor availability by diprenorphine, an unspecific opioidergic antagonist in the human insular cortex during caloric stimulation in healthy volunteers (103).

It is obvious that the roles of these and other neuroactive substances in subcortical-cortical pathways warrant further studies on vestibular processing and compensation.

CONCLUSIONS

Our previous rat data showing that GVS activates rCGM in distinct cortical and subcortical regions characterized those as part of a vestibular network. Our present data of a rat model with unilateral thalamic lesions demonstrate that GVS resulted in augmented activation of contralateral cerebellum and distinct subcortical structures such as superior colliculus as well as diminished activation of ipsilateral sensory cortical regions, showing a distinct pattern measured during 20 days post lesion. These rat data resemble the reduced activation of the ipsilateral cortex during caloric stimulation in patients with acute unilateral thalamic infarction (11). The changes in rCGM observed after lesion may be interpreted as brain plasticity mechanisms associated with vestibular compensation and substitution. Axonal tracings confirmed connections between subcortical and cortical sites identified in the PET-studies. These tracings combined with immunofluorescence showed that thalamic projections to S1 and ACC meet neurons expressing opioid receptors, but apparently do not involve neurotransmission based on serotonin, substance P, dopamine/noradrenaline, or nitric oxide.

DATA AVAILABILITY STATEMENT

The datasets generated for this study are available on request to the corresponding author.

ETHICS STATEMENT

All applicable international, national, and/or institutional guidelines for the care and use of animals were followed. This article does not contain any studies with human participants performed by any of the authors.

CONSENT FOR PUBLICATION

Consent to submit has been received explicitly from all co-authors.

AUTHOR CONTRIBUTIONS

SR: study concept and design, study supervision, analysis and interpretation of data, draft manuscript for intellectual content, and critical revision of manuscript for intellectual content. ES: acquisition of data, analysis and interpretation of data, and critical revision of manuscript for intellectual content. US, NB, NS, and AK: acquisition and analysis of data. H-GB: acquisition, analysis and interpretation of data, and critical revision of manuscript for intellectual content. MD: study concept and design, and critical revision of manuscript for intellectual content. MS: study concept and design.

FUNDING

Study funded by Stiftung Rheinland-Pfalz für Innovation (to MD), Röttger-Stiftung (to SR), and Hoffmann-Klose-Stiftung (to SR). None of the sponsors had any influence in the study design, the collection, analysis and interpretation of data, the writing of the manuscript and in the decision to submit the article for publication.

ACKNOWLEDGMENTS

The authors thank PD Dr. Christoph Best (University of Marburg, Germany, present address: Vitos-Klinik für Neurologie, Weilmünster, Germany) for valuable help. The manuscript contains data from the Ph.D.-thesis of ES and the MD-theses of US and NS.

SUPPLEMENTARY MATERIAL

The Supplementary Material for this article can be found online at: https://www.frontiersin.org/articles/10.3389/fneur.2020.00441/full#supplementary-material

REFERENCES

1. Brandt T, Dieterich M. The vestibular cortex. Its locations, functions, and disorders. *Ann NY Acad Sci.* (1999) 871:293–312.
2. Darlington CL, Smith PF. Molecular mechanisms of recovery from vestibular damage in mammals: recent advances. *Prog Neurobiol.* (2000) 62:313–25. doi: 10.1016/s0301-0082(00)00002-2
3. Dutheil S, Brezun JM, Leonard J, Lacour M, Tighilet B. Neurogenesis and astrogenesis contribution to recovery of vestibular functions in the adult cat following unilateral vestibular neurectomy: cellular and behavioral evidence. *Neuroscience.* (2009) 164:1444–56. doi: 10.1016/j.neuroscience.2009.09.048
4. Roucoux-Hanus M, Boisacq-Schepens N. Ascending vestibular projections: further results at cortical and thalamic levels in the cat. *Exp Brain Res.* (1977) 29:283–92.

5. Faugier-Grimaud S, Ventre J. Anatomic connections of inferior parietal cortex (area 7) with subcortical structures related to vestibulo-ocular function in a monkey (Macaca fascicularis). *J Comp Neurol.* (1989) 280:1–14. doi: 10.1002/cne.902800102
6. de Waele C, Vibert N, Baudrimont M, Vidal PP. NMDA receptors contribute to the resting discharge of vestibular neurons in the normal and hemilabyrinthectomized guinea pig. *Exp Brain Res.* (1990) 81:125–33.
7. Grüsser OJ, Pause M, Schreiter U. Vestibular neurones in the parieto-insular cortex of monkeys (*Macaca fascicularis*): visual and neck receptor responses. *J Physiol.* (1990) 430:559–83.
8. Guldin WO, Akbarian S, Grüsser OJ. Cortico-cortical connections and cytoarchitectonics of the primate vestibular cortex: a study in squirrel monkeys (*Saimiri sciureus*). *J Comp Neurol.* (1992) 326:375–401. doi: 10.1002/cne.903260306
9. Dieterich M, Bense S, Lutz S, Drzezga A, Stephan T, Bartenstein P, et al. Dominance for vestibular cortical function in the non-dominant hemisphere. *Cereb Cortex.* (2003) 13:994–1007. doi: 10.1093/cercor/13.9.994
10. Bense S, Bartenstein P, Lochmann M, Schlindwein P, Brandt T, Dieterich M. Metabolic changes in vestibular and visual cortices in acute vestibular neuritis. *Ann Neurol.* (2004) 56:624–30. doi: 10.1002/ana.20244
11. Dieterich M, Bartenstein P, Spiegel S, Bense S, Schwaiger M, Brandt T. Thalamic infarctions cause side-specific suppression of vestibular cortex activations. *Brain.* (2005) 128:2052–67. doi: 10.1093/brain/awh551
12. Becker-Bense S, Dieterich M, Buchholz HG, Bartenstein P, Schreckenberger M, Brandt T. The differential effects of acute right- vs. left-sided vestibular failure on brain metabolism. *Brain Struct Funct.* (2014) 219:1355–67. doi: 10.1007/s00429-013-0573-z
13. Dieterich M. Functional brain imaging: a window into the visuo-vestibular systems. *Curr Opin Neurol.* (2007) 20:12–8. doi: 10.1097/WCO.0b013e328013f854
14. Dutia MB. Mechanisms of vestibular compensation: recent advances. *Curr Opin Otolaryngol Head Neck Surg.* (2010) 18:420–4. doi: 10.1097/MOO.0b013e32833de71f
15. Cullen KE, Minor LB, Beraneck M, Sadeghi SG. Neural substrates underlying vestibular compensation: contribution of peripheral versus central processing. *J Vestib Res.* (2009) 19:171–82. doi: 10.3233/VES-2009-0357
16. Balaban CD. Neurotransmitters in the vestibular system. *Handb Clin Neurol.* (2016) 137:41–55. doi: 10.1016/b978-0-444-63437-5.00003-0
17. Tighilet B, Bordiga P, Cassel R, Chabbert C. Peripheral vestibular plasticity vs central compensation: evidence and questions. *J Neurol.* (2019). 266(Suppl.1):27–32. doi: 10.1007/s00415-019-09388-9
18. Smith PF, Darlington CL. Neurochemical mechanisms of recovery from peripheral vestibular lesions (vestibular compensation). *Brain Res Rev.* (1991) 16:117–33.
19. Petrosini L, Dell'Anna ME. Vestibular compensation is affected by treatment with dopamine active agents. *Arch Ital Biol.* (1993) 131:159–71.
20. Drago F, Nardo L, Rampello L, Raffaele R. Vestibular compensation in aged rats with unilateral labyrinthectomy treated with dopaminergic drugs. *Pharmacol Res.* (1996) 33:135–40. doi: 10.1006/phrs.1996.0020
21. Saika T, Takeda N, Kiyama H, Kubo T, Tohyama M, Matsunaga T. Changes in preproenkephalin mRNA after unilateral and bilateral labyrinthectomy in the rat medial vestibular nucleus. *Mol Brain Res.* (1993) 19:237–40.
22. Zwergal A, Schlichtiger J, Xiong G, Beck R, Günther L, Schniepp R, et al. Sequential [^{18}F]FDG μPET whole-brain imaging of central vestibular compensation: a model of deafferentation-induced brain plasticity. *Brain Struct Funct.* (2016) 221:159–70. doi: 10.1007/s00429-014-0899-1
23. Kitahara T, Takeda N, Saika T, Kubo T, Kiyama H. Effects of MK801 on Fos expression in the rat brainstem after unilateral labyrinthectomy. *Brain Res.* (1995) 700:182–90.
24. Kitahara T, Nakagawa A, Fukushima M, Horii A, Takeda N, Kubo T. Changes in fos expression in the rat brainstem after bilateral labyrinthectomy. *Acta Oto Laryngol.* (2002) 122:620–6. doi: 10.1080/000164802320396295
25. Kitahara T, Kaneko T, Horii A, Fukushima M, Kizawa-Okumura K, Takeda N, et al. Fos-enkephalin signaling in the rat medial vestibular nucleus facilitates vestibular compensation. *J Neurosci Res.* (2006) 83:1573–83. doi: 10.1002/jnr.20830
26. Dieterich M, Bense S, Stephan T, Brandt T, Schwaiger M, Bartenstein P. Medial vestibular nucleus lesions in Wallenberg's syndrome cause decreased activity of the contralateral vestibular cortex. *Ann NY Acad Sci.* (2005) 1039:368–83. doi: 10.1196/annals.1325.035
27. Dieterich M, Bauermann T, Best C, Stoeter P, Schlindwein P. Evidence for cortical visual substitution of chronic bilateral vestibular failure (an fMRI study). *Brain.* (2007) 130:2108–16. doi: 10.1093/brain/awm130
28. Becker-Bense S, Buchholz HG, Best C, Schreckenberger M, Bartenstein P, Dieterich M. Vestibular compensation in acute unilateral medullary infarction: FDG-PET study. *Neurology.* (2013) 80:1103–9. doi: 10.1212/WNL.0b013e31828868a6
29. Becker-Bense S, Buchholz HG, Baier B, Schreckenberger M, Bartenstein P, Zwergal A, et al. Functional plasticity after unilateral vestibular midbrain infarction in human positron emission tomography. *PLoS ONE.* (2016) 11:e0165935. doi: 10.1371/journal.pone.0165935
30. Best C, Lange E, Buchholz HG, Schreckenberger M, Reuss S, Dieterich M. Left hemispheric dominance of vestibular processing indicates lateralization of cortical functions in rats. *Brain Struct Funct.* (2014) 219:2141–58. doi: 10.1007/s00429-013-0628-1
31. Okami K, Sekitani T, Ogata M, Matsuda Y, Ogata Y, Kanaya K, et al. GABA distribution in the central vestibular system after retroauricular galvanic stimulation. An immunohistochemical study *Acta Otolaryngol.* (1991) 481:150–2.
32. Fitzpatrick RC, Day BL. Probing the human vestibular system with galvanic stimulation. *J Appl Physiol.* (2004) 96:2301–16. doi: 10.1152/japplphysiol.00008.2004
33. Utz KS, Dimova V, Oppenländer K, Kerkhoff G. Electrified minds: transcranial direct current stimulation (tDCS) and galvanic vestibular stimulation (GVS) as methods of non-invasive brain stimulation in neuropsychology–a review of current data and future implications. *Neuropsychologia.* (2010) 48:2789–810. doi: 10.1016/j.neuropsychologia.2010.06.002
34. Schniepp R, Boerner JC, Decker J, Jahn K, Brandt T, Wuehr M. Noisy vestibular stimulation improves vestibulospinal function in patients with bilateral vestibulopathy. *J Neurol.* (2018) 265(Suppl.1):57–62. doi: 10.1007/s00415-018-8814-y
35. Paxinos G, Watson C. *The Rat Brain in Stereotaxic Coordinates.* San Diego: Academic Press (2014).
36. Tai YC, Ruangma A, Rowland D, Siegel S, Newport DF, Chow PL, et al. Performance evaluation of the microPET focus: a third-generation microPET scanner dedicated to animal imaging. *J Nucl Med.* (2005) 46:455–63.
37. Reuss S, Decker K. Anterograde tracing of retinohypothalamic afferents with Fluoro-Gold. *Brain Res.* (1997) 745:197–204.
38. Reuss S, Disque-Kaiser U, DeLiz S, Ruffer M, Riemann R. Immunfluorescence study of neuropeptides in identified neurons of the rat auditory superior olivary complex. *Cell Tissue Res.* (1999) 297:13–21.
39. Reuss S, Disque-Kaiser U, Antoniou-Lipfert P, Najaf Gholi M, Riemann E, Riemann R. Neurochemistry of olivocochlear neurons in the hamster. *Anat Rec.* (2009) 292:461–71. doi: 10.1002/ar.20881
40. Reuss S, Banica O, Elgurt M, Mitz S, Disque-Kaiser U, Riemann R, et al. Neuroglobin expression in the mammalian auditory system. *Mol Neurobiol.* (2016) 53:1461–77. doi: 10.1007/s12035-014-9082-1
41. Schmued LC, Fallon JH. Fluoro-Gold: a new fluorescent retrograde axonal tracer with numerous unique properties. *Brain Res.* (1986) 377:147–54.
42. McLean IW, Nakane PK. Periodate-lysine-paraformaldehyde fixative. A new fixation for immunoelectron microscopy. *J Histochem Cytochem.* (1974) 22:1077–83.
43. Reuss S, Kühn I, Windoffer R, Riemann R. Neurochemistry of identified motoneurons of the tensor tympani muscle in rat middle ear. *Hear Res.* (2009) 248:69–79. doi: 10.1016/j.heares.2008.12.003
44. Curthoys IS. Vestibular compensation and substitution. *Curr Opin Neurol.* (2000) 13:27–30. doi: 10.1097/00019052-200002000-00006
45. Cullen KE. Physiology of central pathways. *Handb Clin Neurol.* (2016) 137:17–40. doi: 10.1016/b978-0-444-63437-5.00002-9
46. Brandt T, Dieterich M. The dizzy patient: don't forget disorders of the central vestibular system. *Nat Rev Neurol.* (2017) 13:352–62. doi: 10.1038/nrneurol.2017.58

47. Brandt T, Dieterich M. Thalamocortical network: a core structure for integrative multimodal vestibular functions. *Curr Opin Neurol.* (2019) 32:154–64. doi: 10.1097/wco.0000000000000638
48. Kirsch V, Keeser D, Hergenroeder T, Erat O, Ertl-Wagner B, Brandt T, et al. Structural and functional connectivity mapping of the vestibular circuitry from human brainstem to cortex. *Brain Struct Funct.* (2016) 221:1291–308. doi: 10.1007/s00429-014-0971-x
49. Dieterich M, Kirsch V, Brandt T. Right-sided dominance of the bilateral vestibular system in the upper brainstem and thalamus. *J Neurol.* (2017) 264(Suppl.1):55–62. doi: 10.1007/s00415-017-8453-8
50. Lopez C, Blanke O. The thalamocortical vestibular system in animals and humans. *Brain Res Rev.* (2011) 67:119–46. doi: 10.1016/j.brainresrev.2010.12.002
51. Lopez C. The vestibular system: balancing more than just the body. *Curr Opin Neurol.* (2016) 29:74–83. doi: 10.1097/wco.0000000000000286
52. Brandt T, Bartenstein P, Janek A, Dieterich M. Reciprocal inhibitory visual-vestibular interaction. Visual motion stimulation deactivates the parieto-insular vestibular cortex. *Brain.* (1998) 121:1749–58.
53. Leong ATL, Gu Y, Chan YS, Zheng H, Dong CM, Chan RW, et al. Optogenetic fMRI interrogation of brain-wide central vestibular pathways. *Proc Natl Acad Sci USA.* (2019) 116:10122–9. doi: 10.1073/pnas.1812453116
54. Ruigrok T, Sillitoe R, Voogd J. Cerebellum and cerebellar connections. In: Paxinos G, editor. *The Rat Nervous System.* Amsterdam: Elsevier (2015). pp. 133–205.
55. Barmack NH. Central vestibular system: vestibular nuclei and posterior cerebellum. *Brain Res Bull.* (2003) 60:511–41. doi: 10.1016/s0361-9230(03)00055-8
56. Schlosser HG, Guldin WO, Grüsser OJ. Tuning in caudal fastigial nucleus units during natural and galvanic labyrinth stimulation. *Neuroreport.* (2001) 12:1443–7. doi: 10.1097/00001756-200105250-00029
57. Jones SM, Jones TA, Mills KN, Gaines GC. Anatomical and physiological considerations in vestibular dysfunction and compensation. *Semin Hear.* (2009) 30:231–41. doi: 10.1055/s-0029-1241124
58. Beraneck M, McKee JL, Aleisa M, Cullen KE. Asymmetric recovery in cerebellar-deficient mice following unilateral labyrinthectomy. *J Neurophysiol.* (2008) 100:945–58. doi: 10.1152/jn.90319.2008
59. zu Eulenburg P, Stoeter P, Dieterich M. Voxel-based morphometry depicts central compensation after vestibular neuritis. *Ann Neurol.* (2010) 68:241–249. doi: 10.1002/ana.22063
60. Newman DB, Liu RP. Nuclear origins of brainstem reticulocortical systems in the rat. *Am J Anat.* (1987) 178:279–99.
61. Rancz EA, Moya J, Drawitsch F, Brichta AM. Widespread vestibular activation of the rodent cortex. *J Neurosci.* (2015) 35:5926–34. doi: 10.1523/JNEUROSCI.1869-14.2015
62. Fredrickson JM, Scheid P, Figge U, Kornhuber HH. Vestibular nerve projection to the cerebral cortex of the rhesus monkey. *Exp Brain Res.* (1966) 2:318–27.
63. Akbarian S, Grüsser OJ, Guldin WO. Thalamic connections of the vestibular cortical fields in the squirrel monkey (*Saimiri sciureus*). *J Comp Neurol.* (1992) 326:423–41. doi: 10.1002/cne.903260308
64. Bottini G, Sterzi R, Paulesu E, Vallar G, Cappa SF, Erminio F, et al. Identification of the central vestibular projections in man: a positron emission tomography activation study. *Exp Brain Res.* (1994) 99:164–9.
65. Bense S, Stephan T, Yousry TA, Brandt T, Dieterich M. Multisensory cortical signal increases and decreases during vestibular galvanic stimulation (fMRI). *J Neurophysiol.* (2001) 85:886–99. doi: 10.1152/jn.2001.85.2.886
66. zu Eulenburg P, Caspers S, Roski C, Eickhoff SB. Meta-analytical definition and functional connectivity of the human vestibular cortex. *Neuroimage.* (2012) 60:162–9. doi: 10.1016/j.neuroimage.2011.12.032
67. Lopez C, Blanke O, Mast FW. The human vestibular cortex revealed by coordinate-based activation likelihood estimation meta-analysis. *Neuroscience.* (2012) 212:159–79. doi: 10.1016/j.neuroscience.2012.03.028
68. Angelaki DE, Cullen KE. Vestibular system: the many facets of a multimodal sense. *Annu Rev Neurosci.* (2008) 31:125–50. doi: 10.1146/annurev.neuro.31.060407.125555
69. Jones EG, Powell TP. Connexions of the somatic sensory cortex of the rhesus monkey. 3. Thalamic connexions. *Brain.* (1970) 93:37–56.
70. Staiger JF, Zilles K, Freund TF. Innervation of VIP-immunoreactive neurons by the ventroposteromedial thalamic nucleus in the barrel cortex of the rat. *J Comp Neurol.* (1996) 367:194–204.
71. Wijesinghe R, Protti DA, Camp AJ. Vestibular interactions in the thalamus. *Front Neural Circuits.* (2015) 9:79. doi: 10.3389/fncir.2015.00079
72. Akbarian S, Grüsser OJ, Guldin WO. Corticofugal connections between the cerebral cortex and brainstem vestibular nuclei in the macaque monkey. *J Comp Neurol.* (1994) 339:421–37. doi: 10.1002/cne.903390309
73. Nagata S. The vestibulothalamic connections in the rat: a morphological analysis using wheat germ agglutinin-horseradish peroxidase. *Brain Res.* (1986) 376:57–70.
74. Doi K, Seki M, Kuroda Y, Okamura N, Ito H, Hayakawa T, et al. Direct and indirect thalamic afferents arising from the vestibular nuclear complex of rats: medial and spinal vestibular nuclei. *Okajimas Folia Anat Jpn.* (1997) 74:9–31.
75. Shiroyama T, Kayahara T, Yasui Y, Nomura J, Nakano K. Projections of the vestibular nuclei to the thalamus in the rat: a *Phaseolus vulgaris* leucoagglutinin study. *J Comp Neurol.* (1999) 407:318–32.
76. Matesz C, Bacskai T, Nagy E, Halasi GA, Kulik A. Efferent connections of the vestibular nuclei in the rat: a neuromorphological study using PHA-L. *Brain Res Bull.* (2002) 57:313–5. doi: 10.1016/s0361-9230(01)00726-2
77. Kim N, Choi MA, Koo H, Park BR, Han SW, Cheong C, et al. Activation of the thalamic parafascicular nucleus by electrical stimulation of the peripheral vestibular nerve in rats. *Exp Brain Res.* (2017) 235:1617–25. doi: 10.1007/s00221-016-4864-5
78. Killackey HP, Sherman SM. Corticothalamic projections from the rat primary somatosensory cortex. *J Neurosci.* (2003) 23:7381–4.
79. Baier B, Conrad J, Stephan T, Kirsch V, Vogt T, Wilting J, et al. Vestibular thalamus: two distinct graviceptive pathways. *Neurology.* (2016) 86:134–40. doi: 10.1212/wnl.0000000000002238
80. Schuerger RJ, Balaban CD. Immunohistochemical demonstration of regionally selective projections from locus coeruleus to the vestibular nuclei in rats. *Exp Brain Res.* (1993) 92:351–9.
81. Horowitz SS, Blanchard J, Morin LP. Medial vestibular connections with the hypocretin (Orexin) system. *J Comp Neurol.* (2005) 487:127–46. doi: 10.1002/cne.20521
82. Akbarian S, Grüsser OJ, Guldin WO. Corticofugal projections to the vestibular nuclei in squirrel monkeys: further evidence of multiple cortical vestibular fields. *J Comp Neurol.* (1993) 332:89–104. doi: 10.1002/cne.903320107
83. Fasold O, von Brevern M, Kuhberg M, Ploner CJ, Villringer A, Lempert T, et al. Human vestibular cortex as identified with caloric stimulation in functional magnetic resonance imaging. *Neuroimage.* (2002) 17:1384–93. doi: 10.1006/nimg.2002.1241
84. Miyamoto T, Fukushima K, Takada T, de Waele C, Vidal PP. Saccular stimulation of the human cortex: a functional magnetic resonance imaging study. *Neurosci Lett.* (2007) 423:68–72. doi: 10.1016/j.neulet.2007.06.036
85. Bohne P, Schwarz MK, Herlitze S, Mark MD. A new projection from the deep cerebellar nuclei to the hippocampus via the ventrolateral and laterodorsal thalamus in mice. *Front Neural Circuits.* (2019) 13:51. doi: 10.3389/fncir.2019.00051
86. Horii A, Russell NA, Smith PF, Darlington CL, Bilkey DK. Vestibular influences on CA1 neurons in the rat hippocampus: an electrophysiological study *in vivo*. *Exp Brain Res.* (2004) 155:245–50. doi: 10.1007/s00221-003-1725-9
87. Brandt T, Schautzer F, Hamilton DA, Brüning R, Markowitsch HJ, Kalla R, et al. Vestibular loss causes hippocampal atrophy and impaired spatial memory in humans. *Brain.* (2005) 128:2732–41. doi: 10.1093/brain/awh617
88. Nakagawa A, Uno A, Horii A, Kitahara T, Kawamoto M, Uno Y, et al. Fos induction in the amygdala by vestibular information during hypergravity stimulation. *Brain Res.* (2003) 986:114–23. doi: 10.1016/s0006-8993(03)03220-7
89. Pompeiano O, d'Ascanio P, Balaban E, Centini C, Pompeiano M. Gene expression in autonomic areas of the medulla and the central nucleus of

the amygdala in rats during and after space flight. *Neuroscience.* (2004) 124:53–69. doi: 10.1016/j.neuroscience.2003.09.027
90. Guldin WO, Grüsser OJ. Is there a vestibular cortex? *Trends Neurosci.* (1998) 21:254–9.
91. Chen A, DeAngelis GC, Angelaki DE. Macaque parieto-insular vestibular cortex: responses to self-motion and optic flow. *J Neurosci.* (2010) 30:3022–42. doi: 10.1523/JNEUROSCI.4029-09.2010
92. Chen A, DeAngelis GC, Angelaki DE. A comparison of vestibular spatiotemporal tuning in macaque parietoinsular vestibular cortex, ventral intraparietal area, and medial superior temporal area. *J Neurosci.* (2011) 31:3082–94. doi: 10.1523/JNEUROSCI.4476-10.2011
93. Stephan T, Deutschländer A, Nolte A, Schneider E, Wiesmann M, Brandt T, et al. Functional MRI of galvanic vestibular stimulation with alternating currents at different frequencies. *Neuroimage.* (2005) 26:721–32. doi: 10.1016/j.neuroimage.2005.02.049
94. Kirsch V, Boegle R, Keeser D, Kierig E, Ertl-Wagner B, Brandt T, et al. Handedness-dependent functional organizational patterns within the bilateral vestibular cortical network revealed by fMRI connectivity based parcellation. *Neuroimage.* (2018) 178:224–37. doi: 10.1016/j.neuroimage.2018.05.018
95. Dieterich M, Brandt T. Functional brain imaging of peripheral and central vestibular disorders. *Brain.* (2008) 131:2538–52. doi: 10.1093/brain/awn042
96. Vidal PP, Cullen K, Curthoys IS, Du Lac S, Holstein G, Idoux E, et al. "The vestibular system," In: Paxinos, editor. *The Rat Nervous System*. Amsterdam: Elsevier (2015). p. 805–864.
97. Reuss S, Wystub S, Disque-Kaiser U, Hankeln T, Burmester T. Distribution of cytoglobin in the mouse brain. *Front Neuroanat.* (2016) 10:47. doi: 10.3389/fnana.2016.00047
98. Smith PF. Age-related neurochemical changes in the vestibular nuclei. *Front Neurol.* (2016) 7:20. doi: 10.3389/fneur.2016.00020
99. Jansen NL, Feuerecker R, Becker-Bense S, Zwergal A, Wulff M, Xiong G, et al. Assessment of cerebral dopamine D 2/3 formula-receptors in patients with bilateral vestibular failure. *J Vestib Res.* (2014) 24:403–13. doi: 10.3233/ves-140526
100. Ryan AF, Simmons DM, Watts AG, Swanson LW. Enkephalin mRNA production by cochlear and vestibular efferent neurons in the gerbil brainstem. *Exp Brain Res.* (1991) 87:259–67.
101. Soto E, Vega R. Neuropharmacology of vestibular system disorders. *Curr Neuropharmacol.* (2010) 8:26–40. doi: 10.2174/157015910790909511
102. Sulaiman MR, Dutia MB. Opioid inhibition of rat medial vestibular nucleus neurones *in vitro* and its dependence on age. *Exp Brain Res.* (1998) 122:196–202.
103. Baier B, Bense S, Birklein F, Buchholz HG, Mischke A, Schreckenberger M, et al. Evidence for modulation of opioidergic activity in central vestibular processing: a [(18)F] diprenorphine PET study. *Hum Brain Mapp.* (2010) 31:550–5. doi: 10.1002/hbm.20886

Conflict of Interest: The authors declare that the research was conducted in the absence of any commercial or financial relationships that could be construed as a potential conflict of interest.

frontiers in Neurology

CLINICAL TRIAL
published: 30 June 2020
doi: 10.3389/fneur.2020.00601

Exergaming With Integrated Head Turn Tasks Improves Compensatory Saccade Pattern in Some Patients With Chronic Peripheral Unilateral Vestibular Hypofunction

Jaap Swanenburg[1,2], *Fabienne Büchi*[1], *Dominik Straumann*[3], *Konrad P. Weber*[3,4] and *Eling D. de Bruin*[5,6*]

[1] Physiotherapy and Occupational Therapy Research Center, Directorate of Research and Education, University Hospital Zurich, University of Zurich, Zurich, Switzerland, [2] Department of Chiropractic Medicine, Integrative Spinal Research ISR, Balgrist University Hospital, Zurich, Switzerland, [3] Department of Neurology, University Hospital Zurich, University of Zurich, Zurich, Switzerland, [4] Department of Ophthalmology, University Hospital Zurich, University of Zurich, Zurich, Switzerland, [5] Department Health Sciences and Technology, Institute of Human Movement Sciences and Sport, ETH Zurich, Zurich, Switzerland, [6] Division of Physiotherapy, Department of Neurobiology, Care Sciences and Society, Karolinska Institute, Stockholm, Sweden

OPEN ACCESS

Edited by:
Stefano Ramat,
University of Pavia, Italy

Reviewed by:
Michael C. Schubert,
Johns Hopkins University, United States
Eric Anson,
University of Rochester, United States

***Correspondence:**
Eling D. de Bruin
eling.debruin@hest.ethz.ch

Specialty section:
This article was submitted to Neuro-Otology, a section of the journal Frontiers in Neurology

Received: 17 March 2020
Accepted: 25 May 2020
Published: 30 June 2020

Citation:
Swanenburg J, Büchi F, Straumann D, Weber KP and de Bruin ED (2020) Exergaming With Integrated Head Turn Tasks Improves Compensatory Saccade Pattern in Some Patients With Chronic Peripheral Unilateral Vestibular Hypofunction. Front. Neurol. 11:601. doi: 10.3389/fneur.2020.00601

Background: This study aimed to determine whether vestibular rehabilitation using active video games (Exergames), including promoted head turns and unsupported locomotion, may facilitate vestibular compensation and gait in subjects with one-sided chronic peripheral vestibular hypofunction (cPVH).

Methods: 12 patients with cPVH (mean age of 65 ± 12 years, 8 male) were recruited for this study. The study consisted of a four-week baseline control period T1-T2 followed by a four-week intervention period T2-T3. The intervention included exergames that required physical tasks such as steps, weight shifts or balance control to cognitive challenges, in a virtual environment to play the game. The subjects participated in a total of 176 min of exergaming in eight sessions. Because of the changing projection direction of the game to the wall, the subjects had to turn their heads constantly while playing the game. Dynamic visual acuity (DVA) was assessed. Vestibulo-Ocular reflex (VOR) gain deficit and cumulative overt saccade amplitude (COSA) were measured with the video head-impulse test. Additionally, the functional gait assessment (FGA), Extended Timed Get-Up-and-Go (ETGUG), and the Dizziness handicap inventory (DHI), were assessed.

Results: DVA showed no significant group level change ($p = 0.475$, $z = -0.714$, $d = 0.295$) with a small effect size and improvements in five out of 12 subjects. Ipsilesional VOR gain did not improve ($p = 0.157$, $z = -1.414$, $d = 0.481$) on group level while there was an intermediate effect size and improvements in six out of 12 subjects. COSA got significant smaller ($p = 0.006$, $z = -2.746$, $d = 1.354$) with improvements in seven out of 12 subjects. The contralesional sides did not change. The FGA for the group significantly improved with an intermediate effect size ($p < 0.001$, $z = -3.08$, $d = 1.617$) and five individuals showed clinically relevant improvements. The ETGUG group value improved significantly with a strong effect size ($p < 0.001$, $z = -2.67$, $d = 1.030$), with

seven individuals contributing to this change. The DHI showed no change ($p = 0.172$, z $= -1.381$, d $= 0.592$) neither on the group nor on the individuals' level. The game scores of the subjects improved during the intervention period of the intervention for every game.

Conclusion: The results of this study demonstrate that exergaming with promoted head turns facilitates vestibular compensation in some subjects with cPVH. This is the first study that shows an improvement in cumulative overt saccade amplitude after exergaming in chronic vestibular subjects.

Keywords: vestibular loss, exergaming, head turns, dynamic visual acuity, saccades

INTRODUCTION

Vestibular disorders are either assessed through cardinal symptoms of vestibular dysfunction, through balance testing or through diagnosing of specific vestibular disorders (1). Subjects with vestibular disorders often experience symptoms like vertigo, dizziness, visual disturbance, and imbalance (2, 3). The lifetime prevalence of vertigo alone in adults aged 18–79 years was 7.4% (4). Furthermore, subjects experience anxiety and distress of depression. Many patients suffer from cognitive impairments, problems with spatial memory and attention (5–7) and sustain repeated falls (8). Having vestibular disorders, hence, relates to reduced quality of life and it negatively affects many aspects of daily living (3).

Non-pharmacological vestibular rehabilitation is thus far the only effective method for improving symptoms related to many chronical vestibular disorders (3) and two recent systematic reviews partly confirm some of this beneficial effects of exercise-based rehabilitation (9, 10). However, both reviews point out the necessity of further non-pharmacological studies into determining the optimal protocol and effect for newly developed therapies, as also reflected in clinical guidelines (11). Therefore, the further development of non-pharmacological approaches for the treatment of vestibular disorders is warranted.

Perceptual and cognitive decline in individuals with vestibular disorders can be counteracted through sustained practice of a martial art or through exposing individuals to a virtual reality environment. Both approaches relate to improved symptoms of vestibular disorders (1, 12, 13). To reduce their sensation of dizziness, patients often move their head as little as possible while moving around (14); e.g., while walking, a strategy associated with negative effects on postural balance and walking behavior on stairs (15, 16) and on community ambulation (17). Therefore, improving gait is an important goal of vestibular rehabilitation (1, 18) and this goal may be achieved by specifically including head movements into the exercise programs (19). Gaze stabilization rehabilitation may lead to some improvements in visual acuity and vestibulo-ocular reflex in these patients (20, 21), especially when applied in early disease stages (22). Next to gaze stabilization, balance training, and walking exercise for endurance, habituation exercise is one of four main exercise categories that can be used for rehabilitation (11). Habituation exercises are used to treat symptoms of dizziness produced by self-motion or that are produced by visual stimuli and are referred to as "the reduction in a behavioral response to repeated exposure to a provocative stimulus, with the goal of reducing symptoms related to the vestibular system (11)."

Neurophysiologically, individuals should in their therapy program be provided with a series of performance tasks that require using the eyes while at the same time moving the head and body (23). A proof-of-concept study from our group showed improved functional gait following training in a virtual environment that integrated visual observation and head turning movements while physically playing the Exergames. This theory-based intervention facilitated gaze stability during head movements in older adults as measured by the computerized dynamic visual acuity (DVA) test (24). The results of this study led to the hypothesis that also chronic subjects with vestibular disorders would be able to train and improve their vestibular functioning.

Video-games that require whole-body physical activity to play the game combine motor and cognitive exercises and are labeled Exergames (25). Exergames provide a motivational and entertaining way to be physically active for patients (12, 26), and recent studies demonstrated a positive effect of virtual reality-based interventions on patients with vestibular hypofunction (27–29). This form of training theoretically allows addressing all four important exercise components for vestibular subjects (11) into one exercise program: gaze stability exercises and habituation exercises (24), balance and gait exercises (30, 31), and endurance (32).

The purpose of this pilot study is to further develop the theory-based exergame intervention and describe its effects on vestibular compensation in multiple subjects with one-sided chronic peripheral vestibular hypofunction (cPVH). We hypothesized that, similar to older adults, individual patient symptoms could be influenced based on the current available evidence (11) for, and the ecological validity of, the training content.

METHODS

Participants

For this pilot study, 12 outpatients with one-sided cPVH were recruited in the Departments of Neurology and Otorhinolaryngology at the University Hospital Zurich (USZ). A senior neurologist identified patients with one-sided cPVH at baseline. A horizontal video head-impulse test (video HIT) to both sides was used to identify cPVH at T1. A video HIT

gain (eye velocity divided by head velocity at peak head acceleration) below 0.7 was considered pathological. Exclusion criteria were; (1) walking disability (independent walking <10 meters), (2) acute pain, (3) medication reducing postural balance (4) weakness resulting from neurological problems, (5), uncontrolled cardiovascular disease (e.g.,: uncontrolled blood pressure) (6) gait disorders putatively attributed to other than primarily vestibular causes, (7) uncorrected severe visual impairment. Additionally, patients with Menière's disease or with benign paroxysmal positional vertigo were excluded. All measurements and exergame sessions took place at the University Hospital Zurich. The measurement assistants were blinded. All subjects provided written informed consent before partaking in the therapy sessions and the study was approved by the ethics committee of the Canton of Zurich under BASEC 2018-00337. Trial registration was done at ClinicalTrials.gov Identifier; NCT03536533.

Design

Subjects were included and primarily assessed using an A-B study design (33). Vestibular function was tested on three separate test sessions T1, T2, and T3 at intervals of one month. The first month served as control period (A) between T1 and T2 whereas, the second month functioned as intervention period (B) between T2 and T3. DVA and VOR gain were used to test for chronicity (T1-T2-T3) of the clinical presentation of symptoms and functional impairment in enrolled subjects with cPVH.

Intervention

Purpose-developed games were used in the study that are targeting to improve cognitive functions such as divided attention, working memory, inhibition, and attention shifting. Physical functions, such as balance and gait, are trained because the games are played through whole body movements in standing position and, preferably, without support from a handrail. By changing the orientation of the projection during the game-play (see Video Exergame) participants need to turn their head to successfully play the games. Additionally, in every session one game had to be played while the participant stood rotated 90° to the left or right and with head turned toward the projection. The detailed exercise protocol is described in detail elsewhere (24). During the intervention, the subjects received one-on-one supervision from the research assistant. In total, eight exergaming sessions were accomplished for each patient over the 4-week intervention period T2–T3. The training principles of progression and overload were applied (31). Each session lasted for 40 min, with an actual exercise duration of 22 min. The total cumulative intervention exercise time of 176 min slightly exceeded the recommended time (150 min) for an efficient virtual reality intervention (12, 24). The certified medical device exercise system Senso (dividat, Schindellegi, Switzerland), a pressure-sensitive plate, was used for the training (24). The Senso pad provided the participants with real-time visual and auditory feedback. The visual angle of the projected game was ±81° in width and ±54°in height. To promote head movements during the exercises the projector was either rotated ±45 degrees horizontally or ±15 degrees vertically. A remote-controlled power panner (Maxwell MPR−202) was used to move the projector with 6° per second horizontally and 2° per second vertically. Misery Score (MISC) was used to determine whether the training could be continued in a given level. The MISC is a simple scale to gather nausea symptoms. It is categorized in 1 = no nausea, 2 = initial symptoms, but no nausea, 3 = mild nausea, 4 = moderate nausea, 5 = severe nausea, and 6 = vomiting. In the present study, MISC 1-3 was accepted during training. A MISC score 4 and more would have led to a training stop (27) or to lowering the exercise level of difficulty. The exercise set-up is shown in a **Video 1** (see Video Exergame).

Games

Four different games were used during the intervention session. As a warm-up, the game "Simple" was used. This game trains focused attention. Thereafter the game "targets" was played. This game trains goal-oriented reacting. Cognitive flexibility was trained with the third game "flexi." The final game was the game "snake," which focuses on visual processing. The difficulty of all games was progressively adapted by speeding up the game according to the performance of the player, or in the fourth game "snake" the length of the snake increased progressively (24) screen images of all games in the **Supplementary File 1**.

Measurements

DVA

DVA measures visual acuity during head movement relative to baseline static visual acuity (SVA) (34, 35). Passive head impulses were performed using a DVA testing system that consisted of a personal computer with a 19-inch monitor (1280 × 1024 pixels, 75 Hz) and a Sparkfun velocity sensor (Sparkfun Electronics, Boulder, Colorado), which was fixed on a headset to the participant's head (36, 37). The test gives information on the vestibulo-ocular reflex (VOR) performance, mainly of the semicircular canal function (36) and has change in visual acuity, when moving the head compared to static acuity, as output (38). For horizontal testing, the head rotation was assessed in both left and right directions, for each patient. (39). One of two experienced examiners conducted testing.

VOR Gain

The video head-impulse-test measurements (vHIT) were used to assess the VOR gain (40, 41). This test gives information about the function of the six semicircular canals individually by measuring the eye rotation response to an abrupt head rotation in the plane of the canal (41). The measurement protocol is described in detail in previous studies (41, 42). An ICS Impulse, Natus Medical Inc., Taastrup, Denmark was used to measure the horizontal canals. One of two experienced examiners conducted testing.

Cumulative Overt Saccades Amplitudes (COSA)

The characteristic saccade pattern responses are highly effective in distinguishing patients with unilateral vestibular loss compared to controls (43). OtosuiteV 2.0 (GN Otometrics) was used to re-analyse VOR gains. To qualify corrective saccades we used a custom-written MATLAB (The MathWorks,

Natick, MA, USA) routine. This provided cumulative overt saccade amplitudes (44–46). Saccades that occurred after the head-impulse are defined as "overt" (46).

Functional Gait Assessment (FGA)

FGA is used to measure disturbances in balance and gait (47) and includes the following 10 items (48): (1) Gait on level surface, (2) Change in gait speed, (3) Gait with horizontal head turns, (4) Gait with vertical head turns, (5) Gait and pivot turn, (6) Step over obstacle, (7) Gait with narrow base of support, (8) Gait with eyes closed, (9) Ambulating backwards, (10) Steps. Each item was scored on a 4-point ordinal scale with scores of 0, 1, 2, and 3 (Maximum total score = 30). Higher scores represented better balance and gait capacity (47). The minimal detectable change is 6 points for the FGA (49) and was used to assess change on individual level.

Extended Timed Get-Up-And-Go (ETGUG)

The ETGUG test (50) measures times in seconds to complete a series of functionally important tasks and the overall time needed (seconds) to complete the test with a multimemory stopwatch. ETGUG test included the following tasks: (1) Rising from a chair, (2) Initiating gait, (3) Walking 6 meters straight, (4) Turning around, (5) Walking back, (6) Sitting down again. The time measured during each task and the overall time depicted the functional mobility of the participant (51). With an ICC of 0.97 for the test-retest reliability the test exhibits excellent reliability in vestibular patients (52). For the minimal detectable change we used the 4 seconds difference between patients with both-sided vestibular loss and healthy controls reported in literature (52).

Dizziness Handicap Inventory (DHI)

The DHI German version is a validated, 25-item-self-report questionnaire to evaluate the self-perceived handicapping effects caused by dizziness (53). The DHI is categorized in three domains; functional (9 questions, 36 points), emotional (9 questions, 36 points), and physical (7 questions, 28 points). Subjects answer the questions with no (0 points), sometimes (2 points), and yes (4 points) (54). The higher the score, the greater the handicap caused by dizziness. The cut-off value of clinical relevance is 9 points (53).

Simulator Sickness Questionnaire (SSQ)

The SSQ questionnaire was used to assess virtual reality users' level of sickness symptoms (55). It contains 16 items which had to be weighed by the participants in terms of severity on a 4-level scale with the options including "none," "slight," "moderate," and "severe."(56). (Minimum score = 0, Maximum total score = 48). After each exercise session and a few hours later the same day, the subjects completed the SSQ.

Game Scores

Game scores and therapy attendance of the exercise sessions were recorded to monitor progression and adherence to the training plan.

Statistical Analysis

Descriptive statistics were used to describe the community dweller's characteristics. Normality of data distribution was tested using the Shapiro-Wilk test. In case of non-normal distribution, the Wilcoxon test was chosen to test the differences between measurement time points. Additionally, for the effect size, Cohen's d (d) values were calculated. Cohen (1988) reports the following intervals for d: 0.1 to 0.3: small effect; 0.3 to 0.5: intermediate effect; 0.5 and higher: strong effect. For sub analysis of FGA and ETGUG tasks a Bonferroni correction was used. Game scores and SSQ were described with descriptive statistics. Additionally a scatterplot with VOR gain and COSA before and after intervention with associated linear regression line was plotted.

IBM SPSS Statistics 25 for Windows (Inc; Chicago, Illinois) was used for all the statistical analyses.

RESULTS

The scores of 12 (mean age of 64.9 ± 11.7 years, 8 male) subjects with one-sided cPVH were analyzed. The mean weight of the subjects was 69.6 ± 10.3 kg and the mean height 168.0 ± 7.7 cm. Two DVA measurements at T1 could not be executed due to technical failure of the measurement device (PT 7 and PT 12). Four subjects received physiotherapy whereof one patient received cervical physiotherapy before the intervention program (PT 3) and the other three subjects were treated for lower extremity issues. Assessed by the MISC no exercise session had to be stopped. There were no adverse events.

Control Period T1–T2

During the control period T1–T2 the DVA lesion side ($p = 0.646$, $z = -0.459$, $d = 0.188$) and the contralateral side ($p = 0.944$, $z = -0.070$, $d = 0.029$) were stable and showed no significant change. A similar result was found with the vHit gain, assessed with the head impulse paradigm, of the affected ($p = 0.694$, $z = -0.393$, $d = 0.161$) and the contralateral side ($p = 0.695$, $z = -0.393$, $d = 0.161$) both showing no significant change.

Intervention Period T2–T3

Vestibular Compensation

DVA showed no significant change ($p = 0.475$, $z = -0.714$, $d = 0.295$) with a small effect size and improvements in five out of 12 subjects. In addition, VOR gain at the ipsilesional side did not improve ($p = 0.157$, $z = -1.414$, $d = 0.481$) on group level and there was an intermediate effect size and improvements in six out of 12 subjects. COSA got significant smaller ($p = 0.006$, $z = -2.746$, $d = 1.354$) with improvements in seven out of 12 subjects. The contralesional sides did not change. A graphical plot example of an impulse test can be seen in **Figure 1**. All data of vestibular compensation can be found in **Table 1**. Results and changes of each individual participant can be found in **Table 2** and **Figures 2–4**.

Scatterplots between DVA and COSA before and after intervention with associated linear regression lines are shown in

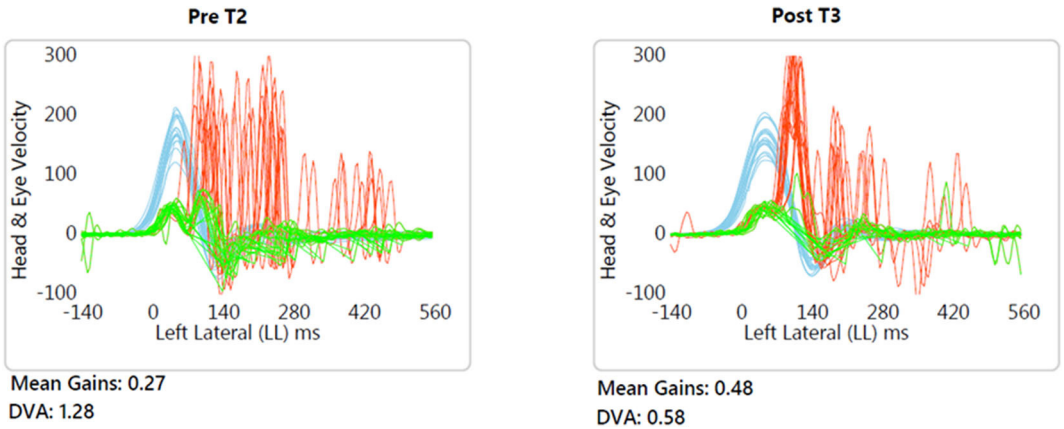

FIGURE 1 | Typical example (patient no. 9) of improved VOR gain and reduced compensatory saccade variability. Blue, head velocity; Green, eye velocity; Red, compensatory saccades.

TABLE 1 | Results of the Vestibular compensation pre and post intervention (T2–T3).

	DVA (logMAR)				VOR Gain				COSA			
	Lesion side		Contralateral side		Lesion side		Contralateral side		Lesion side		Contralateral side	
	T2	T3	T2	T3	T2	T3	T2	T3	T2	T3	T2	T3
Mean	0.630	0.633	0.470	0.439	0.518	0.667	0.911	0.933	3.502	2.543	0.546	0.623
SD	0.367	0.2.80	0.147	0.140	0.213	0.162	0.148	0.078	1.301	1.040	0.666	0.380
Z	−0.714		−0.512		−1.414		−1.070		−2.746		−0.941	
p	0.475		0.609		0.157		0.347		0.006*		0.941	

*SD, standard deviation; Range, min/max; Z, p, Wilcoxon Signed Rank Test; *p < 0.05 significant.*

Figure 5. A scatterplot with VOR gain and COSA before and after intervention with associated linear regression line is shown in **Figure 6**.

Gait Function

The FGA showed significant group-level improvement with a large concomitant Effect Size ($p < 0.001$, $z = -3.08$, $d = 1.617$). The total points improved from 19.58 at T2 to 26.17 points at T3. Five subjects who improved more than the minimal detectable change of six points drove this change. For the sub-tasks gait with horizontal head turns ($p < 0.001$), gait with eyes closed ($p < 0.001$), and ambulating backward ($p < 0.001$) significantly improved. All results of all FGA tasks can be found in **Supplementary Table 1**.

The ETGUG improved significantly on the group level with a strong effect size ($p < 0.001$, $z = -2.67$, $d = 1.030$). The total time decreased from 19.95 s at T2 to 15.61 s at T3. Seven subjects improved more than 4 seconds. The ETGUG sixth task "slow down, stop, turnaround, and sit down" significantly ($p < 0.001$) improved for the group of twelve individuals. All results of all individual ETGUG component tasks can be found in the **Supplementary Table 2**.

Dizziness

There was a non-significant decrease in DHI after the intervention session albeit there was a strong effect size ($p = 0.172$, $z = -1.381$, $d = 0.592$). The total points were 32.83 at T2 and 29.48 points at T3. Four subjects improved more than nine points. All DHI results can be found in **Supplementary Table 3**.

Simulator Sickness

The SSQ showed a decrease immediately following each intervention session. The total points improved from 7.4 at the first session to 4.2 points at the last session. They mainly recorded "fullness of the head" and "sweating during the exercise." Some noted general discomfort or moderate dizziness. During the evening hours of the same day, none of the participants experienced any symptom(s). The mean results of all SSQ measurements after each intervention session are presented in **Supplementary Table 4**.

Game Scores

The subjects' game high scores showed in the beginning continuous improvement in game performance. About half of the course of the intervention period there was a leveling off

TABLE 2 | Individual descriptive data.

Nr	Age range	Diagnosis	Lesion side	Medication	Additional non-vestibular therapy*	DVA	VOR gain	COSA	FGA	ETGUG	DHI
						Change ± 0.05	Change ± 0.05	Change ± 0.1°	Change ± 6 points	Change ± 4 s	Change ± 9 points
1	55-60	cPVH	Right	None	None	+	~	+	~	+	~
2	60-65	cPVH	Left	Aspirin Cardio	None	+	–	~	~	~	~
3	50-55	cPVH	Right	None	Physiotherapy cervical	~	+	–	~	+	+
4	45-50	cPVH	Right	Insulin	None	+	+	~	+	+	~
5	55-60	cPVH	Left	Cholesterol-lowering	Physiotherapy lower extremity	–	~	+	~	+	~
6	60-65	cPVH	Right	Aspirin Cardio, Antihypertensive	None	~	+	+	~	~	~
7	80-85	cPVH	Right	Aspirin Cardio Antihypertensive, Cholesterol-lowering, rare: temesta	Physiotherapy lower extremity	+	+	+	+	~	~
8	65-70	cPVH	Left	Aspirin Cardio, Cholesterol-lowering	None	~	~	–	~	~	+
9	80-85	chronic dizziness under stress	Left	Antihypertensive drug, Aspirin Cardio	None	+	+	+	+	+	~
10	75-80	cPVH	Left	Antihypertensive drug	Physiotherapy lower extremity	–	~	–	+	+	~
11	60-65	cPVH	Left	Aspirin Cardio	None	~	–	+	+	+	+
12	55-60	chronic neuritis vestibularis	Left	None	None	–	+	+	~	~	+

+, *improvement*, –, *deterioration*, ~, *no change by minimal detectable values or by clinical judgment in case of VOR gain.*
**Additional non-vestibular complaints related therapy received during this study.*

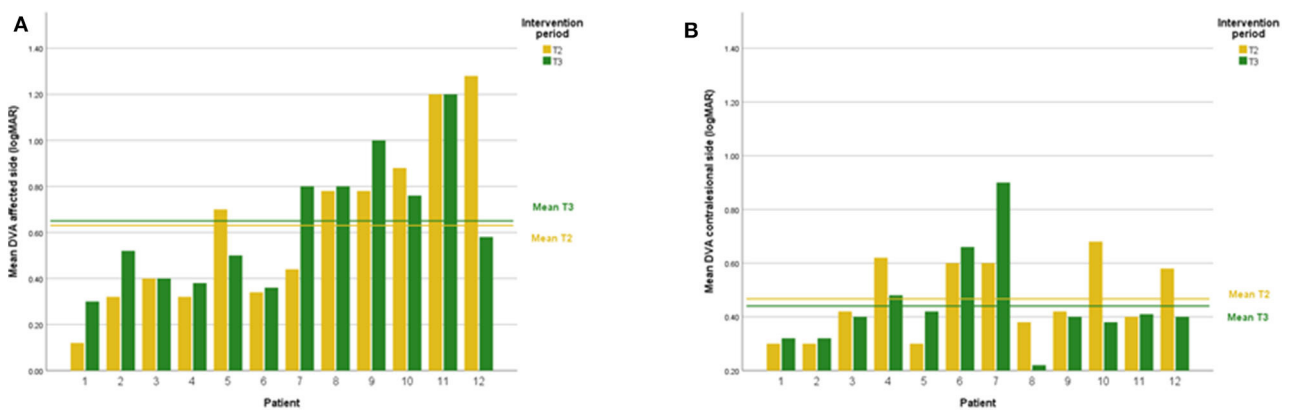

FIGURE 2 | (A) Individual DVA results lesion side at T2 and T3. **(B)** Individual DVA results contralesional side at T2 and T3.

in performance increments. The game scores can be found **Supplementary Figures 1A–H**.

DISCUSSION

Vestibular Compensation

The goal of this study was to evaluate the effects of a purpose-designed Exergaming rehabilitation program, including challenging conditions such as combined visual observation, head turns and unsupported stepping movements, on the vestibular compensation in subjects with cPVH. Based on the combined group and individual patient level assessment using an A-B research design there was clinically relevant improvement in some of the chronic subjects following the Exergame intervention phase. This might indicate that processes underlying central vestibular compensation were activated following the exergaming therapy in subjects with cPVH as opposed to non-observable change in the control phase. We found significantly smaller cumulative overt saccades amplitudes in more than half of the subjects. However, there was no change in VOR gain. A similar

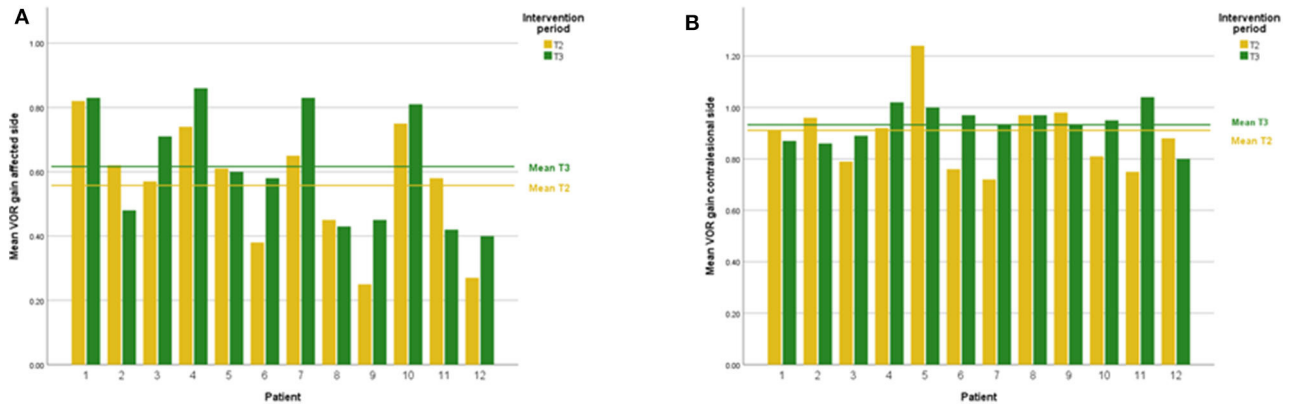

FIGURE 3 | (A) Individual VOR gain results lesion side at T2 and T3. **(B)** Individual VOR gain results contralesional side at T2 and T3.

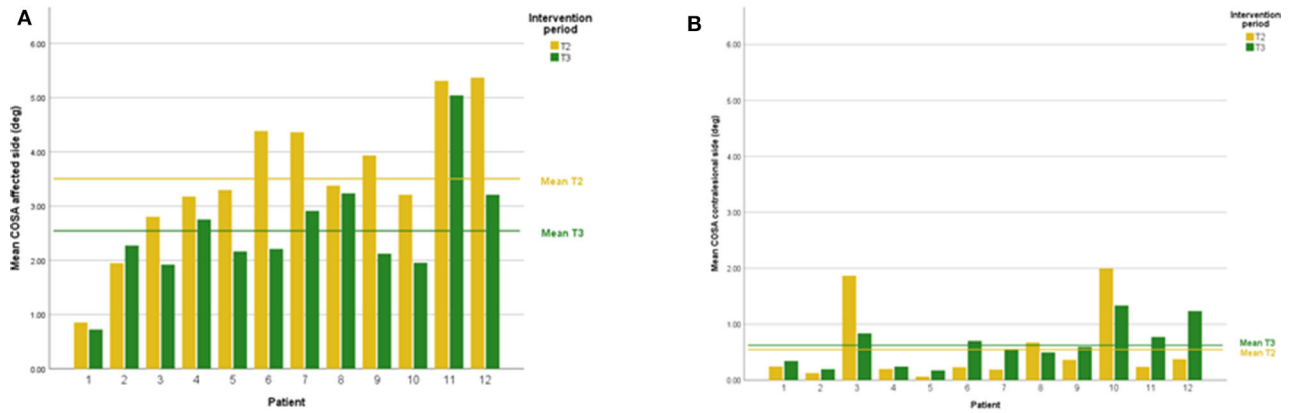

FIGURE 4 | (A) Individual COSA results lesion side at T2 and T3. **(B)** Individual COSA results contralesional side at T2 and T3.

result was recently reported by Millar et al. (57). In their study, a progressive vestibular rehabilitation program was conducted with subjects after unilateral vestibular deafferentation surgery. Their subjects clinically and statistically improved despite absent change in VOR gain (57). The interventions compared to this study were different. The vestibular physical therapy used in the study by Millar et al. was five times longer (total of 945 min over five weeks) than the exergaming performed in this study (total of 176 min over four weeks).

The COSA in this study positively correlated with DVA. Thus, smaller COSA mean better visual acuity.

After the intervention, the correlation between COSA and VOR gains was no longer significant, suggesting that the patients were able to compensate their VOR deficit with covert saccades during the head impulses, which are not accounted for in the COSA measure.

Gait Function

The subjects' gait function showed significant improvements. The FGA improved significantly and five subjects improved their FGA scores by at least nine points, which lies well above the minimal detectable change value for this measure (49). This makes the chance of a measurement error less likely as possible alternative explanation. When the training principle of specificity applies, the improved FGA task "gait with horizontal head turns" might be caused by the training content of provoked head turns while exergaming. The exergaming led to a safer locomotion. It is important to stress that the individuals partaking in our program were all chronic subjects from whom further treatment effects were expected being more difficult to achieve (22) based on their chronicity status. Seeing an improvement in half of the chronic patients in our sample is encouraging for the relevance of exergaming as a novel intervention and important on an individual subjects' daily living level. Finally, subjects' game scores showed continuous improvement in game performance meaning they could play the Exergames better and faster over the intervention course.

Study Limitations

The approach for the data analysis we used may be seen as a limitation of our study. The combination of group- and individual-level data analysis has intuitive appeal allowing

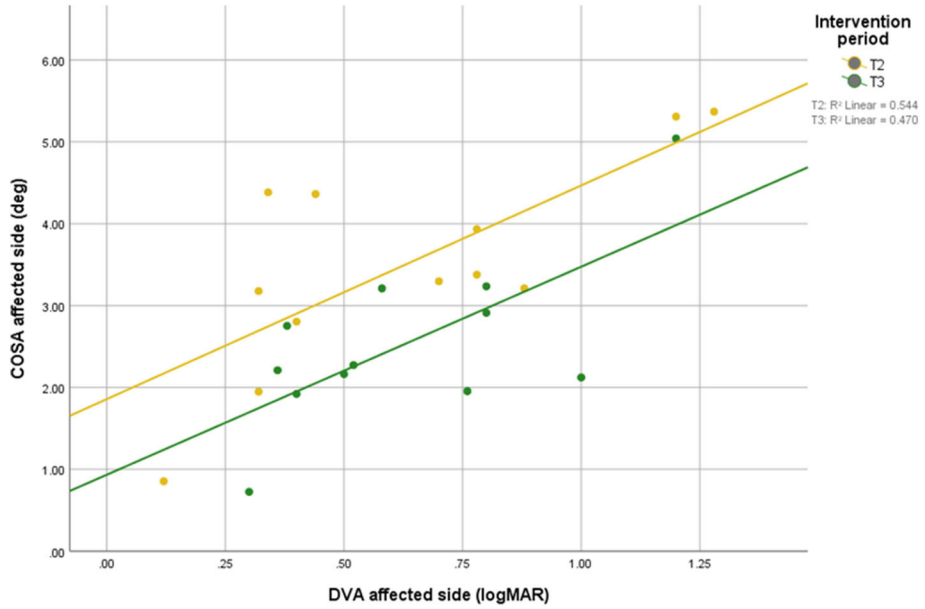

FIGURE 5 | Relationship between DVA and overt saccade amplitude before and after intervention with associated linear regression line.

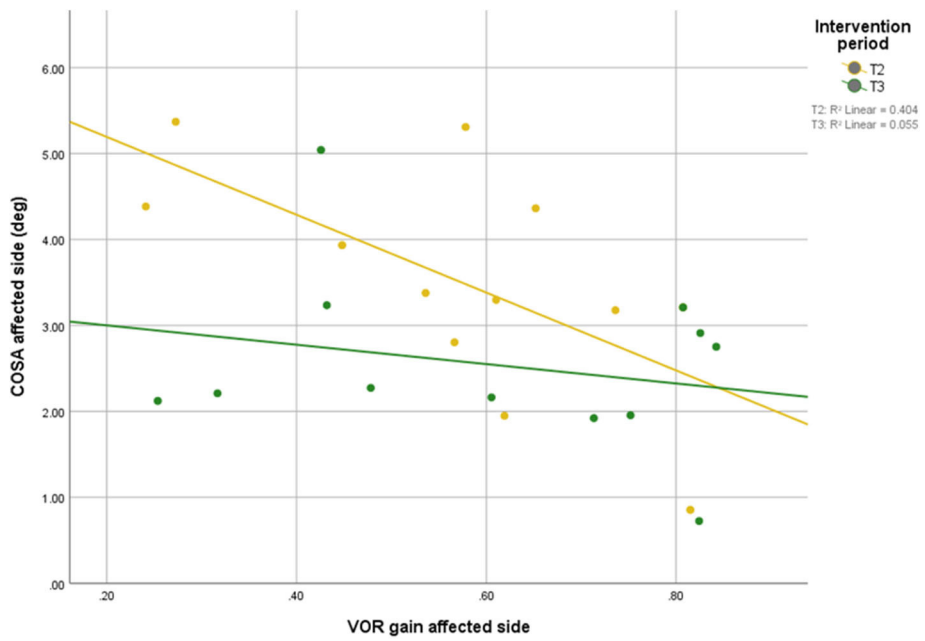

FIGURE 6 | Relationship between VOR gain and overt saccade amplitude before and after intervention with associated linear regression line.

individual-level associations through the mechanisms of bias control (AB design), the separation of contextual within and between-group effects, and the repeated checking of the treatment underlying model (58). However, such an approach theoretically necessitates knowledge about previous rehabilitation programs which each individual experienced as these may effect on the observable treatment effects of individuals (59). Gathering such detailed information for our participants was beyond the means of our study. A further limitation of the present study is the rather small sample size of 12 subjects that led to a weak statement regarding the population level, thus, limiting the generalizability of our treatment. However, in the current stage of intervention development we were mainly interested in individual patient responses to the intervention, since the expectation for these individuals to improve were rather low based on the chronicity of their symptoms and the years of previous therapy these individuals had undergone.

CONCLUSION

The results of the present study demonstrate that exergaming with promoted head turns facilitates vestibular compensation in some subjects with cPVH. This is the first study that shows an improvement in cumulative overt saccade amplitude after exergaming in several chronic vestibular subjects. The findings of this study warrant further research in which more complex research designs in larger samples should be employed.

DATA AVAILABILITY STATEMENT

All datasets generated for this study are included in the article/**Supplementary Material**.

ETHICS STATEMENT

The studies involving human participants were reviewed and approved by Ethics committee of the Canton of Zurich under BASEC 2018-00337. Trial registration was done at ClinicalTrials.gov Identifier; NCT03536533. The patients/participants provided their written informed consent to participate in this study.

AUTHOR CONTRIBUTIONS

JS developed the research question. The concept and design part were established by FB and JS. FB executed the intervention. FB, JS, and KW did the analysis of the results. KW, DS, and JS did the interpretation of the results. JS and FB produced an early version of the manuscript. EB, KW, and DS critically revised the manuscript to bring it to its current version. All authors have read and approved the final manuscript.

SUPPLEMENTARY MATERIAL

The Supplementary Material for this article can be found online at: https://www.frontiersin.org/articles/10.3389/fneur.2020.00601/full#supplementary-material

REFERENCES

1. Agrawal Y, Ward BK, Minor LB. Vestibular dysfunction: prevalence, impact and need for targeted treatment. *J Vestib Res.* (2013) 23:113–7. doi: 10.3233/VES-130498
2. Swanenburg J, Babler E, Adelsberger R, Straumann D, de Bruin ED. Patients with chronic peripheral vestibular hypofunction compared to healthy subjects exhibit differences in gaze and gait behaviour when walking on stairs and ramps. *PLoS ONE.* (2017) 12:e0189037. doi: 10.1371/journal.pone.0189037
3. McDonnell MN, Hillier SL. Vestibular rehabilitation for unilateral peripheral vestibular dysfunction. *Cochrane Database Syst Rev.* (2015) 1:CD005397. doi: 10.1002/14651858.CD005397.pub4
4. Neuhauser HK, von Brevern M, Radtke A, Lezius F, Feldmann M, Ziese T, et al. Epidemiology of vestibular vertigo: a neurotologic survey of the general population. *Neurology.* (2005) 65:898–904. doi: 10.1212/01.wnl.0000175987.59991.3d
5. Monzani D, Casolari L, Guidetti G, Rigatelli M. Psychological distress and disability in patients with vertigo. *J Psychosom Res.* (2001) 50:319–23. doi: 10.1016/S0022-3999(01)00208-2
6. Gufoni M, Guidetti G, Nuti D, Pagnini P, Vicini C, Tinelli C, et al. [The relationship between cognitive impairment, anxiety-depression symptoms and balance and spatial orientation complaints in the elderly]. *Acta Otorhinolaryngol Ital.* (2005) 25:12–21.
7. Smith PF, Zheng Y, Horii A, Darlington CL. Does vestibular damage cause cognitive dysfunction in humans? *J Vestib Res.* (2005) 15:1–9.
8. Agrawal Y, Carey JP, Della Santina CC, Schubert MC, Minor LB. Diabetes, vestibular dysfunction, and falls: analyses from the national health and nutrition examination survey. *Otol Neurotol.* (2010) 31:1445–50. doi: 10.1097/MAO.0b013e3181f2f035
9. Kendall JC, Hartvigsen J, Azari MF, French SD. Effects of nonpharmacological interventions for dizziness in older people: systematic review. *Phys Ther.* (2016) 96:641–9. doi: 10.2522/ptj.20150349
10. Kundakci B, Sultana A, Taylor AJ, Alshehri MA. The effectiveness of exercise-based vestibular rehabilitation in adult patients with chronic dizziness: a systematic review. *F1000Res.* (2018) 7:276. doi: 10.12688/f1000research.14089.1
11. Hall CD, Herdman SJ, Whitney SL, Cass SP, Clendaniel RA, Fife TD, et al. Vestibular rehabilitation for peripheral vestibular hypofunction: an evidence-Based clinical practice guideline: from the american physical therapy association neurology section. *J Neurol Phys Ther.* (2016) 40:124–55. doi: 10.1097/NPT.0000000000000120
12. Bergeron M, Lortie CL, Guitton MJ. Use of virtual reality tools for vestibular disorders rehabilitation: a Comprehensive analysis. *Adv Med.* (2015) 2015:916735. doi: 10.1155/2015/916735
13. Muinos M, Ballesteros S. Sports can protect dynamic visual acuity from aging: a study with young and older judo and karate martial arts athletes. *Atten Percept Psycho.* (2015) 77:2061–73. doi: 10.3758/s13414-015-0901-x
14. Whitney SL, Alghwiri AA, Alghadir A. An overview of vestibular rehabilitation. *Handb Clin Neurol.* (2016) 137:187–205. doi: 10.1016/B978-0-444-63437-5.00013-3
15. Cromwell R, Wellmon R. Sagittal plane head stabilization during level walking and ambulation on stairs. *Physiother Res Int.* (2001) 6:179–92. doi: 10.1002/pri.226
16. Swanenburg J, Zurbrugg A, Straumann D, Hegemann SCA, Palla A, de Bruin ED. A pilot study investigating the association between chronic bilateral vestibulopathy and components of a clinical functional assessment tool. *Physiother Theory Pract.* (2017) 33:454–61. doi: 10.1080/09593985.2017.1323362
17. Paul SS, Dibble LE, Walther RG, Shelton C, Gurgel RK, Lester ME. Reduced purposeful head movements during community ambulation following unilateral vestibular loss. *Neurorehabil Neural Repair.* (2018) 32:309–16. doi: 10.1177/1545968318770271
18. Han BI, Song HS, Kim JS. Vestibular rehabilitation therapy: review of indications, mechanisms, key exercises. *J Clin Neurol.* (2011) 7:184–96. doi: 10.3988/jcn.2011.7.4.184
19. Sulway S, Whitney SL. Advances in vestibular rehabilitation. *Adv Otorhinolaryngol.* (2019) 82:164–9. doi: 10.1159/000490285
20. Scherer M, Migliaccio AA, Schubert MC. Effect of vestibular rehabilitation on passive dynamic visual acuity. *J Vestib Res.* (2008) 18:147–57.
21. Schubert MC, Migliaccio AA, Clendaniel RA, Allak A, Carey JP. Mechanism of dynamic visual acuity recovery with vestibular rehabilitation.

Arch Phys Med Rehabil. (2008) 89:500–7. doi: 10.1016/j.apmr.2007.11.010
22. Michel L, Laurent T, Alain T. Rehabilitation of dynamic visual acuity in patients with unilateral vestibular hypofunction: earlier is better. *Eur Arch Otorhinolaryngol.* (2020) 277:103–13. doi: 10.1007/s00405-019-05690-4
23. Hain TC. Neurophysiology of vestibular rehabilitation. *NeuroRehabilitation.* (2011) 29:127–41. doi: 10.3233/NRE-2011-0687
24. Swanenburg J, Wild K, Straumann D, de Bruin ED. Exergaming in a moving virtual world to train vestibular functions and gait; a proof-of-Concept-Study with older adults. *Front Physiol.* (2018) 9:988. doi: 10.3389/fphys.2018.00988
25. McCaskey MA, Schattin A, Martin-Niedecken AL, de Bruin ED. Making more of iT: enabling intensive motor cognitive rehabilitation exercises in geriatrics using information technology solutions. *Biomed Res Int.* (2018) 2018:4856146. doi: 10.1155/2018/4856146
26. Meldrum D, Herdman S, Vance R, Murray D, Malone K, Duffy D, et al. Effectiveness of conventional versus virtual reality-based balance exercises in vestibular rehabilitation for unilateral peripheral vestibular loss: results of a randomized controlled trial. *Arch Phys Med Rehabil.* (2015) 96:1319–28 e1. doi: 10.1016/j.apmr.2015.02.032
27. Hondebrink MS, Mert A, van der Lint R, de Ru JA, van der Wurff P. Motion-based equilibrium reprocessing therapy a novel treatment method for chronic peripheral vestibulopathies: a pilot study. *Medicine (Baltimore).* (2017) 96:e7128. doi: 10.1097/MD.0000000000007128
28. Hsu SY, Fang TY, Yeh SC, Su MC, Wang PC, Wang VY. Three-dimensional, virtual reality vestibular rehabilitation for chronic imbalance problem caused by meniere's disease: a pilot study<sup/>. *Disabil Rehabil.* (2017) 39:1601–6. doi: 10.1080/09638288.2016.1203027
29. Viziano A, Micarelli A, Augimeri I, Micarelli D, Alessandrini M. Long-term effects of vestibular rehabilitation and head-mounted gaming task procedure in unilateral vestibular hypofunction: a 12-month follow-up of a randomized controlled trial. *Clin Rehabil.* (2019) 33:24–33. doi: 10.1177/0269215518788598
30. Eggenberger P, Wolf M, Schumann M, de Bruin ED. Exergame and balance training modulate prefrontal brain activity during walking and enhance executive function in older adults. *Front Aging Neurosci.* (2016) 8:66. doi: 10.3389/fnagi.2016.00066
31. Schattin A, Arner R, Gennaro F, de Bruin ED. Adaptations of prefrontal brain activity, executive functions, and gait in healthy elderly following exergame and balance training: a Randomized-Controlled study. *Front Aging Neurosci.* (2016) 8:278. doi: 10.3389/fnagi.2016.00278
32. Rebsamen S, Knols RH, Pfister PB, de Bruin ED. Exergame-Driven high-Intensity interval training in untrained community dwelling older adults: a Formative one group quasi- experimental feasibility trial. *Front Physiol.* (2019) 10:1019. doi: 10.3389/fphys.2019.01019
33. Tate RL, Perdices M, Rosenkoetter U, Shadish W, Vohra S, Barlow DH, et al. The single-Case reporting guideline in bEhavioural interventions (SCRIBE) 2016 statement. *Phys Ther.* (2016) 96:e1–e10. doi: 10.2522/ptj.2016.96.7.e1
34. Schubert MC, Migliaccio AA, Della Santina CC. Dynamic visual acuity during passive head thrusts in canal planes. *J Assoc Res Otolaryngol.* (2006) 7:329–38. doi: 10.1007/s10162-006-0047-6
35. Herdman SJ, Tusa RJ, Blatt P, Suzuki A, Venuto PJ, Roberts D. Computerized dynamic visual acuity test in the assessment of vestibular deficits. *Am J Otol.* (1998) 19:790–6.
36. Vital D, Hegemann SC, Straumann D, Bergamin O, Bockisch CJ, Angehrn D, et al. A new dynamic visual acuity test to assess peripheral vestibular function. *Arch Otolaryngol Head Neck Surg.* (2010) 136:686–91. doi: 10.1001/archoto.2010.99
37. Wettstein VG, Weber KP, Bockisch CJ, Hegemann SC. Compensatory saccades in head impulse testing influence the dynamic visual acuity of patients with unilateral peripheral vestibulopathy1. *J Vestib Res.* (2016) 26:395–402. doi: 10.3233/VES-160591
38. Mohammad MT, Whitney SL, Marchetti GF, Sparto PJ, Ward BK, Furman JM. The reliability and response stability of dynamic testing of the vestibulo-ocular reflex in patients with vestibular disease. *J Vestib Res.* (2011) 21:277–88. doi: 10.3233/VES-2011-0430
39. Petersen JA, Straumann D, Weber KP. Clinical diagnosis of bilateral vestibular loss: three simple bedside tests. *Ther Adv Neurol Disord.* (2013) 6:41–5. doi: 10.1177/1756285612465920
40. Eza-Nunez P, Farinas-Alvarez C, Fernandez NP. Comparison of three diagnostic tests in detecting vestibular deficit in patients with peripheral vestibulopathy. *J Laryngol Otol.* (2016) 130:145–50. doi: 10.1017/S0022215115003114
41. Weber KP, MacDougall HG, Halmagyi GM, Curthoys IS. Impulsive testing of semicircular-canal function using video-oculography. *Ann Ny Acad Sci.* (2009) 1164:486–91. doi: 10.1111/j.1749-6632.2008.03730.x
42. Curthoys IS, MacDougall HG, Manzari L, Burgess AM, Bradshaw AP, McGarvie L, et al. Clinical application of a new objective test of semicircular canal dynamic function-the video head impulse test (vHIT). A safe, simple, and fast clinical vestibular test. In: *Vertigo-Kontroverses und Bewährtes 8. Hennig Symposium*, New York, NY: SpringerWien (2011). p. 53–64. doi: 10.1007/978-3-7091-0736-2_6
43. MacDougall ML, Halmagyi GM. Anti-compensatory saccades as an indicator of peripheral vestibular function in a new complementary video head impulse test paradigm. *Eur J Neurol.* (2015) 22.
44. Weber KP, Aw ST, Todd MJ, McGarvie LA, Curthoys IS, Halmagyi GM. Head impulse test in unilateral vestibular loss: vestibulo-ocular reflex and catch-up saccades. *Neurology.* (2008) 70:454–63. doi: 10.1212/01.wnl.0000299117.48935.2e
45. Weber KP, Aw ST, Todd MJ, McGarvie LA, Curthoys IS, Halmagyi GM. Horizontal head impulse test detects gentamicin vestibulotoxicity. *Neurology.* (2009) 72:1417–24. doi: 10.1212/WNL.0b013e3181a18652
46. Tarnutzer AA, Bockisch CJ, Buffone E, Weiler S, Bachmann LM, Weber KP. Disease-specific sparing of the anterior semicircular canals in bilateral vestibulopathy. *Clin Neurophysiol.* (2016) 127:2791–801. doi: 10.1016/j.clinph.2016.05.005
47. Wrisley DM, Marchetti GF, Kuharsky DK, Whitney SL. Reliability, internal consistency, and validity of data obtained with the functional gait assessment. *Phys Ther.* (2004) 84:906–18. doi: 10.1093/ptj/84.10.906
48. Walker ML, Austin AG, Banke GM, Foxx SR, Gaetano L, Gardner LA, et al. Reference group data for the functional gait assessment. *Phys Ther.* (2007) 87:1468–77. doi: 10.2522/ptj.20060344
49. Marchetti GF, Lin CC, Alghadir A, Whitney SL. Responsiveness and minimal detectable change of the dynamic gait index and functional gait index in persons with balance and vestibular disorders. *J Neurol Phys Ther.* (2014) 38:119–24. doi: 10.1097/NPT.0000000000000015
50. Wall JC, Bell C, Campbell S, Davis J. The timed get-up-and-Go test revisited: measurement of the component tasks. *J Rehabil Res Dev.* (2000) 37:109–13.
51. Swanenburg J, Humphreys K, Langenfeld A, Brunner F, Wirth B. Validity and reliability of a german version of the neck disability index (NDI-G). *Man Ther.* (2014) 19:52–8. doi: 10.1016/j.math.2013.07.004
52. Swanenburg J, Hegemann SC, Zurbrugg A, Palla A, de Bruin ED. Reliability and validity of the extended timed-get-up-and-go test in patients with bilateral vestibular loss. *NeuroRehabilitation.* (2014) 34:799–807. doi: 10.3233/NRE-141083
53. Kurre Annette BCH, van Gool Christel JAW, Gloor-Juzi T, De Bruin Eling D, Straumann D. Exploratory factor analysis of the dizziness handicap inventory (German version). *BMC Ear, Nose Throat Disorders.* (2010) 10:3. doi: 10.1186/1472-6815-10-3
54. Jacobson GP, Newman CW. The development of the Dizziness Handicap Inventory. *Arch Otolaryngol Head Neck Surg.* (1990) 116:424–7. doi: 10.1001/archotol.1990.01870040046011
55. Keshavarz B, Hecht H. Validating an efficient method to quantify motion sickness. *Hum Factors.* (2011) 53:415–26. doi: 10.1177/0018720811403736

56. Kennedy RS, Lane NE, Berbaum KS, Lilienthal MG. Simulator sickness questionnaire: an enhanced method for quantifying simulator sickness. *Int J Avi Psychol.* (1993) 3:203–20. doi: 10.1207/s15327108ijap0303_3
57. Millar JL, Gimmon Y, Roberts D, Schubert MC. Improvement after vestibular rehabilitation not explained by improved passive vOR gain. *Front Neurol.* (2020) 11:79. doi: 10.3389/fneur.2020.00079
58. Haneuse S, Bartell S. Designs for the combination of group- and individual-level data. *Epidemiology.* (2011) 22:382–9. doi: 10.1097/EDE.0b013e3182125cff
59. Wirtz MA. [Multilevel analysis as a tool to analyze research questions in rehabilitation science]. *Rehabilitation (Stuttg).* (2019) 58:274–81. doi: 10.1055/s-0043-124334

Conflict of Interest: EB was a co-founder of Dividat; the spin-off company that developed the exergame platform used in this study, and is associated to the company as an external advisor. No revenue was paid (or promised to be paid) directly to EB or his institution over the 36 months prior to submission of the work. KW acts as an unpaid consultant and has received funding for travel from Otometrics.

The remaining authors declare that the research was conducted in the absence of any commercial or financial relationships that could be construed as a potential conflict of interest.

Advantages of publishing in Frontiers

OPEN ACCESS
Articles are free to read for greatest visibility and readership

FAST PUBLICATION
Around 90 days from submission to decision

HIGH QUALITY PEER-REVIEW
Rigorous, collaborative, and constructive peer-review

TRANSPARENT PEER-REVIEW
Editors and reviewers acknowledged by name on published articles

Frontiers
Avenue du Tribunal-Fédéral 34
1005 Lausanne | Switzerland

Visit us: www.frontiersin.org
Contact us: frontiersin.org/about/contact

REPRODUCIBILITY OF RESEARCH
Support open data and methods to enhance research reproducibility

DIGITAL PUBLISHING
Articles designed for optimal readership across devices

FOLLOW US
@frontiersin

IMPACT METRICS
Advanced article metrics track visibility across digital media

EXTENSIVE PROMOTION
Marketing and promotion of impactful research

LOOP RESEARCH NETWORK
Our network increases your article's readership